

Monofunctionalized Gold Nanoparticles via Branched Thioether-Based Ligands

Inauguraldissertation

zur

Erlangung der Würde eines Doktors der Philosophie

vorgelegt der

Philosophisch-Naturwissenschaftlichen Fakultät

der Universität Basel

von

Erich Henrik Peters

aus Arbon (TG), Schweiz

Basel, 2023

Genehmigt von der Philosophisch-Naturwissenschaftlichen Fakultät auf
Antrag von

Prof. Dr. Marcel Mayor

Prof. Dr. Jonathan De Roo

Basel, den 21.04.2020

Prof. Dr. Martin Spiess (Dekan)

...für E. P. und R. H.

*Gold und Silber lieb ich sehr,
kann's auch gut gebrauchen,
hätt ich nur ein ganzes Meer,
mich hineinzutauchen;
braucht ja nicht geprägt zu sein,
hab's auch so ganz gerne,
sei's des Mondes Silberschein.
sei's das Gold der Sterne.*

*Doch viel schöner ist das Gold,
das vom Lockenköpfchen
meines Liebchens niederrollt
in zwei blonden Zöpfen.
Darum, du, mein liebes Kind,
laß uns Herzen, küssen,
bis die Locken silbern sind
und wir scheiden müssen.*

*Seht, wie blinkt der goldne Wein
hier in meinem Becher;
horcht, wie klingt so silberrein
froher Sang der Zecher!
Daß die Zeit einst golden war,
will ich nicht bestreiten,
denk ich doch im Silberhaar
gern vergangner Zeiten.*

—August Schnelzer

Acknowledgments

Four years have passed during which I was privileged to hone my prowess in preparative organic chemistry with a glimpse outside the box. Considering my education in nanoscience with a prominent penchant to physics, I might not have been an obvious choice for a PhD candidate in this field, yet my advisor, Prof. Dr. Marcel Mayor chose to grant me the opportunity to work for his group for which I express my sincerest gratitude (and also for noticing my vast selection of band t-shirts). I would also like to thank Prof. Dr. Jonathan De Roo for kindly accepting to be my co-referee and Prof. Dr. Oliver Wenger for chairing my defense.

At this point, before I thank my colleagues in this group, I feel obliged to apologize for the suffering my horrible sense of humor has brought over these accursed halls and the innumerable times my dull puns enticed my poor co-workers to cringe and roll their eyes. The only gesture I can offer—which can, by no means, account for the abysmally bad impression my shallow jests must have left—is a wide-grinned, ironic “I’m sorry.”

Special thanks go to Dr. Mario Lehmann for converting me into an enthused chemist and showing me the ways of *proper* organic synthesis as well as my predecessors on the nanoparticle project who paved the way to my success: Dr. Thorsten Peterle, Dr. Jens Hermes, Dr. Fabian Sander and Dr. Ulrike Fluch without whose efforts my humble contribution would have been far less yielding. Alas, it is well-known that the dark side all too easily lures the weak-minded—especially if they are prone to fall victim to an equally appalling notion of humor. For this reason, I’d like to thank Dr. Yves Aeschi for teaching me the ways of *improper* organic synthesis, the fruitful expansion of my musical horizon and exchange of quotes from *Lustiges Taschenbuch*, the fruitless exchange of shallow dad jokes and for being a fantastic labmate.

My greatest appreciation shall be expressed to Adriano D’Addio, Laurent Jucker and Dr. Tomáš Šolomek whose sober insight in proofreading allowed turning this toilet paper-grade document into an actual dissertation.

Many thanks go to lab 4, my home and shelter for four years, to Laurent Jucker and Dr. Tomáš Šolomek for taking the relay in helping me explore the vast space of music, Juraj Malinčík for his rare gift of appreciation for my impossible wisecracks, the dank memes we shared and his devotion to learn the *most essential* (Swiss) German expressions, Hsin-Hua Huang whose different cultural background lead to many most amusing situations and Dr. Cristián Gozávez Martínez with whom I shared many conversations in my rusty Spanish which would otherwise suffer the fate of the age-related physiologic cerebral deterioration.

A great contribution to my well-being was brought by the *Gräslclub* whose past and present members Adriano D’Addio, Charlotte Kress, Florian Degen, Dr. Linda Bannwart, Dr. Lorenzo Delarue Bizzini, Patrick Zwick and Dr. Yves Aeschi helped sate my ogreish appetite for countless Mondays’ lunches. Equally beneficial for keeping my sanity were the many, many drinks—and then some—I was provided by *Rauchi*, *Schnaufi* and *Saufi*. Finally, the entirety of my PhD education wouldn’t have been near half as bearable without the help of and the interaction with all the past and current members of the Mayor group that have had the doubtful pleasure of spending their work life with me. It was a joyous time and I will miss you dearly.

At this place, it is only appropriate to thank all the people involved in helping me shed light on the many structural conundrums and analytic challenges beyond my limited intellectual capabilities: Dr. Annika Büttner, Cédric Wobill, PD Dr. Daniel Häussinger, Dr. Heinz Nadig, Dr. Michael Pfeffer, Patrik Eckert, Dr. Sylvie Mittelheisser, Dr. Viviane Lutz-Bueno and the MoBiAS Lab at ETH Zürich. Just as important for the functioning of this organization are the administrative staff, the Werkstatt, Oliver Ilg, Markus Hauri, and our charming secretary Brigitte Howald with whom I spent much time not letting the little Swedish I’m capable of speaking wither and eventually fall victim to my lack of memorizing ability.

Immeasurable gratitude shall be addressed to the two people to whom I owe my very existence: my parents without whose constant support in all my endeavors (and there were quite some of questionable nature) gradually forged the person I am now. I’m also thanking my sister for—despite all the badgering—having my back at all times and being a person I will always look up to.

Finally, I thank my *Vaai* Senta for bearing with me through our best and worst times. I could not imagine a better companion and lover to grow old and miserable with.

Not all that Is Gold Does Glitter

When I was introduced to gold colloids, I was amazed about the observation that from quantum mechanics—until this moment a merely theoretical construct in my educational life—effects manifest to the unaided eye can indeed arise. This fascination has persisted throughout the entirety of my pursuit for ligands enwrapping gold nanoparticles that give the colloids a high stability and allow the introduction of a singular functional unit for further chemical processing.

Standing on the shoulders of my predecessors in this endeavor, my efforts in pushing the reach of this field were rewarded by three publications. The first of which shows a proof of concept for the approach I chose to work on: the introduction of a branching point allowing linear oligomers to cover the surface of a nanoparticle more effectively. It was published in *Particles and Particle Systems Characterization*. For the second paper—published in *European Journal of Inorganic Chemistry*—the branching point was decorated with a chemically addressable unit allowing the controlled building of larger superstructures. The final manuscript enhanced the scope of my work towards a cage-type ligand which stabilized particles of unprecedented resilience, yet challenging our way of thinking about chemistry by their unexpected catalytic behavior. The latter was, at the point this thesis was handed in, pending its imminent submission to *Chemical Communications* and was, meanwhile, published. Preceding these three manuscripts, a review which was published in *CHIMIA* upon invitation shortly after completion of this dissertation, titled “Monofunctionalized Gold Nanoparticles: Fabrication and Applications” is presented in order to give an overview over the many approaches to monofunctionalized gold nanoparticles and their even larger number of applications.

This cumulative dissertation starts with a brief introduction to the vast field of gold nanoparticles and, in particular, their monofunctionalized variant, followed by the aforementioned review article. Subsequently, the approach to monofunctionalized gold nanoparticles by branched thioethers—to which all my efforts towards completing my doctorate were dedicated—is succinctly outlined before the three first-author research publications are presented in chronologic order. For the ease of reading, the supplementary information documents to all experimental manuscripts are placed as an appendix after the Conclusion and Outlook section.

E. Henrik Peters

Basel, March 2020

edited March 2023

Table of Contents

Overview of the Thesis	1–8
Monofunctionalized Gold Nanoparticles: Fabrication and Applications	9–21
<i>CHIMIA</i> , 2021 , 75, 5, 414–426 E. H. Peters, M. Mayor DOI: 10.2533/chimia.2021.414	
About the Project	23–24
Gold Nanoparticles Stabilized by Single Tripodal Ligands	25–34
<i>Particle and Particle Systems Characterization</i> , 2018 , 1800015 E. H. Peters, M. Lehmann, M. Mayor DOI: 10.1002/ppsc.201800015	
Alkyne-Monofunctionalized Gold Nanoparticles as Massive Molecular Building Blocks	35–44
<i>European Journal of Inorganic Chemistry</i> , 2020 , 24, 2325–2334 E. H. Peters, M. Mayor DOI: 10.1002/ejic.202000273	
An Organic Cage Controlling the Dimension and Stability of Gold Nanoparticles	45–48
<i>Chemical Communication</i> , 2023 , 59 E. H. Peters, M. Mayor DOI: 10.1039/D3CC00277B	
Conclusion and Outlook	49
Appendix	
A: Supporting Information for Particle and Particle Systems Characterization	51–70
B: Supporting Information for European Journal of Inorganic Chemistry	71–84
C: Supporting Information for Chemical Communications	85–103
Curriculum Vitae	105–106

Overview of the Thesis

Gold nanoparticles, despite being an extensively researched field for well over 150 years, have lost none of their fascination. Several approaches have been investigated to find ligands that passivate the highly reactive surface of these colloids featuring non-classical optical and electrical properties and, moreover, provide them with chemical, biological or physical functionality. In this cumulative thesis, three publications on the pathway to gold nanoparticles bearing a single functional unit—*i.e.* monofunctionalized gold nanoparticles—shall be presented as well as a review highlighting alternate pathways that ultimately lead to the same goal. For a better understanding, the concept of gold nanoparticles will be briefly introduced before summarizing the included publications in short.

From Shiny Metal to Nanoparticle—A Succinct Introduction

Arguably, metal nanoparticles are humankind's oldest form of nanotechnology, for it is well before the Roman Empire—from whence the famous *Lycurgus cup* cometh—that gold colloids were used as an additive for the fabrication of dichroic ceramics and glasses.^[1] A modern example of this art is shown in Figure 1. In medieval and post-Renaissance Europe, gold elixirs were used for various medical treatments such as, among others, *sore limbs* (archaic term for arthritis) in the form of *Aurum Potabile* (potable gold)^[2] and as stains for decorative glass for *e.g.* church windows.^[3,4] It is not before the pioneering works of Faraday, however, that the wet chemical synthesis of colloidal gold was mastered and their optical properties phenomenologically described.^[5] In 1908, at the dawn of quantum mechanics, the German scientist Gustav Mie solved the Maxwell equations for electrons in a finitely deep spherical potential well and thus delivered the theoretical description of the surface plasmon resonance phenomena observed in nanoparticles, explaining their size-dependent color.^[6]

In the middle of the twentieth century, Turkevich and co-workers reported the first synthesis of gold nanoparticles of narrow size distribution via reduction of hydrogen tetrachloroaurate (HAuCl_4) by citrate which acts as both the reducing agent and the weakly stabilizing ligand.^[7] Later, the two-phase reduction of HAuCl_4 by sodium borohydride in presence of a hydrophobic alkylthiol ligand exploiting the sulfur's affinity to gold and giving exceptionally stable colloids, was proposed by Brust *et al.* in 1994.^[8]



Figure 1 Example of a dichroic cup. The glass has been stained with gold nanoparticles which appear brown when light is reflected and purple when light is transmitted. Reproduced from Ref. 9.

In a world of electronics dominated by Moore's law,^[10] these seminal works sparked great efforts for the implementation of gold nanoparticles in molecular electronics.^[11–15] Several conditions need to be fulfilled in order to obtain gold nanoparticles which can be used as components for nanometer-sized circuits. The nanoparticles must (1) be uniform and of suitable size, (2) exhibit a controlled (small) number of functional units addressable via common chemical transformations, and (3) the functional unit must allow precise spatial arrangement in superstructural assembly protocols. These conditions pose a considerable challenge to the architecture and chemical properties of the ligands stabilizing the nanoparticles. Several approaches have been reported for the incorporation of a single addressable unit into the ligand shell of gold nanoparticles. Methods using a single^[16–19] or multiple ligands whereof only one bears a chemical functionality of interest^[20–23] are known. In the former case, Brust's thiol approach^[8] shows limitations in regard of ligand architecture scope since thiols are

terminal functions. In 2001, Pankau *et al.* demonstrated that, in order to overcome these constraints, the thiols could be swapped for thioethers,^[24] giving ligands that do rather physisorb than chemisorb on the nanoparticle surface via quasi-reversible bonds.^[25–27] This feature is expected to allow the ligand to adapt into a favorable conformation upon stabilizing the nucleating gold nanoparticle and thus opens the door to thioether-based multidentate oligomers^[28,29] and dendrimers^[19,30] as well as cages^[31] which allow more precise control over size of the particle and number of functional units per particle^[32] via their tailored architecture. The works presented in this thesis were inspired by Pankau's approach using benzylic thioethers as stabilizing moieties.

Publications in this Thesis

I. Monofunctionalized Gold Nanoparticles: Fabrication and Applications (2021, Invited Review, CHIMIA)

As briefly discussed above, the installation of one single chemically addressable unit on a gold nanoparticle often demands for sophisticated solutions. There are many aspects to take into consideration: the size of the nanoparticles, the number of ligands stabilizing them, the ligand architecture and its chemical accessibility, the desired application scope et cetera. In order to tackle this challenging endeavor, many approaches have been reported, resulting in a plethora of implementations. In general, monofunctionalized gold nanoparticles can be classified into two classes: gold nanoparticles stabilized by a single ligand (Type I) or by multiple ligands (Type II), whereby only one of these ligands contains the functionality of interest. Both types result from different approaches. In Type I nanoparticles, the ligand, to a certain limit, templates their size by its pre-organized oligo-,^[33] poly-,^[16,34–36] dendrimeric^[37,38] or cage-type^[31] structure. Type II particles are subjected to single-ligand place-exchange reactions in order to achieve monofunctionalization^[22,23] or they are synthesized in presence of a finely tuned statistical ligand mixture.^[39,40] Figure 2 shows a tentative graphical abstract explaining both Types of monofunctionalized gold nanoparticles and how to synthesize them.

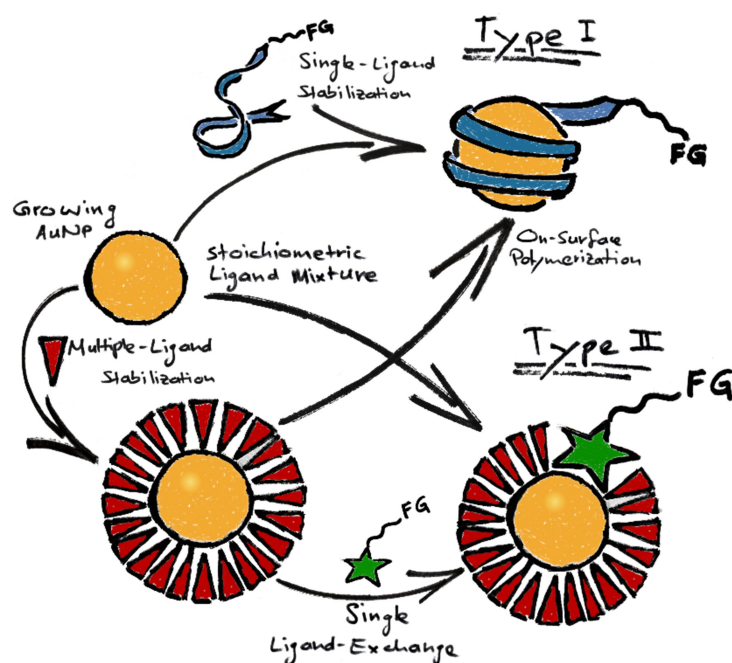


Figure 2 Original graphical abstract for the review 'Monofunctionalized Gold Nanoparticles: Fabrication and Applications'. A nucleating particle is stabilized by either one ligand with a single functional unit (Type I) or multiple small ligands which can be on-surface polymerized to a single ligand to give Type I particles as well. Alternatively, Gold nanoparticles can be stabilized by multiple small ligands and a single ligand can be place-exchanged to a small ligand with a functional unit (Type II). Another way to synthesize Type II nanoparticles is by synthesizing them in presence of a statistical ligand mixture. AuNP = gold nanoparticle, FG = functional group.

Figure 2 shows a tentative graphical abstract explaining both Types of monofunctionalized gold nanoparticles and how to synthesize them. In our review "Monofunctionalized Gold Nanoparticles: Fabrication and Applications" (2021), we summarize the different approaches to introduce a single functional group into the ligand shell of gold nanoparticles and their numerous variations. We, furthermore, discuss the applications of such

systems which cover—to cite only the most prominent examples—labeling,^[40–42] supramolecular assembly,^[43–45] molecular electronics,^[46–48] and plasmonics.^[49–51]

II. Gold Nanoparticles Stabilized by Single Tripodal Ligands (2018, Full Paper, Particle & Particle Systems Characterization)

In previous works, it was found that in Type I gold nanoparticles stabilized by benzylic thioether-based ligands, it is the bulkiness of the ligand and not the number of sulfur atoms that controls the stability and size of the particles as well as the number of ligands coating them.^[29] Also, the ligand's bite angle was shown to have only limited influence on the particle size.^[52] For these reasons, previously reported linear ligands^[28,29] were attached to a tetraphenylmethane-based central linking point comprising benzylic bromides in the *para* position of three of its phenyls in order to enable more effective surficial covering in contrast to linear oligomers. Further, the unfunctionalized phenyl was expected to stand in upright position^[53] and would therefore be an ideal position for the introduction of a single chemically (and ultimately, electronically) addressable unit. Interestingly, variation of the side-chains showed no influence on the particle size within statistical error. A comprehensive drawing of this ligand system is shown in Scheme 1. Figure 3 was used as a graphical abstract for the publication. This preliminary work represents a proof of principle in which it was shown that the nonlinearity of the ligand offers

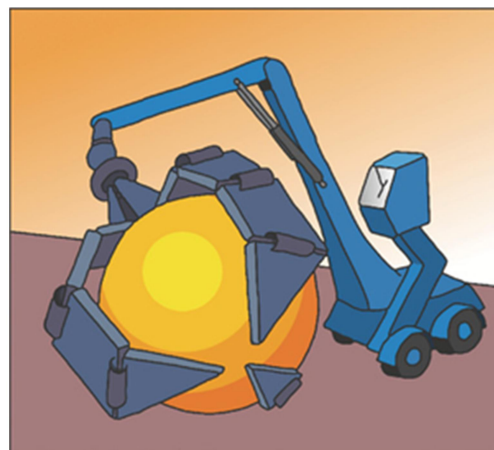
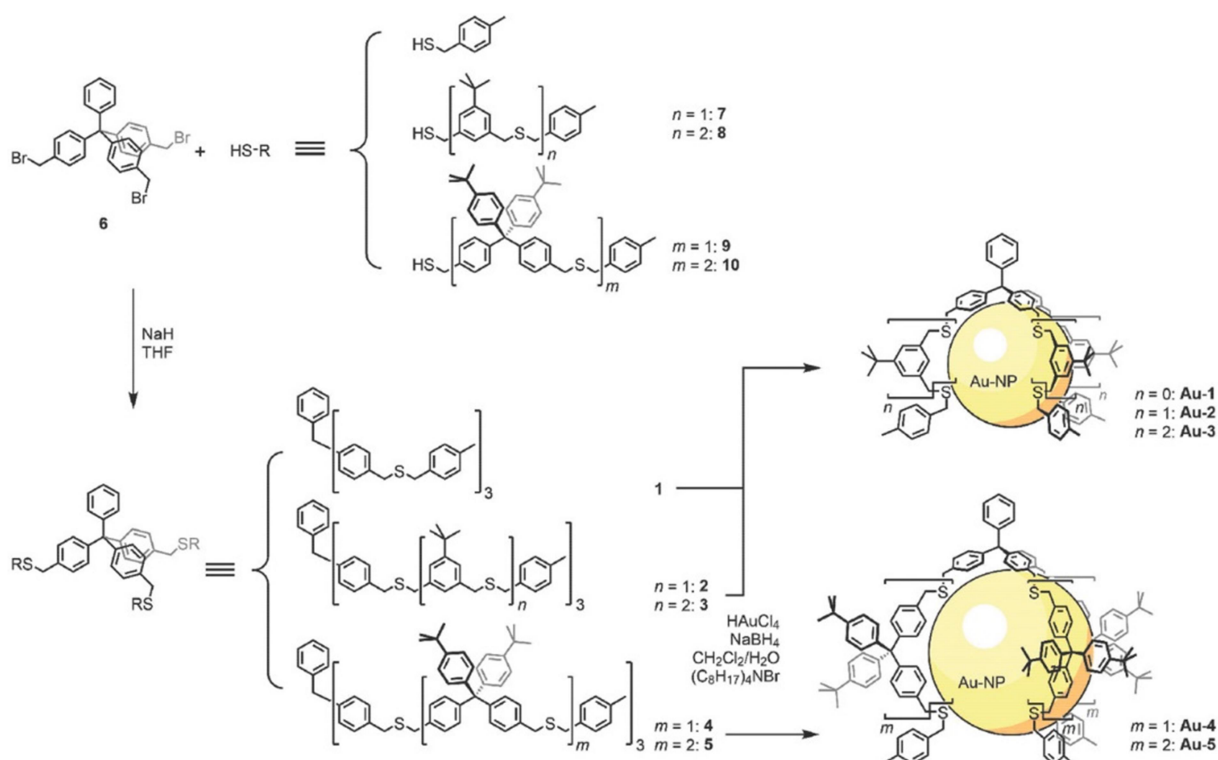


Figure 3 Graphical abstract of „Gold Nanoparticles Stabilized by Single Tripodal Ligands“. The claw of the crane represents the ligand which has a branching point to which three side-chains are attached. Here, the side-chains have three joints representing the sulfur atoms between the individual constituents: two repeating units and one terminus. Reproduced from Ref. 54.



Scheme 1 Molecular concept for the branched ligand: Side-chain thiols **7–10** substitute the bromides of **6**. Resulting ligands **4** and **5** stabilize AuNPs in a 1:1 ligand-to-particle ratio. Ligands **1** and **2** don't yield stable gold nanoparticles. Particles synthesized in presence of **3** are typically stabilized by three to four ligands. Reproduced from Ref. 50.

enhanced thermal and bench stability and enables reliable coating by a single ligand.

The manuscript titled “Gold Nanoparticle Stabilized by Single Tripodal Ligands” published in *Particle & Particle Systems Characterization* in 2018 serves as the cornerstone on which all other articles presented in this thesis—with the exception of the abovementioned review—are based. At this point, it is most important to point out that this work would not have been possible without the preceding work of Dr. Mario Lehmann who established the synthetic route to our favored ligand side-chain and performed the full characterization by ^1H - and ^{13}C -NMR as well as HRMS thereof. The few missing pieces toward the full characterization of the ligands and their precursors were complemented by PD Dr. Daniel Häussigner who recorded ^{13}C -NMR spectra when the material when deeper insight was necessary, Dr. Heinz Nadig and MoBiAS laboratory of ETH Zürich who measured HRMS of the molecules. The gold nanoparticles were characterized by transmission electron microscopy, UV-vis absorption and ^1H -NMR spectroscopy, thermogravimetric analysis performed by Cedric Wobill from the Constable–Housecroft group (University of Basel) and thermal stability experiments. Further, we were interested in exploring the size limits of the nanoparticles by using more gold equivalents for their synthesis. It was found that gold nanoparticles fare best in regard to stability, size-distribution and ligand-to-particle ratio when one gold equivalent for each sulfur per ligand was used.

III. Alkyne-Monofunctionalized Gold Nanoparticles as Massive Molecular Building Blocks (2021, Full Paper, *European Journal of Inorganic Chemistry*)

As a direct continuation of the previous work, here the central linking tetraphenylmethane unit was decorated with a short oligo(phenyleneethynylene) (OPE) with a terminal protected acetylene, giving a ligand which was not only able to enwrap an entire gold nanoparticle but also exhibited a single functional unit. It was demonstrated that—once the acetylene was deprotected—the nanoparticles could be used in the same manner as conventional molecules in wet chemistry. Proof of principle was shown with two reactions: first, acetylene deprotection–homocoupling to give gold nanoparticle dimers and second, copper(I)-catalyzed azide-alkyne 1,3-cycloaddition (CuAAC) “click” reaction with 1,3,5-tris(*p*-(azidomethyl)phenyl)benzene to yield trimer structures, both of which reflected the one-to-one ligand-to-particle ratio measured by thermogravimetric analysis (Cedric Wobill). Much in contrast to previous reports,^[32,37,55] both these superstructures withstood repeated size-exclusion column conditions. Unfortunately, it was only possible to isolate the dimer structures. The fact that only few larger aggregates were found testifies of the ligand’s ideal monofunctionalization properties of the nanoparticles. The obtained nanoparticles, furthermore, showed thermal stability up to 105 °C, pointing at the excellent properties of the ligand. Scheme 2 depicts the functionalized ligand published in this report, showing deprotection–homocoupling as an example of supramolecular assembly.

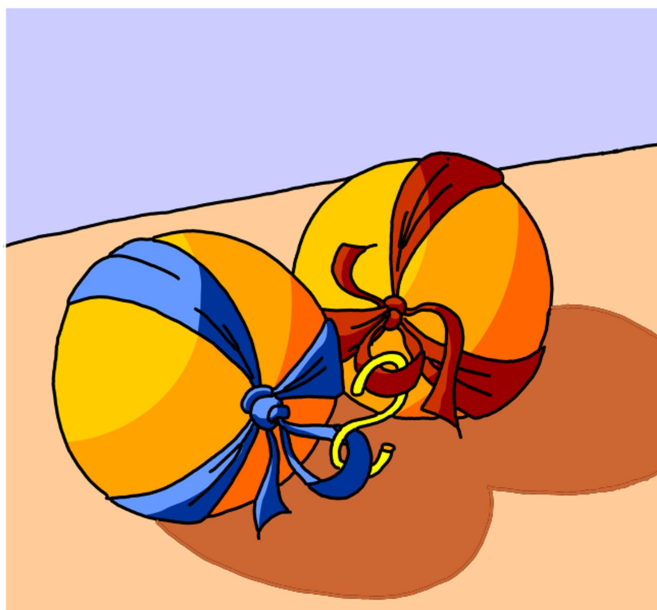
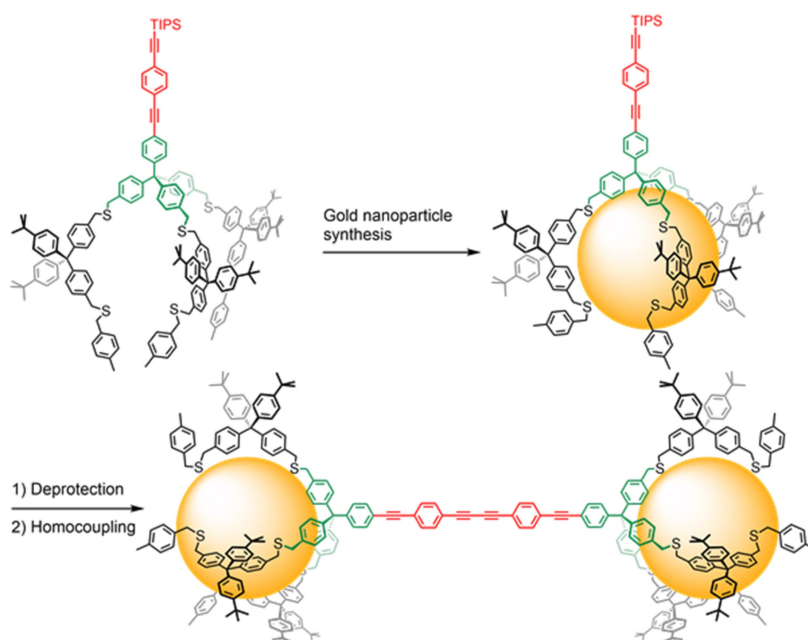


Figure 4 Concept picture for “Alkyne-Monofunctionalized Gold Nanoparticles as Massive Molecular Building Blocks”. The ribbons represent the single ligand per nanoparticle while the hook shows the homocoupled acetylene. Reproduced from Ref. 64.

In this work, the synthesis of the central linking tripod had to be redesigned, for the introduction of an OPE required a Pd-catalyzed coupling reaction and it could, therefore, not be introduced in the last synthetic step, given the presence of the benzylic sulfides. Further, the OPE can—to our best knowledge—not be installed to a tetraphenylmethane in presence of benzylic bromides via *Sonogashira* cross-coupling. For these reasons, the OPE had to be introduced at an earlier stage, namely to tris(*p*-bromophenyl)-*p*-iodophenylmethane at room temperature to prevent reaction with the bromophenyl moieties. The subsequent installation of the three benzylic bromides proved to be a non-trivial task that required careful screening for optimal bromination conditions as bromine has a strong tendency to brominate the acetylene moieties, thus disrupting the rigidity of the OPE and making us lose control over the spatial arrangement in the superstructures.

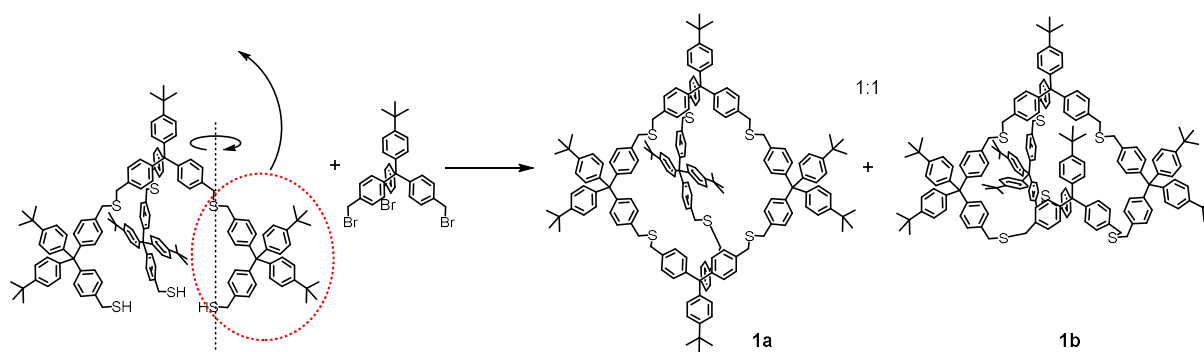


Scheme 2 Functional ligand concept. Green: central linking unit functionalized with a protected acetylene in red, black: bulky side-chains. The ligand monofunctionalizes the particles and forms AuNP dimers upon acetylene deprotection and subsequent oxidative homocoupling.

This paper was published in 2020 in *European Journal of Inorganic Chemistry* titled “Alkyne-Monofunctionalized Gold Nanoparticles as Massive Molecular Building Blocks” with Figure 4 as the concept art.

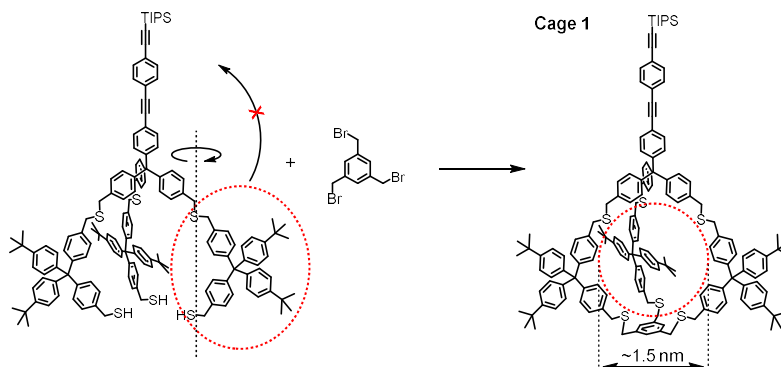
IV. An Organic Cage Controlling the Dimension and Stability of Gold Nanoparticles (2023, Communication, Chemical Communications)

In continuation of this work, our focus was directed towards increasing the particle size and obtaining narrower size-distributions. Inspired by a publication of McCaffrey *et al.*,^[31] we chose to macrocyclize the ends of the three side-chains of our successfully OPE-functionalized ligand reported in the previous manuscript. With this, a cage-type thioether-based ligand was obtained—so far only the second of its kind. We found, with the help of molecular modeling, that the cavity of the envisaged cage would be of the order of 1.5 nm. Yet, the realization of this endeavor was anything but straightforward. First attempts at statistically forming a cage from two tetraphenylmethane



Scheme 3 Cage design by Dr. Mario Lehmann. The precursor side-chain can flip over the branching unit or the bottom branching unit can insert in the wrong way, giving an inseparable mixture of two cage-type structures (1a and 1b).

tribromides with three side-chain dithiols resulted in inseparable mixtures of complex pseudo-cage structures.^[33] A second approach attaching first the side-chain bars to one of the branching points and then closing the cage with a second tetraphenylmethane-based branching unit yielded an inseparable mixture of two compounds: the target cage **1a** in Scheme 3 and the cage with one inverted branching point **1b** in Scheme 3.^[33] In order to overcome these challenges, we decided to



*Scheme 4 Optimized design for **Cage 1**. The bulky OPE in the central linking unit prevents flipping of the side-chain and the planar 1,3,5-tris(bromomethyl)benzene cannot be inserted in the wrong way, giving only one accessible cage conformation.*

attach the cage bars to our OPE-bearing branching unit and to close the cage with a simple 1,3,5-tris(bromomethyl)benzene via threefold S_N2 -type macrocyclization reaction, giving **Cage 1** in Scheme 4. Using this strategy, the flipping of the side-chains presented a sterically impossible hurdle as can be seen in Scheme 4. Using 1,3,5-tris(*p*-(bromomethyl)phenyl)benzene to close the cage was also investigated, giving a ligand which had cage bars that freely, yet slowly rotated in and out of the cage's cavity, thus giving a cage of little use. Despite the unfavorable odds, we tried to grow gold nanoparticles inside this larger cage but only obtained particles of a size which by far exceeded the size of the ligand and, moreover, aggregated after few days. PD Dr. Daniel Häussinger measured variable temperature NMR spectra up to 125 °C. Only at this temperature, a coalescence behavior of the molecule could be observed at NMR timescale. For these reasons, we decided to focus on **Cage 1**. We were able to synthesize **Cage 1** in surprisingly high yields and fully characterize it by ^1H - and ^{13}C -NMR as well as HRMS (MoBiAs laboratory at ETH Zürich). Our first gold nanoparticle synthesis efforts were, alas, unfruitful as the nanoparticles seemed to prefer to nucleate outside the cage and swiftly formed aggregates much larger than the cage's cavity with a very broad size distribution and low thermal stability. Careful scoping for conditions revealed that the gold salt needed to be reduced in solutions as concentrated as possible in order to give reproducible samples of gold nanoparticles of the size expected by the cage's dimensions (1.42 ± 0.46 nm). Thermogravimetric analysis (Patrik Eckert, FHNW) suggested that each ligand covers an average of 53.5 gold atoms which stands in very close agreement with the Au_{55} Schmid cluster (1.4 ± 0.4 nm),^[56,57] indicating the effective monofunctionalization of the particles. Further indication that the particles willingly nucleated inside the cage was given by measuring their thermal stability limit which was, with 130 °C, found to be significantly higher than gold nanoparticles stabilized by non-cage parent structures. It is with great surprise, however, that we observed that these particles need not be subjected to our standard acetylene deprotection–homocoupling protocol in order to dimerize or form larger aggregates, suggesting the nucleating $\text{Au}(0)$ nanoparticles catalyze oxidative acetylene homocoupling as has been reported for $\text{Au}(0)$ species before.^[58–63] Despite our greatest efforts in reproducing gold nanoparticle-catalyzed acetylene homocoupling on model compounds, we were only able to find the particles catalyzed the reduction

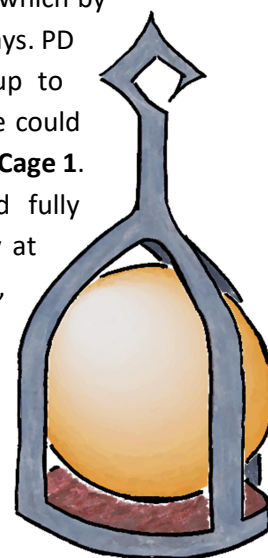


*Figure 5 Tentative concept picture for "An Organic Cage Controlling the Dimension and Stability of Gold Nanoparticles". The bird cage with the hook represents the monofunctionalized **Cage 1**.*

of terminal acetylenes to terminal olefins, only adding more mystery to the apparent homocoupling conundrum than solving it. For this reason, we decided to leave the scoping of catalytic activity and investigations in the control over the acetylene chemistry to future research.

Figure 5 shows a tentative concept picture for the manuscript which was, at the point of defending this work, to be submitted for publication to *Chemical Communications* and has meanwhile (2023) been accepted in the latter.

Summary and Future Prospects

In this thesis, a series of ligands for the passivation of gold nanoparticles is presented. Their architecture is based on the branched interlinking of three benzylic thioether side-chains by a central tetraphenylmethane tripod. This central unit possesses one unfunctionalized phenyl. The resulting gold nanoparticles have unprecedented thermal stability when a bulky tetraphenylmethane side-chain is used and stabilize the gold nanoparticles in a 1:1 ligand-to-gold ratio. For this reason, we regard this system as the preferred candidate for the introduction of a single rigid TIPS-protected acetylene derivative at the central branching unit's free phenyl, allowing further chemical modification as well as electronic addressability. The promising chemical features are demonstrated by acetylene homocoupling dimerization reaction as well as CuAAC "click" reaction to 1,3,5-tris(4-(azidomethyl)phenyl)benzene to give trimers. In a final step, the ligand is macrocyclized to give a monofunctionalized cage-type structure with a cavity of defined size. Surprisingly, we observe this structure to readily undergo dimerization under standard *Brust-Schiffrin* gold nanoparticle synthesis conditions^[8] without the need for a separate deprotection step. The mechanism of this observation is not yet understood and has to be elucidated in the near future. It is expected that the forming Au(0) nanoparticle play the role of the active catalyst during nucleation, as Au(0)-catalyzed acetylene homocoupling has been reported on several occasions.^[58–63] Catalytic screening of the obtained structures reveals that the nanoparticles are catalytically active in acetylene reduction, yet no acetylene homocoupling was so far observed, let alone deprotection of the TIPS moiety. Further tests in gold nanoparticle-catalyzed acetylene chemistry should allow gaining deeper insight.

Once their catalytic scope is understood, the here presented gold nanoparticles should be implemented in labeling applications of, for instance, lysine or insulin or as functional devices for molecular electronics. Further progress in this work is thought to lie in the decoration of the ligands by water-solubilizing groups—e.g. polyethylene glycol chains or sugars—in order to obtain water-soluble nanoparticles stabilized by only one benzylic thioether-based ligand bearing a single functional group. In further efforts, enlarging the cavity of the cage by introduction of suitable larger bottom connectors should be investigated as well.

References

- [1] M.-C. Daniel, D. Astruc, *Chem. Rev.* **2004**, *104*, 293–346.
- [2] N. Culpeper, *Mr. Culpepper's Treatise of Aurum Potabile Being a Description of the Three-Fold World, Viz. Elementary Celestial Intellectual Containing the Knowledge Necessary to the Study of Hermetick Philosophy. Faithfully Written by Him in His Life-Time, and since His Death, Published by His Wife.*, London, **1657**.
- [3] J. Kunckel von Löwenstern, *Utiles observationes sive animadversiones de salibus fixis et volatilibus, auro et argento potabili (etc.)*, Austria, **1678**.
- [4] S. R. N. Gupta, *Int. Res. J. Sci. Eng.* **2018**, *6*, 181–198.
- [5] M. Faraday, *Philos. Trans. R. Soc. Lond.* **1857**, *147*, 145–181.
- [6] G. Mie, *Ann. Phys.* **1908**, *330*, 377–445.
- [7] J. Turkevich, P. C. Stevenson, J. Hillier, *Discuss. Faraday Soc.* **1951**, *11*, 55–75.
- [8] M. Brust, M. Walker, D. Bethell, D. J. Schiffrin, R. Whyman, *J. Chem. Soc. Chem. Commun.* **1994**, 801–802.
- [9] L. Kool, A. Bunschoten, A. H. Velders, V. Saggiomo, *Beilstein J. Nanotechnol.* **2019**, *10*, 442–447.
- [10] G. E. Moore, *Electronics* **1965**, *38*, 114–116.
- [11] G. Schmid, *Chem. Rev.* **1992**, *92*, 1709–1727.

- [12] G. Schmid, U. Simon, *Chem. Commun.* **2005**, 697–710.
- [13] G. Schmid, *Adv. Eng. Mater.* **2001**, *3*, 737–743.
- [14] T. A. Gschneidtner, Y. A. D. Fernandez, K. Moth-Poulsen, *J. Mater. Chem. C* **2013**, *1*, 7127–7133.
- [15] J. Liao, S. Blok, S. J. van der Molen, S. Diefenbach, A. W. Holleitner, C. Schönenberger, A. Vladyka, M. Calame, *Chem. Soc. Rev.* **2015**, *44*, 999–1014.
- [16] R. Wilson, *Chem. Commun.* **2003**, 108–109.
- [17] W. M. Pankau, S. Mönninghoff, G. von Kiedrowski, *Angew. Chem. Int. Ed.* **2006**, *45*, 1889–1891.
- [18] C. Krüger, S. Agarwal, A. Greiner, *J. Am. Chem. Soc.* **2008**, *130*, 2710–2711.
- [19] J. P. Hermes, F. Sander, T. Peterle, R. Urbani, T. Pfohl, D. Thompson, M. Mayor, *Chem. – Eur. J.* **2011**, *17*, 13473–13481.
- [20] J. E. Reardon, P. A. Frey, *Biochemistry (Mosc.)* **1984**, *23*, 3849–3856.
- [21] H. Yang, J. E. Reardon, P. A. Frey, *Biochemistry (Mosc.)* **1984**, *23*, 3857–3862.
- [22] D. Zanchet, C. M. Micheel, W. J. Parak, D. Gerion, A. P. Alivisatos, *Nano Lett.* **2001**, *1*, 32–35.
- [23] J. G. Worden, A. W. Shaffer, Q. Huo, *Chem. Commun.* **2004**, 518–519.
- [24] W. M. Pankau, K. Verbist, G. von Kiedrowski, *Chem Commun* **2001**, 519–520.
- [25] J. R. Reimers, M. J. Ford, S. M. Marcuccio, J. Ulstrup, N. S. Hush, *Nat. Rev. Chem.* **2017**, *1*, s41570-017-0017-017.
- [26] M. S. Inkpen, Z.-F. Liu, H. Li, L. M. Campos, J. B. Neaton, L. Venkataraman, *Nat. Chem.* **2019**, *11*, 351.
- [27] H. Häkkinen, *Nat. Chem.* **2012**, *4*, 443–455.
- [28] T. Peterle, A. Leifert, J. Timper, A. Sologubenko, U. Simon, M. Mayor, *Chem. Commun.* **2008**, 3438–3440.
- [29] M. Lehmann, E. H. Peters, M. Mayor, *Chem. – Eur. J.* **2016**, *22*, 2261–2265.
- [30] A. D'Aléo, R. M. Williams, F. Osswald, P. Edamana, U. Hahn, J. van Heyst, F. D. Tichelaar, F. Vögtle, L. De Cola, *Adv. Funct. Mater.* **2004**, *14*, 1167–1177.
- [31] R. McCaffrey, H. Long, Y. Jin, A. Sanders, W. Park, W. Zhang, *J. Am. Chem. Soc.* **2014**, *136*, 1782–1785.
- [32] J. P. Hermes, F. Sander, U. Fluch, T. Peterle, D. Thompson, R. Urbani, T. Pfohl, M. Mayor, *J. Am. Chem. Soc.* **2012**, *134*, 14674–14677.
- [33] M. Lehmann, Multidentate Thioether-Based Ligands Controlling the Stability and Size of Gold Nanoparticles, Thesis, University of Basel, **2017**.
- [34] Z. Fan, M. K. Serrano, A. Schaper, S. Agarwal, A. Greiner, *Adv. Mater.* **2015**, *27*, 3888–3893.
- [35] G. Yao, H. Pei, J. Li, Y. Zhao, D. Zhu, Y. Zhang, Y. Lin, Q. Huang, C. Fan, *NPG Asia Mater.* **2015**, *7*, e159–e159.
- [36] H. Xing, Y. Bai, Y. Bai, L. H. Tan, J. Tao, B. Pedretti, G. A. Vincil, Y. Lu, S. C. Zimmerman, *J. Am. Chem. Soc.* **2017**, *139*, 3623–3626.
- [37] F. Sander, U. Fluch, J. P. Hermes, M. Mayor, *Small* **2014**, *10*, 349–359.
- [38] K. C.-F. Leung, X.-B. Li, X. Li, S.-F. Lee, J. C. Yu, P. M. Mendes, K. E. Hermann, M. A. V. Hove, *Mater. Chem. Front.* **2019**, *3*, 1555–1564.
- [39] R. Lévy, Z. Wang, L. Duchesne, R. C. Doty, A. I. Cooper, M. Brust, D. G. Fernig, *ChemBioChem* **2006**, *7*, 592–594.
- [40] D. Safer, L. Bolinger, J. S. Leigh, *J. Inorg. Biochem.* **1986**, *26*, 77–91.
- [41] D. Safer, J. F. Hainfeld, J. S. Wall, *Biophys. J.* **1985**, *47*, 128a.
- [42] R. Lévy, *ChemBioChem* **2006**, *7*, 1141–1145.
- [43] A. J. Mastroianni, S. A. Claridge, A. P. Alivisatos, *J. Am. Chem. Soc.* **2009**, *131*, 8455–8459.
- [44] D. Zanchet, C. M. Micheel, W. J. Parak, D. Gerion, S. C. Williams, A. P. Alivisatos, *J. Phys. Chem. B* **2002**, *106*, 11758–11763.
- [45] F. Huo, A. K. R. Lytton-Jean, C. A. Mirkin, *Adv. Mater.* **2006**, *18*, 2304–2306.
- [46] Y.-S. Chen, M.-Y. Hong, G. S. Huang, *Nat. Nanotechnol.* **2012**, *7*, 197–203.
- [47] M. A. Rahman, H.-B. Noh, Yoon-Bo Shim, *Anal. Chem.* **2008**, *80*, 8020–8027.
- [48] Y. Xiao, F. Patolsky, E. Katz, J. F. Hainfeld, I. Willner, *Science* **2003**, *299*, 1877–1881.
- [49] Y. Jun, S. Sheikholeslami, D. R. Hostetter, C. Tajon, C. S. Craik, A. P. Alivisatos, *Proc. Natl. Acad. Sci.* **2009**, *106*, 17735–17740.
- [50] S. Bidault, F. J. García de Abajo, A. Polman, *J. Am. Chem. Soc.* **2008**, *130*, 2750–2751.
- [51] J. Elbaz, A. Ceconello, Z. Fan, A. O. Govorov, I. Willner, *Nat. Commun.* **2013**, *4*, 2000.
- [52] M. Lehmann, E. H. Peters, M. Mayor, *Helv. Chim. Acta* **2017**, *100*, e1600395.
- [53] M. Valášek, M. Mayor, *Chem. Eur. J.* **2017**, *23*, 13538–13548.
- [54] E. H. Peters, M. Lehmann, M. Mayor, *Part. Part. Syst. Charact.* **2018**, *35*, 1800015.
- [55] J. P. Hermes, F. Sander, T. Peterle, M. Mayor, *Chim. Aarau* **2011**, *65*, 219–220.
- [56] G. Schmid, R. Pfeil, R. Boese, F. Bandermann, S. Meyer, G. H. M. Calis, J. W. A. van der Velden, *Chem. Ber.* **1981**, *114*, 3634–3642.
- [57] D. H. Rapoport, W. Vogel, H. Cölfen, R. Schlögl, *J. Phys. Chem. B* **1997**, *101*, 4175–4183.
- [58] G. Li, R. Jin, *Nanotechnol. Rev.* **2013**, *2*, 529–545.
- [59] Y.-Q. Zhang, N. Kepčija, M. Kleinschrodt, K. Diller, S. Fischer, A. C. Papageorgiou, F. Allegretti, J. Björk, S. Klyatskaya, F. Klappenberger, et al., *Nat. Commun.* **2012**, *3*, 1–8.
- [60] M. Boronat, D. Combata, P. Concepción, A. Corma, H. García, R. Juárez, S. Laursen, J. de Dios López-Castro, *J. Phys. Chem. C* **2012**, *116*, 24855–24867.
- [61] M. Boronat, S. Laursen, A. Leyva-Pérez, J. Oliver-Meseguer, D. Combata, A. Corma, *J. Catal.* **2014**, *315*, 6–14.
- [62] G. Kyriakou, S. K. Beaumont, S. M. Humphrey, C. Antonetti, R. M. Lambert, *ChemCatChem* **2010**, *2*, 1444–1449.
- [63] V. K. Kanuru, G. Kyriakou, S. K. Beaumont, A. C. Papageorgiou, D. J. Watson, R. M. Lambert, *J. Am. Chem. Soc.* **2010**, *132*, 8081–8086.
- [64] E. H. Peters and M. Mayor, *Eur. J. Inorg. Chem.* **2020**, *24*, 2325–2334

Monofunctionalized Gold Nanoparticles: Fabrication and Applications

E. Henrik Peters^a and Marcel Mayor^{*abc}

Abstract: An overview of various approaches to synthesize gold nanoparticles (AuNPs) bearing one single chemically addressable unit and their diverse fields of application is presented. This *comprehensive review* not only describes the strategies pursued to obtain monofunctionalized AuNPs, but also reports their behavior as ‘massive’ molecules in wet chemical protocols and the scope of their applications. The latter reaches from site-specific labels in biomolecules over mechanical barriers in superstructures to building blocks in hybrid nano-architectures. The complementing physical properties of AuNPs combined with precise chemical control of their attachment makes these objects promising building blocks for numerous proof-of-concept experiments and applications.

Keywords: Gold Nanoparticle · Labeling · Monofunctional · Plasmonics · Superstructure



Erich Henrik Peters (right) obtained his MSc in Nanoscience (2015) as well as his PhD in chemistry (2020) at the University of Basel under the supervision of Professor Marcel Mayor on the subject of monofunctionalized gold nanoparticles stabilized by branched thioether-based ligands. He is currently working in the group of Professor Robert Häner at the University of Bern on the supramolecular self-assembly of DNA-inspired oligomers in aqueous media.

Marcel Mayor (left) received his PhD in 1995 supervised by Professor Rolf Scheffold and Professor Lorenz Walder at the University of Bern. After working with Professor Jean-Marie Lehn at the University Louis Pasteur in Strasbourg and at the Collège de France in Paris, he founded his own research group at the Karlsruhe Institute of Technology in 1998. On defending his habilitation in 2002, he became Professor of Chemistry at the University of Basel in 2004. His current research interests are supramolecular chemistry, molecular electronics, nanoscale architectures, functional materials and hybrid materials.

1. Introduction

Due to the reactivity of their surface, nucleating Au(0) clusters need to be passivated by ligands in order to prevent aggregation. With the recognition of the potential of gold nanoparticles (AuNPs) as functional subunits in nanoscale architectures and molecular devices, the focus of research moved from the bare investigation of their physical properties to their integration in larg-

er systems. Consequently, their ligand shell was no longer solely stabilizing the AuNP, but became also of interest as the interface with the chemical environment. Consequently, the decoration of the AuNPs' surface with functional groups enabling their integration as massive ‘artificial molecules’ by wet chemical protocols moved into the focus of interest. Owing to their non-classical optical^[1,2] and physical^[3] properties, in the past decades, considerable research efforts were geared towards functional ligand shells for the implementation of AuNPs in sensing,^[4,5] catalysis,^[6–8] plasmonics,^[9–12] labeling,^[13–17] molecular electronics,^[18–20] and biomedical applications.^[16,21,22] For many of these applications, control over the number and spatial arrangement of addressable moieties, *i.e.* functional groups, exposed on the ligand shell of the AuNPs is of primary interest since it allows the integration of AuNPs with molecular precision.

In this *comprehensive review*, we provide an overview of various strategies to synthesize monofunctionalized AuNPs as well as the reported proof-of-concept experiments and applications. We differentiate between two strategic approaches to obtain monofunctionalized AuNPs, which are sketched in Fig. 1. In the first part, strategies towards AuNPs stabilized by a single macromolecular ligand exposing a single functional moiety (Type I) are presented. In the second part, the approach consists of AuNPs stabilized by multiple ligands – typically dozens or even hundreds – whereof only one possesses the functionality of interest (Type II). To keep the dimension of this review reasonable, exclusively AuNPs possessing a single functional unit in their ligand shell are considered. Also, we will only occasionally mention AuNPs functionalized with antibodies, as this topic has been extensively reviewed elsewhere.^[5,23,24]

2. Single-ligand-coated Gold Nanoparticles (Type I)

The most straightforward way to synthesize monofunctionalized AuNPs is to design ligands that are large enough to stabilize an entire particle by steric crowding,^[25–29] yet the introduction of a single functional unit per ligand demands sophisticated synthetic strategies.

*Correspondence: Prof. Dr. M. Mayor, E-mail: marcel.mayor@unibas.ch

^aDepartement of Chemistry, University of Basel, St. Johannis-Ring 19, CH-4056 Basel, Switzerland;

^bInstitute for Nanotechnology (INT); Karlsruhe Institute of Technology (KIT); P. O. Box 3640, 76021 Karlsruhe, Germany;

^cLehn Institute of Functional Materials (LIFM), Sun Yat-Sen University (SYSU), Xingang Xi Rd. 135, 510275 Guangzhou, P. R. China

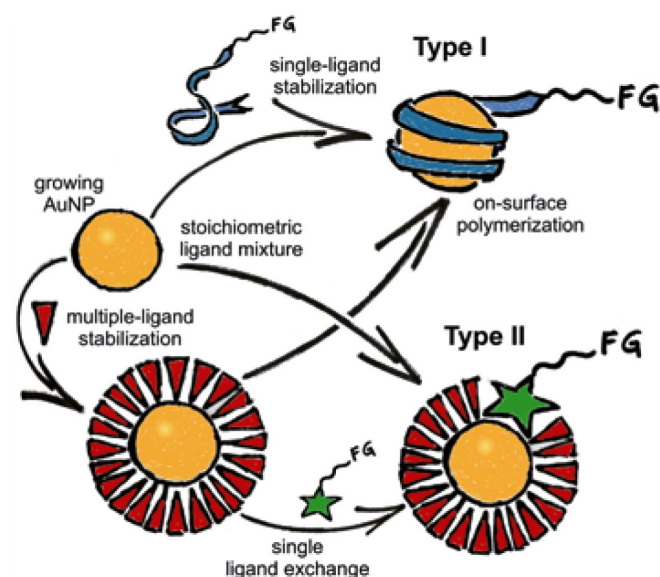


Fig. 1. Illustration of the two strategies geared towards monofunctionalized AuNPs considered in this review. FG = functional group.

2.1 Oligomers and Polymers

2.1.1 Pre-polymerized Ligands

The first report of AuNPs that were monofunctionalized via a single polymer ligand comprising only one functional unit was published by Wilson.^[30] He reported the use of a dextran-based ligand that was decorated with 15 thiol anchors for the stabilization of AuNPs as well as a single 2,4-dinitrophenyl hapten as a recognition site for antibodies. The latter was attached to the ligand by a short hydrophobic linker in order to pierce its aqueous solvation shell. The 12 nm AuNPs were prepared by citrate reduction of HAuCl_4 . Subsequently, the citrate shell was conjugated with various amounts of monofunctionalized dextran polymers. Stability tests against phosphate-buffered saline (PBS)-induced flocculation of the AuNPs revealed that a minimum of four ligands was needed to give AuNPs with satisfactory stability, yielding AuNPs with a minimum of four functional units per particle. Increasing the number of sulfur anchors on the ligand by an order of magnitude gave sufficiently stable AuNPs that were passivated by a single ligand.^[31] In this further developed system, the single hapten was replaced by 15 biotins for the detection of streptavidin. Later reports included studies on the functionalization degree dependence for bovine serum albumin detection in lateral flow immunoassays,^[32] single-stranded deoxyribonucleic acid (ssDNA) detection^[33] and DNA labeling.^[34]

A variation of this approach was proposed by Yao *et al.*^[35] in which phosphine-stabilized AuNPs were subjected to ligand-exchange with a poly-adenine chain long enough to enwrap an entire AuNP, and functionalized with a polynucleotide chain. The latter acted as a recognition motif for the detection of complementary DNA strands or as an anchor for the formation of more complex AuNP superstructures upon DNA hybridization since the number of DNA strands per NP was precisely tuned by the NP size.

An elegant approach to monofunctionalized AuNPs based on tailor-made block co-polymers was reported recently. As sketched in Fig. 2, a linear block co-polymer comprising a block exposing numerous olefins and a terminal azide was obtained by ring-opening metathesis polymerization (ROMP, Fig. 2a). Upon cross-linking with Grubb's catalyst, the olefin-rich block-copolymer formed a cage-like organic NP (ONP) scaffold (Fig. 2b). By oxidizing the olefins of the block co-polymer, a hydroxyl-rich water-soluble ONP was obtained, which still

exposed an azide group (Fig. 2c). The latter was engaged in a 'click' protocol to attach a single DNA strand (Fig. 2d). This structure was used to graft AuCl_4^- to the hydroxyl groups of the organic NP (Fig. 2e). Reduction by addition of ascorbic acid led to AuNP nucleation inside the organic scaffold (Fig. 2f). The preserved function of the single DNA strand was demonstrated by titration with the complementary DNA strand comprising a fluorescence quencher. The monofunctionalization was corroborated by dimer formation with an AuNP functionalized with a complementary DNA strand (Figs. 2g–h).^[36] In continuation of this work, the influence of the polymer size, degree of polymer crosslinking, and monomer-to-polymerization initiator ratio on the organic nanoparticle size were investigated in order to tune the size of the formed metal NPs.^[37] Monofunctionalized metal NPs of diameters up to 40 nm were obtained by this strategy.

2.1.2 On-Surface Polymerization

A different approach to the monofunctionalization of AuNPs by polymers was proposed by the research group of Andreas Greiner.^[38] In contrast to the previously discussed approach, the polymerization of thiol-derivatives of styrene-based ligand monomers was performed after AuNP synthesis, *i.e.* on the particle surface. The functional group was introduced by a suitable radical starter initiating the polymer formation. First, AuNPs were synthesized according to the *Brust-Schiffrin* two-phase synthesis in presence of 4-mercaptostyrene as a small passivating ligand.^[39] Subsequently, 4,4'-azobis(4-cyanopentanoic acid) was used as a radical initiator to induce the free-radical polymerization of the ligands' vinyl moieties, giving AuNPs stabilized by a single poly(4-mercaptostyrene) polymer cage. The formed ligand shell had a single carboxyl – the residue of the radical starter – accessible for further chemistry at the terminus of the formed polymer shell (Fig. 3). Monofunctionalization was demonstrated by amide condensation reaction with 1,7-diaminoheptane or with polyallylamine which resulted in either AuNP dimers, or linear AuNP chains respectively.^[38] Based on these results, the scope of this monofunctionalization method was enhanced by decorating the radical initiator with a methylcoumarine dye.^[40] Free-radical polymerization of the ligand shell gave AuNPs functionalized with a single remote methylcoumarin, making these 'artificial molecules' appealing candidates for labeling applications. In a further study, the particle-coating surface polymer was engaged in a second polymerization reaction. Therefore, the single exposed carboxylic acid was forming an amide bond with 4-aminostyrene which was engaged in the polymerization of methyl methacrylate to give acrylate/AuNP–styrene copolymers.^[41] Interestingly, these poly(methyl methacrylate)-grafted polymer ligand shells were acting as 'fishing rods' for size-selective capture of various metal nanoparticles once the ligand shells were liberated from the encapsulated AuNPs templates by NaCN etching (Fig. 3).^[42,43]

2.2 Dendrons, Dendrimers and Branched Oligomers

Dendrimers as ligands for AuNPs have found significant interest in drug delivery and sensing,^[44] catalysis,^[45,46] and biomedical applications.^[47] The sheer number of end groups in dendrimers, however, poses a major challenge in the monofunctionalization of AuNPs since reliable methods for the modification of a single dendrimer subunit have, to the best of our knowledge, not been reported yet. In first-generation dendrimers with a low number of branches, a single functional group can be statistically introduced. This has been demonstrated by labeling of ssDNA with Au_{55} clusters that were stabilized by a monofunctionalized benzylic thioether-based dendrimer.^[48] Inspired by these studies from Kiedrowski *et al.*, we investigated the potential of benzylic thioether-based oligomers and dendrimers for the stabilization of AuNPs. Already first experiments resulted in AuNPs with nar-

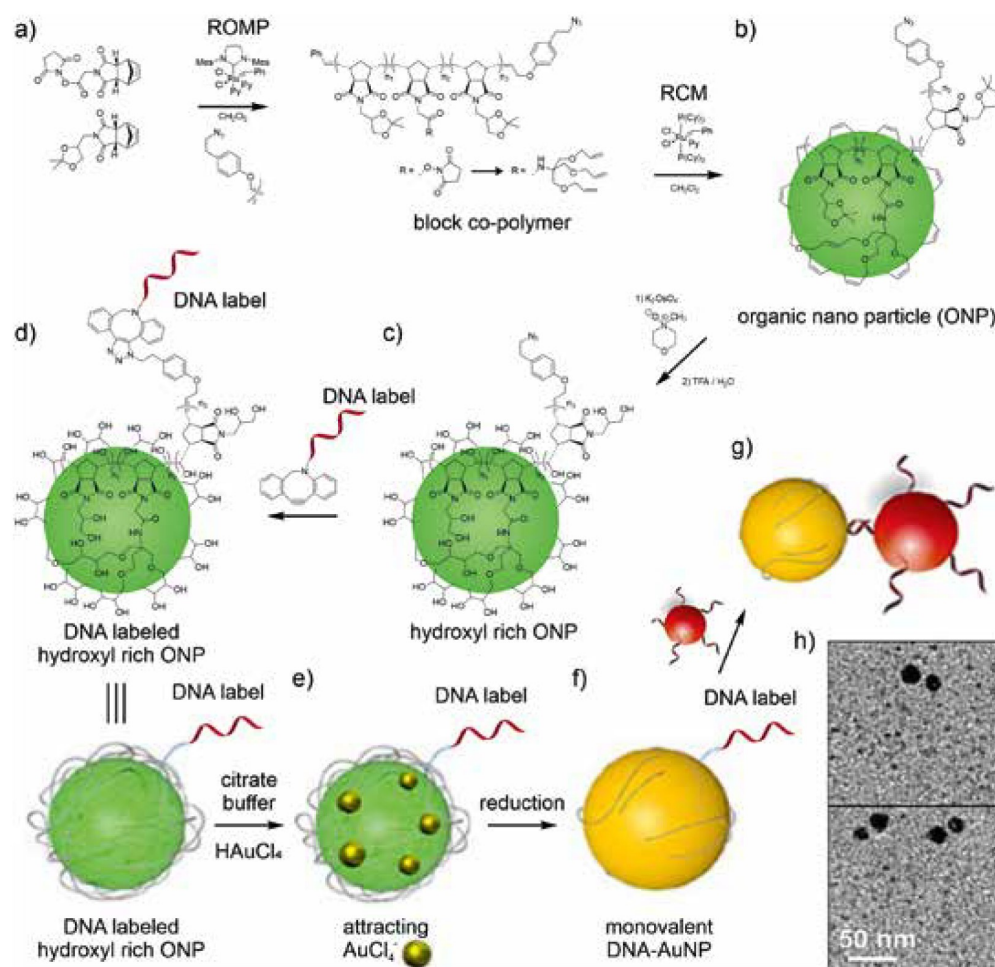


Fig. 2. a) Synthesis of the linear block co-polymer comprising a terminal azide and exposing alkene side-chains. b) Formation of the organic nanoparticle (ONP) by crosslinking the side-chain alkenes via ring closing olefin metathesis (RCM). c) Oxidizing the olefins to 1,2-diols results in a water-soluble hydroxyl-rich ONP exposing a single azide. d) Conjugating the ssDNA to the exposed azide of the ONP. e) Collecting AuCl₄⁻ in the ONP. f) Reduction of the Au salt, yielding the monofunctionalized AuNP. g) Hybridization to parent DNA-functionalized AuNP to form dimers. h) TEM pictures of the dimers. All images adapted with permission from ref. [36]. Copyright (2017) American Chemical Society.

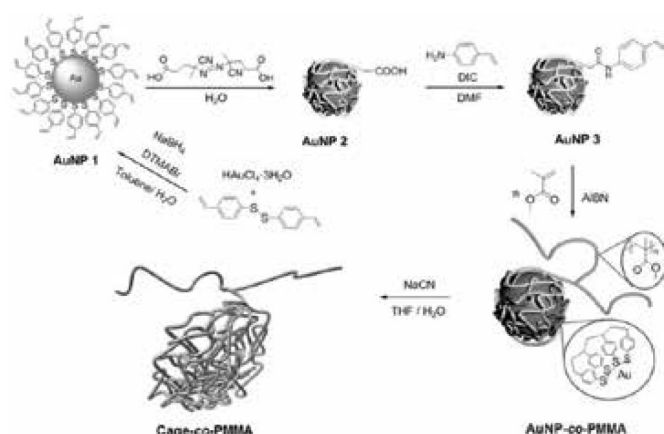


Fig. 3. On-surface polymerization of mercaptostyrene to give mono-carboxy AuNP 2. Subsequent amide condensation with aminostyrene and co-polymerization to methyl methacrylate yields acrylate/AuNP-styrene co-polymers. Etching with NaCN demetalates the polymer cage chains that can be used for size-selective 'fishing' of metal NPs. Reproduced from ref. [43] according to the CC BY-NC-ND 4.0 license. Copyright (2015) John Wiley and Sons.

row dispersity suggesting a discrete number of ligands coating the particle.^[27] Decorating the ligands with a single functional group enabled to corroborate the presence of a pair of ligands for *meta*-benzyl thioether based linear oligomers.^[49,50] The AuNP surface covered by the macromolecule was increased by introduc-

ing branching units and, indeed, the second-generation dendrimer was not only catching AuNPs of 1.2 nm diameter during their growth, but also stabilizing the entire particle.^[51] Introduction of an exposed alkyne group at the central dendrimer subunit provided dumbbell-type AuNP dimers upon oxidative acetylene coupling^[52] and trimeric or tetrameric AuNP architectures upon exposure to copper(I)-catalyzed alkyne-azide cycloaddition (CuAAC) 'click' reaction conditions with central linking units comprising three or four benzylic azides respectively,^[53] all corroborating the 1:1 dendrimer:AuNP ratio. Enlarging the steric demand of the coating benzyl thioether ligand by tetraphenylmethane subunits even provided linear^[28] and threefold branched^[29] oligomers able to coat entire AuNPs. The central tetraphenyl subunit of the latter was ideally suited to expose a single alkyne group enabling again the formation of AuNP dimers or trimers by wet chemical protocols based on oxidative acetylene homocoupling or CuAAC respectively (Fig. 4).^[54]

Dendrimers and dendrons were used as host structures for AuNPs mainly as an instrument to profit from the particles' catalytic activity. Parent thioester-based second-generation dendron structures were attached to SiO₂ beads as support for AuNPs which were used as a reusable catalyst for the oxidation of alcohols.^[55] Dendronized polymers^[56] were used for the AuNP-catalyzed reduction of 4-nitrophenol to 4-aminophenol in both aqueous^[57] and organic^[58] media. An alternate dendron motif based on CuAAC-'clicked' triazols^[59] was proposed.^[60] Upon functionalizing the focal point of the dendron with a disulfide as anchor, it was shown that the resulting AuNPs were indeed stabilized by a single ligand. The parent ligands, functionalized with free acetylene or

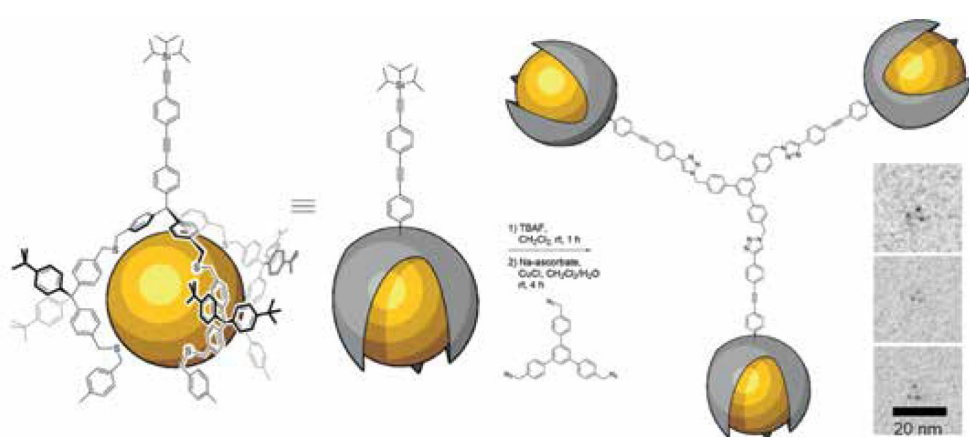


Fig. 4. a) Threefold branched ligand structure coating the AuNP. b) Sketch of its engagement like a huge molecule in a CuAAC 'click' reaction after deprotection of the masked alkyne group. c) TEM micrographs of the obtained AuNP trimers. Reproduced from ref. [54] according to the CC BY 4.0 license. Copyright (2020) John Wiley and Sons.

N-hydroxysuccinimide yielded AuNPs stabilized with two dendrons each under otherwise identical reaction conditions, pointing at the importance of the anchoring group for the controlled nucleation of AuNPs to yield a 1:1 ligand-to-particle ratio.

Grafting poly(amido)amine (PAMAM) dendrimers *via* amide condensation to solid polymer supports^[61] has been reported as a means for the facile monofunctionalization of dendrimers: first, the dendrimers were grafted to cellulose nanocrystals, subsequently, the AuNPs were synthesized in presence of these superstructures *via* sodium borohydride-mediated reduction of chloroauric acid, giving organic superstructures covered by AuNPs.^[62] These AuNP superclusters were used as catalysts in the reduction of 4-nitrophenol to 4-aminophenol and were recyclable multiple times. A similar approach was used to monitor laccase activity in an electronic monitoring sensor for electron-transfer events upon oxidation of catechin.^[63]

3. Multiple-ligand-coated Gold Nanoparticles (Type II)

As an alternative to large molecules, AuNPs can be stabilized by dozens or even hundreds of small ligands such as citrate,^[64] 4-(dimethylamino)pyridine,^[65] tetra-*n*-octylammonium bromide (TOAB),^[66] cetyltrimethylammonium bromide (CTAB),^[67] triphenylphosphine^[68,69] or alkyl thiols.^[69] In order to obtain monofunctionalized AuNPs from such multiple-ligand-coated AuNPs, two approaches have found widespread application: (1) the synthesis of AuNPs in a stoichiometric ligand mixture containing a carefully chosen ratio of functional and non-functional ligands or (2) exploiting the ligand place-exchange reaction that occurs in presence of a ligand of similar or better affinity to gold than the ligand coating the NP^[70,71] in order to introduce a single functional ligand per NP *via* statistical ligand-exchange events. In this section, methods documenting one of the two approaches are presented.

3.1 Stoichiometric Ligand Mixtures

3.1.1 Au₁₁ Clusters

The first report of trace evidence of a gold cluster with mixed ligands whereof only one exposed a single chemically addressable functional group was published as early as 1980,^[72] but it is not before 1984 that parent clusters were isolated.^[73,74] In an elaborate protocol based on stoichiometric functionalization, one single amine of tricyanoheptakis [4,4',4''-phosphinidynetris(benzenemethanamine)]undecagold ($[(P(PhCH_2NH_2)_3)_7]X_3Au_{11}$, where X = halogen) was functionalized with succinimide or phthalimide respectively.^[73] Alternatively, $[(P(PhCH_2NH_2)_3)_7]X_3Au_{11}$ was modified with a stoichiometric mixture of phthalic anhydride and acetic anhydride to give a mono-(*N*-phthalyl) undecagold cluster which was further functionalized for tailored needs.^[74] These rather laborious methods were optimized by Safer *et al.*^[75,76] who, to synthesize monofunctionalized Au₁₁ clusters, used a stoichiometric

mixture of two triphenylphosphine-based ligands, one bearing a single free amine while the other was not functionalized. The monofunctionalized clusters were readily separated in excellent yields from their un- and overfunctionalized parent structures by liquid chromatography. After adequate manipulation of the single free amine per cluster, they were used as site-specific labeling agents for actin, myosin and propomyosin. Alternatively, monofunctionalized Au₁₁ clusters were obtained by stoichiometric ligand place-exchange with suitably functionalized phosphine ligands^[72] and subsequent chromatography.^[77] These facilitated synthetic approaches allowed reliable labeling of a multitude of biomolecules for TEM detection such as proteins,^[13,78] antibodies^[79] and RNA,^[80–82] whereby, in the latter case, it was shown that the undecagold label did not interfere with the translation process in the ribosome due to its minuscule size^[83,84] – in contrast to its Au₅₅ counterpart.^[85] Recently, *N*-heterocyclic carbene-monofunctionalized undecagold was reported to have unprecedented thermal stability and catalytic activity in the electroreduction of CO₂.^[86]

3.1.2 Au₅₅ Clusters

The stoichiometric ligand mixture approach was expanded to the monofunctionalization of Au₅₅ Schmid clusters^[69] and was commercialized in 1990 together with the Au₁₁ parent clusters under the name 'Nanoprobes'.^[17,87,88] These commercial gold clusters were used for the synthesis of precisely organized Au₅₅ dimers and trimers by substitution to ssDNA which could hybridize to complementary Au₅₅-labeled strands in pre-defined orientations.^[89] Owing to their minute size, they were further used for the labeling of sterically challenging sites on antigens.^[85] Their ease of handling was further exploited in the fabrication of organic/inorganic Au₅₅-conjugated double-stranded DNA (dsDNA) and RNA structures.^[90] In the same study it was demonstrated that streptavidin covalently labeled with the Au₅₅-DNA conjugates was still performing its natural immunoglobulin G (IgG) recognition function.

Au₅₅-labeled DNA was further used to study the DNA de- and re-hybridization as a function of magnetic field-induced temperature increase: a 38-nucleotide DNA hairpin with self-complementary ends over 7 bases was labeled with a Au₅₅ cluster (Fig. 5a).^[91,92] The de- and re-hybridization of the 7-base sequence upon radiation with a radio-frequency magnetic field was monitored by measuring the optical absorbance at 260 nm which reflects the hybridization state of the loop (Fig. 5b). The temperature calibration of the experiment was obtained by profiting from an immobilized DNA strand which was conjugated with a complementary DNA strand decorated with a Au₅₅ cluster and a fluorophore at opposed ends (Fig. 5c). De-hybridization was triggered by either heat or the radio-frequency magnetic field with the extent of de-hybridization monitored by the fluorophore concentration in the

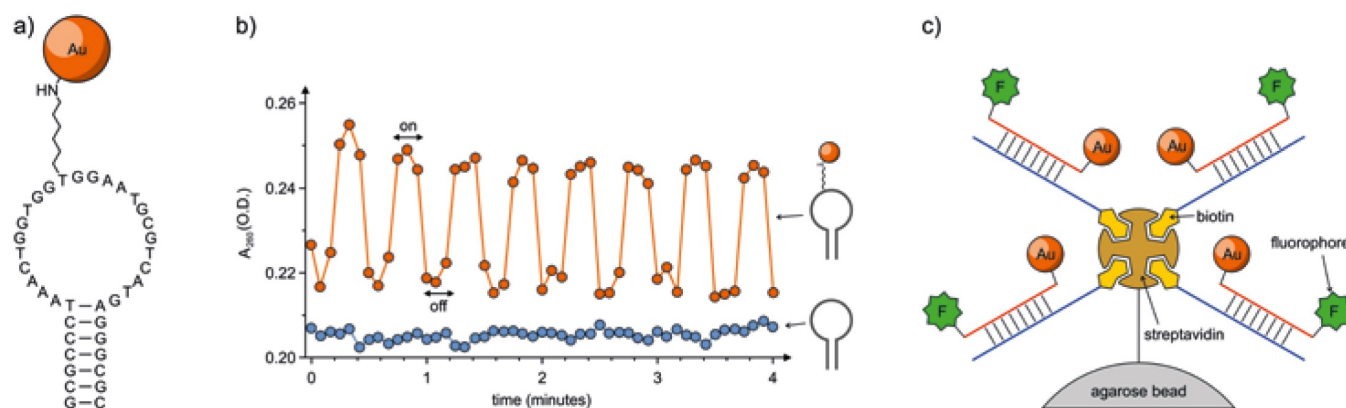


Fig. 5. a) DNA hairpin loop labeled with Au₅₅. b) Change in absorbance at 260 nm upon switching of the radio-frequency magnetic field, reflecting the de- and re-hybridization of the DNA duplex. c) Set-up of paired DNA strands used for temperature calibration in the experiment. Sketched from ref. [91] and ref [92].

supernatant. Equal fluorophore concentrations in the supernatant point at comparable effective temperatures experienced by the paired DNA strands in the set-up.

Willner and co-workers covalently attached Au₅₅ to a DNA intercalator and profited from a dsDNA as a template to obtain wire-like arrays of AuNPs.^[93] In the same article, the exposed amino groups of polylysine were functionalized with mono-*N*-hydroxysuccinimido-Au₅₅ from ‘Nanoprobes’ as alternative approach to AuNP wires.^[93] The same group profited from Au₅₅ as functional unit in a biology-inspired electrochemical experiment monitoring the apo-glucose oxidase activity in real-time.^[94] By wet chemical control, a single Au₅₅ was coupled to flavin adenine dinucleotide (FAD). The AuNPs were further place-exchanged to a gold wire electrode *via* thiolated bridge molecules. Upon oxidizing glucose, an electron was transferred from FAD to the attached AuNP, giving a detectable signal on the electrode. The natural enzyme relying on electron transfer from FAD to oxygen was outperformed by a factor of seven.^[94]

Pons *et al.* investigated the fluorescence quenching of CdSe–ZnS quantum dots (QDs) by AuNPs by controlling the spacing between both particles with a beta-sheet-forming repeating sequence.^[95] By variation of the length of the beta-sheet rod, the distance-dependence of the quenching was studied and, indeed, quenching occurred even beyond separation distances of 200 Å, suggesting nonradiative energy dissipation and dipole-to-metal nanoparticle energy transfer to be a better model for quantum dot photoluminescence quenching than Förster resonance energy transfer.

3.1.3 Ligand-exchange with Stoichiometric Ligand Mixtures

In order to stabilize larger gold colloids with stoichiometric ligand mixtures, Brust’s group proposed to exchange the entire ligand shell of 13 nm and 40 nm citrate-stabilized AuNPs with a carefully tuned mixture comprising an unfunctionalized, cysteine-containing pentapeptide and its DNA-functionalized parent peptide, allowing the controlled supramolecular assembly of AuNP nanoarchitectures *via* DNA hybridization.^[96] The scope of the method was enlarged by replacing the DNA-conjugated functional peptide by a biotin-labeled pentadecapeptide containing a His₆-tag which can chelate to transition metals.^[97] In the latter case, isolation of the monofunctionalized AuNPs was achieved by metal ion affinity chromatography. In order to prove the versatility of the approach, different functional peptide chains were used, enabling the AuNPs to bind to proteins.^[98] The approach was

later generalized by using an alkyl-poly(ethyleneglycol) ligand as the non-functionalized ligand.^[99] Peptide-monomer-functionalized AuNPs were used to label various proteins,^[99–102] target lipid rafts of cell membranes,^[103] and to study the effect of NP surface functionalization density on the supramolecular assembly behavior of bis(sulfosuccinimideyl)suberate (BS3) with peptide chains on the AuNP surface.^[104] Interestingly, the experimental data suggest that thus-synthesized AuNP labels do not interfere with the function of their target protein.^[100]

Using a comparable statistical ligand-exchange protocol, Jun *et al.* reported a study monitoring the cleavage of peptide-linked AuNP superstructures by caspase-3: AuNPs monofunctionalized with a biotinylated peptide bearing the caspase-3 cleavage site were attached to NeutrAvidin-coated AuNPs attached to a solid support. Monitoring the plasmon resonance wavelength as well as the scattering intensity allowed the recording of single caspase-3 cleaving events by a blue-shift of the plasmon band and a drop in intensity for each cleaving (Fig. 6).^[105] In the same report, this method was implemented into *in vivo* systems in order to monitor caspase-3 activity in apoptosis processes.

Similar studies used mixtures of unfunctionalized hydrophobic ligands and linear oligo(phenylene-ethynylene)(OPE) dithiols to create AuNP dimers or star-shaped OPE trithiols to create AuNP trimers respectively.^[106] While the existence of both AuNP dimers and trimers was corroborated by transmission electron microscopy (TEM), the AuNP superstructures were not isolated. Mechanically interlinked structures with an AuNP as intrinsic subunit of the catenated macrocycle were also reported.^[107] Both phenantroline ligands of a copper complex were terminally decorated with short ethyleneglycol chains exposing a terminal thiol, allowing to close the macrocycle by immobilizing both ends of each ligand to an AuNP. The concentration ratios between copper complex and AuNP were optimized for catenated dimer formation.

3.2 Single Ligand-exchange Events

For AuNPs stabilized by multiple ligands beyond the 1.4 nm-Au₅₅ cluster, often more elaborate procedures have to be used in order to obtain reliable monofunctionalization. Single ligand place-exchange events were reported in liquid phase as well as on solid support. In the first case, between various assembly and purification strategies has to be differentiated, namely exploiting the negative charge of *e.g.* (but not limited to) DNA in gel electrophoresis, using single polymerase chain reaction (PCR) cycles, place-exchange at the liquid-liquid interface of biphasic mixtures,

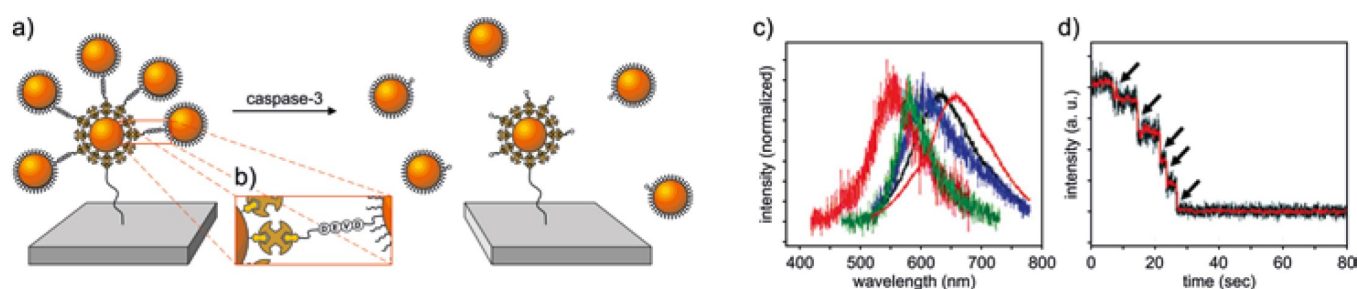


Fig. 6. a) Monofunctionalized AuNPs attached to stationary AuNP via a peptide chain bearing the caspase recognition motif (DEVD) and caspase-mediated degrading of the superstructure. b) Sketch of the avidin-biotin immobilization chemistry and the caspase-sensitive DEVD peptide sequence (Asp-Glu-Val-Asp). c) Gradual plasmon band blue-shift and decreasing of signal-to-noise ratio with increasing number of cleaving events. The solid red line is the absorption of the intact structure, the increasing fuzziness of the curves reflects the decrease of signal-to-noise ratio when AuNPs are cleaved off the central AuNP. d) Scattering intensity as a function of time, showing a distinct decrease for each cleaving event. Reproduced from ref. [105].

or separation by centrifugation. Solid-support place-exchange reactions require pre-functionalized stationary chromatography phases that will be discussed in the second part of this chapter.

3.2.1 Liquid-phase Place-exchange

3.2.1.1 DNA-monofunctionalized Gold Nanoparticles by Electrophoresis

In order to circumvent the challenges faced by embedding a single functional group into the ligand shell, Alivisatos and co-workers exploited the negative charge of DNA and its influence on separation behavior: they place-exchanged phosphine-,^[108–110] tannic acid-,^[111] or citrate-stabilized^[110,111] AuNPs with stoichiometric amounts of thiolated ssDNA and separated the obtained products by number of attached DNA strands via electrophoresis,^[108,110,111] or anion-exchange HPLC.^[109] The ability for reliable control over the degree of functionalization allowed, via DNA strand hybridization, the fabrication of precisely organized AuNP dimers and trimers,^[108,112,113] structurally switchable di-,^[114] tri- and tetramers,^[115] extendable hairpin DNA-AuNP tetramers,^[116] chains,^[117] chiral and achiral AuNP tetrahedrons,^[118] AuNP transport machineries^[119] as well as highly organized 2-dimensional AuNP arrays,^[120,121] or DNA origami slabs^[122] on surfaces (Fig. 7).

This method further allowed to probe the NP-NP distance-dependence of the surface plasmon resonance of AuNP dimers.^[123,124] Both studies found that a significant redshift can be observed if the AuNPs are moved closer together. Temperature-dependent UV-vis monitoring of the plasmon absorption signal in dsDNA-linked AuNP dimers showed a drastic redshift of the plasmon band upon heating.^[125] Further, the size-dependence of the individual AuNPs in dsDNA-linked heterodimer structures was investigated.^[124] Förster resonance energy transfer amplification for fluorescent donor-acceptor pairs located at the center between AuNP dimers with well-defined interparticle distance was reported.^[126] Trimer assemblies with interparticle gaps in the subnanometer regime were shown to act as plasmon nanolenses.^[127]

The method was used to fabricate rotaxanes consisting of a partially double-stranded DNA axle with AuNPs acting as stoppers on each end. The macrocycle consisted of a circular ssDNA which was hybridized with a single-stranded domain of the axle as well as a third ssDNA-functionalized AuNP or a fluorophore (Fig. 8a).^[128] The thus-functionalized macrocycle was able to shuttle between the stoppers upon addition of suitable DNA fuel strands (Fig. 8b). With these structures, geometry-dependent plasmon resonance behavior of AuNP assemblies as well as distance-dependent fluorescence quenching and amplifying was investigated, being in close agreement with theoretically predicted surface plasmon-enhanced luminescence in noble metal nanoparticles.^[129,130] In a closely related work, both plasmonics and fluorescence quenching and amplifying behavior of precisely

organized AuNP assemblies were further investigated with the help of complex catenated AuNP-macrocylic DNA structures which were able to change morphology by exchange of DNA fuel strands.^[131] Further, mono-DNA AuNPs served as probes for the measurement of rotary and shuttling motions of DNA rotaxanes.^[132]

The distance-dependent plasmon properties of AuNP dimers were exploited to fabricate a ‘plasmon ruler’ where AuNPs functionalized with a single biotinylated ssDNA were anchored to surface-immobilized, streptavidin-coated AuNPs. With higher NaCl concentration in the buffer, the DNA strand curled up, bringing the AuNPs closer together and thus resulting in a plasmon redshift, while, with lower NaCl concentration, stretching of the DNA strand resulted in a plasmon blueshift.^[133] This type of ‘plasmon ruler’ was used to monitor endonuclease activity with high time-resolution as single Au-DNA-Au cutting events resulted in a drastic drop of scattering intensity upon release of AuNPs into the buffer solution.^[134]

DNA hybridization was exploited for the attachment of sin-

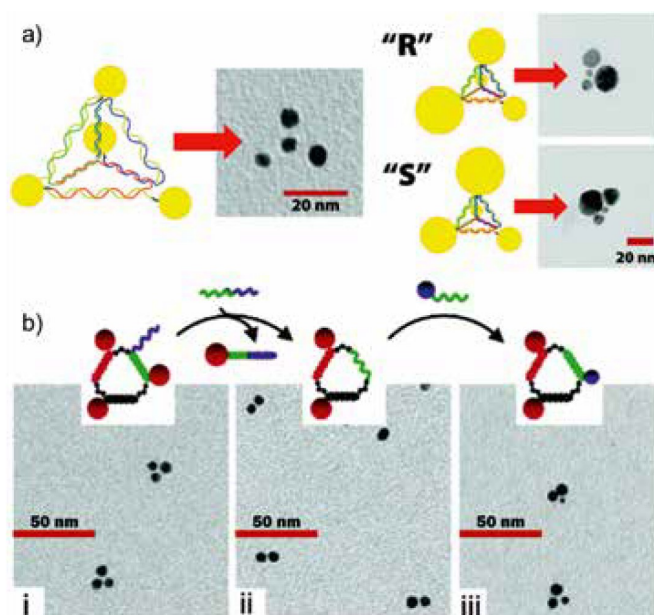


Fig. 7. a) Examples of superstructure assemblies from DNA-monofunctionalized AuNPs. a) Chiral and achiral AuNP tetrahedrons. Reprinted with permission from ref. [118]. Copyright (2009) American Chemical Society. b) Controlled NP exchange in a trimer structure by a ‘write/erase’ procedure. Adapted with permission from ref. [115]. Copyright (2007) American Chemical Society.

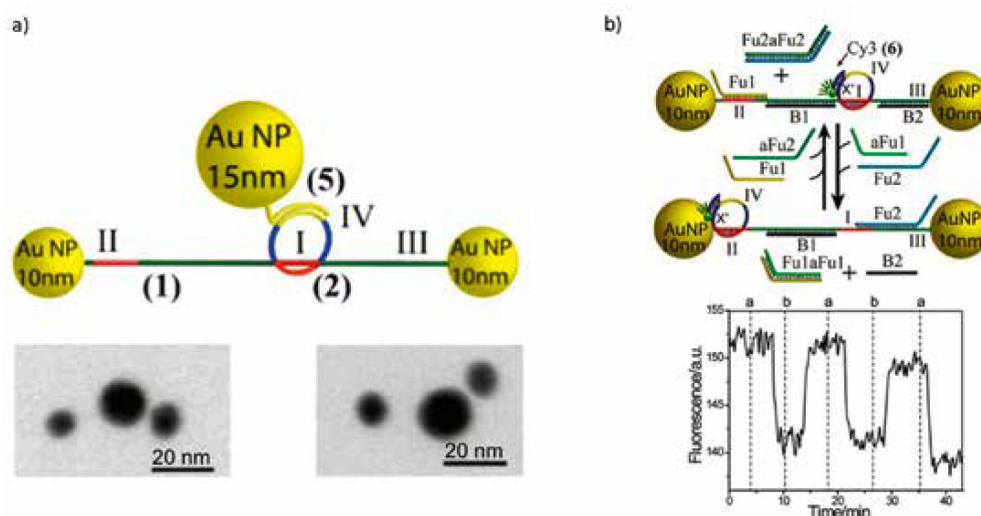


Fig. 8. a) AuNP–DNA–rotaxane with a third AuNP attached to the macrocycle. Domains I and II (red): ssDNA part of the axle. Domain III (green): dsDNA part of the axle. Domain IV (yellow): recognition site for the ssDNA-functionalized AuNP. The AuNP can shuttle between domains I and II. b) ssDNA macrocycle labeled with fluorescence marker for fluorescence quenching experiments. Adapted with permission from ref. [128]. Copyright (2017) American Chemical Society.

gle inactive thiolated hairpin DNA strands to AuNPs: an asymmetric DNA hairpin bearing a thiol at its sterically crowded hybridized end while the overhang is not functionalized cannot bind to a gold surface. In order to attach the inactive hairpin, phosphine-stabilized AuNPs were subjected to single place-exchange reaction with thiolated helper DNA strands. Those acted as competitive strands, allowing the loop to open upon hybridization and to expose the unreachable thiol. With this approach, the attached DNA lost its loop structure, but left an overhang for further functionalization of the AuNPs (Fig. 9a). Alternatively, a helper DNA with a hybridizable sequence and an overhang was first hybridized with the overhang of the loop DNA, thus freeing the inactive thiol while leaving the loop intact and finally, enabling the attaching to the AuNP surface (Fig. 9b). Using this procedure left the loop able to hybridize with further ssDNA as well as a hybridizable overhang from the helper DNA for individually accessible functionalizations of the AuNPs. These two methods allowed the controlled fabrication of AuNP superstructures such as di-, tri- and tetramers upon hybridization with either the intact loop, the helper DNA overhang or the stretched loop overhang (Fig. 9c).^[135] In continuation of this work, controlled strand displacement events on the helper strands were used to create AuNP-based ‘AND’, ‘OR’ and ‘YES’ logic circuit functions.^[136]

3.2.1.2 Alternate Functional Groups Using Electrophoresis for Purification

Several groups have shown that the versatility of electrophoresis as a means of isolating AuNPs bearing a single functional group

is not limited to DNA functionalization. A similar procedure based on electrophoretic separation was implemented for the monofunctionalization of AuNPs by monoamino poly(ethyleneglycol) chains.^[137] This modified method allowed to trace the accumulation of AuNPs in living animals from both intravenous injection and intratracheal instillation.^[138] In another approach, AuNPs were stabilized by 11-mercaptopundecanoic acid. Ligand-exchange with stoichiometric amounts of 1,6-hexanedithiol gave interconnected AuNP structures which could be separated by gel electrophoresis owing to the anionic charge on the structure’s surface. With this method, precisely ordered di- and trimers were isolated.^[139] The potential of electrophoresis for AuNPs was demonstrated with the self-assembly of protein cage–AuNP hybrid nanoarchitectures obtained by surface engineering.^[140] The AuNP exposed a single Ni²⁺ complex which was introduced by place-exchanging citrate with a thiolated molecule exposing a nitrilotriacetic acid subunit coordinating Ni²⁺ ions. This Ni-complex at the AuNP surface interacts with the polyhistidine tag exposed by a protein cage. Depending on the concentrations of the surface-engineered nano-objects, a variety of discrete AuNP–protein hybrid architectures were obtained (Fig. 10).

Recently, *p*-mercaptobenzoic acid-coated Au₁₀₂ and Au₂₅₀ clusters were subjected to stoichiometric place-exchange reaction with biphenyl-4,4'-dithiol. After separation of the dimers from the unreacted monomers and oligomers, it was found that the dimers were formed by disulfide formation of the exposed thiol. These well-defined structures of moderate size made them excellent model compounds for connecting *ab initio* theoretical studies and experimental quantum plasmonics. These dimers not

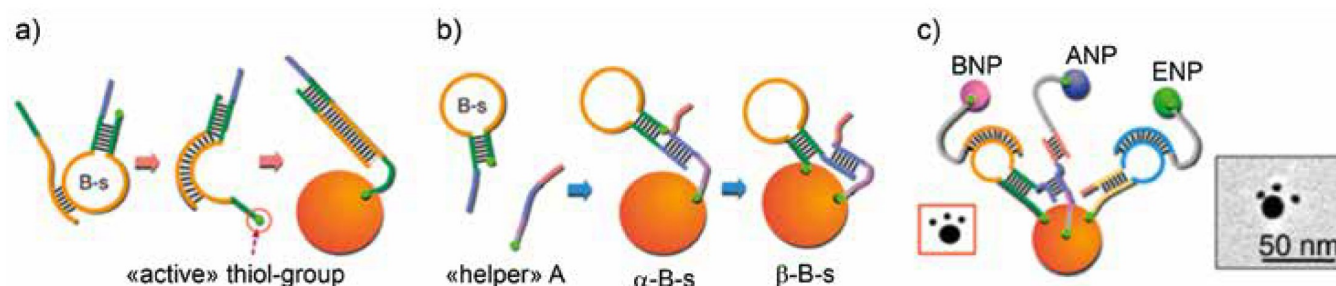


Fig. 9. a) Opening the hairpin DNA loop via hybridization allows access to the sterically crowded thiol, leaving the loop overhang exposed; b) Helper DNA hybridizes to DNA loop overhang, exposing the thiol. The helper DNA overhang is accessible for hybridization; c) AuNP tetramer structure demonstrating the presence of the corresponding DNA architectures at the AuNP surface. Small, ssDNA-monofunctionalized AuNPs hybridize to the specific target functional units on the large AuNP. Adapted with permission from ref. [135]. Copyright (2013) American Chemical Society.

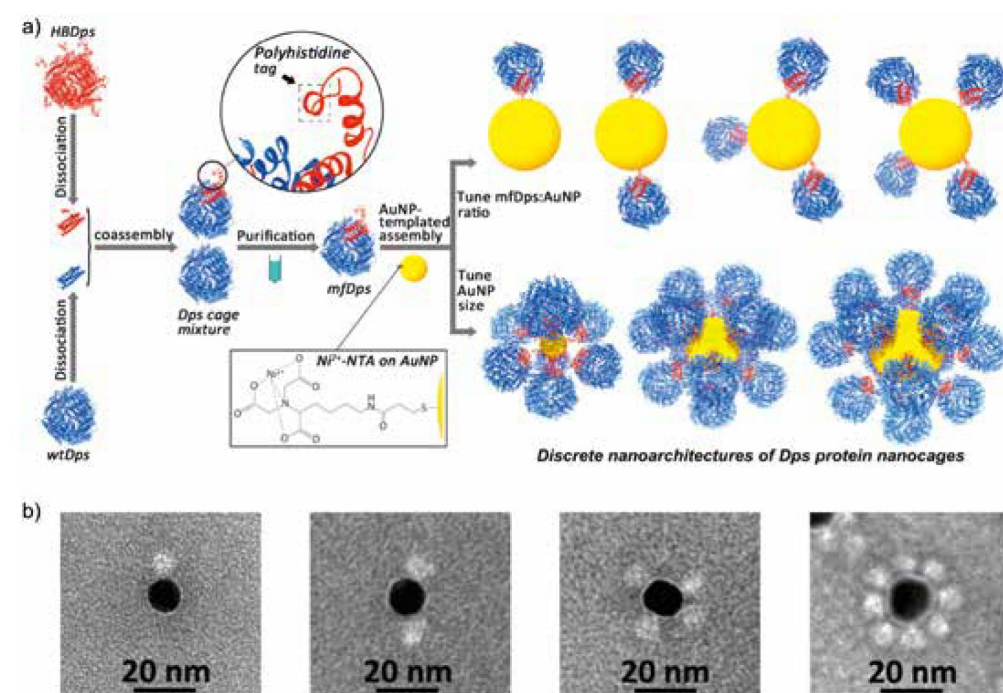


Fig. 10. a) Sketch of the conceptual approach assembling discrete hybrid nanoarchitectures controlled by the protein-cage/AuNP ratio. b) TEM images of discrete hybrid nano objects isolated by electrophoresis. Adapted with permission from ref. [140]. Copyright (2015) American Chemical Society.

only showed large red-shift in their plasmon resonance, but also a second plasmon resonance mode most likely stemming from tunneling charge transfer phenomena.^[141] In a later study, a series of alternate dithiol linkers was investigated in order to gain insight into the influence of the linker structure on the AuNP superstructure polymerization behavior.^[142] This approach was further used as a proof-of-principle method for the imaging of individual disulfide bonds *via* electron energy-loss spectroscopy in scanning transmission electron microscopy experiments on AuNP dimers.^[143]

3.2.1.3 Polymerase Chain Reaction for the Monofunctionalization of Gold Nanoparticles

In order to functionalize AuNPs with single DNA strands, PCR was used on AuNPs coated with DNA primers.^[144] It was demonstrated that, for single PCR cycles, monofunctionalization is achieved while multiple cycles give AuNPs functionalized with two or more DNA strands, making this method a powerful candidate for automated AuNP superstructure assembly. The scope of this approach was shown by DNA pairing-driven assembly of chiral core-satellite and dendriform structures^[145] as well as two-sized AuNP heterodimers^[146] and chiral pyramids that show optical activity in circular dichroism spectroscopy measurements.^[144,147] Further, alternating heterochains of different-sized AuNPs fabricated by PCR have been shown to exhibit a direct dependence of structure chain length with plasmon absorption intensity and strength of surface-enhanced Raman scattering.^[148]

3.2.1.4 Two-phase Mixtures

An alternative approach to functionalize AuNPs with a single DNA strand was proposed by Jhaveri *et al.* They used methyl triethyleneglycol thiol for the stabilization of AuNPs. After place-exchanging the ligand with sub-stoichiometric amounts of thiolated ssDNA in a two-phase mixture (water and ethanol/dichloromethane), unreacted AuNPs preferred migrating to the organic phase while DNA-functionalized AuNPs preferably stayed in the aqueous phase. Salting out the free DNA was found to be a facile purification method. Proof of purity of monofunctionalized AuNPs was shown by gel electrophoresis.^[149]

In another study, citrate-stabilized AuNPs in aqueous phase were brought into contact with an organic phase containing stoichiometric amounts of 11-mercaptopundecyl methacrylate which place-exchanged with the ligands at the liquid-liquid interface. In presence of styrene and a radical initiator, styrene-acrylate-copolymer chains carrying AuNPs were synthesized. Since the backbone of the polymer was hydrophobic and the AuNPs had a hydrophilic ligand shell, AuNP chains were formed in organic media while the structures aggregated to micelles in water.^[150] This method proved to be an attractive pathway for the formation of AuNP vesicles and core-shell-corona structures^[151] as well as vesicles containing Fe₃O₄ NPs embedded in the wall.^[152] In later reports, this strategy was used to fabricate cross-linked one- and multi-component hollow capsules which acted as nanocontainers for organic solvents in aqueous media *via* radical polymerization^[153] or anthracene photodimerization.^[154]

In an inverted variant of this protocol, AuNPs stabilized by a hydrophobic ligand shell were dispersed in toluene and place-exchanged with a stoichiometric aqueous solution of tiopronin, giving AuNPs carrying a single carboxylic acid function as demonstrated by synthesis of AuNP dimers *via* amide condensation with ethylenediamine for the assembly of plasmonic superstructures.^[155]

3.2.1.5 Centrifugation

Since place-exchange reactions are not limited to intrinsically charged ligands, the obvious limitations of gel electrophoresis regarding the nature of the ligand shell and mere sample size have pushed researchers to find alternate means for the isolation of discrete AuNP structures. In order to isolate precise AuNP assemblies by degree of functionalization, centrifugation has been used, yielding AuNP dimers connected by a single dithiol for the measurement of conductance through a single molecule^[156] or to exploit the Raman scattering properties of Au NP dimers in cancer detection.^[157]

A more elaborate protocol for the assembly of AuNP core-satellite structures was proposed by the group of Chad Mirkin: to ssDNA-functionalized SiO₂ NPs, 27-mer DNA strands were hybridized on 7 base-pairs to give a 20-base ssDNA overhang

to which complementary ssDNA-functionalized AuNPs can hybridize over 12 base-pairs. An excess of AuNPs guarantees full passivation of the SiO₂-bound DNA. In order to passivate the free DNA strands attached to the AuNPs, complementary strands were incubated with the superstructures. Because of the difference in hybridization lengths on the respective part of the bridging DNA between the Au and SiO₂ NPs (7 base-pairs vs 12 base-pairs), the DNA was selectively de-hybridized *via* careful temperature tuning to give AuNPs with one single 15-base overhang. These structures were used to form planet–satellite-type structures with larger, ssDNA-saturated AuNPs, which can be effectively purified by centrifugation (Fig. 11).^[158]

More recently, isolation by centrifugation was used to stopper a thiol-derivatized cucurbit[7]uril ferrocene pseudorotaxane with AuNPs to study the electrochemical electron transfer kinetics of the ferrocene in the rotaxane axle.^[159]

3.2.2 Solid-phase Place-exchange

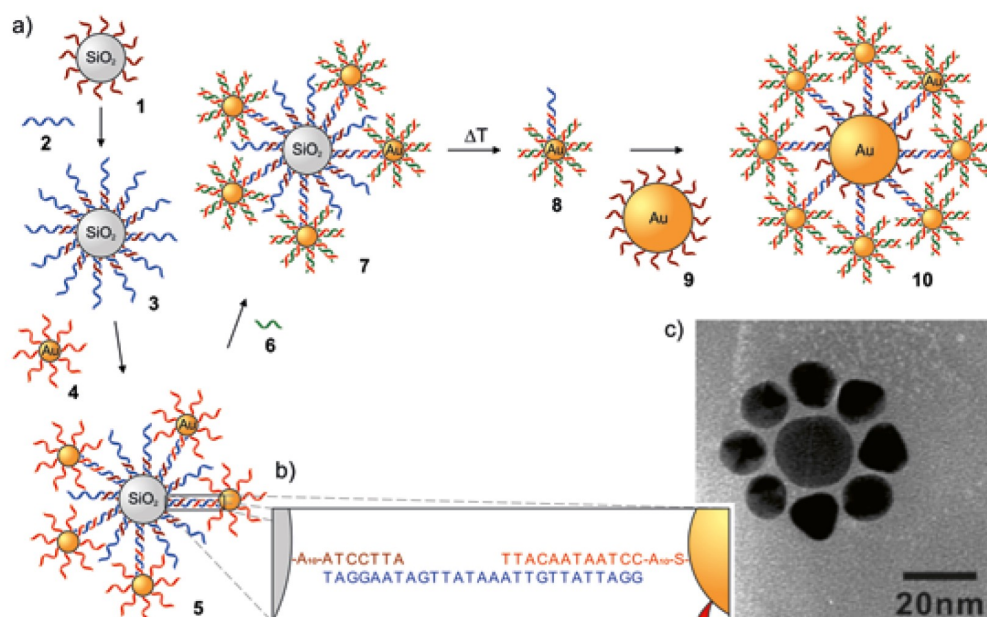
In solid-phase place-exchange strategies, the extent of the ligand-exchange reaction shall be limited to the small interaction surface between the AuNP and the solid substrate. The first protocol profiting from such an approach for the monofunctionalization of AuNPs was reported by Worden *et al.* in 2004^[160] and optimized soon thereafter.^[161] In their approach, Worden *et al.* loaded *n*-butanethiolate-stabilized AuNPs onto a polystyrene Wang resin which was functionalized by 6-mercaptohexanoic acid *via* an ester bond on the carboxyl moiety. In contact with the resin's free thiols, a single place-exchange reaction occurred on the AuNPs due to the limited interaction surface between NP and solid support. In a subsequent step, the ester bond was cleaved upon addition of trifluoroacetic acid (TFA), thus releasing the AuNPs exposing a single carboxyl group. Proof of concept was brought by amide condensation reaction with 1,7-diaminoheptane to give AuNP dimers.^[160,161] This procedure opened the doors to the formation of larger, highly ordered AuNP structures such as trimers,^[162] necklace-type macrocycles *via* amide condensation to polylysine and subsequent cyclization to AuNP necklace structures^[163] and amide condensation to oligo-AuNP PAMAM dendrimers.^[164] The necklace structures served as a template for the investigation of the optical, plasmonic and electromagnetic coupling behavior of AuNPs located in close proximity to each other. The studies favored a dipole–dipole interaction model for the de-

scription of optical AuNP–AuNP interaction^[165] and suggested inefficient electron surface scattering as the limiting phenomena in the optical experiment.^[166]

Variations of the Worden procedure were reported using boronic ester-functionalized polymer resins which had a free thiolate that place-exchanged with non-functional ligands on AuNPs. The boronic ester was cleaved by transesterification, giving AuNP functionalized with a single diol ligand.^[167] A further publication reported AuNPs functionalized with carboxylic acids that underwent amide condensation on Fmoc-protected lysine-decorated polystyrene and poly(ethylene glycol)acrylamide beads. Passivation of the free carboxyl groups on the AuNP and subsequent cleavage of the ester gave mono-carboxyl-terminated AuNPs as proven by dimerization reaction with ethylenediamine.^[168] Another closely similar approach used magnetic beads covered with crown ether acting as hosts for ammonium guests comprising a disulfide anchor, forming a pseudorotaxane with a dithiol axle. Place-exchange reaction with non-functional ligands on AuNPs and subsequent deprotonation of the ammonium caused pseudorotaxane de-threading, releasing monofunctional AuNPs. These readily formed pseudorotaxane-based supramolecular assemblies with suitable guests.^[169] In a later publication, the single amine moiety of the pseudorotaxane axle was further functionalized with maleimide which was then ‘clicked’ to thiolated single-stranded bacterial DNA sequences. This system showed promising potential in sensing and medical applications *via* hybridization to target DNA strands.^[170] Alternatively, silica beads or a Rink resin were functionalized with free amines that bound to the carboxylate of 11-mercaptoundecanoic acid ionically. Upon ligand place-exchange with unfunctionalized AuNPs and subsequent treatment with acetic acid, mono-carboxyl AuNPs were generated as proven by dimer formation *via* amide condensation with ethylenediamine.^[171,172] The usage of cellulose as the solid support was reported in a further variation of the method in order to create mono- and divalent AuNPs for the formation of AuNP chains and rings.^[173]

An interesting solid-phase mono-functionalization approach was reported by Dewi *et al.*, providing AuNPs exposing a terpyridine subunit as coordination site. Silica nanoparticles functionalized with a terminal carboxylic acid were subjected to amide condensation with an amine-functionalized terpyridine derivate first. Upon complexation with an iron ion and another equivalent of the amine-functionalized terpyridine derivate, the silicon

Fig. 11. a) Strategy for the formation of planet–satellite AuNP structures. ssDNA-coated silica bead (1) is hybridized with DNA strand 2, leaving a single-stranded overhang (3). ssDNA-functionalized AuNPs (4) hybridize to the free DNA overhang to give superstructure 5. DNA strand 6 passivates all non-hybridized DNA strands on the AuNPs (7). Careful heating releases AuNPs with a single DNA overhang strand (8) which can be hybridized to ssDNA-saturated AuNP 9 to give planet–satellite structure 10. b) DNA pairing sequences of various lengths between the SiO₂NP and the AuNP. c) TEM image of a planet–satellite AuNP structures. Adapted from ref. [158].



nanoparticle was decorated by iron terpyridine complexes exposing an amine, which were engaged in an amide formation with carboxy-functionalized AuNPs. Subsequent extraction of the iron ion gave AuNPs functionalized with a single terpyridine subunit. The monofunctionality of the AuNPs was corroborated by forming dumbbell-type dimers resulting from the addition of iron ions forming the homoleptic iron complex.^[174]

3.2.2.1 Janus Nanoparticles

'Janus' particles are micro- and nanoparticles with two different surface compositions, named after the two-faced ancient Roman god.^[175] Although efforts of asymmetrical functionalization of AuNPs with few functional groups by partial surface-masking approaches have been reported,^[176–178] only very few publications on reliable monofunctionalization exist in this field. Li *et al.* proposed the fabrication of monofunctionalized AuNPs by a combination of Janus-type surface modification and exploiting the challenging sterics of bulky ligands.^[179] In their approach, AuNPs were stabilized with phosphine ligands, giving the AuNPs a net negative charge which allowed them to bind to positively charged silica beads. Ligand place-exchange with glutathione passivated the exposed surface while the silica-bound surface was still accessible for further ligand-exchange with clover-shaped thiolated DNA after HF-mediated release. Due to its bulkiness, the clover DNA strand hindered further functionalization of the AuNPs as proven by hybridization with larger, DNA-functionalized AuNPs, giving core-satellite structures.

In a similar approach, citrate-stabilized AuNPs were ligand-exchanged to a glass slide functionalized with 3-mercaptopropyl-trimethoxy-silane. The exposed surface of the AuNPs was ligand-exchanged with cysteamine which was then attached to Cytochrome C, yielding AuNPs functionalized with a single protein. The absorption spectrum of these structures showed distinct dips next to the typical plasmon band in comparison with their unfunctionalized counterparts. This sharpening of the plasmon absorption was attributed to plasmon resonance energy transfer and identified as a promising property towards activity monitoring of biomarker proteins or *in vivo* electron transfer events.^[180]

3.3 Ligand-exchange in Living Systems

Based on the pioneering accounts on the immunological response of biological systems on colloids by Steabben in the early twentieth century,^[181] Huang and co-workers proposed *in vivo* ligand-exchange to obtain AuNPs carrying one single immunoglobulin G for the measurement of the flexibility of immunoglobulin *via* TEM images^[182] or the construction of a piezoelectric sensor chip.^[183] In a later report, they fabricated a transistor where the source-drain contact was established by an immunoglobulin G to which AuNPs were attached at each end, giving a molecular transistor which was not only gate-voltage dependent, but also modulated by the wavelength of the incident light.^[184]

4. Conclusion

In the present review, the variety of methods yielding AuNPs exposing a single functional group are summarized. The so-obtained AuNPs become addressable by wet chemical protocols and behave like massive molecules. The reported AuNPs can be coarsely categorized in two types: Type I AuNPs that are stabilized by a single ligand comprising only one functional moiety and Type II AuNPs that are stabilized by multiple ligands, whereof only one bears the additional functionality of interest. The examples show that, despite their size and mass, monofunctionalized AuNPs in solution behave molecule-like with respect to their chemical function, exhibiting plasmonic and electrochemical behavior and are powerful tags in TEM experiments. With the methods presented here, large, highly ordered plasmonic AuNP assemblies can be fabricated with good control at the single-particle level. The re-

ported AuNP assemblies act as model systems giving access to a variety of physical features such as plasmon quenching, fluorescence amplification, plasmon lensing, heat transfer *via* inductive coupling, as well as Förster- and plasmon resonance energy transfer processes. Alternatively, AuNPs, with a properly tuned functionality, act as effective, site-selective labels for a plethora of biomolecules and as physical barriers in mechanically interlinked superstructures. While the diversity of applications and the level of control achieved are impressive, the challenging aspect of most approaches is the limited sample size. While this is not an issue for biological systems where the handled sample size is usually equally tiny, it limits more the application potential of the methods in material science. There is plenty of room for improvements as far as the strategies towards larger batches of monofunctionalized AuNPs are concerned.

Acknowledgements

Financial support by the Swiss National Science Foundation (Grant no. 200020_178808), M. M. acknowledges support by the 111 project (90002-18011002).

Received: March 1, 2021

- [1] M. Faraday, *Phil. Trans. R. Soc. Lond.* **1857**, *147*, 145, <https://doi.org/10.1098/rstl.1857.0011>.
- [2] G. Mie, *Ann. Phys.* **1908**, *330*, 377, <https://doi.org/10.1002/andp.19083300302>.
- [3] G. Schmid, U. Simon, *Chem. Commun.* **2005**, 697, <https://doi.org/10.1039/B411696H>.
- [4] G. Yue, S. Su, N. Li, M. Shuai, X. Lai, D. Astruc, P. Zhao, *Coord. Chem. Rev.* **2016**, *311*, 75, <https://doi.org/10.1016/j.ccr.2015.11.009>.
- [5] R. Wilson, *Chem. Soc. Rev.* **2008**, *37*, 2028, <https://doi.org/10.1039/B712179M>.
- [6] P. Zhao, X. Feng, D. Huang, G. Yang, D. Astruc, *Coord. Chem. Rev.* **2015**, *287*, 114, <https://doi.org/10.1016/j.ccr.2015.01.002>.
- [7] C. Wang, D. Astruc, *Chem. Soc. Rev.* **2014**, *43*, 7188, <https://doi.org/10.1039/C4CS00145A>.
- [8] L. Pasquato, P. Pengo, P. Scrimin, *Supramol. Chem.* **2005**, *17*, 163, <https://doi.org/10.1080/10610270412331328817>.
- [9] S. Link, M. A. El-Sayed, *J. Phys. Chem. B* **1999**, *103*, 4212, <https://doi.org/10.1021/jp984796o>.
- [10] H. Xu, M. Käll, *Sens. Actuators B Chem.* **2002**, *87*, 244, [https://doi.org/10.1016/S0925-4005\(02\)00243-5](https://doi.org/10.1016/S0925-4005(02)00243-5).
- [11] W. Rechberger, A. Hohenau, A. Leitner, J. R. Krenn, B. Lamprecht, F. R. Aussenegg, *Opt. Commun.* **2003**, *220*, 137, [https://doi.org/10.1016/S0030-4018\(03\)01357-9](https://doi.org/10.1016/S0030-4018(03)01357-9).
- [12] N. Zohar, L. Chuntunov, G. Haran, *J. Photochem. Photobiol. C* **2014**, *21*, 26, <https://doi.org/10.1016/j.jphotochemrev.2014.10.002>.
- [13] D. Safer, *J. Struct. Biol.* **1999**, *127*, 101, <https://doi.org/10.1006/jsbi.1999.4110>.
- [14] J. F. Hainfeld, 'Colloidal Gold: Principles, Methods, and Applications', Elsevier, **2012**.
- [15] Y. Wu, M. R. K. Ali, K. Chen, N. Fang, M. A. El-Sayed, *Nano Today* **2019**, *24*, 120, <https://doi.org/10.1016/j.nantod.2018.12.006>.
- [16] R. A. Sperling, P. R. Gil, F. Zhang, M. Zanella, W. J. Parak, *Chem. Soc. Rev.* **2008**, *37*, 1896, <https://doi.org/10.1039/B712170A>.
- [17] J. F. Hainfeld, R. D. Powell, *J. Histochem Cytochem.* **2000**, *48*, 471, <https://doi.org/10.1177/002215540004800404>.
- [18] T. A. Gschneidner, Y. A. D. Fernandez, K. Moth-Poulsen, *J. Mater. Chem. C* **2013**, *1*, 7127, <https://doi.org/10.1039/C3TC31483A>.
- [19] G. Schmid, *Adv. Eng. Mater.* **2001**, *3*, 737, [https://doi.org/10.1002/1527-2648\(200110\)3:10<737::AID-ADEM737>3.0.CO;2-8](https://doi.org/10.1002/1527-2648(200110)3:10<737::AID-ADEM737>3.0.CO;2-8).
- [20] J. Liao, S. Blok, S. J. van der Molen, S. Diefenbach, A. W. Holleitner, C. Schönenberger, A. Vladyka, M. Calame, *Chem. Soc. Rev.* **2015**, *44*, 999, <https://doi.org/10.1039/C4CS00225C>.
- [21] J. Wang, J. Li, J. Li, F. Liu, Y. Gu, J. Fan, B. Dong, C. Wang, L. Qiu, L. Gao, S. Seong Lee, P. Jiang, *Curr. Org. Chem.* **2016**, *20*, 1786, <https://doi.org/10.2174/1385272820666151105193200>.
- [22] H.-H. Wang, C.-H. Su, Y.-J. Wu, C.-A. J. Lin, C.-H. Lee, J.-L. Shen, W.-H. Chan, W. H. Chang, H.-I. Yeh, *Int. J. Gerontol.* **2012**, *6*, 1, <https://doi.org/10.1016/j.ijge.2011.09.015>.
- [23] W. Baschong, N. G. Wrigley, *J. Elec. Microsc. Tech.* **1990**, *14*, 313, <https://doi.org/10.1002/jemt.1060140405>.

- [24] T. Carter, P. Mulholland, K. Chester, *Immunotherapy* **2016**, *8*, 941, <https://doi.org/10.2217/imt.16.11>.
- [25] P. Kesharwani, H. Choudhury, J. G. Meher, M. Pandey, B. Gorain, *Prog. Mater. Sci.* **2019**, *103*, 484, <https://doi.org/10.1016/j.pmatsci.2019.03.003>.
- [26] P. Zhao, N. Li, D. Astruc, *Coord. Chem. Rev.* **2013**, *257*, 638, <https://doi.org/10.1016/j.ccr.2012.09.002>.
- [27] T. Peterle, A. Leifert, J. Timper, A. Sologubenko, U. Simon, M. Mayor, *Chem. Commun.* **2008**, 3438, <https://doi.org/10.1039/B802460J>.
- [28] M. Lehmann, E. H. Peters, M. Mayor, *Chem. Eur. J.* **2016**, *22*, 2261, <https://doi.org/10.1002/chem.201504575>.
- [29] E. H. Peters, M. Lehmann, M. Mayor, *Part. Part. Syst. Character.* **2018**, *35*, 1800015, <https://doi.org/10.1002/ppsc.201800015>.
- [30] R. Wilson, *Chem. Commun.* **2003**, 108, <https://doi.org/10.1039/B208170A>.
- [31] R. Wilson, Y. Chen, J. Aveyard, *Chem. Commun.* **2004**, 1156, <https://doi.org/10.1039/B402786H>.
- [32] J. Aveyard, P. Nolan, R. Wilson, *Anal. Chem.* **2008**, *80*, 6001, <https://doi.org/10.1021/ac800699k>.
- [33] Y. Chen, J. Aveyard, R. Wilson, *Chem. Commun.* **2004**, 2804, <https://doi.org/10.1039/B411181H>.
- [34] M. Mehrabi, R. Wilson, *Small* **2007**, *3*, 1491, <https://doi.org/10.1002/sml.200700230>.
- [35] G. Yao, H. Pei, J. Li, Y. Zhao, D. Zhu, Y. Zhang, Y. Lin, Q. Huang, C. Fan, *NPG Asia Mater* **2015**, *7*, e159, <https://doi.org/10.1038/am.2014.131>.
- [36] H. Xing, Y. Bai, Y. Bai, L. H. Tan, J. Tao, B. Pedretti, G. A. Vincil, Y. Lu, S. C. Zimmerman, *J. Am. Chem. Soc.* **2017**, *139*, 3623, <https://doi.org/10.1021/jacs.7b00065>.
- [37] Y. Bai, H. Xing, Y. Bai, L. H. Tan, K. Hwang, J. Li, Y. Lu, S. C. Zimmerman, *Chem. Sci.* **2020**, *11*, 1564, <https://doi.org/10.1039/C9SC05656D>.
- [38] C. Krüger, S. Agarwal, A. Greiner, *J. Am. Chem. Soc.* **2008**, *130*, 2710, <https://doi.org/10.1021/ja0763495>.
- [39] M. Brust, M. Walker, D. Bethell, D. J. Schiffrin, R. Whyman, *J. Chem. Soc., Chem. Commun.* **1994**, 801, <https://doi.org/10.1039/C3994000080I>.
- [40] S. Bokern, K. Gries, H.-H. Görtz, V. Warzelhan, S. Agarwal, A. Greiner, *Adv. Funct. Mater.* **2011**, *21*, 3753, <https://doi.org/10.1002/adfm.201100590>.
- [41] K. Gries, M. El Helou, G. Witte, S. Agarwal, A. Greiner, *Polymer* **2012**, *53*, 1632, <https://doi.org/10.1016/j.polymer.2012.02.008>.
- [42] Z. Fan, X. Chen, M. Köhn Serrano, H. Schmalz, S. Rosenfeldt, S. Förster, S. Agarwal, A. Greiner, *Angew. Chem. Int. Ed.* **2015**, *54*, 14539, <https://doi.org/10.1002/anie.201506415>.
- [43] Z. Fan, M. K. Serrano, A. Schaper, S. Agarwal, A. Greiner, *Adv. Mater.* **2015**, *27*, 3888, <https://doi.org/10.1002/adma.201501306>.
- [44] S. R. Barman, A. Nain, S. Jain, N. Punjabi, S. Mukherji, J. Satija, *J. Mater. Chem. B* **2018**, *6*, 2368, <https://doi.org/10.1039/C7TB03344C>.
- [45] A. K. Ilunga, R. Meijboom, *Catal. Lett.* **2019**, *149*, 84, <https://doi.org/10.1007/s10562-018-2584-0>.
- [46] B. I. Kharisov, H. V. R. Dias, O. V. Kharissova, A. Vázquez, *J. Nanopart. Res.* **2014**, *16*, 2665, <https://doi.org/10.1007/s11051-014-2665-y>.
- [47] X. Li, K. Kono, *Polym. Int.* **2018**, *67*, 840, <https://doi.org/10.1002/pi.5583>.
- [48] W. M. Pankau, S. Mönninghoff, G. von Kiedrowski, *Angew. Chem. Int. Ed.* **2006**, *45*, 1889, <https://doi.org/10.1002/anie.200502370>.
- [49] T. Peterle, P. Ringler, M. Mayor, *Adv. Funct. Mater.* **2009**, *19*, 3497, <https://doi.org/10.1002/adfm.200901410>.
- [50] J. P. Hermes, F. Sander, T. Peterle, C. Cioffi, P. Ringler, T. Pfohl, M. Mayor, *Small* **2011**, *7*, 920, <https://doi.org/10.1002/sml.201002101>.
- [51] J. P. Hermes, F. Sander, T. Peterle, R. Urbani, T. Pfohl, D. Thompson, M. Mayor, *Chem. Eur. J.* **2011**, *17*, 13473, <https://doi.org/10.1002/chem.201101837>.
- [52] J. P. Hermes, F. Sander, U. Fluch, T. Peterle, D. Thompson, R. Urbani, T. Pfohl, M. Mayor, *J. Am. Chem. Soc.* **2012**, *134*, 14674, <https://doi.org/10.1021/ja306253t>.
- [53] F. Sander, U. Fluch, J. P. Hermes, M. Mayor, *Small* **2014**, *10*, 349, <https://doi.org/10.1002/sml.201300839>.
- [54] E. H. Peters, M. Mayor, *Eur. J. Inorg. Chem.* **2020**, *2020*, 2325, <https://doi.org/10.1002/ejic.202000273>.
- [55] S. H. Kashani, A. Landarani-Isfahani, M. Moghadam, S. Tangestaninejad, V. Mirkhani, I. Mohammadpoor-Baltork, *Appl. Organomet. Chem.* **2018**, *32*, e4440, <https://doi.org/10.1002/aoc.4440>.
- [56] X. Liu, Q. Ling, L. Zhao, G. Qiu, Y. Wang, L. Song, Y. Zhang, J. Ruiz, D. Astruc, H. Gu, *Macromol. Rapid. Commun.* **2017**, *38*, 1700448, <https://doi.org/10.1002/marc.201700448>.
- [57] X. Liu, S. Mu, Y. Long, G. Qiu, Q. Ling, H. Gu, W. Lin, *Catal. Lett.* **2019**, *149*, 544, <https://doi.org/10.1007/s10562-019-02662-5>.
- [58] F. Liu, X. Liu, D. Astruc, H. Gu, *J. Colloid. Interface. Sci.* **2019**, *533*, 161, <https://doi.org/10.1016/j.jcis.2018.08.062>.
- [59] S.-F. Lee, Q. Wang, D. K.-L. Chan, P.-L. Cheung, K.-W. Wong, J. C. Yu, B. S. Ong, K. C.-F. Leung, *New J. Chem.* **2014**, *38*, 3362, <https://doi.org/10.1039/C4NJ00318G>.
- [60] K. C.-F. Leung, X.-B. Li, X. Li, S.-F. Lee, J. C. Yu, P. M. Mendes, K. E. Hermann, M. A. V. Hove, *Mater. Chem. Front.* **2019**, *3*, 1555, <https://doi.org/10.1039/C9QM00132H>.
- [61] L. Chen, W. Cao, N. Grishkewich, R. M. Berry, K. C. Tam, *J. Colloid. Interface. Sci.* **2015**, *450*, 101, <https://doi.org/10.1016/j.jcis.2015.03.002>.
- [62] L. Chen, W. Cao, P. J. Quinlan, R. M. Berry, K. C. Tam, *ACS Sustainable Chem. Eng.* **2015**, *3*, 978, <https://doi.org/10.1021/acssuschemeng.5b00110>.
- [63] Md. A. Rahman, H.-B. Noh, Yoon-Bo Shim, *Anal. Chem.* **2008**, *80*, 8020, <https://doi.org/10.1021/ac801033s>.
- [64] J. Turkevich, P. C. Stevenson, J. Hillier, *Discuss. Faraday Soc.* **1951**, *11*, 55, <https://doi.org/10.1039/DF9511100055>.
- [65] F. Griffin, D. Fitzmaurice, *Langmuir* **2007**, *23*, 10262, <https://doi.org/10.1021/la061261a>.
- [66] M. Brust, R. Etchenique, E. J. Calvo, G. J. Gordillo, *Chem. Commun.* **1996**, 1949, <https://doi.org/10.1039/CC9960001949>.
- [67] B. Nikoobakht, M. A. El-Sayed, *Langmuir* **2001**, *17*, 6368, <https://doi.org/10.1021/la0105300>.
- [68] F. Cariati, L. Naldini, *Inorganica Chim. Acta* **1971**, *5*, 172, [https://doi.org/10.1016/S0020-1693\(00\)95906-1](https://doi.org/10.1016/S0020-1693(00)95906-1).
- [69] G. Schmid, R. Pfeil, R. Boese, F. Bändermann, S. Meyer, G. H. M. Calis, J. W. A. van der Velden, *Chem. Ber.* **1981**, *114*, 3634, <https://doi.org/10.1002/cber.1981114116>.
- [70] M. J. Hostetler, A. C. Templeton, R. W. Murray, *Langmuir* **1999**, *15*, 3782, <https://doi.org/10.1021/la981598f>.
- [71] A. W. Shaffer, J. G. Worden, Q. Huo, *Langmuir* **2004**, *20*, 8343, <https://doi.org/10.1021/la049308k>.
- [72] F. A. Vollenbroek, J. P. Van den Berg, J. W. A. Van der Velden, J. J. Bour, *Inorg. Chem.* **1980**, *19*, 2685, <https://doi.org/10.1021/ic50211a041>.
- [73] J. E. Reardon, P. A. Frey, *Biochemistry* **1984**, *23*, 3849, <https://doi.org/10.1021/bi00312a009>.
- [74] H. Yang, J. E. Reardon, P. A. Frey, *Biochemistry* **1984**, *23*, 3857, <https://doi.org/10.1021/bi00312a010>.
- [75] D. Safer, L. Bolinger, J. S. Leigh, *J. Inorg. Biochem.* **1986**, *26*, 77, [https://doi.org/10.1016/0162-0134\(86\)80001-0](https://doi.org/10.1016/0162-0134(86)80001-0).
- [76] D. Safer, J. F. Hainfeld, J. S. Wall, *Biophys. J.* **1985**, *47*, 128a, [https://doi.org/10.1016/S0006-3495\(85\)83902-3](https://doi.org/10.1016/S0006-3495(85)83902-3).
- [77] W. Jahn, *Z. Naturforsch. B* **1989**, *44b*, 1313, <https://doi.org/10.1515/znB-1989-1027>.
- [78] J. Crum, K. J. Gruys, T. G. Frey, *Biochemistry* **1994**, *33*, 13719, <https://doi.org/10.1021/bi00250a024>.
- [79] J. F. Hainfeld, *Science* **1987**, *236*, 450, <https://doi.org/10.1126/science.3563522>.
- [80] J. F. Hainfeld, M. Sprinzl, V. Mandiyan, S. J. Tumminia, M. Boublik, *J. Struct. Biol.* **1991**, *107*, 1, [https://doi.org/10.1016/1047-8477\(91\)90024-Q](https://doi.org/10.1016/1047-8477(91)90024-Q).
- [81] A. Zlotnick, N. Cheng, S. J. Stahl, J. F. Conway, A. C. Steven, P. T. Wingfield, *PNAS* **1997**, *94*, 9556, <https://doi.org/10.1073/pnas.94.18.9556>.
- [82] B. Blechschmidt, W. Jahn, J. F. Hainfeld, M. Sprinzl, M. Boublik, *J. Struct. Biol.* **1993**, *110*, 84, <https://doi.org/10.1006/jsbi.1993.1007>.
- [83] E. Skripkin, G. Yusupova, M. Yusupov, P. Kessler, C. Ehresmann, B. Ehresmann, *Bioconjugate Chem.* **1993**, *4*, 549, <https://doi.org/10.1021/bc00024a019>.
- [84] B. Blechschmidt, V. Shirokov, M. Sprinzl, *Eur. J. Biochem.* **1994**, *219*, 65, <https://doi.org/10.1111/j.1432-1033.1994.tb19915.x>.
- [85] J. F. Hainfeld, F. R. Furuya, *J. Histochem. Cytochem.* **1992**, *40*, 177, <https://doi.org/10.1177/40.2.1552162>.
- [86] M. R. Narouz, K. M. Osten, P. J. Unsworth, R. W. Y. Man, K. Salorinne, S. Takano, R. Tomihara, S. Kaappa, S. Malola, C.-T. Dinh, J. D. Padmos, K. Ayoo, P. J. Garrett, M. Nambo, J. H. Horton, E. H. Sargent, H. Häkkinen, T. Tsukuda, C. M. Crudden, *Nat. Chem.* **2019**, *11*, 419, <https://doi.org/10.1038/s41557-019-0246-5>.
- [87] NANOPROBES: Gold nanoparticles and Nanogold for immunolabeling, EM, LM, fluorescence microscopy, and micro-CT x-ray contrast agents, <http://www.nanoprob.com/>, accessed November 14, 2019.
- [88] J. F. Hainfeld, R. D. Leone, F. R. Furuya, R. D. Powell, US Patent 5,521,289, **1996**.
- [89] A. P. Alivisatos, K. P. Johnsson, X. Peng, T. E. Wilson, C. J. Loweth, M. P. Bruchez, P. G. Schultz, *Nature* **1996**, *382*, 609, <https://doi.org/10.1038/382609a0>.
- [90] C. M. Niemeyer, W. Bürger, J. Peplies, *Angew. Chem. Int. Ed.* **1998**, *37*, 2265, [https://doi.org/10.1002/\(SICI\)1521-3773\(19980904\)37:16<2265::AID-ANIE2265>3.0.CO;2-F](https://doi.org/10.1002/(SICI)1521-3773(19980904)37:16<2265::AID-ANIE2265>3.0.CO;2-F).
- [91] K. Hamad-Schifferli, J. J. Schwartz, A. T. Santos, S. Zhang, J. M. Jacobson, *Nature* **2002**, *415*, 152, <https://doi.org/10.1038/415152a>.
- [92] K. Hamad-Schifferli, J. J. Schwartz, A. T. Santos, S. Zhang, J. M. Jacobson, *Mat. Res. Soc. Symp. Proc.* **2001**, *676*, Y8.43.1, <https://doi.org/10.1557/PROC-676-Y8.43>.
- [93] F. Patolsky, Y. Weizmann, O. Lioubashevski, I. Willner, *Angew. Chem. Int. Ed.* **2002**, *41*, 2323, [https://doi.org/10.1002/1521-3773\(20020703\)41:13<2323::AID-ANIE2323>3.0.CO;2-H](https://doi.org/10.1002/1521-3773(20020703)41:13<2323::AID-ANIE2323>3.0.CO;2-H).

- [94] Y. Xiao, F. Patolsky, E. Katz, J. F. Hainfeld, I. Willner, *Science* **2003**, *299*, 1877, <https://doi.org/10.1126/science.1080664>.
- [95] T. Pons, I. L. Medintz, K. E. Sapsford, S. Higashiya, A. F. Grimes, D. S. English, H. Mattoussi, *Nano Lett.* **2007**, *7*, 3157, <https://doi.org/10.1021/nl071729+>.
- [96] Z. Wang, R. Lévy, D. G. Fernig, M. Brust, *Bioconjugate Chem.* **2005**, *16*, 497, <https://doi.org/10.1021/bc050047f>.
- [97] R. Lévy, Z. Wang, L. Duchesne, R. C. Doty, A. I. Cooper, M. Brust, D. G. Fernig, *ChemBioChem* **2006**, *7*, 592, <https://doi.org/10.1002/cbic.200500457>.
- [98] R. Lévy, *ChemBioChem* **2006**, *7*, 1141, <https://doi.org/10.1002/cbic.200600129>.
- [99] L. Duchesne, D. Gentili, M. Comes-Franchini, D. G. Fernig, *Langmuir* **2008**, *24*, 13572, <https://doi.org/10.1021/la802876u>.
- [100] L. Duchesne, V. Oceau, R. N. Bearon, A. Beckett, I. A. Prior, B. Lounis, D. G. Fernig, *PLoS Biology* **2012**, *10*, e1001361, <https://doi.org/10.1371/journal.pbio.1001361>.
- [101] C. Leduc, S. Si, J. Gautier, M. Soto-Ribeiro, B. Wehrle-Haller, A. Gautreau, G. Giannone, L. Cognet, B. Lounis, *Nano Lett.* **2013**, *13*, 1489, <https://doi.org/10.1021/nl304561g>.
- [102] D. J. Nieves, N. S. Azmi, R. Xu, R. Lévy, E. A. Yates, D. G. Fernig, *Chem. Commun.* **2014**, *50*, 13157, <https://doi.org/10.1039/C4CC05909C>.
- [103] D. Paramelle, D. Nieves, B. Brun, R. S. Kraut, D. G. Fernig, *Adv. Healthc. Mater.* **2015**, *4*, 911, <https://doi.org/10.1002/adhm.201400730>.
- [104] L. Duchesne, G. Wells, D. G. Fernig, S. A. Harris, R. Lévy, *ChemBioChem* **2008**, *9*, 2127, <https://doi.org/10.1002/cbic.200800326>.
- [105] Y. Jun, S. Sheikholeslami, D. R. Hostetter, C. Tajon, C. S. Craik, A. P. Alivisatos, *PNAS* **2009**, *106*, 17735, <https://doi.org/10.1073/pnas.0907367106>.
- [106] L. C. Brousseau III, J. P. Novak, S. M. Marinakos, D. L. Feldheim, *Adv. Mater.* **1999**, *11*, 447, [https://doi.org/10.1002/\(SICI\)1521-4095\(199904\)11:6<447::AID-ADMA447>3.0.CO;2-I](https://doi.org/10.1002/(SICI)1521-4095(199904)11:6<447::AID-ADMA447>3.0.CO;2-I).
- [107] C. A. Otter, P. J. Patty, M. A. K. Williams, M. R. Waterland, S. G. Telfer, *Nanoscale* **2011**, *3*, 941, <https://doi.org/10.1039/C0NR00801J>.
- [108] C. J. Loweth, W. B. Caldwell, X. Peng, A. P. Alivisatos, P. G. Schultz, *Angew. Chem. Int. Ed.* **1999**, *38*, 1808, [https://doi.org/10.1002/\(SICI\)1521-3773\(19990614\)38:12<1808::AID-ANIE1808>3.0.CO;2-C](https://doi.org/10.1002/(SICI)1521-3773(19990614)38:12<1808::AID-ANIE1808>3.0.CO;2-C).
- [109] S. A. Claridge, H. W. Liang, S. R. Basu, J. M. J. Fréchet, A. P. Alivisatos, *Nano Lett.* **2008**, *8*, 1202, <https://doi.org/10.1021/nl0802032>.
- [110] T. Pellegrino, R. A. Sperling, A. P. Alivisatos, W. J. Parak, *J. Biomed. Biotechnol.* **2007**, *26796*, <https://doi.org/10.1155/2007/26796>.
- [111] D. Zanchet, C. M. Micheel, W. J. Parak, D. Gerion, A. P. Alivisatos, *Nano Lett.* **2001**, *1*, 32, <https://doi.org/10.1021/nl005508e>.
- [112] D. Zanchet, C. M. Micheel, W. J. Parak, D. Gerion, S. C. Williams, A. P. Alivisatos, *J. Phys. Chem. B* **2002**, *106*, 11758, <https://doi.org/10.1021/jp026144c>.
- [113] Y. Akiyama, H. Shikagawa, N. Kanayama, T. Takarada, M. Maeda, *Small* **2015**, *11*, 3153, <https://doi.org/10.1002/smll.201500045>.
- [114] L. Lermusiaux, A. Sereda, B. Portier, E. Larquet, S. Bidault, *ACS Nano* **2012**, *6*, 10992, <https://doi.org/10.1021/nn304599d>.
- [115] F. A. Aldaye, H. F. Sleiman, *J. Am. Chem. Soc.* **2007**, *129*, 4130, <https://doi.org/10.1021/ja0700171>.
- [116] S. A. Claridge, S. L. Goh, J. M. J. Fréchet, S. C. Williams, C. M. Micheel, A. P. Alivisatos, *Chem. Mater.* **2005**, *17*, 1628, <https://doi.org/10.1021/cm0484089>.
- [117] Z. Deng, Y. Tian, S.-H. Lee, A. E. Ribbe, C. Mao, *Angew. Chem. Int. Ed.* **2005**, *44*, 3582, <https://doi.org/10.1002/anie.200463096>.
- [118] A. J. Mastroianni, S. A. Claridge, A. P. Alivisatos, *J. Am. Chem. Soc.* **2009**, *131*, 8455, <https://doi.org/10.1021/ja808570g>.
- [119] H. Gu, J. Chao, S.-J. Xiao, N. C. Seeman, *Nature* **2010**, *465*, 202, <https://doi.org/10.1038/nature09026>.
- [120] J. Zheng, P. E. Constantinou, C. Micheel, A. P. Alivisatos, R. A. Kiehl, N. C. Seeman, *Nano Lett.* **2006**, *6*, 1502, <https://doi.org/10.1021/nl060994c>.
- [121] J. Sharma, R. Chhabra, Y. Liu, Y. Ke, H. Yan, *Angew. Chem. Int. Ed.* **2006**, *45*, 730, <https://doi.org/10.1002/anie.200503208>.
- [122] J. Sharma, R. Chhabra, C. S. Andersen, K. V. Gothelf, H. Yan, Y. Liu, *J. Am. Chem. Soc.* **2008**, *130*, 7820, <https://doi.org/10.1021/ja802853r>.
- [123] L. Lermusiaux, V. Maillard, S. Bidault, *ACS Nano* **2015**, *9*, 978, <https://doi.org/10.1021/nn506947g>.
- [124] M. P. Busson, B. Rolly, B. Stout, N. Bonod, E. Larquet, A. Polman, S. Bidault, *Nano Lett.* **2011**, *11*, 5060, <https://doi.org/10.1021/nl2032052>.
- [125] L. Lermusiaux, S. Bidault, *Langmuir* **2018**, *34*, 14946, <https://doi.org/10.1021/acs.langmuir.8b00133>.
- [126] S. Bidault, A. Devilez, P. Ghenuche, B. Stout, N. Bonod, J. Wenger, *ACS Photonics* **2016**, *3*, 895, <https://doi.org/10.1021/acsphotonics.6b00148>.
- [127] S. Bidault, F. J. García de Abajo, A. Polman, *J. Am. Chem. Soc.* **2008**, *130*, 2750, <https://doi.org/10.1021/ja711074n>.
- [128] A. Ceconello, C.-H. Lu, J. Elbaz, I. Willner, *Nano Lett.* **2013**, *13*, 6275, <https://doi.org/10.1021/nl403884w>.
- [129] H. Mertens, A. F. Koenderink, A. Polman, *Phys. Rev. B* **2007**, *76*, 115123, <https://doi.org/10.1103/PhysRevB.76.115123>.
- [130] E. Fort, S. Gréssillon, *J. Phys. D: Appl. Phys.* **2007**, *41*, 013001, <https://doi.org/10.1088/0022-3727/41/1/013001>.
- [131] J. Elbaz, A. Ceconello, Z. Fan, A. O. Govorov, I. Willner, *Nat. Commun.* **2013**, *4*, 2000, <https://doi.org/10.1038/ncomms3000>.
- [132] J. List, E. Falgenhauer, E. Kopperger, G. Pardatscher, F. C. Simmel, *Nat. Commun.* **2016**, *7*, <https://doi.org/10.1038/ncomms12414>.
- [133] C. Sönnichsen, B. M. Reinhard, J. Liphardt, A. P. Alivisatos, *Nat. Biotechnol.* **2005**, *23*, 741, <https://doi.org/10.1038/nbt1100>.
- [134] B. M. Reinhard, S. Sheikholeslami, A. Mastroianni, A. P. Alivisatos, J. Liphardt, *PNAS* **2007**, *104*, 2667, <https://doi.org/10.1073/pnas.0607826104>.
- [135] C. Zhang, J. Ma, J. Yang, S. Liu, J. Xu, *Anal. Chem.* **2013**, *85*, 11973, <https://doi.org/10.1021/ac402908y>.
- [136] C. Zhang, R. Wu, Y. Li, Q. Zhang, J. Yang, *Langmuir* **2017**, *33*, 12285, <https://doi.org/10.1021/acs.langmuir.7b02620>.
- [137] R. A. Sperling, T. Pellegrino, J. K. Li, W. H. Chang, W. J. Parak, *Adv. Funct. Mater.* **2006**, *16*, 943, <https://doi.org/10.1002/adfm.200500589>.
- [138] J. Lipka, M. Semmler-Behnke, R. A. Sperling, A. Wenk, S. Takenaka, C. Schleh, T. Kissel, W. J. Parak, W. G. Kreyling, *Biomaterials* **2010**, *31*, 6574, <https://doi.org/10.1016/j.biomaterials.2010.05.009>.
- [139] J.-Y. Kim, H.-B. Kim, D.-J. Jang, *Electrophoresis* **2013**, *34*, 911, <https://doi.org/10.1002/elps.201200492>.
- [140] L. Ma, F. Li, T. Fang, J. Zhang, Q. Wang, *ACS Appl. Mater. Interfaces* **2015**, *7*, 11024, <https://doi.org/10.1021/acsami.5b02823>.
- [141] T. Lahtinen, E. Hultkko, K. Sokołowska, T.-R. Tero, V. Saarnio, J. Lindgren, M. Pattersson, H. Häkkinen, L. Lehtovaara, *Nanoscale* **2016**, *8*, 18665, <https://doi.org/10.1039/C6NR05267C>.
- [142] K. Sokołowska, E. Hultkko, L. Lehtovaara, T. Lahtinen, *J. Phys. Chem. C* **2018**, *122*, 12524, <https://doi.org/10.1021/acs.jpcc.8b02988>.
- [143] K. Sokołowska, Z. Luan, E. Hultkko, C. Rameshan, N. Barrabés, V. A. Apkarian, T. Lahtinen, *J. Phys. Chem. Lett.* **2020**, *11*, 796, <https://doi.org/10.1021/acs.jpcclett.9b03496>.
- [144] W. Chen, A. Bian, A. Agarwal, L. Liu, H. Shen, L. Wang, C. Xu, N. A. Kotov, *Nano Lett.* **2009**, *9*, 2153, <https://doi.org/10.1021/nl900726s>.
- [145] Y. Zhao, L. Xu, H. Kuang, L. Wang, C. Xu, *J. Mater. Chem.* **2012**, *22*, 5574, <https://doi.org/10.1039/C2JM15800K>.
- [146] W. Yan, W. Ma, H. Kuang, L. Liu, L. Wang, L. Xu, C. Xu, *J. Phys. Chem. C* **2013**, *117*, 17757, <https://doi.org/10.1021/jp405925q>.
- [147] W. Yan, L. Xu, C. Xu, W. Ma, H. Kuang, L. Wang, N. A. Kotov, *J. Am. Chem. Soc.* **2012**, *134*, 15114, <https://doi.org/10.1021/ja3066336>.
- [148] Y. Zhao, L. Xu, L. M. Liz-Marzán, H. Kuang, W. Ma, A. Asenjo-García, F. J. García de Abajo, N. A. Kotov, L. Wang, C. Xu, *J. Phys. Chem. Lett.* **2013**, *4*, 641, <https://doi.org/10.1021/jz400045s>.
- [149] S. D. Jhaveri, E. E. Foos, D. A. Lowy, E. L. Chang, A. W. Snow, M. G. Ancona, *Nano Lett.* **2004**, *4*, 737, <https://doi.org/10.1021/nl0499591>.
- [150] X. Zhang, L. Liu, J. Tian, J. Zhang, H. Zhao, *Chem. Commun.* **2008**, 6549, <https://doi.org/10.1039/B815778B>.
- [151] J. Tian, F. Zheng, Q. Duan, H. Zhao, *J. Mater. Chem.* **2011**, *21*, 16928, <https://doi.org/10.1039/C1JM11384D>.
- [152] X. Zhang, Y. Yang, J. Tian, H. Zhao, *Chem. Commun.* **2009**, 3807, <https://doi.org/10.1039/B906967D>.
- [153] J. Tian, L. Yuan, M. Zhang, F. Zheng, Q. Xiong, H. Zhao, *Langmuir* **2012**, *28*, 9365, <https://doi.org/10.1021/la301453n>.
- [154] J. Tian, G. Liu, C. Guan, H. Zhao, *Polym. Chem.* **2013**, *4*, 1913, <https://doi.org/10.1039/C2PY20967E>.
- [155] T.-J. Yim, Y. Wang, X. Zhang, *Nanotechnology* **2008**, *19*, 435605, <https://doi.org/10.1088/0957-4484/19/43/435605>.
- [156] T. Dadosh, Y. Gordin, R. Krahn, I. Khivrich, D. Mahalu, V. Frydman, J. Sperling, A. Yacoby, I. Bar-Joseph, *Nature* **2005**, *436*, 677, <https://doi.org/10.1038/nature03898>.
- [157] A. S. D. S. Indrasekara, B. J. Paladini, D. J. Naczynski, V. Starovoytov, P. V. Moghe, L. Fabris, *Adv. Healthc. Mater.* **2013**, *2*, 1370, <https://doi.org/10.1002/adhm.201200370>.
- [158] F. Huo, A. K. R. Lytton-Jean, C. A. Mirkin, *Adv. Mater.* **2006**, *18*, 2304, <https://doi.org/10.1002/adma.200601178>.
- [159] A. Ulfkjær, F. W. Nielsen, H. Al-Kerdi, T. Ruß, Z. K. Nielsen, J. Ulstrup, L. Sun, K. Moth-Poulsen, J. Zhang, M. Pittelkow, *Nanoscale* **2018**, *10*, 9133, <https://doi.org/10.1039/C8NR01622D>.
- [160] J. G. Worden, A. W. Shaffer, Q. Huo, *Chem. Commun.* **2004**, 518, <https://doi.org/10.1039/B312819A>.
- [161] J. G. Worden, Q. Dai, A. W. Shaffer, Q. Huo, *Chem. Mater.* **2004**, *16*, 3746, <https://doi.org/10.1021/cm048907+>.
- [162] Z. Zhang, F. Rong, Y. Xie, Y. Wang, H. Yang, D. Fu, *J. Nanosci. Nanotech.* **2011**, *11*, 2163, <https://doi.org/10.1166/jnn.2011.3132>.
- [163] Q. Dai, J. G. Worden, J. Trullinger, Q. Huo, *J. Am. Chem. Soc.* **2005**, *127*, 8008, <https://doi.org/10.1021/ja042610v>.
- [164] J. G. Worden, Q. Dai, Q. Huo, *Chem. Commun.* **2006**, 1536, <https://doi.org/10.1039/B600641H>.
- [165] W. Sun, Q. Dai, J. G. Worden, Q. Huo, *J. Phys. Chem. B* **2005**, *109*, 20854, <https://doi.org/10.1021/jp055109d>.
- [166] G. Ramakrishna, Q. Dai, J. Zou, Q. Huo, T. Goodson, *J. Am. Chem. Soc.* **2007**, *129*, 1848, <https://doi.org/10.1021/ja067123p>.
- [167] O. Abed, A. Vaskevich, R. Arad-Yellin, A. Shanzer, I. Rubinstein, *Chem. Eur. J.* **2005**, *11*, 2836, <https://doi.org/10.1002/chem.200401171>.
- [168] K.-M. Sung, D. W. Mosley, B. R. Peelle, S. Zhang, J. M. Jacobson, *J. Am. Chem. Soc.* **2004**, *126*, 5064, <https://doi.org/10.1021/ja049578p>.

- [169] C.-P. Chak, S. Xuan, P. M. Mendes, J. C. Yu, C. H. K. Cheng, K. C.-F. Leung, *ACS Nano* **2009**, *3*, 2129, <https://doi.org/10.1021/nn9005895>.
- [170] C.-P. Chak, J. M. Y. Lai, K. W. Y. Sham, C. H. K. Cheng, K. C.-F. Leung, *RSC Adv.* **2011**, *1*, 1342, <https://doi.org/10.1039/C1RA00304F>.
- [171] X. Liu, J. G. Worden, Q. Dai, J. Zou, J. Wang, Q. Huo, *Small* **2006**, *2*, 1126, <https://doi.org/10.1002/smll.200600162>.
- [172] J. Zou, Q. Dai, J. Wang, X. Liu, Q. Huo, *J. Nanosci. Nanotech.* **2007**, *7*, 2382, <https://doi.org/10.1166/jnn.2007.424>.
- [173] J.-H. Kim, J.-W. Kim, *Langmuir* **2008**, *24*, 5667, <https://doi.org/10.1021/la800506g>.
- [174] M. R. Dewi, T. A. Gschneidner, S. Elmas, M. Ranford, K. Moth-Poulsen, T. Nann, *ACS Nano* **2015**, *9*, 1434, <https://doi.org/10.1021/nn5058408>.
- [175] C. Casagrande, M. Veyssié, *C. R. Acad. Sci. Paris* **1988**, *306*, 1423.
- [176] B. Dong, B. Li, C. Y. Li, *J. Mater. Chem.* **2011**, *21*, 13155, <https://doi.org/10.1039/C1JM12866C>.
- [177] B. Li, C. Y. Li, *J. Am. Chem. Soc.* **2007**, *129*, 12, <https://doi.org/10.1021/ja0668318>.
- [178] V. Paraschiv, S. Zapotoczny, M. R. de Jong, G. J. Vancso, J. Huskens, D. N. Reinhoudt, *Adv. Mater.* **2002**, *14*, 722, [https://doi.org/10.1002/1521-4095\(20020517\)14:10<722::AID-ADMA722>3.0.CO;2-T](https://doi.org/10.1002/1521-4095(20020517)14:10<722::AID-ADMA722>3.0.CO;2-T).
- [179] Z. Li, E. Cheng, W. Huang, T. Zhang, Z. Yang, D. Liu, Z. Tang, *J. Am. Chem. Soc.* **2011**, *133*, 15284, <https://doi.org/10.1021/ja205712a>.
- [180] G. L. Liu, Y.-T. Long, Y. Choi, T. Kang, L. P. Lee, *Nature Methods* **2007**, *4*, 1015, <https://doi.org/10.1038/nmeth1133>.
- [181] D. B. Steabben, *Br. J. Exp. Pathol.* **1925**, *6*, 1.
- [182] G. S. Huang, Y.-S. Chen, H.-W. Yeh, *Nano Lett.* **2006**, *6*, 2467, <https://doi.org/10.1021/nl061598x>.
- [183] G. S. Huang, Yu-Shiun Chen, Xin-Yau Lin, in '2007 7th IEEE Conference on Nanotechnology (IEEE NANO)', **2007**, pp. 7, <https://doi.org/10.1109/NANO.2007.4601129>.
- [184] Y.-S. Chen, M.-Y. Hong, G. S. Huang, *Nat. Nanotechnol.* **2012**, *7*, 197, <https://doi.org/10.1038/nnano.2012.7>.

License and Terms



This is an Open Access article under the terms of the Creative Commons Attribution License CC BY 4.0. The material may not be used for commercial purposes.

The license is subject to the CHIMIA terms and conditions: (<http://chimia.ch/component/sppagebuilder/?view=page&id=12>).

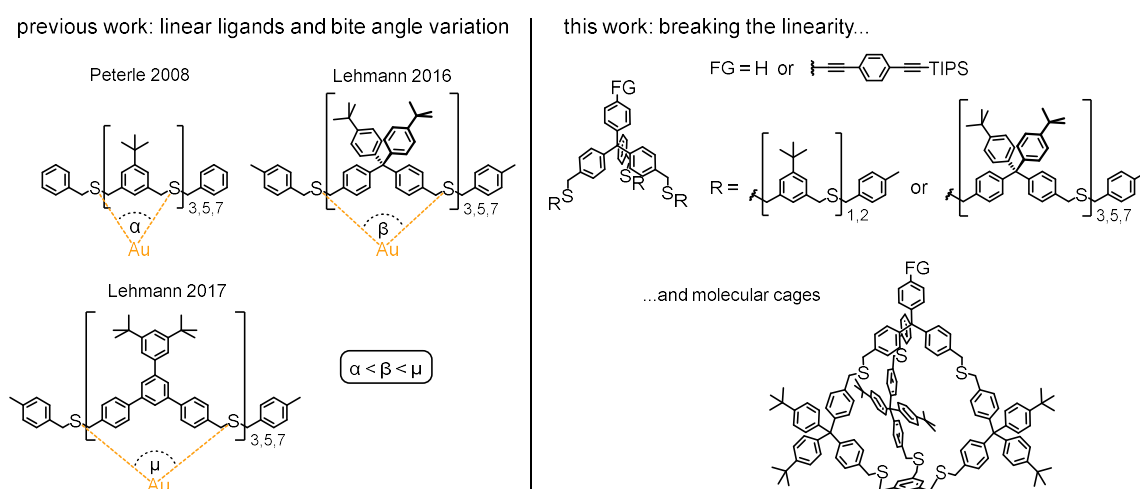
The definitive version of this article is the electronic one that can be found at <https://doi.org/10.2533/chimia.2021.414>

About the Project

This project aims at the reliable synthesis of stable, monofunctionalized gold nanoparticles. As outlined in the preceding review article, there are, in principle, two ways of achieving this goal: (1) using a single, large enough ligand which passivates the entire surface of a nanoparticle and contains a single chemically addressable moiety or (2) stabilizing the particles with multiple ligands whereof only one bears a functionality of interest. Our attention was drawn to the former case since it allows insight into the ligand architecture-dependence of the size and stability of the gold nanoparticles. In order to follow this endeavor, we chose to use ligands bearing benzylic thioethers as anchoring group for the surface of the particles, exploiting the flexibility of the benzylic position and the thioether's quasi-reversible, physisorbed-type bond to the gold.^[1,2] Earlier contributions in this group comprised variation of the number of sulfur atoms in oligomeric ligand chains,^[3–5] studies on the bite angle of the ligand^[6] as well as monofunctionalized dendrimer structures that enable the controlled synthesis of nanoparticle superstructures.^[7,8] In direct continuation of these foregoing efforts the benzylic thioether ligand design was improved by the introduction of a branching point which enabled surficial rather than linear coverage of the particles and allowed the study of the influence of different side-chains on the particle size and stability (see Scheme 5).

As a proof of concept, we were able to show that branched ligands can stabilize gold nanoparticles in a 1:1 ligand-to-particle fashion, which are, moreover, highly stable against thermal stress. Hereby, elongating or exchanging the side-chain had very little influence on the particle size but on the stability: it was found that bulky side-chains gave more stable particles. The exceptional stability of our gold nanoparticles was further exploited by the introduction of a rigid TIPS-protected acetylene-terminated OPE to the free phenyl. The OPE was used for oxidative acetylene homocoupling as well as CuAAC “click” chemistry with 1,3,5-tris(4-(azidomethyl)phenyl)benzene as shown by di- and trimerization reaction protocols without losses in particle stability. It is noteworthy that, in contrast to our earlier systems,^[9,10] the nanoparticle superstructures presented in this thesis were repeatedly dried, redispersed and columned without any material perdition, corroborating the ligand's excellent stabilization properties. In a last step, the branched tripodal structure was macrocyclized to form a cage which gave monofunctionalized gold nanoparticles of so far unmatched stability for thioether-based systems. Contrary to our previous systems, here it is the cage cavity that templated the nanoparticle size and not the nucleating particle that governed the ligand conformation.

The detailed concepts, syntheses and characterizations of the ligands as well as the gold nanoparticles are described in the ensuing manuscripts.



Scheme 5 Previously published systems relied on a high number of sulfides per ligand, variation of the bite angle and were linear. The approach presented in this thesis uses a two-dimensional ligand architecture to give better coverage of the gold nanoparticle surface. Additionally, functional groups (FG) for monofunctionalization are introduced to the free phenyl in the branching subunit.

References

- [1] M. S. Inkpen, Z.-F. Liu, H. Li, L. M. Campos, J. B. Neaton, L. Venkataraman, *Nat. Chem.* **2019**, *11*, 351.
- [2] H. Häkkinen, *Nat. Chem.* **2012**, *4*, 443–455.
- [3] T. Peterle, A. Leifert, J. Timper, A. Sologubenko, U. Simon, M. Mayor, *Chem. Commun.* **2008**, 3438–3440.
- [4] M. Lehmann, E. H. Peters, M. Mayor, *Chem. – Eur. J.* **2016**, *22*, 2261–2265.
- [5] T. Peterle, P. Ringler, M. Mayor, *Adv Funct Mater* **2009**, *19*, 3497–3506.
- [6] M. Lehmann, E. H. Peters, M. Mayor, *Helv. Chim. Acta* **2017**, *100*, e1600395.
- [7] J. P. Hermes, F. Sander, U. Fluch, T. Peterle, D. Thompson, R. Urbani, T. Pfohl, M. Mayor, *J. Am. Chem. Soc.* **2012**, *134*, 14674–14677.
- [8] F. Sander, U. Fluch, J. P. Hermes, M. Mayor, *Small* **2014**, *10*, 349–359.
- [9] J. P. Hermes, F. Sander, U. Fluch, T. Peterle, D. Thompson, R. Urbani, T. Pfohl, M. Mayor, *J. Am. Chem. Soc.* **2012**, *134*, 14674–14677.
- [10] F. Sander, U. Fluch, J. P. Hermes, M. Mayor, *Small* **2014**, *10*, 349–359.

FULL PAPER

Nanoparticles

Particle

& Particle Systems Characterization

www.particle-journal.com

Gold Nanoparticles Stabilized by Single Tripodal Ligands

Erich Henrik Peters, Mario Lehmann, and Marcel Mayor*

In order to coat the entire surface of gold nanoparticles (AuNPs) by a single ligand, tripodal macromolecules comprising benzylic thioethers coordinating to the AuNP surface are synthesized and their abilities to stabilize AuNPs are investigated. Out of the five studied ligands 1–5, the tetraphenylmethane-based oligomers 4 and 5 display excellent AuNP coating features. Both ligand structures are able to control the dimensions of the AuNPs by stabilizing particles of narrow size distributions during their syntheses (1.05 ± 0.28 nm for Au-4, and 1.15 ± 0.34 nm for Au-5). Closer inspection of these AuNPs by transmission electron microscopy and thermogravimetric analyses suggests that single ligands 4 and 5 are able to stabilize entire AuNPs. These particles Au-4 and Au-5 are obtained in good yields and display promising thermal stabilities (110 °C for Au-4, and 95 °C for Au-5), making them interesting nanoscale inorganic–organic building blocks for further functionalization/processing by wet chemistry.

1. Introduction

Beyond its monetary value and inertness as a bulk material, colloidal gold has exerted great fascination on scientists in the past century and beyond.^[1–6] Due to their availability and ease of handling, thiol-based organic ligands have been in the focus of interest for the stabilization of gold nanoparticles (AuNPs) which found application in various fields such as catalysis,^[7–9] medical diagnostics,^[10] and therapeutics,^[11–14] chemical^[15–17] and biological sensing,^[18–23] molecular electronics^[24–26] or as building blocks for hybrid materials.^[27]

In the past decade, the variety of ligand designs has been enlarged toward benzylic sulfide-based oligomers due to their reversible binding to gold surfaces, enabling supramolecular approaches toward AuNP stabilization. The flexibility of the benzylic sulfide linkers enables favorable conformations of the ligands upon passivation of the AuNP and various ligand designs

have been investigated, ranging from oligomeric,^[28–33] tripodal,^[34,35] and dendrimeric^[36–41] to even cage-like^[42] thioether-based ligands, most of them yielding AuNPs with narrow size distributions. Cages controlling the size of the nanoparticles were also developed for other noble metals like palladium, displaying catalytic activity.^[43–45] Also, the periodically arranged cavities of a covalent organic framework were used as “caging” structure for catalytically active palladium and platinum particles.^[46]

It has furthermore been shown that such oligomeric benzyl sulfide ligand-stabilized AuNPs are accessible by wet chemical procedures, and ligand-coated AuNPs exposing reactive functional groups have been interlinked forming nanoarchitectures.^[29–31,37,38] In the approach, the ligand

not only controls the particles' sizes, but also the number and the spatial orientation of exposed functional groups.

While rather complex and synthetically demanding dendritic ligands already displayed their ability to stabilize an entire AuNP,^[36–39] a more recent ligand design showed that also linear oligomers are able to stabilize an entire particle when bulky enough to sterically protect the surface of the ligand-coated AuNP.^[32] With a series of linear oligomers of various sulfur–sulfur distances, a correlation between the size of the stabilized AuNP and both parameters, the distance between coordination points of these multivalent ligand structures and the equivalents of gold salt used has been observed.^[33] The study, however, also unraveled some limitations of the approach, namely an increasing loss over the control of the NP's size going along with a decrease in the stability of these AuNPs with increasing size.

An alternative approach to increase both the number of coordinating sulfide groups and the AuNP surface covered by the ligand is the use of suitable branching points, increasing the number of oligomeric branches per ligand. Further, such architectures break the linearity of the ligand, enabling better coverage of the surface of AuNPs upon passivation. Of particular interest was to which extent a local density of concave, pre-organized coordinating sites might steer the dimensions of the stabilized particle.

Already slightly larger AuNPs with diameters in the order of about 2 nm display surface plasmon bands and are thus interesting target structures opening the door for sensing and labeling applications.^[3] The here reported research is motivated by our interest in optically active, ligand-stabilized AuNPs with a controlled exposition of functional groups as potential building blocks for hybrid nanoarchitectures interacting with optical signals.

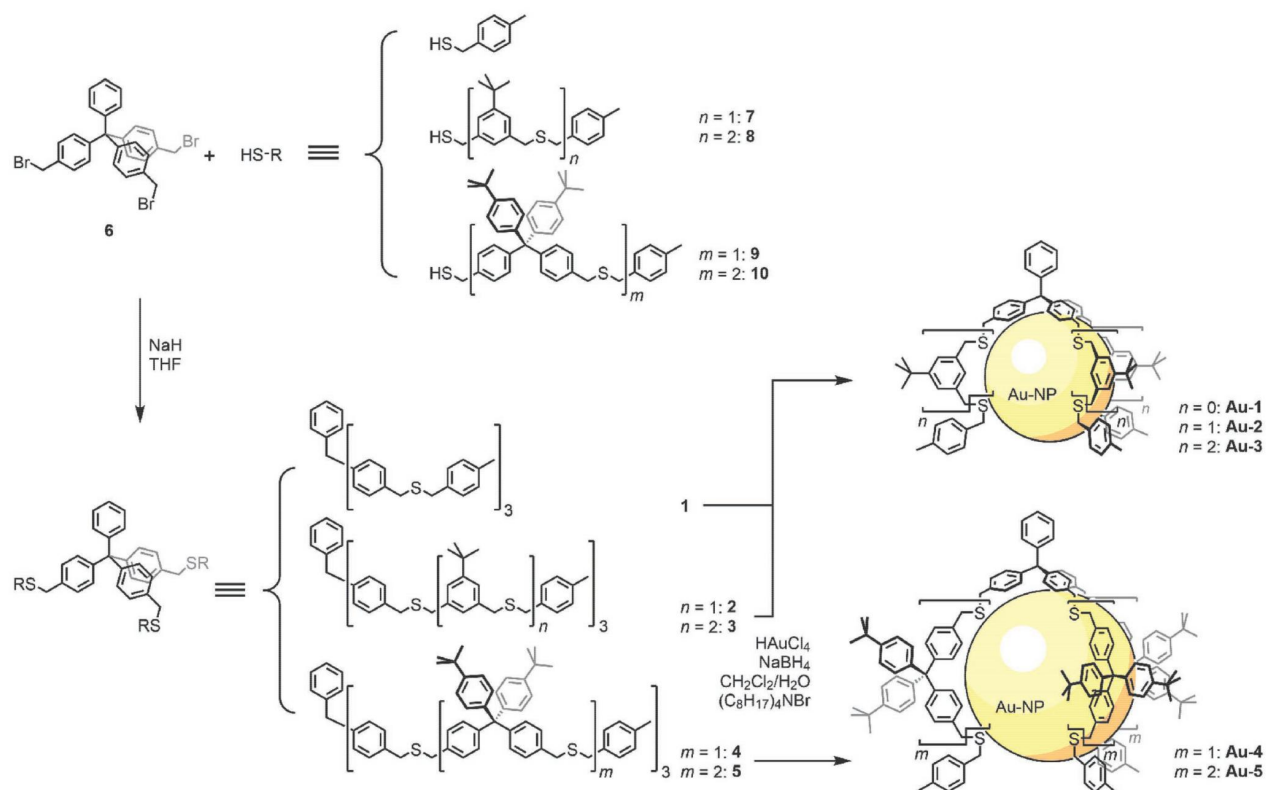
In order to benefit from surficial rather than linear coverage, we introduce a central tetraphenylmethane-based tripodal unit, which interlinks three oligomeric side-chains. In addition, the

E. H. Peters, Dr. M. Lehmann, Prof. M. Mayor
Department of Chemistry
University of Basel
St. Johanns-Ring 19, 4056 Basel, Switzerland
E-mail: marcel.mayor@unibas.ch

Prof. M. Mayor
Institute for Nanotechnology (INT)
Karlsruhe Institute of Technology (KIT)
P. O. Box 3640, 76021 Karlsruhe, Germany
Prof. M. Mayor
Lehn Institute of Functional Materials (LIFM)
Sun Yat-Sen University (SYSU)
Xingang Xi Rd. 135, 510275 Guangzhou, P. R. China

The ORCID identification number(s) for the author(s) of this article can be found under <https://doi.org/10.1002/ppsc.201800015>.

DOI: 10.1002/ppsc.201800015



Scheme 1. Overview over the ligand concept and the resulting AuNPs. The tripodal central linking unit **6** offers a free phenyl moiety for further functionalization. **6** reacts with oligomeric thioether side-chain thiols **7–10** or *p*-methylbenzylthiol via S_N2-substitution to give ligands **1–5**, which stabilize AuNPs by surface passivation.

fourth phenyl ring is expected to be arranged in an upright position, pointing away from the AuNP's surface and is thus ideally suited for the decoration with functional groups in a latter molecular design (see **Scheme 1**). Tripodal tetraphenylmethane-based structures exposing benzylic thiols have already been reported^[47–50] and we recently investigated similar model compounds exposing three phenylic thiols.^[50–53]

2. Results and Discussion

The approach toward ligand-stabilized AuNPs is sketched in Scheme 1. The series of benzylic thioether-based multidentate tripodal oligomers **1–5** were assembled and gold particles were synthesized by reduction of chloroauric acid in the presence of the ligand of interest. The ligand-stabilized particles **Au-1–Au-5** were purified by size-exclusion chromatography (SEC) and characterized. The thermal stability of the ligand-coated particles was investigated to explore the suitability of the ligand structure as potential building block for hybrid architectures based on covalently interlinked coated AuNPs.

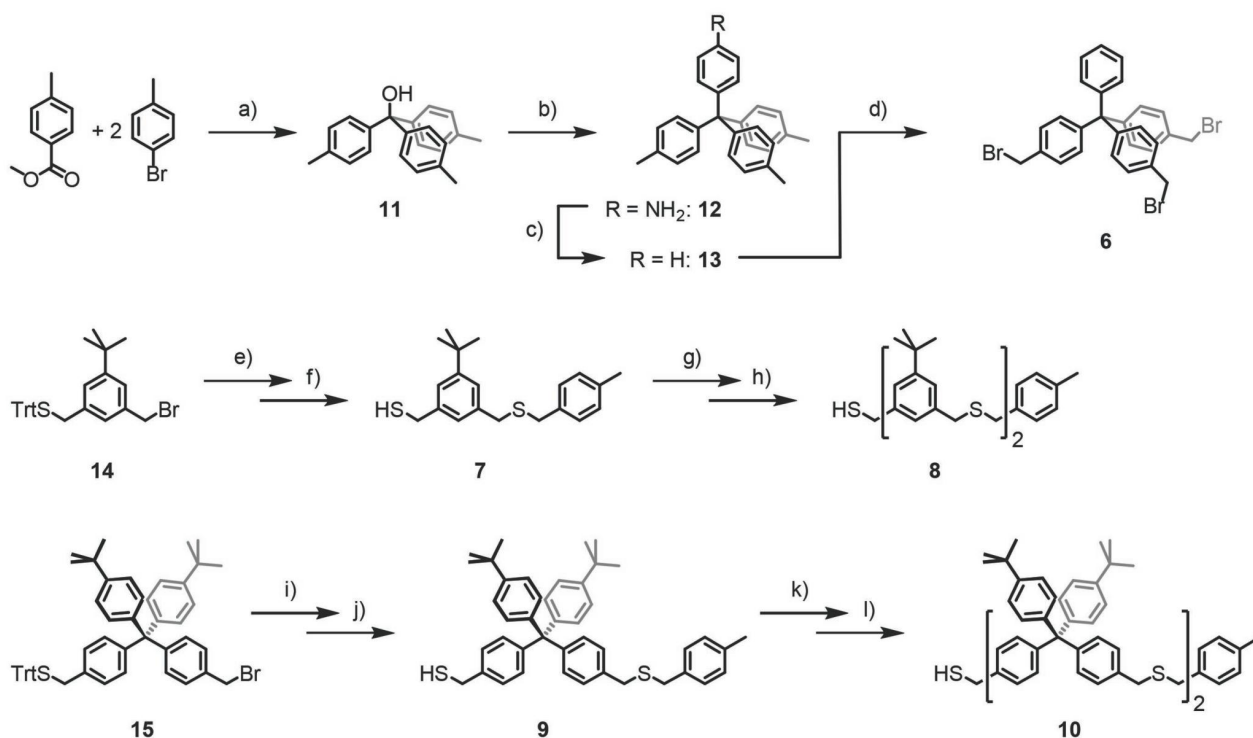
2.1. Ligand Syntheses

The syntheses of the tripodal ligand structures **1–5** are displayed in Scheme 1. The three benzylic bromides of **6** were substituted

with terminally thiol-functionalized linear oligomers **7–10** of various length and bulkiness.

The smallest tripodal ligand **1** was assembled by treating **6** with a considerable excess (6 equivalents) of the commercially available *p*-tolylmercaptan and 10 equivalents of sodium hydride (NaH) in degassed tetrahydrofuran (THF) for 15 h at room temperature. After aqueous work-up, the ligand **1** was isolated by column chromatography (CC) as pale yellow oil in very good 92% yield. The synthesis of **2** serves as representative example of the assembly of tripodal ligands with the more precious mercaptans that had to be synthesized. The central tetraphenyltribromide **6** and 3.5 equivalents of the benzylmercaptan **7** were treated with an excess (5–10 equivalents) of NaH in degassed THF for 2 h at room temperature. After aqueous workup, CC provided the tripodal ligand **2** in 77% isolated yield. Applying similar reaction conditions with the benzylic mercaptans **8**, **9**, and **10** provided the ligands **3**, **4**, and **5**. While **4** was isolated in 61% yield after CC, the two second generation ligands **3** and **5** were isolated by gel permeation chromatography (GPC) in 39%, respectively 89% yield.

The syntheses of the central tripodal building block **6** and the oligomers exposing a benzylic thiol **7–10** are displayed in **Scheme 2**. Both series of oligomers were assembled with a comparable strategy. With a bifunctional monomer (**14** and **15**) comprising a masked benzylic mercaptan and a benzylic bromide, the controlled elongation of the oligomer by a single repeat unit was possible. The terminal thiol of the *n*-generation



Scheme 2. Syntheses of the tripodal central linking subunit **6** and the benzyl thioether oligomers **7–10** with a terminal benzylic thiol. Reagents and conditions: a) 1) Mg, THF, reflux, 24 h; 2) H₂O, sat. NH₄Cl, 98%; b) aniline, HCl, AcOH, 140 °C, 3 h, 66 %; c) 1) BF₃OEt₂, ^tBuNO₂, THF, –10 °C, 2 h; 2) FeSO₄, DMF, 2.5 h; 3) H₂O, 0 °C 80%; d) NBS, AIBN, *hν*, methyl formate, reflux, 15 h, 50%; e) *p*-methylbenzylthiol, NaH, THF, rt, 2 h, 91%; f) Et₃SiH, TFA, DCM, rt, 1 h, 91%; g) **14**, NaH, THF, rt, 2 h, 79%; h) Et₃SiH, TFA, DCM, rt, 1 h, 77%; i) *p*-methylbenzylthiol, NaH, THF, rt, 2 h, 93% j) Et₃SiH, TFA, DCM, rt, 1 h, quant.; k) **15**, NaH, THF, rt, 2 h, 85%; l) Et₃SiH, TFA, DCM, rt, 1 h, 89%. rt: room temperature; Trt: trityl.

oligomer attacked the benzylic bromide of the bifunctional monomer, resulting in the *n*+1 generation oligomer after liberation of the masked benzylic mercaptan.

The central linking subunit **6** (Scheme 2) was synthesized using a modified literature protocol.^[54] Triphenylmethanol derivative **11** was obtained via twofold Grignard reaction of the Grignard reagent obtained from 1-bromo-4-methylbenzene and solid magnesium in THF with methyl *p*-toluate. Subsequent electrophilic aromatic substitution to aniline in glacial acetic acid (AcOH) with hydrochloric acid as catalyst gave tetraphenylmethane derivative **12**. Defunctionalization of the amine moiety towards compound **13** was carried out via in situ formation of the diazonium salt in dichloromethane (DCM) and subsequent treatment with iron sulfate in dimethylformamide. Finally, the central subunit **6** was obtained via Wohl-Ziegler reaction to compound **13** with *N*-bromosuccinimide (NBS) as a bromine source and azobis(isobutyronitril) (AIBN) as a radical starter in methyl formate, exploiting the solvent's low boiling point and therefore hindering the overbromination of the benzylic position upon illumination with a halogen lamp. The threefold benzylic bromide **6** as central building block was isolated by CC as white solid in a moderate yield of 26% over the four steps.

Mono- and dimeric side-chains **7** and **8** were obtained via a controlled stepwise deprotection–elongation strategy following a modification from a protocol previously reported by Peterle et al.^[28] (see Scheme 2). Asymmetrically trityl-protected benzylic

thiol **14** was end-capped with *p*-methylbenzylthiol and subsequently deprotected by treatment with trifluoroacetic acid (TFA) and Et₃SiH as cation scavenger in DCM to yield monomeric side-chain **7**. In contrast to the reported protocol, benzylthiol was replaced by *p*-methylbenzylthiol, providing more characteristic features in the ¹H NMR spectra of the model compounds. The S_N2-reaction of compounds **7** and **14** in THF in presence of NaH yielded the protected dimeric side-chain, which was converted to the free benzylic thiol **8**, using the same deprotection conditions as stated above.

For the mono- and dimeric side-chains **9** and **10**, the bifunctional monomer **15** was assembled in six steps following an already reported protocol.^[32] In short, a similar elongation–deprotection strategy as described for the side-chains **7** and **8** above was applied: monomeric side-chain **9** was obtained by end-capping with *p*-methylbenzylthiol followed by trityl deprotection under similar reaction conditions. Elongation with the bifunctional building block **15** followed by deprotection gave the dimer **10** with a terminal benzylic thiol.

All ligand precursors as well as ligands **1** and **2** were fully characterized by ¹H and ¹³C NMR spectroscopy, and high-resolution ESI–ToF mass spectrometry. The NMR-based characterizations of ligands **3–5** were complemented by their MALDI–ToF mass spectrometry data. Syntheses of previously published compounds **6**, **11–15**, as well as the trityl-protected side-chain precursors can be found in the Supporting Information.

2.2. Gold Particle Syntheses

AuNP syntheses from all five ligands 1–5 were carried out following an already implemented protocol^[28–33,36–38] based on a variation of the AuNP synthesis proposed by Brust et al.,^[55] but also considering the dimensional differences of the various ligands. In the aqueous phase of a biphasic system, one equivalent of gold salt (HAuCl₄) for each sulfur atom in the ligand, dissolved in the organic phase (DCM), was added. This means that 3 equivalents of HAuCl₄ were used for the tridentate ligand 1, 6 equivalents of the gold salt for the hexadentate ligands 2 and 4, and 9 equivalents of gold for the nonadentate ligands 3 and 5. The transfer of the gold salt from the aqueous to the organic phase was achieved by addition of tetra-*n*-octylammonium bromide (TOAB, 2 equivalents with respect to HAuCl₄) to the organic phase. Nucleation of the AuNPs was induced via reduction by addition of an aqueous solution of sodium borohydride (NaBH₄, 8 equivalents with respect to HAuCl₄). Upon addition of the reducing agent, an immediate color change of the organic phase from bright red to opaque dark brown was observed. After rigorous stirring for 15 min, the phases were separated and the particles were precipitated by addition of excess ethanol. Separation of the AuNPs from excess TOAB, NaBH₄ and ligand molecules was achieved by centrifugation and SEC. It is noteworthy that the colloidal gold particles were the only detectable form of gold throughout all syntheses, pointing at the favorable mass balance with respect to the precious metal. In the following, we will refer to the AuNPs by the coating ligands. For example, the AuNP coated with 1 will be named **Au-1**, the one coated with 2 **Au-2** and so on.

2.3. AuNP Analysis and Characterization

During synthesis, **Au-1** and **Au-2** did not show any signs of precipitation, suggesting reasonable ability of the ligands 1 and 2 to stabilize colloidal gold. However, their stability was limited to a few hours at RT, as formation of insoluble black powdery residue was observed during workup, pointing at aggregation of the particles. We therefore concluded that the ligands 1 and 2 provide only limited particle stabilization features, at least under the conditions of interest here. Also **Au-3** displayed limited stability features, but in a different time window. While it was stable for 5 d at room temperature, it took more than 10 d at –20 °C before indispersible black powdery residues were observed. While the delayed aggregation of **Au-3** enabled its characterization, the limited temporal stability reduces considerably its application potential and consequently also our interest in the structure. In general, it seems that only transiently stable AuNPs were obtained with these merely *p*-methylbenzylthiyl- and *m*-xylene-based oligomer-decorated tripodal ligand structures 1–3, and thus these particles **Au-1**, **Au-2**, and **Au-3** moved out of the focus of interest.

Much more promising were the features of **Au-4** and **Au-5**, which did not display any stability issues during the observation period (several months). The UV/UV-vis absorption spectra of **Au-4** and **Au-5** dissolved in DCM remain

constant over months with the samples stored at room temperature. Also, these AuNPs can be dried in vacuum and redissolved in DCM with neither any remaining indissoluble residue nor any observable alteration of the UV-vis spectra. It is important to note that the stability claims are exclusively for the here reported AuNPs, which were synthesized with one equivalent HAuCl₄ per sulfur atom in the ligand. Experiments using larger ratios of chloroauric acid resulted in larger particles with considerably reduced stability features, as will be discussed below. We attribute the large difference in the AuNP stabilities to the variation in bulkiness of the attached side-chains. It seems that the voluminous tetraphenylmethane-based side-chains of **Au-4** and **Au-5** sterically protect the coated AuNP much more efficiently than the considerably less bulky *m*-xylene-based side-chain of **Au-2** and **Au-3**.

The AuNPs **Au-3**, **Au-4**, and **Au-5** were analyzed and characterized by UV-vis absorption spectroscopy, ¹H NMR spectrometry, transmission electron microscopy (TEM) and thermogravimetric analysis (TGA). **Au-4** and **Au-5** were furthermore subjected to thermal stability experiments.

The UV-vis spectra of the three AuNPs are displayed in **Figure 1**. The very comparable spectra of the three AuNPs samples are pointing at comparable dimensions of the stabilized nanoparticles. Of particular interest is the absence of a plasmon band, which is characteristic for small particles with diameters smaller than 2 nm.^[3]

The ¹H NMR spectra of the AuNPs **Au-3**, **Au-4**, and **Au-5** are displayed in the Supporting Information of the article (Figure S1–S3, Supporting Information). They display the characteristic broadening of the ligand signals due to the reduced tumbling motion of the ¹H labels in comparison to the free ligands 3–5, corroborating that the ligands are tightly immobilized in a coating layer at the particle surface. Furthermore, the ¹H NMR spectra also document the successful separation of the coated AuNPs from the phase transfer catalyst TOAB and the excess ligand by repeated centrifugation and SEC.

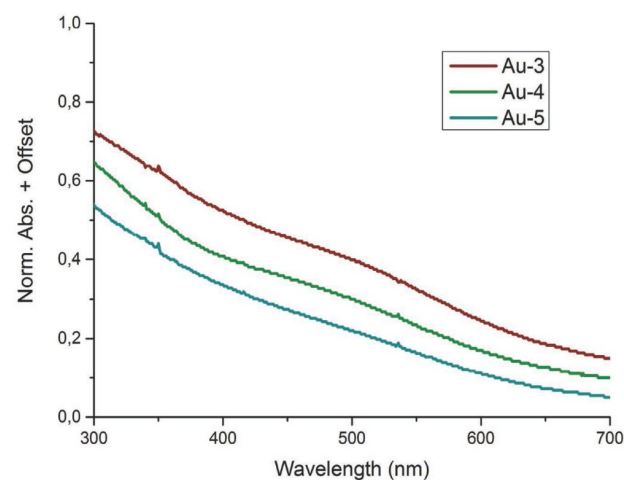


Figure 1. UV-vis absorption spectra of **Au-3**, **Au-4**, and **Au-5** recorded in DCM at room temperature and offset for clarity. The absence of a plasmon band points at AuNPs with diameters below 2 nm. The similarity of all three spectra suggests comparable particle sizes for all three samples.

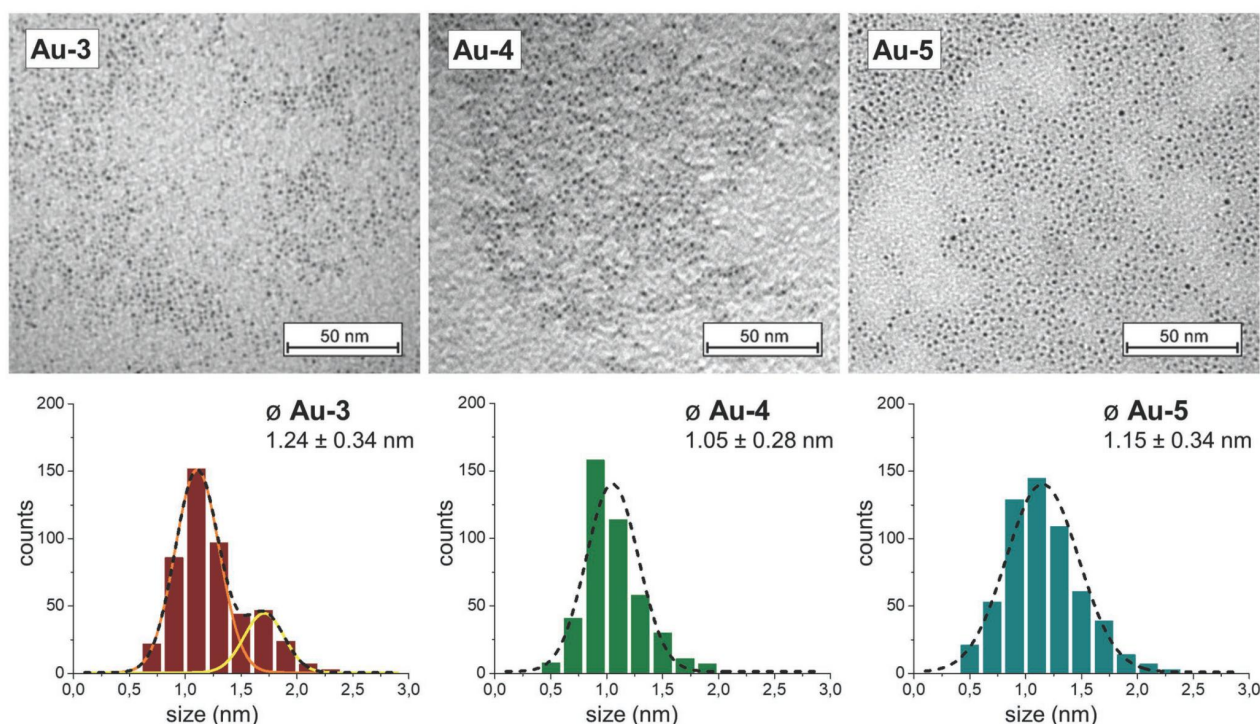


Figure 2. Representative TEM micrographs for the AuNPs **Au-3**, **Au-4**, and **Au-5** complemented by the size distributions extracted from the micrographs (Gaussian fits: black dashed lines).

The dimensions of the central Au-core of the three particles were analyzed by recording TEM pictures from samples prepared by spreading a DCM solution of the AuNP of interest on a TEM grid. Representative examples of the recorded TEM images are displayed in **Figure 2**. For the size determination of the AuNPs based on the recorded TEM images, the threshold and particle analysis functions of ImageJ^[56] were used. Profiting from the automated particle analyzing features of the program, the following diameters and size distributions were obtained: 1.24 ± 0.34 nm for **Au-3**, 1.05 ± 0.28 nm for **Au-4**, and 1.15 ± 0.34 nm for **Au-5**. The diameters of the AuNPs considerably below 2 nm are in agreement with the absence of a plasmon band in the UV-vis absorption spectra. While for **Au-4** and **Au-5** a reasonable size distribution was observed, the one obtained for **Au-3** seems to be the combination of particles of two different sizes. Applying a twofold Gaussian fit revealed about 80% of the particles belonging to a distribution with a maximum at 1.11 ± 0.20 nm (Gaussian fit: orange solid line in **Figure 2**), and about 20% of the AuNPs belonging to a second distribution with a maximum at about 1.71 ± 0.18 nm (Gaussian fit: yellow solid line). The sum of both distributions results in the size distribution of 1.24 ± 0.34 nm for **Au-3**.

It is tempting to hypothesize that this second maximum is the consequence of the AuNP agglomeration resulting in the limited stability of **Au-3**, already described before.

Of particular interest is the stoichiometry between coating ligand and stabilized AuNP. Profiting from the fact that the AuNPs have been purified by SEC and thus the samples comprise neither excess ligand nor remaining phase transfer catalysts, the ratio between coating ligand and Au-core was

determined by TGA after excessive drying of the AuNP samples in vacuum to get rid of solvent molecules. For all three samples (**Au-3**, **Au-4**, and **Au-5**), a considerable weight loss between 100 °C and 600 °C was observed which is due to the degradation/evaporation of the organic coating (see **Figure S4** in the Supporting Information). The recorded weight losses were 38.54% for **Au-3**, 25.97% for **Au-4**, and 30.71% for **Au-5**. With the diameters of the AuNPs determined by the TEM analyses, the volumes of the particles were estimated assuming perfect ball shapes. With these volumes and the bulk density of gold (19.32 g cm^{-3}), the mass of the average particle was determined and consequently also the number of gold atoms present in the average sized particle. The obtained numbers are summarized in **Table 1**.

In spite of the simplifying assumptions required for the estimation of the stoichiometry, the obtained ligand-to-particle ratios provide key information about each ligand's ability to enwrap the AuNP. As our strategy is to profit from the coating to introduce functional groups at the particles' periphery, ligands able to stabilize an entire particle are particularly appealing. While approximately 4 ligands **3** are required to cover the surface of the AuNP **Au-3**, the calculations suggest that a single ligand **4** or **5** seems to be able to passivate the entire surfaces of the AuNPs **Au-4** and **Au-5**, respectively.

An equally important feature as the ligand-to-particle ratio is the stability of the coated AuNP, determining the window of potential reaction conditions for subsequent wet chemical transformations. As experimentally accessible parameter, the thermal stabilities of the AuNPs were investigated. The AuNPs of interest were dispersed in *p*-xylene and starting at 40 °C, the temperature was ramped in 5 °C steps every 30 min while

Table 1. Ligand-to-gold ratio based on TGA analysis data.

Entry	m_{Lig} [mg]	M_{Lig} [g mol ⁻¹]	n_{Lig} [mol]	m_{Au} [mg]	n_{Au} [mol]	n_{Au} [mol]	NP \varnothing [nm]	Au/NP	Lig/NP
Au-3	1.53	1925	7.94×10^{-7}	2.44	1.23×10^{-5}	15.51	1.24 ± 0.34	58.97	3.80
Au-4	1.54	2243	6.87×10^{-7}	4.39	2.22×10^{-5}	32.30	1.05 ± 0.28	35.80	1.11
Au-5	1.25	3716	3.36×10^{-7}	2.82	1.42×10^{-5}	42.35	1.15 ± 0.34	47.04	1.11

m_{Lig} : mass of disappearing ligand; M_{Lig} : ligand molar mass; n_{Lig} : number of moles of ligand; m_{Au} : mass of remaining gold; n_{Au} : number of moles of gold; Au/Lig: average number of gold atoms per ligand; NP \varnothing : NP diameter; Au/NP: average number of gold atoms per NP; Lig/NP: average number of ligand per NP; Molar mass of gold: M_{Au} : 196.97 g mol⁻¹.

monitoring the sample by UV–vis spectroscopy. No alterations in the UV–vis spectra of **Au-4** and **Au-5** were observed up to 110 and 95 °C, respectively (see Figure S5 in the Supporting Information). At higher temperatures, the broad and featureless UV–vis absorption assigned to the Au core disappeared and the precipitation of black, insoluble material was observed, pointing at the uncontrolled agglomeration of AuNPs.

Interestingly, the AuNPs **Au-4** coated with the one generation smaller and thus synthetically easier accessible ligand **4** are thermally about 15 °C more stable than **Au-5** with the extended ligand structure **5**. It seems that the four central tetraphenylmethane subunits of **4** and **5** are coating the AuNP and that the additional three subunits of **5** do not contribute further to the AuNP surface passivation. In contrast, these bulky extensions either handicap the coating sterically or destabilize the coated particle by other effects like, e.g., offering additional coordination sites, which might lead to a less tight arrangement of the coating ligand.

2.4. Variation of the Ligand to Gold Salt Stoichiometry

While these AuNPs **Au-4** and **Au-5** stabilized by a single ligand are promising building blocks for hybrid architectures, they are too small to interact with visible light efficiently. To be able to compare the particle stabilization potential of the different ligand structures, the amount of gold salt employed during the AuNPs synthesis was so far fixed to the number of sulfur atoms present in the ligand structure. The limited availability of gold salt during the particles' syntheses is one of the factors defining the AuNP size and it might be that the dimensions of AuNPs being stabilized by a particular ligand structure are not fully explored with this restricted protocol. In order to explore the size limits of potentially stabilized AuNPs by **4** and **5**, the amount of HAuCl₄ used for the particle synthesis was doubled systematically.^[33,57,58] Thus the AuNP passivation features of **4** were also investigated with particles formed with 12 and 24 equivalents of chloroauric acid. It seems that the maximum size of AuNPs stabilized by **4** was already reached with 6 equivalents of gold salt, as the size distributions of these samples recorded by TEM all displayed very comparable maxima for the AuNP diameter of about 1 nm (see Figure S6 in the Supporting Information). The increased concentration of gold salt however, considerably reduced the stability of the particles. The particles **Au-4**_{24eq} obtained with 24 equivalents were not even stable enough for SEC to remove the remaining ligand and phase transfer catalyst. The samples **Au-4**_{12eq} synthesized with 12 equivalents were a little bit more stable and did not decompose during chromatography. However, the deposition of a gold film upon

extended storage (7 d) dissolved in DCM at –20 °C indicated as well a reduced stability compared to the parent sample **Au-4**_{6eq}.

With a comparable approach, the dimensional limits for AuNPs stabilized with **5** were investigated. The size distributions of the AuNPs synthesized with 18, 36, 72, and 144 equivalents of HAuCl₄ in the presence of **5** are displayed in Figure S7 in the Supporting Information. Also in the case of **5**, it seems that the ideal dimension of the AuNP coated by **5** is already reached with the initial protocol using 9 equivalents chloroauric acid, as the size distribution of **Au-5**_{18eq} with a maximum of 1.18 nm is barely shifted to larger diameters. With increasing equivalents of gold salt present, the maximum of the distributions shifts slightly to larger dimensions, accompanied by a pronounced broadening of the shoulder of the distribution towards larger particles. Also in the case of **5**-coated AuNPs, a reduced stability of too large AuNPs was observed, but at considerable larger dimensions compared to **4**. The sample **Au-5**_{72eq}, for example, was stable enough for the purification processes and for drying/re-dispersing cycles. Dispersed in DCM, however, **Au-5**_{72eq} displayed limited stability features comparable with those of **Au-4**_{12eq}. The samples **Au-5**_{18eq} and **Au-5**_{36eq} were even stable enough to determine the ligand-to-gold ratio by TGA (see Table S1 in the Supporting Information). While **Au-5**_{18eq} is, with 1.29 ligands per particle, only slightly above the favored 1/1 ratio, more than two ligands **5** are required to stabilize the average particle in **Au-5**_{36eq}.

3. Conclusion

A new tripodal central ligand motif has been developed to improve the surface coverage of benzylthioether-based oligomers upon passivation of AuNPs. The potential of the tripodal architecture has been explored by two different oligomer motifs, namely a *meta*-xylene-based motive (in **2** and **3**) and a tetraphenylmethane-based repeat unit (in **4** and **5**). In particular, the second series **4** and **5** displayed promising AuNP stabilization features. The particles **Au-4** and **Au-5** are not only isolated in excellent yields with respect to the gold salt, they are stable enough for purification by SEC. They have comparable dimensions of about 1.1 nm and in both cases, a single ligand is able to cover and stabilize the entire AuNP. Interestingly, improved thermal stability was recorded for **Au-4**, coated with the smaller ligand of the two.

We are currently further developing the easily accessible ligand motif by introducing functional groups at the remaining phenyl of the central tetraphenylmethane unit, in order to provide coated AuNPs as “heavy” molecules and labels attached by wet chemical coupling reactions.

4. Experimental Section

Materials: All commercially available starting materials were of reagent grade and used as received, unless stated differently. Absolute THF was purchased from J. T. Baker, stored over 4 Å molecular sieves, pre-dried with CaH, handled under argon and freshly distilled before each use. Pure DCM was purchased from J. T. Baker. Pure toluene was purchased from Romil. Pure DMF was purchased from Acros Organics. *tert*-butylmethyl ether (TBME), *c*-hexane, ethyl acetate (EtOAc), and DCM were used for purification and were of technical grade. CC purifications were carried out on SilicaFlash P60 (particle size 40–63 μm) from SiliCycle. Deuterated solvents were purchased from Cambridge Isotope Laboratories.

Equipment and Measurements: ¹H and ¹³C NMR spectra were recorded with a Bruker DPX 400 instrument (¹H resonance 400 MHz, ¹³C resonance 101 MHz) or a Bruker DRX 500 instrument (¹H resonance 500 MHz, ¹³C resonance 126 MHz) at 298 K. The chemical shifts (δ) are reported in ppm and are referenced to the residual proton signal of the deuterated solvent (CDCl₃: 7.26 ppm) for ¹H spectra or the carbon of the solvent (CDCl₃: 77.1 ppm) for ¹³C spectra. The coupling constants (J) are given in Hertz (Hz), the multiplicities are denoted as: s (singlet), d (doublet), t (triplet), m (multiplet), and br (broad). MALDI-ToF mass spectra were performed on a Bruker microflex mass spectrometer, calibrated with CsI₃, and α-cyano-4-hydroxycinnamic acid (unless stated differently) was used as matrix. Important signals are given in *m/z*. Gas chromatography-mass spectrometry (GC-MS) was performed on a Shimadzu GCMS-QP2010 SE gas chromatography system with a ZB-5HT inferno column (30 m × 0.25 m × 0.25 m), at 1 mL min⁻¹ He-flow rate (split = 20:1) with a Shimadzu mass detector (EI 70 eV). High-resolution mass spectra (HRMS) were measured as HR-ESI-ToF-MS with a Maxis 4G instrument from Bruker with the addition of formic acid. SEC for the purification of AuNPs was performed manually using Bio-Rad Bio-Beads S-X1 (operating range 600–14 000 g mol⁻¹) with DCM as eluent. For purification of the ligands, a (automated) Shimadzu Prominence System was used with SDV preparative columns from Polymer Standards Service (two Showdex columns in series, 20 mm × 600 mm each, exclusion limit: 30 000 g mol⁻¹) with chloroform as eluent. UV-vis measurements were recorded on a Shimadzu UV spectrometer UV-1800 using optical 1115F-QS Hellma cuvettes (10 mm light path). TEM was performed on a Philips CM100 TEM at 80 kV using copper grids (Cu-400HD) from Pacific Grid Tech. TGA was measured on a Mettler Toledo TGA/SDTA851^e with a heating rate of 10 °C min⁻¹.

(3-(*tert*-Butyl)-5-(((4-methylbenzyl)thio)methyl)benzyl)(trityl)sulfane (16): In a dry, degassed 25 mL one-neck flask, compound 14 (693 mg, 1.34 mmol, 1 eq.) and *p*-tolylmercaptan (273 μL, 2.02 mmol, 1.5 eq.) were dissolved in dry, degassed THF (7 mL). NaH (60% dispersed in mineral oil, 268.4 mg, 6.7 mmol, 5 eq.) was added to the solution, which was then allowed to stir at room temperature for 2 h. The reaction mixture was quenched with water, then extracted three times with TBME dried over Na₂SO₄ and the solvent removed in vacuo. The crude product was subjected to CC (c-hexane 10:1 DCM) to yield 16 as a white solid (698 mg, 91%). ¹H NMR (400 MHz, CDCl₃, δ): 7.49–7.46 (m, 6H), 7.33–7.19 (m, 9H), 7.18–7.07 (m, 4H), 7.00–6.97 (m, 1H), 6.90–6.87 (m, 1H), 3.52 (d, *J* = 2.9 Hz, 4H), 3.31 (d, *J* = 1.4 Hz, 2H), 2.32 (s, 3H), 1.27 (s, 9H). ¹³C NMR (101 MHz, CDCl₃, δ): 151.57, 144.88, 137.99, 137.02, 136.59, 135.17, 129.78, 129.21, 129.03, 128.01, 126.97, 126.77, 125.03, 124.82, 67.62, 37.30, 35.72, 35.35, 34.70, 31.41, 21.20. HRMS (ESI): *m/z* = [M + Na]⁺ calcd for C₃₉H₄₀NaS₂ 595.2464; found, 595.2464.

(3-(*tert*-Butyl)-5-(((4-methylbenzyl)thio)methyl)phenyl)methanethiol (7): In a 25 mL one-neck flask, compound 16 (698 mg, 1.22 mmol, 1 eq.) was dissolved in DCM (6 mL). Triethylsilane (590 μL, 3.66 mmol, 3 eq.) was added to the solution, which was then bubbled with argon for 15 min after which time trifluoroacetic acid (240 μL, 4% of DCM volume) was added to the solution. An immediate color change to a bright yellow hue which faded a few seconds after was observed. The mixture was stirred for another hour at room temperature before quenching upon addition of saturated aqueous sodium bicarbonate. The aqueous phase was extracted three times with DCM, the combined organic phase was

dried over Na₂SO₄ and the solvent was removed in vacuo. The crude product was subjected to column chromatography (c-hexane 10:1 DCM) to yield 7 as colorless oil (368 mg, 91%). ¹H NMR (400 MHz, CDCl₃, δ): 7.21–7.10 (m, 6H), 7.07 (t, *J* = 1.6 Hz, 1H), 3.72 (d, *J* = 7.5 Hz, 2H), 3.57 (s, 4H), 1.27 (s, 3H), 1.76 (t, *J* = 7.5 Hz, 1H), 1.31 (s, 9H). ¹³C NMR (101 MHz, CDCl₃, δ): 151.78, 140.92, 138.26, 136.60, 135.08, 129.18, 128.95, 125.88, 125.00, 123.73, 35.73, 35.46, 34.73, 31.39, 29.18, 21.16. HRMS (ESI): *m/z* = [M + Na]⁺ calcd for C₂₀H₂₆NaS₂ 353.1369; found 353.1368.

(3-(*tert*-Butyl)-5-(((3-(*tert*-butyl)-5-(((4-methylbenzyl)thio)methyl)benzyl)thio)methyl)benzyl)(trityl)sulfane (17): In a dry, degassed 25 mL one-neck flask, compound 7 (56.2 mg, 0.17 mmol, 1 eq.) and compound 14 (87.4 mg, 0.17 mmol, 1 eq.) were dissolved in dry THF (10 mL), and bubbled with argon for 15 min. NaH (60% dispersion in mineral oil, 17.1 mg, 0.428 mmol, 7.4 eq.) was added to the mixture, which was then stirred for 2 h at room temperature, and then quenched by addition of water. The aqueous phase was extracted three times with TBME, and the combined organic fraction was dried over Na₂SO₄. The solvent was removed in vacuo. The crude product was subjected to CC (c-hexane 10:1 DCM) to afford 17 as pale, colorless solid (102.8 mg, 79%). ¹H NMR (400 MHz, CDCl₃, δ): 7.53–7.41 (m, 6H), 7.36–7.01 (m, 17H), 6.99 (s, 1H), 6.91 (s, 1H), 3.55 (d, *J* = 2.2 Hz, 8H), 3.31 (s, 2H), 2.31 (s, 3H), 1.30 (s, 9H), 1.27 (s, 9H). ¹³C NMR (101 MHz, CDCl₃, δ): 151.61, 151.52, 144.82, 138.05, 138.03, 138.00, 137.11, 136.55, 135.14, 129.74, 129.19, 128.98, 127.98, 126.86, 126.84, 126.74, 124.90, 124.85, 124.70, 67.61, 37.26, 35.97, 35.84, 35.46, 34.70, 34.68, 31.46, 31.42, 21.18. HRMS (ESI): *m/z* = [M + Na]⁺ calcd for C₅₁H₅₆NaS₂ 787.3437; found 787.3436.

(3-(*tert*-Butyl)-5-(((3-(*tert*-butyl)-5-(((4-methylbenzyl)thio)methyl)benzyl)thio)methyl)phenyl)methanethiol (8): In a 25 mL one-neck flask, dimeric branch compound 17 (100 mg, 0.131 mmol, 1 eq.) was dissolved in DCM (5 mL). Triethylsilane (63.4 μL, 0.393 mmol, 3 eq.) was added to the mixture, which was then bubbled with argon for 15 min. Trifluoroacetic acid (200 μL, 4% of DCM volume) was added to the mixture upon which an immediate color change to bright yellow and a subsequent fading of the color was observed. The reaction mixture was allowed to stir at room temperature for 2 h, then quenched by addition of saturated aqueous sodium bicarbonate. The aqueous phase was extracted three times with DCM. The combined organic phase was dried over Na₂SO₄ and the solvent was removed in vacuo. The crude product was subjected to CC (c-hexane 10:1 DCM) to afford 8 as colorless oil (53 mg, 77%). ¹H NMR (400 MHz, CDCl₃, δ): 7.24–7.15 (m, 6H), 7.14–7.07 (m, 4H), 3.73 (d, *J* = 7.5 Hz, 2H), 3.60 (dd, *J* = 6.8, 2.3 Hz, 8H), 2.34 (s, 3H), 1.77 (t, *J* = 7.5 Hz, 1H), 1.33 (s, 9H), 1.33 (s, 9H). ¹³C NMR (101 MHz, CDCl₃, δ): 151.90, 151.55, 140.96, 138.28, 138.00, 136.57, 135.11, 129.19, 128.96, 126.86, 125.90, 124.94, 124.86, 124.70, 123.80, 35.99, 35.89, 35.85, 35.50, 34.76, 34.70, 31.44, 31.43, 29.18, 21.17. HRMS (ESI): *m/z* = [M + Na]⁺ calcd for C₃₂H₄₂NaS₂ 545.2341; found 545.2341.

(4-(*Bis*(4-(*tert*-butyl)phenyl)-4-(((4-methylbenzyl)thio)methyl)phenyl)methyl)benzyl)(trityl)sulfane (18): To a dry, degassed 25 mL one-neck flask, compound 15 (35 mg, 0.043 mmol, 1 eq.) was added and dissolved in dry THF (2 mL). *p*-tolylmercaptan (8.8 μL, 0.065 mmol, 1.5 eq.) was added to the solution, which was then bubbled for 15 min. NaH (60% dispersed in mineral oil, 8.6 mg, 0.215 mmol, 5 eq.) was added to the reaction mixture. The mixture was stirred at room temperature for 2 h, and then quenched by addition of water, extracted two times with TBME, dried over Na₂SO₄ and the solvent was removed in vacuo. The crude product was subjected to CC (c-hexane 10:1 DCM) to afford 18 as pale, yellowish solid (35 mg, 93%). ¹H NMR (400 MHz, CDCl₃, δ): 7.48–7.42 (m, 6H), 7.30–6.98 (m, 29H), 3.56 (d, *J* = 10.5 Hz, 4H), 3.28 (s, 2H), 2.31 (s, 3H), 1.29 (s, 18H). ¹³C NMR (101 MHz, CDCl₃, δ): 148.45, 146.00, 145.85, 144.73, 143.66, 136.55, 135.52, 135.13, 134.33, 131.24, 130.67, 129.66, 129.16, 128.91, 128.10, 127.94, 126.70, 124.21, 67.42, 63.69, 36.66, 35.49, 35.23, 34.33, 31.40, 29.74, 21.14. HRMS (ESI): *m/z* = [M + Na]⁺ calcd for C₆₂H₆₂NaS₂ 893.4186; found 893.4185.

(4-(*Bis*(4-(*tert*-butyl)phenyl)-4-(((4-methylbenzyl)thio)methyl)phenyl)methyl)phenyl)methanethiol (9): In a 25 mL one-neck flask, compound 18 (91 mg, 0.104 mmol, 1 eq.) was dissolved in DCM (5 mL). After addition of triethylsilane (150.9 μL, 0.936 mmol, 9 eq.), the solution was bubbled with argon for 20 min after which time trifluoroacetic acid

(200 μL , 4% of DCM volume) was added to the mixture. An immediate color change to yellow, lasting for 30 s was observed. The mixture was stirred 1 h at room temperature. The reaction was quenched by addition of saturated aqueous sodium bicarbonate. The aqueous phase was extracted three times with DCM, dried over Na_2SO_4 and the solvent was removed in vacuo. The crude product was subjected to CC (c-hexane 10:1 DCM) to afford 9 as colorless oil (65.6 mg, quant.). ^1H NMR (400 MHz, CDCl_3 , δ): 7.26–7.21 (m, 4H), 7.20–7.12 (m, 10H), 7.12–7.06 (m, 6H), 3.70 (d, $J = 7.5$ Hz, 2H), 3.57 (d, $J = 9.8$ Hz, 4H), 2.31 (s, 3H), 1.75 (t, $J = 7.5$ Hz, 1H), 1.30 (s, 18H). ^{13}C NMR (101 MHz, CDCl_3 , δ): 148.54, 146.06, 145.84, 143.65, 138.40, 136.57, 135.62, 135.14, 131.47, 131.28, 130.72, 129.18, 128.93, 127.98, 127.00, 124.27, 63.72, 35.54, 35.26, 34.36, 31.43, 28.58, 21.17. HRMS (ESI): $m/z = [\text{M} + \text{Na}]^+$ calcd for $\text{C}_{43}\text{H}_{48}\text{NaS}_2$ 651.3090; found 651.3090.

(4-(Bis(4-(*tert*-butyl)phenyl) (4-(((4-methylbenzyl)thio)methyl)phenyl)methyl)benzyl) (4-(bis(4-(*tert*-butyl)phenyl) (4-(tritylthio)methyl)phenyl)methyl)benzyl) sulfane (19): In a dry, degassed 25 mL one-neck flask, compound 9 (73.2 mg, 0.119 mmol, 1 eq.) and branch precursor 15 (107 mg, 0.131 mmol, 1.1 eq.) were dissolved in dry THF (5 mL), and bubbled with argon for 15 min. NaH (60% dispersion in mineral oil, 23.8 mg, 0.595, 5 eq.) was added to the mixture, which was then stirred for 2 h at room temperature, and then quenched by addition of water. The mixture was extracted three times with TBME, dried over Na_2SO_4 and the solvent was removed in vacuo. The crude product was subjected to CC (c-hexane 10:1 DCM) to afford 19 as pale solid (136 mg, 85%). ^1H NMR (400 MHz, CDCl_3 , δ): 7.48–7.43 (m, 6H), 7.35–7.01 (m, 43H), 7.02–6.98 (m, 2H), 3.60 (d, $J = 2.4$ Hz, 4H), 3.58 (d, $J = 9.5$ Hz, 4H), 3.27 (s, 2H), 2.32 (s, 3H), 1.29 (s, 18H), 1.28 (s, 18H). ^{13}C NMR (101 MHz, CDCl_3 , δ): 148.49, 148.42, 145.96, 145.92, 145.90, 145.84, 144.70, 143.65, 143.62, 136.54, 135.55, 135.43, 135.36, 135.10, 134.30, 131.28, 131.25, 131.19, 130.68, 130.63, 129.68, 129.63, 129.14, 128.88, 128.40, 128.08, 127.92, 127.77, 127.72, 126.67, 124.21, 124.19, 67.39, 63.70, 63.66, 35.49, 35.37, 35.23, 34.32, 34.30, 34.28, 31.38, 31.37, 21.12. HRMS (ESI): $m/z = [\text{M} + \text{Na}]^+$ calcd for $\text{C}_{97}\text{H}_{100}\text{NaS}_3$ 1384.6913; found 1384.6912.

(4-(((4-(((4-(Bis(4-(*tert*-butyl)phenyl) (4-(((4-methylbenzyl)thio)methyl)phenyl)methyl)benzyl)thio)methyl)phenyl)bis(4-(*tert*-butyl)phenyl)methyl)phenyl)methanethiol) (10): To a solution of compound 19 (117 mg, 0.086 mmol, 1 eq.) in DCM (5 mL) in a 25 mL one-neck flask, triethylsilane (41.6 μL , 0.258 mmol, 3 eq.) was added. After bubbling the solution with argon for 15 min, trifluoroacetic acid (200 μL , 4% of DCM volume) was added upon which a brief color to bright yellow was observed. The reaction mixture was allowed to stir at room temperature for 1 h, and was thereafter quenched by addition of saturated aqueous sodium bicarbonate. The aqueous phase was extracted three times with DCM, dried over Na_2SO_4 and the solvent was removed in vacuo. The crude product was subjected to CC (c-hexane 10:1 DCM) to afford 10 as pale solid (86 mg, 89%). ^1H NMR (400 MHz, CDCl_3 , δ): 7.25–7.03 (m, 36H), 3.71 (d, $J = 7.5$ Hz, 2H), 3.63–3.54 (m, 8H), 2.32 (s, 3H), 1.75 (t, $J = 7.5$ Hz, 1H), 1.29 (s, 18H), 1.29 (s, 18H). ^{13}C NMR (101 MHz, CDCl_3 , δ): 148.65, 146.16, 146.08, 146.03, 145.98, 143.79, 143.73, 143.69, 138.50, 136.69, 135.69, 135.57, 135.53, 135.55, 135.24, 131.56, 131.43, 131.40, 131.38, 130.82, 130.79, 129.28, 129.02, 128.09, 128.06, 127.09, 124.37, 124.35, 63.84, 63.82, 35.65, 35.51, 35.38, 34.46, 31.52, 28.67, 21.26. HRMS (ESI): $m/z = [\text{M} + \text{Na}]^+$ calcd for $\text{C}_{78}\text{H}_{88}\text{NaS}_3$ 1141.5784; found 1141.5784.

((Phenylmethanetriyl)tris(benzene-4,1-diyl)tris(methylene)tris(4-methylbenzyl)sulfane) (1): In a dry, degassed 15 mL two-neck flask, compound 6 (52.4 mg, 0.087 mmol, 1 eq.) and *p*-tolylmercaptan (71.1 μL , 0.53 mmol, 6 eq.) were dissolved in dry THF (5 mL). After bubbling the mixture with argon for 15 min, NaH (60% dispersed in mineral oil, 35 mg, 0.87 mmol, 10 eq.) was added. The mixture was allowed to stir at room temperature for 15 h, after which time the reaction was quenched upon addition of water. The aqueous phase was extracted three times with TBME. The combined organic phases were washed three times with water, dried over MgSO_4 , and evaporated to dryness. The product 1 was afforded by CC (c-hexane 5:1 DCM, and c-hexane 3:2 DCM) as a yellowish oil (61.9 mg, 92%). ^1H NMR (400 MHz, CDCl_3 , δ): 7.25–7.06 (m, 29H), 3.58 (d, $J = 11.6$ Hz, 12H), 2.31 (s, 9H). ^{13}C NMR (101 MHz, CDCl_3 , δ): 146.72, 145.47, 136.61, 135.85, 135.07, 131.19, 131.08, 129.19,

128.91, 128.14, 127.53, 126.00, 64.32, 35.60, 35.22, 21.15. HRMS (ESI): $m/z = [\text{M} + \text{Na}]^+$ calcd for $\text{C}_{52}\text{H}_{50}\text{NaS}_3$ 793.2967; found 793.2967.

((Phenylmethanetriyl)tris(benzene-4,1-diyl)tris(methylene)tris(3-(*tert*-butyl)-5-(((4-methylbenzyl)thio)methyl)benzyl)sulfane) (2): In a dry, degassed 25 mL one-neck flask, compound 6 (50 mg, 0.083 mmol, 1 eq.) and thiol 7 (96.5, 0.292 mol, 3.5 eq.) were dissolved in dry THF (5 mL). After bubbling the mixture with argon for 15 min, NaH (60% dispersed in mineral oil, 16.7 mg, 0.86 mmol, 5 eq.) was added. The mixture was allowed to stir at room temperature for 2 h, after which time the reaction was quenched upon addition of water. The aqueous phase was extracted three times with TBME. The combined organic phases were dried over Na_2SO_4 , and evaporated to dryness. The product was afforded after CC (1:1 DCM) as a yellowish oil (86 mg, 77%). ^1H NMR (400 MHz, CDCl_3 , δ): 7.23–7.06 (m, 38H), 3.59 (d, $J = 14.4$ Hz, 12H), 3.55 (d, $J = 3.8$ Hz, 12H), 2.31 (s, 9H), 1.29 (s, 27H). ^{13}C NMR (101 MHz, CDCl_3 , δ): 151.48, 146.72, 145.51, 138.07, 137.89, 136.56, 135.73, 135.10, 131.21, 131.07, 129.18, 128.95, 128.19, 127.57, 126.83, 126.02, 124.92, 124.81, 64.35, 36.17, 35.79, 35.43, 35.29, 34.68, 31.42, 21.17. HRMS (ESI): $m/z = [\text{M} + \text{Na}]^+$ calcd for $\text{C}_{88}\text{H}_{98}\text{NaS}_6$ 1369.5885; found 1369.5868.

((Phenylmethanetriyl)tris(benzene-4,1-diyl)tris(methylene)tris(3-(*tert*-butyl)-5-(((3-(*tert*-butyl)-5-(((4-methylbenzyl)thio)methyl)benzyl)thio)methyl)benzyl)sulfane) (3): To a dry, degassed 25 mL one-neck flask, compound 6 (17.4 mg, 0.029 mmol, 1 eq.) and thiol 8 (53.1, 0.102 mol, 3.5 eq.) were added and dissolved in dry THF (5 mL). After bubbling the mixture with argon for 15 min, NaH (60% dispersed in mineral oil, 11.6 mg, 0.29 mmol, 10 eq.) was added. The mixture was allowed to stir at room temperature for 2 h, after which time the reaction was quenched upon addition of water. The aqueous phase was extracted three times with TBME. The combined organic phases were dried over Na_2SO_4 , and evaporated to dryness. The crude product was filtrated and purified by automated GPC (chloroform) thereafter to recover 3 as yellowish oil (22 mg, 39%). ^1H NMR (400 MHz, CDCl_3 , δ): 7.22–7.12 (m, 35H), 7.11–7.08 (m, 9H), 7.06 (s, 3H), 3.62 (s, 6H), 3.59–3.55 (m, 30H), 2.32 (s, 9H), 1.30 (s, 27H), 1.29 (s, 27H). ^{13}C NMR (101 MHz, CDCl_3 , δ): 151.54, 151.51, 146.69, 145.47, 138.09, 137.98, 137.90, 136.54, 135.69, 135.09, 131.19, 131.04, 129.16, 128.93, 128.15, 127.54, 126.84, 126.79, 125.99, 124.90, 124.86, 124.76, 124.68, 64.32, 36.24, 35.92, 35.80, 35.44, 35.35, 34.66, 31.42, 31.41, 21.15. HRMS (MALDI-ToF): $m/z = [\text{M} + \text{Na}]^+$ calcd for $\text{C}_{124}\text{H}_{146}\text{NaS}_9$ 1945.8803; found 1945.8803.

((Phenylmethanetriyl)tris(benzene-4,1-diyl)tris(methylene)tris(4-(bis(4-(*tert*-butyl)phenyl) (4-(((4-methylbenzyl)thio)methyl)phenyl)methyl)benzyl)sulfane) (4): In a dry, degassed 25 mL one-neck flask, compound 6 (20 mg, 0.033 mmol, 1 eq.) and thiol 9 (71.9 mg, 0.117 mol, 3.5 eq.) were dissolved in dry THF (5 mL). After bubbling the mixture with argon for 15 min, NaH (60% dispersed in mineral oil, 13.4 mg, 0.334 mmol, 10 eq.) was added. The mixture was allowed to stir at room temperature for 2 h, after which time the reaction was quenched upon addition of water. The aqueous phase was extracted three times with TBME. The combined organic phases were dried over Na_2SO_4 , and evaporated to dryness. The product 4 was afforded by CC (c-hexane 2:1 DCM) as a yellowish oil (44 mg, 61%). ^1H NMR (400 MHz, CDCl_3 , δ): 7.22–7.12 (m, 35H), 7.11–7.08 (m, 9H), 7.06 (s, 3H), 3.62 (s, 6H), 3.59–3.55 (m, 30H), 2.32 (s, 9H), 1.30 (s, 27H), 1.29 (s, 27H). ^{13}C NMR (101 MHz, CDCl_3 , δ): 148.63, 146.78, 146.09, 145.97, 145.61, 143.78, 136.67, 135.84, 135.70, 135.54, 135.24, 131.43, 131.38, 131.29, 131.12, 130.82, 129.27, 129.02, 128.26, 128.05, 128.04, 127.65, 126.10, 124.34, 64.44, 63.84, 35.65, 35.63, 35.54, 35.38, 34.45, 31.52, 21.25. HRMS (MALDI-ToF): $m/z = [\text{M} + \text{Na}]^+$ calcd for $\text{C}_{157}\text{H}_{164}\text{NaS}_6$ 2264.1050; found 2264.1050.

((Phenylmethanetriyl)tris(benzene-4,1-diyl)tris(methylene)tris(4-(((4-(bis(4-(*tert*-butyl)phenyl) (4-(((4-methylbenzyl)thio)methyl)phenyl)methyl)benzyl)thio)methyl)phenyl)bis(4-(*tert*-butyl)phenyl)methyl)benzyl)sulfane) (5): In a dry, degassed 25 mL one-neck flask, compound 6 (13.1 mg, 0.022 mmol, 1 eq.) and thiol 10 (85.8 mg, 0.077 mol, 3.5 eq.) were dissolved in dry THF (5 mL). After bubbling the mixture with argon for 15 min, NaH (60% dispersed in mineral oil, 8.8 mg, 0.219 mmol, 10 eq.) was added. The mixture was allowed to stir at room temperature for 2 h, after which time it was quenched upon addition of water. The aqueous phase was extracted three times with TBME. The combined organic

phases were dried over Na_2SO_4 , and evaporated to dryness. The crude product was filtrated, and purified by automated GPC (chloroform) thereafter to recover 5 as yellowish oil (72 mg, 89%). ^1H NMR (400 MHz, CDCl_3 , δ): 7.25–7.16 (m, 35H), 7.14–7.11 (m, 57H), 7.09–7.04 (m, 33H), 3.60–3.54 (m, 36H), 2.31 (s, 9H), 1.28 (s, 54H), 1.27 (s, 54H). ^{13}C NMR (101 MHz, CDCl_3 , δ): 148.67, 148.66, 146.82, 146.11, 146.11, 146.09, 146.02, 145.65, 143.84, 143.82, 136.71, 135.90, 135.74, 135.62, 135.62, 135.59, 135.29, 131.48, 131.46, 131.43, 131.34, 131.17, 130.87 ($\times 2$), 130.85, 129.33, 129.07, 128.31, 128.13, 128.12, 128.11, 128.10, 127.70, 126.15, 124.40 ($\times 2$), 64.48, 63.89 ($\times 2$), 35.69 ($\times 2$), 35.60, 35.58, 35.58, 35.41, 34.51, 34.50, 31.58 ($\times 2$), 21.32. HRMS (MALDI-ToF): $m/z = [\text{M} + \text{Na}]^+$ calcd for $\text{C}_{262}\text{H}_{278}\text{NaS}_9$ 3734.9132; found 3734.9132.

General Procedure for AuNP Formation and Purification: AuNP syntheses were carried out on a 30–50 μmol scale with respect to the Au equivalents. Tetrachloroauric acid (n eq., where n is the number of sulfur atoms in the used ligand) was dissolved in deionized water (2.5 mL). A solution of tetraoctylammonium bromide ($2n$ eq.) dissolved in DCM (2.5 mL) was added and the two-phase mixture was stirred for 15 min after which time the aqueous phase had turned colorless. The ligand (1 eq.), dissolved in DCM (2.5 mL), was added to the reaction mixture, which was stirred for 15 min, allowing the thioether moieties and the gold to preorganize their conformation. A freshly prepared solution of sodium borohydride ($8n$ eq.) in water (2.5 mL) was then added quickly to the reaction mixture, causing an immediate color change to dark brown. After 15 min stirring, the resulting opaque organic phase was separated from the aqueous phase via Pasteur pipette and the aqueous phase was extracted twice with DCM. The combined organic fractions were concentrated to a volume of approximately 0.5 mL in a Falcon tube by constant bubbling of protection gas. 35 mL ethanol was added in order to precipitate the particles, which were then centrifuged three times at during 25 min at 5 $^\circ\text{C}$ and 4000 rpm, discarding the supernatant after every centrifugation step. After redispersion in DCM, the AuNPs were separated from excess ligand via SEC, evaporated to dryness and stored in the freezer.

Supporting Information

Supporting Information is available from the Wiley Online Library or from the author.

Acknowledgements

The authors thank the Swiss National Science Foundation (Grant no. 200020_159730) for financial support, Annika Büttner and Cedric Wobill for providing the TGA measurements and Dr. Daniel Häussinger for his help with ^{13}C NMR measurements and interpretation thereof.

Conflict of Interest

The authors declare no conflict of interest.

Keywords

gold nanoparticles, macromolecular ligands, oligomers, organic coatings, tetraphenylmethane

Received: January 10, 2018

Revised: February 11, 2018

Published online: March 25, 2018

[1] P. Mulvaney, *MRS Bull.* **2001**, 26, 1009.

[2] M.-C. Daniel, D. Astruc, *Chem. Rev.* **2004**, 104, 293.

[3] G. Schmid, M. Bäuml, M. Geerkens, I. Heim, C. Osemann, T. Sawitowski, *Chem. Soc. Rev.* **1999**, 28, 179.

[4] F. Kretschmer, S. Mühligh, S. Hoepfener, A. Winter, M. D. Hager, C. Rockstuhl, T. Pertsch, U. S. Schubert, *Part. Part. Syst. Charact.* **2014**, 31, 721.

[5] M. Faraday, *Philos. Trans. R. Soc. London* **1857**, 147, 145.

[6] P. Zhao, N. Li, D. Astruc, *Coord. Chem. Rev.* **2013**, 257, 638.

[7] M. Bartz, J. Küther, R. Seshadri, W. Tremel, *Angew. Chem., Int. Ed.* **1998**, 37, 2466.

[8] W. K. Cho, J. K. Lee, S. M. Kang, Y. S. Chi, H.-S. Lee, I. S. Choi, *Chem. Eur. J.* **2007**, 13, 6351.

[9] R. Sardar, A. M. Funston, P. Mulvaney, R. W. Murray, *Langmuir* **2009**, 25, 13840.

[10] D. G. Georganopoulou, L. Chang, J.-M. Nam, C. S. Thaxton, E. J. Mufson, W. L. Klein, C. A. Mirkin, *Proc. Natl. Acad. Sci. USA* **2005**, 102, 2273.

[11] N. L. Rosi, D. A. Giljohann, C. S. Thaxton, A. K. R. Lytton-Jean, M. S. Han, C. A. Mirkin, *Science* **2006**, 312, 1027.

[12] M. Homberger, U. Simon, *Philos. Trans. R. Soc., A* **2010**, 368, 1405.

[13] P. Podsiadlo, V. A. Sinani, J. H. Bahng, N. W. S. Kam, J. Lee, N. A. Kotov, *Langmuir* **2008**, 24, 568.

[14] M.-C. Bowman, T. E. Ballard, C. J. Ackerson, D. L. Feldheim, D. M. Margolis, C. Melander, *J. Am. Chem. Soc.* **2008**, 130, 6896.

[15] F. J. Ibañez, F. P. Zamborini, *ACS Nano* **2008**, 2, 1543.

[16] C.-C. Huang, Z. Yang, K.-H. Lee, H.-T. Chang, *Angew. Chem.* **2007**, 119, 6948.

[17] Y. Guo, Z. Wang, H. Shao, X. Jiang, *Analyst* **2011**, 137, 301.

[18] L. M. Demers, C. A. Mirkin, R. C. Mucic, R. A. Reynolds, R. L. Letsinger, R. Elghanian, G. Viswanadham, *Anal. Chem.* **2000**, 72, 5535.

[19] J. J. Storhoff, A. A. Lazarides, R. C. Mucic, C. A. Mirkin, R. L. Letsinger, G. C. Schatz, *J. Am. Chem. Soc.* **2000**, 122, 4640.

[20] R. Wilson, *Chem. Commun.* **2003**, 108.

[21] D. C. Hone, A. H. Haines, D. A. Russell, *Langmuir* **2003**, 19, 7141.

[22] D. S. Seferos, D. A. Giljohann, H. D. Hill, A. E. Prigodich, C. A. Mirkin, *J. Am. Chem. Soc.* **2007**, 129, 15477.

[23] P. Miao, Y. Tang, Z. Mao, Y. Liu, *Part. Part. Syst. Charact.* **2017**, 34, 1600405.

[24] M. A. Mangold, M. Calame, M. Mayor, A. W. Holleitner, *ACS Nano* **2012**, 6, 4181.

[25] J. Liao, L. Bernard, M. Langer, C. Schönenberger, M. Calame, *Adv. Mater.* **2006**, 18, 2444.

[26] D. Huang, F. Liao, S. Moles, D. Redinger, V. Subramanian, *J. Electrochem. Soc.* **2003**, 150, G412.

[27] R. Costi, A. E. Saunders, U. Banin, *Angew. Chem., Int. Ed.* **2010**, 49, 4878.

[28] T. Peterle, A. Leifert, J. Timper, A. Sologubenko, U. Simon, M. Mayor, *Chem. Commun.* **2008**, 3438.

[29] T. Peterle, P. Ringler, M. Mayor, *Adv. Funct. Mater.* **2009**, 19, 3497.

[30] J. P. Hermes, F. Sander, T. Peterle, C. Cioffi, P. Ringler, T. Pfohl, M. Mayor, *Small* **2011**, 7, 920.

[31] J. P. Hermes, F. Sander, T. Peterle, M. Mayor, *Chimia* **2011**, 65, 219.

[32] M. Lehmann, E. H. Peters, M. Mayor, *Chem. Eur. J.* **2016**, 22, 2261.

[33] M. Lehmann, E. H. Peters, M. Mayor, *Helv. Chim. Acta* **2017**, 100, e1600395.

[34] W. M. Pankau, K. Verbist, G. von Kiedrowski, *Chem. Commun.* **2001**, 519.

[35] Y. Hosokawa, S. Maki, T. Nagata, *Bull. Chem. Soc. Jpn.* **2005**, 78, 1773.

[36] J. P. Hermes, F. Sander, T. Peterle, R. Urbani, T. Pfohl, D. Thompson, M. Mayor, *Chem. Eur. J.* **2011**, 17, 13473.

[37] J. P. Hermes, F. Sander, U. Fluch, T. Peterle, D. Thompson, R. Urbani, T. Pfohl, M. Mayor, *J. Am. Chem. Soc.* **2012**, 134, 14674.

[38] F. Sander, U. Fluch, J. P. Hermes, M. Mayor, *Small* **2014**, 10, 349.

[39] W. M. Pankau, S. Mönninghoff, G. von Kiedrowski, *Angew. Chem., Int. Ed.* **2006**, 45, 1889.

[40] A. D'Aléo, R. M. Williams, F. Osswald, P. Edamana, U. Hahn, J. van Heyst, F. D. Tichelaar, F. Vögtle, L. De Cola, *Adv. Funct. Mater.* **2004**, 14, 1167.

- [41] A. Fahmi, A. D'Aléo, R. M. Williams, L. De Cola, N. Gindy, F. Vögtle, *Langmuir* **2007**, *23*, 7831.
- [42] R. McCaffrey, H. Long, Y. Jin, A. Sanders, W. Park, W. Zhang, *J. Am. Chem. Soc.* **2014**, *136*, 1782.
- [43] B. Mondal, K. Acharyya, P. Howlader, P. S. Mukherjee, *J. Am. Chem. Soc.* **2016**, *138*, 1709.
- [44] L. Qiu, R. McCaffrey, Y. Jin, Y. Gong, Y. Hu, H. Sun, W. Park, W. Zhang, *Chem. Sci.* **2018**, *9*, 676.
- [45] L. Qiu, R. McCaffrey, W. Zhang, *Chem. Asian J.* **2018**, *13*, 362.
- [46] S. Lu, Y. Hu, S. Wan, R. McCaffrey, Y. Jin, H. Gu, W. Zhang, *J. Am. Chem. Soc.* **2017**, *139*, 17082.
- [47] T. Sakata, S. Maruyama, A. Ueda, H. Otsuka, Y. Miyahara, *Langmuir* **2007**, *23*, 2269.
- [48] L. Wei, K. Padmaja, W. J. Youngblood, A. B. Lysenko, J. S. Lindsey, D. F. Bocian, *J. Org. Chem.* **2004**, *69*, 1461.
- [49] L. Wei, H. Tiznado, G. Liu, K. Padmaja, J. S. Lindsey, F. Zaera, D. F. Bocian, *J. Phys. Chem. B* **2005**, *109*, 23963.
- [50] M. Valášek, M. Mayor, *Chem. Eur. J.* **2017**, *23*, 13538.
- [51] M. Lindner, M. Valášek, J. Homberg, K. Edelmann, L. Gerhard, W. Wulfhekel, O. Fuhr, T. Wächter, M. Zharnikov, V. Kolivoška, L. Pospíšil, G. Mészáros, M. Hromadová, M. Mayor, *Chem. Eur. J.* **2016**, *22*, 13218.
- [52] M. Lindner, M. Valášek, M. Mayor, T. Frauhammer, W. Wulfhekel, L. Gerhard, *Angew. Chem., Int. Ed.* **2017**, *56*, 8290.
- [53] M. Valášek, M. Lindner, M. Mayor, *Beilstein J. Nanotechnol.* **2016**, *7*, 374.
- [54] J. Tian, Y.-D. Ding, T.-Y. Zhou, K.-D. Zhang, X. Zhao, H. Wang, D.-W. Zhang, Y. Liu, Z.-T. Li, *Chem. Eur. J.* **2014**, *20*, 575.
- [55] M. Brust, M. Walker, D. Bethell, D. J. Schiffrin, R. Whyman, *J. Chem. Soc., Chem. Commun.* **1994**, 801.
- [56] "ImageJ," can be found as free download under <http://imagej.net/> Welcome (accessed: Jun 17, 2016).
- [57] M. J. Hostetler, C.-J. Zhong, B. K. H. Yen, J. Andereg, S. M. Gross, N. D. Evans, M. Porter, R. W. Murray, *J. Am. Chem. Soc.* **1998**, *120*, 9396.
- [58] I. Hussain, Z. Wang, A. I. Cooper, M. Brust, *Langmuir* **2006**, *22*, 2938.

Monofunctionalized Au Nanoparticles | Very Important Paper |

Alkyne-Monofunctionalized Gold Nanoparticles as Massive Molecular Building Blocks

Erich Henrik Peters^[a] and Marcel Mayor^{*[a,b,c]}

Abstract: Using a tripodal, thioether-based ligand comprising a remote protected acetylene, we efficiently stabilize small gold nanoparticles ($\varnothing \approx 1.2$ nm) which are isolated and purified by chromatography. The 1:1 ligand-to-particle ratio is obtained by comparing the particles' dimensions measured by transmission electron microscopy with the weight fraction of the coating ligand determined by thermogravimetric analysis. The single ligand coating of the gold particle guarantees the presence of a single masked alkyne per particle. It can be addressed by wet chemical protocols providing the particles with the properties

of "massive molecules". The "massive molecule" nature of the particles is demonstrated by involving them in wet chemical coupling protocols like oxidative acetylene coupling providing gold nanoparticle dimers (34 % isolated yield) or alkyne-azide "click"-chemistry with a suitable triazide, giving trimeric particle architectures (30 % determined by transmission electron microscopy). The particle stabilization obtained by the coating ligand allows, for the first time, to treat these multi-particle architectures by size exclusion chromatography.

Introduction

Colloidal gold has experienced large interest due to its optical and physical properties.^[1–5] Since the pioneering work by *Brust* et al.,^[6,7] various thiol-based organic ligands have been investigated for the stabilization of gold nanoparticles (Au NPs), owing to their synthetic tunability and availability, ease of handling, and favorable stabilization properties. Thiol-stabilized Au NPs were applied in a plethora of fields including catalysis,^[8–10] sensing and labeling applications,^[11–19] medical diagnostics and therapeutics^[20–24] or as building blocks for hybrid materials^[25] and molecular electronics.^[26–28] For many of these applications, Au NPs exposing a single functional group, behaving like "massive molecules" enabling their positioning and integration by covalent chemistry are desirable.^[29–32] Several approaches resulting in monofunctionalized Au NPs stabilized with thiol-based ligands have been reported, including single-

ligand place-exchange reactions on solid support^[33,34] or in solution, followed by separation by electrophoresis,^[35] on-Au NP surface polymerization of suitable ligands^[36] or exchange of the entire ligand shell with carefully tuned thiol mixtures on citrate-stabilized Au NPs.^[37] Recently, the scope of sulfur-containing ligands for Au NPs has been enhanced towards more complex benzylic thioether-based ligands. The reversible coordinative binding of the thioether to the Au NP surface and the flexible adaptive structure of the multidentate coating ligand holds the promise of efficient and size-selective Au NP passivation. Indeed, oligomeric,^[38–43] tripodal,^[44–46] dendrimeric,^[46–50] and even cage-like^[51] thioether-based ligands yielded Au NPs with, in some cases, narrow size-distributions, good yields and remarkable stability features. We reported earlier about the favorable Au NP stabilization features of a family of ligands consisting of a central tetraphenylmethane subunit decorated three-fold with multidentate oligomeric chains.^[52] Particularly appealing were these ligands with tetraphenylmethane-based benzylic thioether oligomers, as in these cases, a single ligand turned out to be able to stabilize an entire Au NP. Interestingly, as only three of the four phenyl units of the central tetraphenylmethane are decorated with an oligomer, the molecular design leaves the fourth phenyl ring upright-standing on the coated Au NP as ideal site for further chemical functionalization.^[53–55]

Here, we report the successful functionalization of the remaining free phenyl ring by an oligo(phenylene-ethynylene) (OPE) rod exposing a triisopropylsilyl (TIPS)-masked alkyne group. As sketched in Scheme 1, the ligand **1** exposing the OPE rod as a functional group keeps the ability to stabilize an entire Au NP, resulting in monofunctionalized Au NPs which readily undergo chemical reactions in a single position. The combination of a reasonably stable Au NP with a reactive functional group makes these particles addressable by wet chemistry and

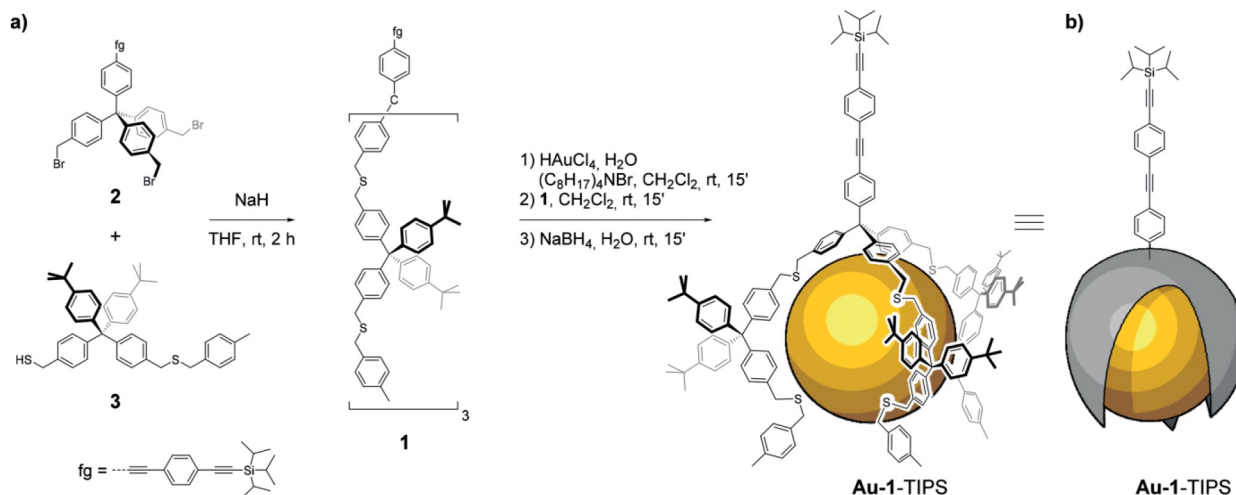
[a] E. H. Peters, Prof. Dr. M. Mayor
Departement of Chemistry, University of Basel,
St. Johanns-Ring 19, 4056 Basel, Switzerland
E-mail: marcel.mayor@unibas.ch
<https://www.chemie1.unibas.ch/~mayor/index.html>

[b] Prof. Dr. M. Mayor
Institute for Nanotechnology (INT), Karlsruhe Institute of Technology (KIT),
P. O. Box 3640, 76021 Karlsruhe, Germany
E-mail: marcel.mayor@kit.edu

[c] Prof. Dr. M. Mayor
Lehn Institute of Functional Materials (LIFM), Sun Yat-Sen University (SYSU),
Xingang Xi Rd. 135, 510275 Guangzhou, P. R. China

Supporting information and ORCID(s) from the author(s) for this article are available on the WWW under <https://doi.org/10.1002/ejic.202000273>.

© 2020 The Authors. Published by Wiley-VCH Verlag GmbH & Co. KGaA. This is an open access article under the terms of the Creative Commons Attribution License, which permits use, distribution and reproduction in any medium, provided the original work is properly cited.



Scheme 1. **a**) Conceptual overview and synthesis of the Au NP exposing a single functional group (fg). **b**) Sketch of the ligand-coated Au NP as massive object exposing a functional group accessible by wet chemistry.

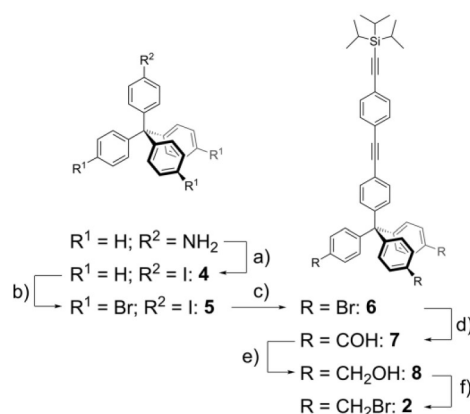
they can be considered as “massive molecules”. The chemical accessibility of the exposed alkyne was demonstrated by standard coupling reactions like oxidative acetylene coupling^[39,41,48] resulting in “dumbbell”-type dimers and alkyne-azide “click” chemistry^[56,57] providing Au NP trimers thanks to a suitable triazide linker. Interestingly, the here reported ligand shell stabilizes the Au NP to an extent enabling to expose these small nano-architectures consisting of interlinked Au NPs to size-exclusion chromatography (SEC), which was not the case for previously reported ligand designs.^[39,41,48,49]

Results and Discussion

Ligand Synthesis

The synthesis of tripodal ligand **1** is shown in Scheme 1. The three benzylic bromides of precursor **2** were substituted with a moderate excess of thiol **3** (1.23 equivalents per bromide), using sodium hydride (NaH) as a base in freshly distilled tetrahydrofuran (THF). After aqueous work-up, the ligand was isolated in 55 % yield by silica plug filtration and automated gel permeation chromatography (GPC, in chloroform).

The synthesis of the central linking unit was performed in six steps with an overall yield of 54 % (Scheme 2). Precursor **4** was obtained via Sandmeyer-type reaction applied to 4-tritylaniline in good 80 % yield. Subsequent treatment with bromine gave the tribromide **5** quantitatively. Profiting from the improved reactivity of the iodine substituent in palladium-catalyzed coupling reactions,^[58] the OPE-rod exposing the TIPS-protected alkyne was introduced via Sonogashira cross-coupling reaction performed at room temperature, providing the OPE-rod **6** exposing three terminal *para*-bromophenyls. Threefold lithium-halogen exchange was achieved with *tert*-butyl-lithium in -78 °C cold THF, and quenching with *N,N*-dimethylformamide (DMF) gave the trialdehyde **7** in excellent 88 % yield after aqueous work-up and column chromatography. The three aldehydes were quantitatively reduced to benzylic alcohols in **8** with so-



Scheme 2. Synthesis of functionalized central linking unit **2**. a) 1) BF₃Et₂O, CH₂Cl₂, -10 °C, 45'; 2) *t*BuONO, CH₂Cl₂, -10 °C, 45'; 3) I₂, KI, -10 °C to r.t., 15 h, 80 %; b) Br₂, neat, r.t., 30', quant.; c) Pd(PPh₃)₂Cl₂, TIPSC≡C-*p*-C₆H₄-C≡CH, CuI, Et₃N, CH₂Cl₂, r.t., 2 h, 76 %; d) 1) *t*BuLi, THF, -78 °C, 2 h, 2) DMF, -78 °C to r.t., 2 h, 88 %; e) 1) NaBH₄, MeOH, 0 °C, 2 h, 2) HCl (aq.), 0 °C, r.t., quant.; f) CBr₄, PPh₃, CH₂Cl₂, -10 °C, 1 h quant.

dium borohydride. Finally, in a threefold Appel-reaction, the benzylic alcohols were converted into the benzylic bromides of **2** quantitatively.

The assembly of the teraphenylmethane building block **3** exposing a benzylic thiol was achieved following a previously published protocol.^[42]

All new compounds were characterized by ¹H- and ¹³C-NMR spectroscopy and high-resolution mass spectrometry.

Au NP Synthesis

The Au NPs stabilized by ligand **1** were synthesized following a previously published protocol^[38] based on a variation of the Au NP synthesis proposed by *Brust* et al.^[6] In the aqueous phase of a biphasic system, one equivalent of gold salt (HAuCl₄) for each sulfur atom in the ligand, i.e. 6 equivalents, was added.

The transfer of the gold salt from the aqueous to the organic phase was achieved by addition of tetra-*n*-butyl ammonium bromide (TOAB, 2 equivalents with respect to HAuCl_4 , i.e. 12 equivalents) to the organic phase. The ligand was added dissolved in CH_2Cl_2 . Nucleation of the Au NPs was induced via reduction by aqueous NaBH_4 (8 equivalents with respect to HAuCl_4 , i.e. 48 equivalents). Upon addition of the reducing agent, an immediate color change of the organic phase from bright orange to opaque dark brown was observed. After rigorous stirring for 15 min, the organic phase was separated and concentrated in a N_2 stream to prevent possible thermal aggregation of NPs. Precipitation of the Au NPs from the concentrated organic solution was achieved by addition of ethanol. Repeated centrifugation and subsequent SEC provided pure samples of the Au NPs without remaining traces of ligand molecules or TOAB. The colloidal gold particles stabilized by ligand **1** are labeled as **Au-1-TIPS** and were isolated in excellent yields above 95%. **Au-1-TIPS** was the only detectable form of gold throughout the synthesis and the mass losses were due to the handling during the purification procedures.

Au NP Analysis and Characterization

The Au NPs were characterized by variable temperature UV/Vis absorption spectroscopy, transmission electron microscopy

(TEM), and thermogravimetric analysis (TGA). Finally, the “molecule-like” behavior of **Au-1-TIPS** was demonstrated by engaging them in wet chemistry coupling protocols producing small nano-architectures like dimers and trimers which could be detected by TEM.

The UV/Vis absorption spectrum of **Au-1-TIPS** (Figure 1c) displays discrete bands between 300–350 nm, characteristic for the absorbance of the OPE subunit of the ligand **1**. Apart from these features, the continuous increase towards shorter wavelength without a surface plasmon band points at Au NPs with diameters below 2 nm. Only with Au NPs of dimensions below 2 nm, the rate of surface scattering exceeds the rate of bulk scattering and the electron-donating character of the coordinating sulfur atoms of the coating ligand increases the surface electron density significantly, reflected in a broadening of the surface plasmon band.^[59] It is noteworthy that very similar optical behavior was reported for the parent ligand structure without the exposed functional group.^[52] The OPE subunit of **1** acts as an optical label and the very comparable absorption of the OPE subunit of **Au-1-TIPS** compared with the free ligand **1** not only proves the presence of the ligand on the Au NP, but also supports the hypothetical picture of an exposed and dissolved OPE rod which does not interfere with the Au NP surface. The dimensions of the Au NPs were further analyzed by TEM (Fig-

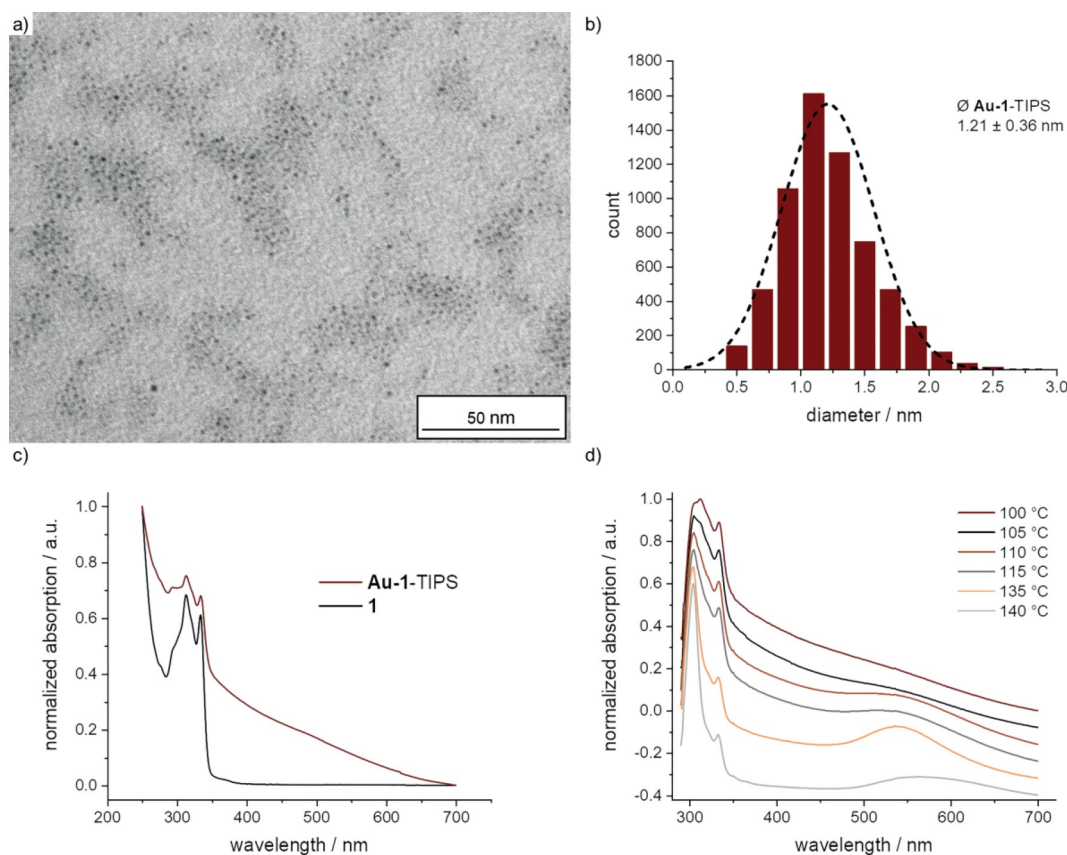


Figure 1. a) TEM micrograph of **Au-1-TIPS**; b) size-distribution of **Au-1-TIPS** obtained from TEM micrographs; c) UV/Vis absorption spectrum of **Au-1-TIPS** in comparison with ligand **1**; d) UV/Vis absorption spectra at selected temperatures, offset for clarity.

ure 1a–b) and the recorded diameters of 1.21 ± 0.36 nm confirmed the initial claims derived from the UV/Vis experiments. The Au NP size distribution was determined with TEM micrographs comprising more than 6000 NPs, using the threshold and particle analysis tools from ImageJ.^[60]

TGA of **Au-1-TIPS** revealed a mass loss of 19.0 % between 200 and 600 °C which was attributed to the combustion of the coating organic ligand **1**. Assuming a spherical shape, the Au NP diameter of 1.21 nm determined by TEM allowed to determine the Au NP's volume (0.93 nm^3). With the density of gold (19.32 g cm^{-3}), the mass of an average Au NP was determined to be 1.79×10^{-20} g, and, by multiplication with Avogadro's number ($N_A: 6.022 \times 10^{23} \text{ mol}^{-1}$), the molecular weight of the average uncoated Au NP was determined to be 10792 g mol^{-1} . The molecular weight of the ligand **1** with the formula $\text{C}_{176}\text{H}_{188}\text{S}_6\text{Si}$ is $2523.89 \text{ g mol}^{-1}$. The molecular weight of the proposed particle **Au-1-TIPS** coated by a single ligand is, with 13316 g mol^{-1} , the sum of both. The weight contribution of the coating ligand **1** fits, with 18.95 %, perfectly the weight loss recorded during TGA (19.0 %), corroborating the claim that a single ligand **1** is coating and stabilizing an entire Au NP. The same issue is examined in Table 1 displaying that the same number of gold atoms per particle is obtained from the TGA and the TEM analysis.

The Au NPs **Au-1-TIPS** coated with a single ligand exposing an OPE rod can be regarded as "massive molecules" with a peripheral TIPS-protected alkyne as functional group. To explore the stability of this "massive molecule" and thus also the scope of potential reaction conditions, samples of **Au-1-TIPS** were dispersed in *ortho*-xylene and gradually heated while their optical features were monitored by UV/Vis spectroscopy. Applying a heating gradient of 10 °C per hour, the UV/Vis spectra of the sample remained unchanged up to 105 °C (Figure 1d). Above this temperature, the samples turned red and the emergence of a plasmon band in the UV/Vis was observed. Upon extended exposure to temperatures above 105 °C, decoloration of the sample due to precipitation was observed. The thermal decomposition of **Au-1-TIPS** above 105 °C is interpreted as agglomeration to larger particles, either due to too violent collisions for the delicate steric protection provided by coating **1** or due to prior thermal detachment of **1**. It is noteworthy that a comparable decomposition temperature was observed for the parent ligand structure (110 °C),^[52] documenting further the separation between the coating ligand subunit of **1** and the attached OPE rod.

After the determination of the thermal stability of **Au-1-TIPS**, its potential as precursor in wet-chemical reactions as building block for nano-architectures was explored.

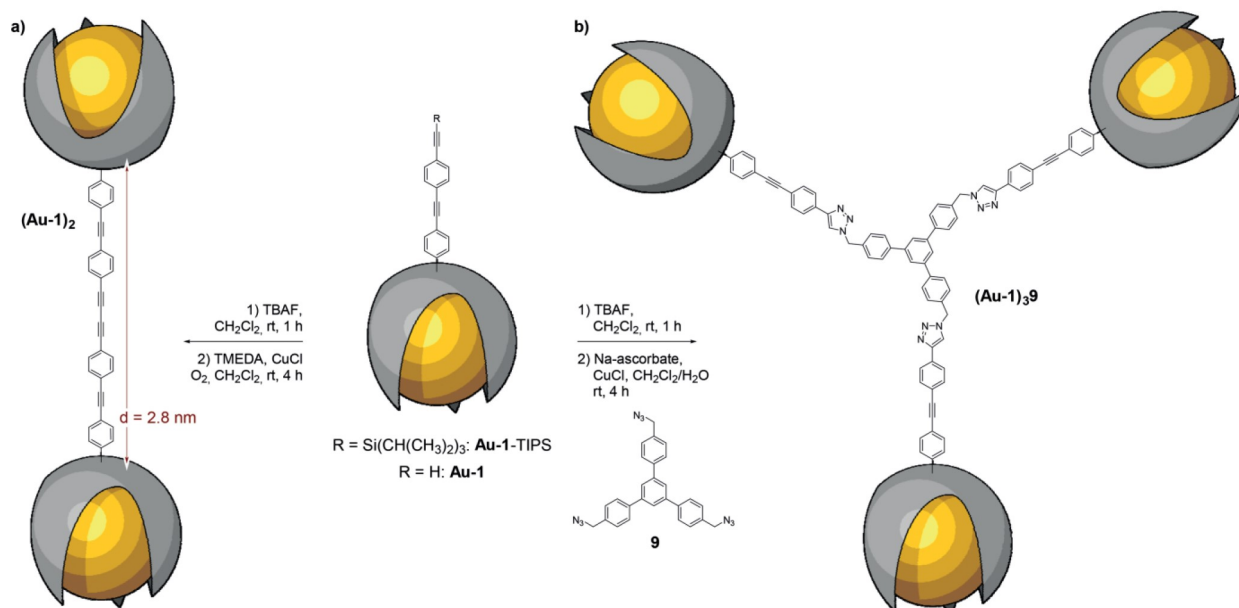
Au-1-TIPS as Precursor in Coupling Reactions I: Dimerization

The analytical data of **Au-1-TIPS** displayed a Au NP coated by a single ligand and, consequently, also only one OPE rod per Au NP. Furthermore, the comparison of the UV/Vis spectra of **Au-1-TIPS** and the free ligand **1** suggested an entirely dissolved and thus wet-chemically addressable OPE subunit exposed at the Au NP surface. The OPE rod exposes a TIPS-protected terminal alkyne as masked but reactive functional group which can be involved e.g. in various coupling protocols. To demonstrate the engagement of **Au-1-TIPS** as "massive molecule" in coupling chemistry, the TIPS-masked alkyne was deprotected profiting from the fluoride ions of tetra-*n*-butylammoniumfluoride (TBAF) in CH_2Cl_2 (Scheme 3). After aqueous work-up, the deprotected Au NPs were exposed to typical Glaser–Hay oxidative acetylene coupling conditions.^[61,62] They were re-dissolved in CH_2Cl_2 and $\text{Cu}^{(I)}$ ions were added together with *N,N,N',N'*-tetramethylethane-1,2-diamine (TMEDA) as ligand dissolving the copper ion. The reaction was vigorously stirred at ambient air to guarantee the presence of dissolved oxygen. To avoid aggregation of the coated gold particles, the reaction was kept for 4 hours at room temperature. After aqueous work-up and subsequent repetitive separation by SEC using CH_2Cl_2 and toluene as eluent, Au NP dimers [**(Au-1)₂**] were isolated in 34 % yield. It is noteworthy that these dimeric Au NP architectures based on the ligand **1** were the first larger systems resisting decomposition on the SEC column, documenting further the superior stability of Au NP coated by the ligand **1**. All our earlier ligand designs based on benzylic thioethers survived SEC conditions as monomers, but the resulting interlinked NP architectures disintegrated when exposed to the shear forces of SEC.^[39,41,48]

The yield of **(Au-1)₂** was also determined by analyzing TEM micrographs of the crude reaction mixture. The reaction mixture was diluted to an extent avoiding the agglomeration of Au NPs on the TEM grid. 53 micrographs (each $340 \text{ nm} \times 260 \text{ nm}$) comprising a total of 2077 Au NPs were analyzed, covering $4.69 \mu\text{m}^2$ of the TEM grid. Pairs of Au NPs with a spacing up to 3.2 nm were considered as **(Au-1)₂**. With 826 of 2077 NPs being part of a dimer corresponding to a yield of 39.8 %, the TEM analysis confirmed the yield isolated by SEC.

Table 1. Ligand-to-gold ratio of **Au-1-TIPS**. The number of gold atoms of an average particle is calculated from the TGA data (top) and from the dimension of the NP determined by TEM (bottom). $m(1)$: mass loss due to burned ligand **1**; $M(1)$: molar mass of **1**; $n(1)$: number of mol of ligand **1**; m_{Au} : mass of remaining gold; n_{Au} : number of mol of gold; $n_{\text{Au}}/n(1)$: average number of gold atoms per ligand according to the TGA data; \varnothing_{NP} : diameter of an average NP determined by TEM; V_{NP} : volume of the NP = $4/3\pi r^3$; m_{NP} : mass of the NP = $V_{\text{NP}}\rho_{\text{Au}}$ (with $\rho_{\text{Au}} = 19.32 \text{ g cm}^{-3}$); M_{Au} : molar mass of gold ($196.97 \text{ g mol}^{-1}$); n_{Au} : number of mol of gold = $m_{\text{NP}}/M_{\text{Au}}$; n_{Au}/NP : average number of gold atoms per NP = n_{Au}/N_A ($N_A = 6.022 \times 10^{23} \text{ mol}^{-1}$).

Au-1-TIPS	$m(1)$ [mg]	$M(1)$ [g/mol]	$n(1)$ [mol]	m_{Au} [mg]	n_{Au} [mol]	$n_{\text{Au}}/n(1)$
TGA	0.545	2523.9	2.18×10^{-7}	2.33	1.18×10^{-5}	54.7
	\varnothing_{NP} [nm]	V_{NP} [nm ³]	m_{NP} [g]	M_{Au} [g/mol]	n_{Au} [mol]	n_{Au}/NP
TEM	1.21 ± 0.36	0.928	1.79×10^{-20}	196.97	9.1×10^{-23}	54.8



Scheme 3. Nano-architectures obtained by using **Au-1-TIPS** as starting materials. **a**) Dimerization by oxidative acetylene coupling. **b**) Trimerization profiting from alkyne-azide "click"-chemistry.

Additional structural features of **(Au-1)₂** were extracted from TEM micrographs (Figure 2a). The size-distribution of the Au NPs after the coupling reaction (Figure 2b) resembles, with 1.18 ± 0.29 nm, within the limits of the method, the one recorded for the parent sample **Au-1-TIPS**. This suggests that, during the entire deprotection–homocoupling protocol, the Au NPs remain stable and protected by the coating ligand, corroborating the "massive molecule" behavior of **Au-1-TIPS** in the reaction sequence.

TEM micrographs of the isolated, "dumbbell-like" Au NP dimers (Figure 2a) enabled to analyze the inter-NP distances in more details. Interestingly, the distribution of the NP spacing clearly displayed two maxima (Figure 2c). The majority of about 80 % of the recorded Au–NP distances was, with 2.62 ± 0.21 nm, in the dimensions of the diethynyl-linker expected as product of the oxidative acetylene coupling, as the distance for the fully stretched linker estimated by simple MM2 simulation was 2.8 nm (distance between both tertiary methane carbon atoms of the rod-terminating tetraphenylmethane subunits, see Scheme 3a). In principle, any shorter distance might be attributed to the projection of the Au NPs of a "dumbbell" dimer not lying flat on the TEM grid. For such an explanation, one would, however, rather expect a continuous tailing to shorter distances and not a discrete maximum. Thus, in similarity to "dumbbell" architectures based on dendrimer-coated Au-NPs,^[48] the shorter inter-NP distance of 1.64 ± 0.20 nm (recorded for about 20 %) most likely points at direct coordinative contacts between an Au NP and the terminal acetylene exposed by the OPE rod of the deprotected **Au-1**.^[63] Such a coordination between alkyne and Au NP requires access to the Au NP surface, showing that the ligand **1** is not covering the entire surface of

the stabilized Au NP in **Au-1**. Interestingly, trimeric structures e.g. consisting of "dumbbell"-type dimers formed by oxidative acetylene coupling with one of its terminal Au NPs engaged in a coupling with the terminal acetylene of a third deprotected **Au-1** were, with only 4 observed cases, too rare to exclude random arrangements on the TEM grid. The Au NP dimers with short spacing are of comparable stability to the longer ones and do also not decompose during the SEC process. Also, we were not able to distinguish both structures during the SEC experiment, which was not surprising, considering the working hypothesis that both structures exclusively differ in the inter-linking of two **Au-1**-type subunits.

Au-1-TIPS as Precursor in Coupling Reactions II: Trimerization

The lack of trimers observed in the homocoupling protocol discussed above raised the question if there could be an intrinsic limitation disqualifying trimerization. As alternative approach to couple three Au NPs to a trimeric nano-architecture, alkyne-azide "click"-chemistry has already been applied successfully for dendrimer-stabilized Au NPs.^[49] Thus, a sample of **Au-1-TIPS** was deprotected and the liberated alkynes were exposed to a "click" protocol with the triazide 1,3,5-tris[*p*-(azidomethyl)phenyl]benzene (**9** in Scheme 3) as threefold central coupling unit. To the deprotected **Au-1** dissolved in CH₂Cl₂, the triazide **9** was added and, while vigorously stirring, aqueous solutions of copper sulfate and sodium ascorbate as reducing agent were added (Scheme 3b). To avoid aggregation of the coated gold particles, the reaction was kept for 4 hours at room tempera-

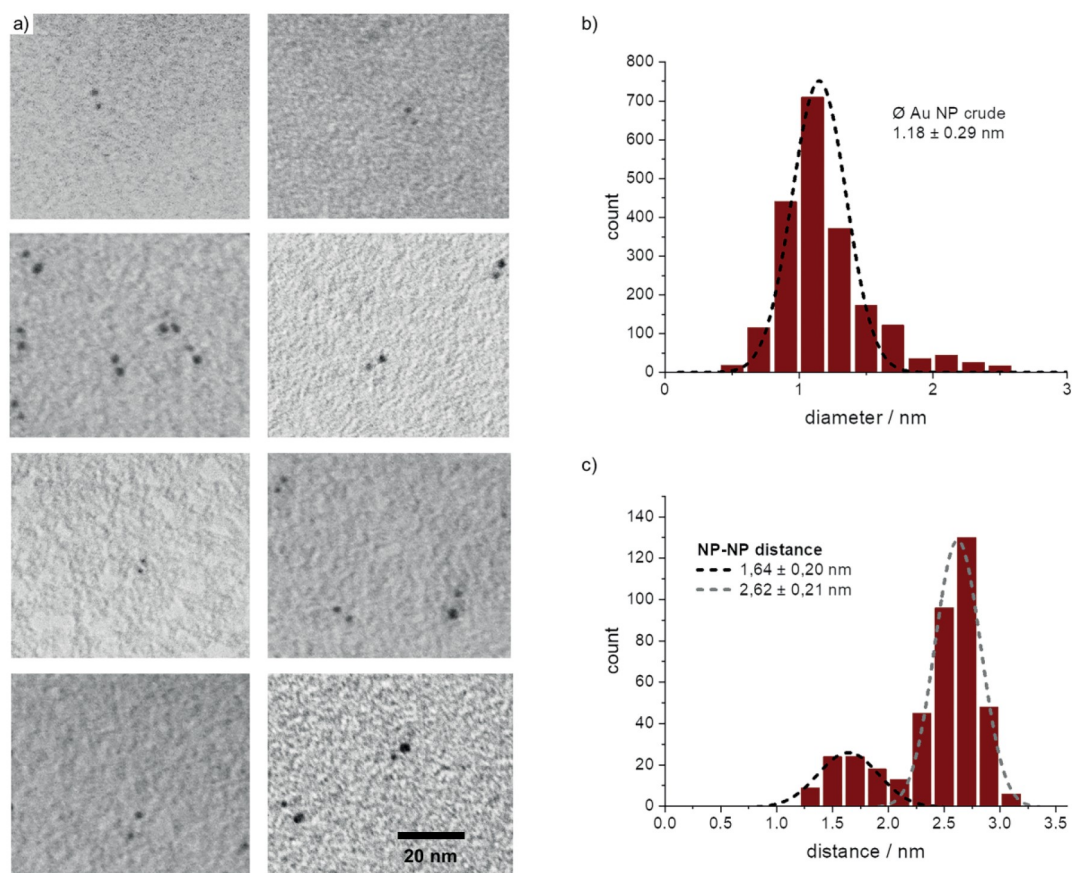


Figure 2. “Dumbbell”-type dimers formed by exposing **Au-1**-TIPS to a deprotection-homocoupling protocol. **a**) TEM micrographs of **(Au-1)₂** (scale bar is valid for all 8 micrographs). **b**) Size-distribution of Au NPs after the deprotection-homocoupling protocol. **c**) Distribution of the interparticle distance in **(Au-1)₂**.

ture. After extraction with CH_2Cl_2 , the composition of the crude reaction mixture was analyzed by TEM. 42 micrographs (each 340×260 nm) comprising a total of 1587 Au NPs were analyzed, covering $3.71 \mu\text{m}^2$ of the TEM grid. Groups of 3 NPs with a maximal separation smaller than 4.5 nm were considered as the trimeric **(Au-1)₃9**. The slightly larger accepted radius compared with the homocoupled **(Au-1)₂** is due to both the larger dimensions and the increased flexibility of the particle-interlinking organic structure. From the 1587 NPs, 477 NPs or 30.1 % were engaged in a **(Au-1)₃9** structure, 324 NPs or 20.4 % were observed as dimers of Au NPs, and 786 NPs or 49.5 % were recorded as monomers. Whether the dimers are formed due to only twofold “click”-chemistry-type coupling to **9**, or to homocoupled **(Au-1)₂**, cannot be distinguished in the TEM micrographs.

Also for the “click”-chemistry protocol, a very comparable size-distribution (Figure 3b, 1.28 ± 0.30 nm) of the Au NPs after the coupling reaction was observed, pointing at the integrity of **Au-1** during the applied reaction conditions. In analogy to the homocoupled **(Au-1)₂**, also **(Au-1)₃9** survived SEC conditions. However, while fractions comprising **(Au-1)₃9** and the di-

meric Au NP architectures could be separated from the monomeric Au NPs, the method failed to isolate pure **(Au-1)₃9** fractions.

TEM micrographs of **(Au-1)₃9** (Figure 3a) enabled the analyses of the interparticle distances (Figure 3c). The rather broad and unspecific distance distribution reflects the increased structural variety in the arrangement of the three Au NP in **(Au-1)₃9**, due to the flexibility of the interlinking scaffold comprising triazole subunits attached at benzylic positions.

While the spatial grouping of Au NPs by TEM analyses of the reaction mixtures support for both coupling reactions the formation of the desired oligo-NP nano-architectures, the method does not comprise any further chemical information. As example, an interesting chemical issue was the rather moderate yield of the desired oligo-NP objects with 39.8 % for **(Au-1)₂** and 30.1 % for **(Au-1)₃9** respectively. Whether these moderate yields reflect the lack of reactivity of the “massive molecule” **Au-1** in the coupling reaction or, in the step before, an incomplete deprotection of **Au-1**-TIPS cannot be distinguished by the here reported studies.

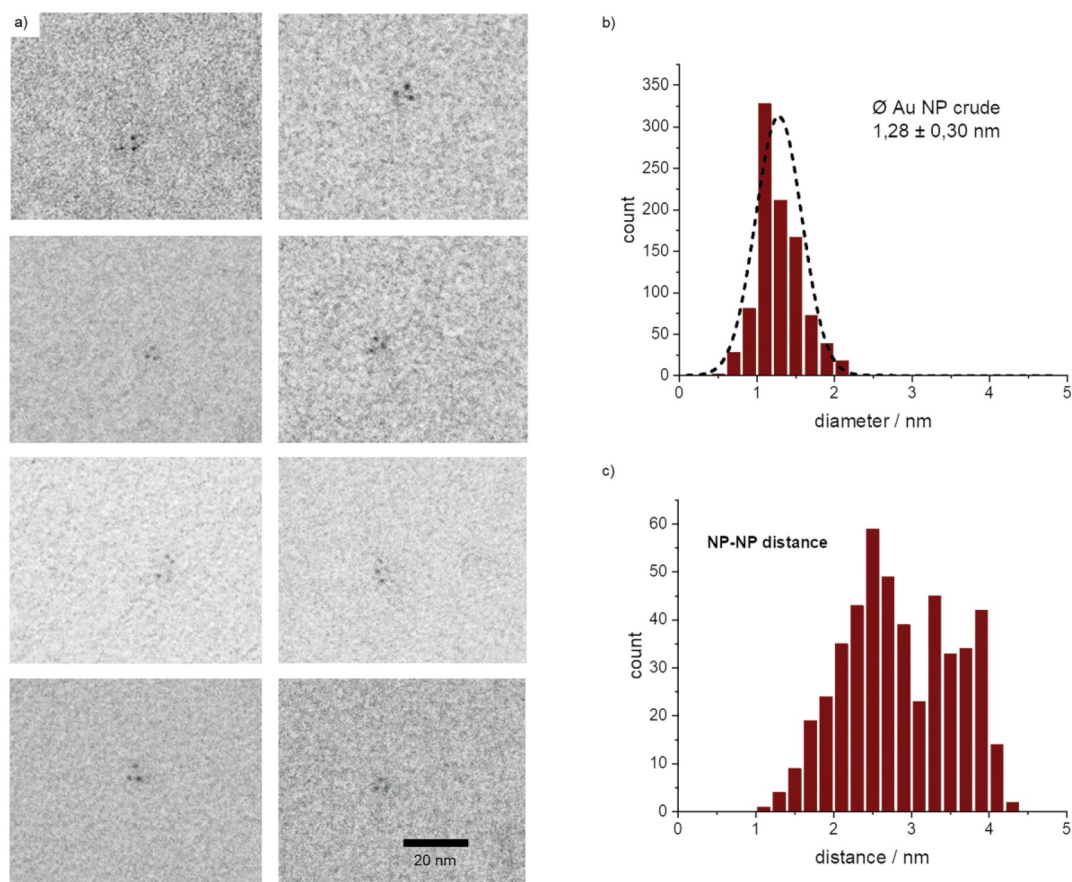


Figure 3. TEM analyses of (Au-1)₃9. **a)** TEM micrographs of (Au-1)₃9 (scale bar is valid for all 8 micrographs). **b)** Size-distribution of Au NPs after the deprotection–click–coupling protocol. **c)** Distribution of the interparticle distance in (Au-1)₃9.

Conclusion

In summary, a new ligand for the efficient and controlled synthesis of monofunctionalized Au NPs combining the massive nature of the particles with the wet chemical addressability of a molecule and thus behaving as “massive molecules” with superior stability properties is reported. The ligand design is based on a central tetraphenylmethane subunit unifying three oligomeric benzyl sulfide chains forming the Au NP-stabilizing subunit and exposing a masked alkyne on an OPE rod attached to the fourth phenyl ring of the central unit. Au NPs with narrow size distribution around 1.2 nm coated by a single ligand are obtained efficiently and display very good stability features, withstanding decomposition up to 105 °C in dispersion. The “massive molecule”-like behavior is displayed by deprotecting the terminal alkyne of the coated Au NP and engaging it in coupling protocols providing interlinked dimeric and trimeric Au NP systems as displayed by TEM analyses. With the here reported coating ligand, the particles of these nano-architectures are stable enough to resist the shear forces during purification by SEC.

We are currently investigating the catalytic activity of these ligand-coated Au NPs and explore their scope as labels in proteins and even larger biological systems.

Experimental Section

Materials

All commercially available starting materials were of reagent grade and used as received, unless stated differently. Absolute THF was purchased from Acros, stored over 4 Å molecular sieves, pre-dried with CaH, handled under argon and freshly distilled from sodium before each use. Pure CH₂Cl₂ was purchased from J. T. Baker. Pure toluene was purchased from Acros. Pure DMF was purchased from Acros Organics. *tert*-butylmethyl ether (TBME), *c*-hexane, ethyl acetate (EtOAc), and CH₂Cl₂ from Biosolve were used for purification and were of technical grade. Column chromatography was carried out on SiliaFlash P60 (particle size 40–63 μm) from SiliCycle. SEC for the purification of Au NPs mono-, di- and trimers was performed manually using Bio-Rad Bio-Beads S-X1 (operating range 600–14 000 g mol⁻¹) with CH₂Cl₂ or toluene as eluent. Deuterated solvents were purchased from Cambridge Isotope Laboratories.

Equipment and Measurements

¹H- and ¹³C-NMR spectra were recorded with a Bruker DPX 400 instrument (¹H resonance 400 MHz, ¹³C resonance 101 MHz) or a Bruker DRX 500 instrument (¹H resonance 500 MHz, ¹³C resonance 126 MHz) at 298 K. The chemical shifts (δ) are reported in ppm and are referenced to the residual proton signal of the deuterated solvent ([D]chloroform: 7.26 ppm) for ¹H spectra or the carbon of the solvent ([D]chloroform: 77.1 ppm) for ¹³C spectra. The coupling con-

stants (*J*) are given in Hertz (Hz), the multiplicities are denoted as: s (singlet), d (doublet), t (triplet), m (multiplet), and br (broad). High-resolution mass spectra (HRMS) were measured as HR-ESI-ToF-MS with a Maxis 4G instrument from Bruker or a Bruker UltraFlex II – MALDI-ToF-MS. For purification of the ligands, a (automated) Shimadzu Prominence System was used with SDV preparative columns from Polymer Standards Service (two Showdex columns in series, 20 mm × 600 mm each, exclusion limit: 30 000 g mol⁻¹) with chloroform as eluent. UV/Vis measurements were recorded on a Jasco V-770 spectrophotometer using 117.100F-QS cuvettes from Hellma Analytics (10 mm light path). TEM was performed on a Philips CM100 TEM at 80 kV using copper grids (Cu-400HD) from Pacific Grid Tech. TGA was measured on a Mettler Toledo TGA/SDTA851[°] with a heating rate of 10 °C min⁻¹.

p-Iodophenyltriphenylmethane (4):^[64] To a degassed 250 mL two-neck flask equipped with rubber septum and thermometer, BF₃OEt₂ (3.67 mL, 29.0 mmol, 2 equiv.) was added and cooled to -10 °C. In a separate flask, 4-tritylaniline (5.01 g, 14.5 mmol, 1 equiv.) was dissolved in 100 mL of degassed CH₂Cl₂ and was added dropwise via transfer cannula. The mixture was stirred at -10 °C for 45 minutes after which time *t*BuNO₂ (3.00 mL, 25.0 mmol, 1.75 equiv.) dissolved in 50 mL of degassed CH₂Cl₂ was added dropwise via transfer cannula. The mixture was stirred at -10 °C during 45 minutes. I₂ (4.78 g, 18.9 mmol, 1.3 equiv.) and KI (3.61 g, 21.8 mmol, 1.5 equiv.) were added to the mixture which was thereafter stirred vigorously during 15 h and allowed to slowly warm up to r.t. Excess halogen was quenched upon addition of saturated aqueous Na₂S₂O₃. After phase separation, the aqueous phase was extracted twice more with CH₂Cl₂ and dried with Na₂SO₄. After evaporation of the volatile in vacuo, compound **4** was purified by column chromatography (c-hexane) as a pale solid (5.2 g, 11.6 mmol, 80 %). ¹H-NMR (400 MHz, [D]Chloroform): δ = 7.60–7.55 (m, 2H), 7.25–7.20 (m, 6H), 7.20–7.17 (m, 6H), 7.17–7.15 (m, 3H), 7.00–6.96 (m, 2H).

p-Iodophenyltri(p-bromophenyl)methane (5):^[65] In a 250 mL flask, **4** (4.91 g, 11.0 mmol, 1 equiv.) was dissolved in Br₂ (20 mL, 385 mmol, 35 equiv.) and stirred at r.t. for 30 minutes. The reaction was diluted with CH₂Cl₂ and crushed ice was added. The mixture was further cooled with an ice bath and saturated aqueous Na₂S₂O₃ was slowly added until all the excess bromine was quenched. The mixture was extracted twice with CH₂Cl₂, dried with Na₂SO₄, and the volatile evaporated in vacuo. The crude was subjected to silica plug filtration (CH₂Cl₂) and recrystallized from hot c-hexane to yield **5** as a pale solid (7.51 g, 11.0 mmol, quant.). ¹H-NMR (400 MHz, [D]Chloroform): δ = 7.63–7.57 (m, 2H), 7.41–7.37 (m, 6H), 7.04–6.99 (m, 6H), 6.92–6.84 (m, 2H).

p-[p-(Triisopropylsilylethynyl)phenylethynyl]phenyltri(p-bromophenyl)methane (6): In a dry, degassed 100 mL flask, **5** (1.4 g, 2.05 mmol, 1 equiv.), bis(triphenylphosphine)palladium(II)chloride (0.24 g, 0.205 mmol, 0.1 equiv., cat.) and CuI (0.195 g, 1.03 mmol, 0.5 equiv., cat.) were dissolved in 40 mL of CH₂Cl₂ and 10 mL of triethylamine (71.2 mmol, 35 equiv.). The mixture was bubbled with Ar for 20 minutes after which time, *p*-(triisopropylsilylethynyl)-phenylethyne (1.16 g, 4.1 mmol, 2 equiv.) was added portionwise while stirring for 2 hours at r.t. The solvent was then evaporated in vacuo and the crude subjected to column chromatography (c-hexane 10:1 CH₂Cl₂) to afford **6** as a yellow foam (1.3 g, 1.55 mmol, 76 %). ¹H-NMR (400 MHz, [D]Chloroform) δ = 7.47–7.39 (m, 12H), 7.17–7.13 (m, 2H), 7.08–7.02 (m, 6H), 1.16 (s, 21H). ¹³C-NMR (101 MHz, [D]Chloroform) δ = 145.71, 144.55, 132.45, 132.00, 131.40, 131.20, 131.09, 130.70, 123.50, 122.93, 121.40, 120.80, 106.64, 92.96, 90.62, 89.77, 63.98, 18.72, 11.35. HRMS (MALDI-ToF): *m/z* = [M]⁺ calcd. for C₄₄H₄₁Br₃Si: 834.0522, found 834.0531.

p-[p-(Triisopropylsilylethynyl)phenylethynyl]phenyltri(p-formyl)phenylmethane (7): In a dry, degassed 250 mL flask, **6** (2.10 g, 2.51 mmol, 1 equiv.) was dissolved in 50 mL of freshly distilled THF and cooled to -78 °C. *t*BuLi (1.7 M in pentane, 20 mL, 34.1 mmol, 13.5 equiv.) was added to the mixture and stirred for 2 hours. DMF (5 mL, 65.3 mmol, 26 equiv.) was added to the mixture which was warmed up to r.t. over 2 hours and was thereafter stirred for 2 more hours. The reaction was cautiously quenched by addition of water, the organic phase separated, and the aqueous phase extracted twice with CH₂Cl₂. The combined organic phase was dried with Na₂SO₄, and the solvent evaporated. The purification was afforded by column chromatography (c-hexane 4:1 EtOAc) to yield **7** as a yellowish solid (1.51 g, 2.20 mmol, 88 %). ¹H-NMR (400 MHz, [D]Chloroform) δ = 10.00 (s, 3H), 7.89–7.77 (m, 6H), 7.51–7.39 (m, 12H), 7.25–7.16 (m, 2H), 1.13 (s, 21H). ¹³C-NMR (63 MHz, [D]Chloroform) δ = 191.43, 151.52, 144.71, 134.75, 131.99, 131.56, 131.40, 131.29, 130.64, 129.50, 123.59, 122.76, 121.89, 106.56, 93.08, 90.38, 90.11, 65.96, 18.69, 11.32. HRMS (ESI): *m/z* = [M + Na]⁺ calcd. for C₄₄H₄₁Br₃SiNa: 707.2952, found 707.2942.

p-[p-(Triisopropylsilylethynyl)phenylethynyl]phenyltri(p-hydroxymethylphenyl)methane (8): In a 100 mL flask, **7** (1.51 mg, 2.20 mmol, 1 equiv.) was dissolved in 20 mL of MeOH and 20 mL of THF and cooled to 0 °C. NaBH₄ (749 mg, 19.8 mmol, 9 equiv.) was added to the solution portionwise over 1 hour. The mixture was allowed to stir for 1 more hour until the reaction was quenched upon careful addition of aqueous HCl (10 %). The mixture was diluted with CH₂Cl₂ and transferred to a separation funnel. The aqueous phase was extracted three times with CH₂Cl₂, the combined organic phase dried with Na₂SO₄ and the solvent removed in vacuo. The crude product was filtered through a silica plug (c-hexane 1:1 EtOAc), to afford **8** as a yellowish solid (1.52 mg, 2.20 mmol, quant.). ¹H-NMR (400 MHz, [D]Chloroform): δ = 7.49–7.41 (m, 4H), 7.39–7.34 (m, 2H), 7.17 (s, 14H), 4.51 (s, 6H), 3.02–2.86 (s, 3H), 1.17 (s, 21H). ¹³C-NMR (63 MHz, [D]Chloroform) δ = 147.23, 145.70, 138.63, 131.98, 131.37, 131.01, 130.94, 130.89, 126.45, 123.33, 123.07, 120.61, 106.69, 92.85, 91.03, 89.34, 64.57, 64.42, 18.71, 11.34. HRMS (ESI-ToF): *m/z* = [M + Na]⁺ calcd. for C₄₇H₅₀NaO₃Si: 713.3421, found 713.3420.

p-[p-(Triisopropylsilylethynyl)phenylethynyl]phenyltri(p-bromomethyl)phenylmethane (2): In a dry, degassed 100 mL flask, **8** (419 mg, 0.606 mmol, 1 equiv.) was dissolved in 10 mL of dry, degassed CH₂Cl₂ and cooled to -10 °C. Triphenylphosphine (965 mg, 3.64 mmol, 2 equiv.) and carbon tetrabromide (1.21 g, 3.64 mmol, 2 equiv.) were added portionwise over 20 minutes. The mixture was allowed to stir 1 more hour and was then quenched by addition of saturated aqueous NaHCO₃. The organic phase was separated, dried with Na₂SO₄ and the solvent evaporated. The crude was subjected to silica plug filtration (CH₂Cl₂) to afford **2** as a yellowish foam (533 mg, 0.606 mmol, quant.). ¹H-NMR (400 MHz, [D]Chloroform): δ = 7.47–7.38 (m, 6H), 7.34–7.27 (m, 6H), 7.23–7.15 (m, 8H), 4.48 (s, 6H), 1.15 (s, 21H). ¹³C-NMR (101 MHz, [D]Chloroform): δ = 146.46, 146.20, 135.75, 131.98, 131.38, 131.24, 131.05, 130.89, 128.53, 123.39, 123.04, 120.98, 106.66, 92.87, 90.85, 89.50, 64.53, 33.07, 18.71, 11.34. HRMS (MALDI-ToF): *m/z* = [M]⁺ calcd. for C₄₇H₄₇Br₃Si: 876.0992, found 876.1003.

Ligand 1 (p-[p-(Triisopropylsilylethynyl)phenylethynyl]phenyltris{p-[(p-bis[p-(tert-butyl)phenyl][p-[(p-methylbenzyl)thio]methyl]phenyl)methyl]benzyl]thio]methyl]phenyl)methane): In a dry, degassed 25 mL flask, **2** (28 mg, 0.032 mmol, 1 equiv.) and **3** (74 mg, 0.118 mmol, 3.7 equiv.) were dissolved in 10 mL of freshly distilled THF. In order to start the reaction, NaH (60 % dispersed in mineral oil, 40 mg, 1.0 mmol, 10 equiv.) was added. The

mixture was allowed to stir at room temperature for 15 hours after which time, the reaction was quenched upon addition of minimum amounts of water. The mixture was dried with Na_2SO_4 , and the solvents evaporated to dryness. The crude was filtered through a silica plug (CH_2Cl_2) and subjected to automated GPC (chloroform) to give an orange oil (44 mg, 0.018 mmol, 55 %). $^1\text{H-NMR}$ (400 MHz, $[\text{D}]\text{Chloroform}$): δ = 7.44 (s, 2H), 7.43–7.33 (m, 2H), 7.26–7.20 (m, 12H), 7.19–7.08 (m, 64H), 3.61 (d, J = 5.3 Hz, 12H), 3.59 (d, J = 9.7 Hz, 12H), 2.33 (s, 9H), 1.30 (s, 54H), 1.15 (s, 21H). $^{13}\text{C-NMR}$ (126 MHz, $[\text{D}]\text{Chloroform}$) δ = 148.53, 147.28, 146.00, 145.85, 145.07, 143.67, 136.55, 135.98, 135.60, 135.41, 135.13, 131.97, 131.70, 131.37, 131.33, 131.26, 131.09, 131.01, 130.85, 130.71, 130.66, 130.57, 129.16, 128.90, 128.29, 127.95, 127.93, 124.55, 124.24, 123.28, 120.62, 106.71, 92.75, 64.33, 63.74, 35.55, 35.39, 35.26, 34.34, 31.41, 21.14, 18.71, 11.35. HRMS (MALDI-ToF): m/z = $[\text{M} + \text{Na}]^+$ calcd. for $\text{C}_{176}\text{H}_{188}\text{S}_6\text{Si}$: 2544.2697, found 2544.2725.

Gold Nanoparticle Formation and Purification

Au NP syntheses were carried out on a 30–50 μmol scale with respect to the Au equivalents. Tetrachloroauric acid (6 equiv., where 6 is the number of sulfur atoms in the used ligand) was dissolved in 2.0 mL of deionized water. A solution of TOAB (12 equiv.) dissolved in 2.0 mL of CH_2Cl_2 was added and the two-phase mixture was stirred for 15 minutes after which time, the aqueous phase had turned colorless and the bright orange color of the organic phase indicated complete phase transfer of the gold. The ligand (1 equiv.), dissolved in 2.5 mL of CH_2Cl_2 , was added to the reaction mixture which was stirred for 15 minutes, allowing the thioether moieties and the gold to pre-organize their conformation. A freshly prepared solution of sodium borohydride (48 equiv.) in 2.0 mL of water was then added quickly to the reaction mixture, reducing the gold species and thereby causing an immediate color change to dark brown. After 15 min stirring, the resulting opaque organic phase was separated from the aqueous phase via Pasteur pipette and the aqueous phase was washed three times with CH_2Cl_2 and separated in the same manner. The combined organic fractions were concentrated to a volume of approximately 0.5 mL in a Falcon tube by constant bubbling of protection gas to avoid possible thermal decomposition. 35 mL of ethanol was added in order to precipitate the particles which were then centrifuged three times at during 25 minutes at 5 $^\circ\text{C}$ and 4000 rpm, discarding the supernatant after every centrifugation step. After redispersion in CH_2Cl_2 , the Au NPs were separated from excess ligand via size-exclusion chromatography, and stored in the freezer dispersed in CH_2Cl_2 at a concentration of 1 mg mL^{-1} .

Gold Nanoparticle Dimerization

The formation of Au NP dimers was done on a 2 mg scale with respect to **Au-1**. The acetylene-functionalized Au NPs (**Au-1-TIPS**) were dispersed in CH_2Cl_2 (200 μL) and TBAF (1 M in THF, 50 μL) was added. The mixture was left stirring for 1 hour, quenched with water, extracted with dichloromethane and dried with Na_2SO_4 . After filtration, the solvent was evaporated and the deprotected particles were redispersed in CH_2Cl_2 (200 μL). TMEDA (50 μL) and copper(I) chloride (2 mg) were added. The dimerization reaction was left stirring for 4 hours and then quenched with a saturated aqueous solution of ammonium chloride, extracted with CH_2Cl_2 and dried with Na_2SO_4 . After filtration, the solution was concentrated and subjected to size-exclusion chromatography (once in CH_2Cl_2 and twice in toluene). The obtained fractions were investigated by TEM on carbon-coated copper S5 grids in order to identify pure dimer fractions. 0.67 mg of dimers were obtained (34 %; with respect to **Au-1-TIPS** containing 54.7 Au atoms in average). Highly diluted solutions were used for deposition on the grids to avoid accidental

proximity of non-linked NPs. Interparticle distances were measured manually from the TEM micrographs.

Gold Nanoparticle Trimerization

The Au NP “click” reactions were carried out with 3 mg of Au NPs (MW 13357 g/mol [one ligand **1** with 55 Au atoms]). The acetylene-monofunctionalized Au NPs were dispersed in dichloromethane (200 μL) and TBAF (1 M in THF, 50 μL) was added. The mixture was left stirring for 1 hour and quenched with water, extracted with dichloromethane and dried with Na_2SO_4 . After filtration, the solution was concentrated by vacuum at 30 $^\circ\text{C}$. The dry, deprotected Au NPs were dissolved in 50 μL dichloromethane. Corresponding to the amount of azide moieties, 0.33 equiv. 1,3,5-tris[*p*-(azidomethyl)phenyl]benzene was dissolved in 50 μL CH_2Cl_2 and added to the solution. While intensely stirring, CuSO_4 (20 mol-% in respect to **Au-1-TIPS** dissolved in 20 μL water) and sodium ascorbate (30 mol-% in respect to **Au-1-TIPS** dissolved in 20 μL water) were added. After 4 h reaction time, the mixture was extracted with dichloromethane and dried with Na_2SO_4 and dried in vacuo to yield a mixture of Au NP mono-, di- and trimers. The crude was subjected to four cycles of SEC with toluene as an eluent to remove unreacted monomers. Di- and trimers were not separated. Highly diluted solutions were used for deposition on the grids to avoid accidental proximity of non-linked NPs. Interparticle distances and di- and trimerization yields were measured manually from the TEM micrographs.

Acknowledgments

The authors thank the Swiss National Science Foundation (Grant no. 200020_178808) for financial support, Cedric Wobill for providing the TGA measurements, Dr. Michael Pfeffer and Dr. Heinz Nadig for measuring ESI-HRMS and the ETH Zürich MoBiAs lab for measurement of MALDI-HRMS. M. M. acknowledges support by the 111 project (90002-18011002).

Keywords: Gold · Nanoparticles · Monofunctionalized particles · Macromolecular ligands · Oligomers · Organic coating

- [1] M. Faraday, *Philos. Trans. R. Soc. London* **1857**, 147, 145–181.
- [2] G. Schmid, M. Bäuml, M. Geerkens, I. Heim, C. Osemann, T. Sawitowski, *Chem. Soc. Rev.* **1999**, 28, 179–185.
- [3] E. Boisselier, D. Astruc, *Chem. Soc. Rev.* **2009**, 38, 1759–1782.
- [4] P. Mulvaney, *MRS Bull.* **2001**, 26, 1009–1014.
- [5] M.-C. Daniel, D. Astruc, *Chem. Rev.* **2004**, 104, 293–346.
- [6] M. Brust, M. Walker, D. Bethell, D. J. Schiffrin, R. Whyman, *J. Chem. Soc., Chem. Commun.* **1994**, 801–802.
- [7] M. Brust, J. Fink, D. Bethell, D. J. Schiffrin, C. Kiely, *J. Chem. Soc., Chem. Commun.* **1995**, 1655–1656.
- [8] M. Bartz, J. Küther, R. Seshadri, W. Tremel, *Angew. Chem. Int. Ed.* **1998**, 37, 2466–2468; *Angew. Chem.* **1998**, 110, 2646.
- [9] W. K. Cho, J. K. Lee, S. M. Kang, Y. S. Chi, H.-S. Lee, I. S. Choi, *Chem. Eur. J.* **2007**, 13, 6351–6358.
- [10] R. Sardar, A. M. Funston, P. Mulvaney, R. W. Murray, *Langmuir* **2009**, 25, 13840–13851.
- [11] F. J. Ibañez, F. P. Zamborini, *ACS Nano* **2008**, 2, 1543–1552.
- [12] C.-C. Huang, Z. Yang, K.-H. Lee, H.-T. Chang, *Angew. Chem. Int. Ed.* **2007**, 46, 6824–6828; *Angew. Chem.* **2007**, 119, 6948–6952.
- [13] Y. Guo, Z. Wang, H. Shao, X. Jiang, *Analyst* **2011**, 137, 301–304.
- [14] L. M. Demers, C. A. Mirkin, R. C. Mucic, R. A. Reynolds, R. L. Letsinger, R. Elghariani, G. Viswanadham, *Anal. Chem.* **2000**, 72, 5535–5541.
- [15] J. J. Storhoff, A. A. Lazarides, R. C. Mucic, C. A. Mirkin, R. L. Letsinger, G. C. Schatz, *J. Am. Chem. Soc.* **2000**, 122, 4640–4650.

- [16] R. Wilson, *Chem. Commun.* **2003**, 108–109.
- [17] D. C. Hone, A. H. Haines, D. A. Russell, *Langmuir* **2003**, *19*, 7141–7144.
- [18] D. S. Seferos, D. A. Giljohann, H. D. Hill, A. E. Prigodich, C. A. Mirkin, *J. Am. Chem. Soc.* **2007**, *129*, 15477–15479.
- [19] P. Miao, Y. Tang, Z. Mao, Y. Liu, *Part. Part. Syst. Charact.* **2017**, *34*, 1600405.
- [20] D. G. Georganopoulou, L. Chang, J.-M. Nam, C. S. Thaxton, E. J. Mufson, W. L. Klein, C. A. Mirkin, *Proc. Natl. Acad. Sci. USA* **2005**, *102*, 2273–2276.
- [21] N. L. Rosi, D. A. Giljohann, C. S. Thaxton, A. K. R. Lytton-Jean, M. S. Han, C. A. Mirkin, *Science* **2006**, *312*, 1027–1030.
- [22] M. Homberger, U. Simon, *Phil. Trans. R. Soc. A* **2010**, *368*, 1405–1453.
- [23] P. Podsiadlo, V. A. Sinani, J. H. Bahng, N. W. S. Kam, J. Lee, N. A. Kotov, *Langmuir* **2008**, *24*, 568–574.
- [24] M.-C. Bowman, T. E. Ballard, C. J. Ackerson, D. L. Feldheim, D. M. Margolis, C. Melander, *J. Am. Chem. Soc.* **2008**, *130*, 6896–6897.
- [25] R. Costi, A. E. Saunders, U. Banin, *Angew. Chem. Int. Ed.* **2010**, *49*, 4878–4897; *Angew. Chem.* **2010**, *122*, 4996.
- [26] M. A. Mangold, M. Calame, M. Mayor, A. W. Holleitner, *ACS Nano* **2012**, *6*, 4181–4189.
- [27] J. Liao, L. Bernard, M. Langer, C. Schönenberger, M. Calame, *Adv. Mater.* **2006**, *18*, 2444–2447.
- [28] D. Huang, F. Liao, S. Moles, D. Redinger, V. Subramanian, *J. Electrochem. Soc.* **2003**, *150*, G412–G417.
- [29] J. Wang, J. Li, J. Li, F. Liu, Y. Gu, J. Fan, B. Dong, C. Wang, L. Qiu, L. Gao, et al., *Curr. Org. Chem.* **2016**, *20*, 1786–1796.
- [30] T. A. Gschneidtnr, Y. A. D. Fernandez, K. Moth-Poulsen, *J. Mater. Chem. C* **2013**, *1*, 7127–7133.
- [31] J. Liao, S. Blok, S. J. van der Molen, S. Diefenbach, A. W. Holleitner, C. Schönenberger, A. Vladyka, M. Calame, *Chem. Soc. Rev.* **2015**, *44*, 999–1014.
- [32] R. Wilson, *Chem. Soc. Rev.* **2008**, *37*, 2028–2045.
- [33] J. G. Worden, A. W. Shaffer, Q. Huo, *Chem. Commun.* **2004**, 518–519.
- [34] X. Liu, J. G. Worden, Q. Dai, J. Zou, J. Wang, Q. Huo, *Small* **2006**, *2*, 1126–1129.
- [35] D. Zanchet, C. M. Micheel, W. J. Parak, D. Gerion, A. P. Alivisatos, *Nano Lett.* **2001**, *1*, 32–35.
- [36] C. Krüger, S. Agarwal, A. Greiner, *J. Am. Chem. Soc.* **2008**, *130*, 2710–2711.
- [37] R. Lévy, Z. Wang, L. Duchesne, R. C. Doty, A. I. Cooper, M. Brust, D. G. Fernig, *ChemBioChem* **2006**, *7*, 592–594.
- [38] T. Peterle, A. Leifert, J. Timper, A. Sologubenko, U. Simon, M. Mayor, *Chem. Commun.* **2008**, 3438–3440.
- [39] T. Peterle, P. Ringler, M. Mayor, *Adv. Funct. Mater.* **2009**, *19*, 3497–3506.
- [40] J. P. Hermes, F. Sander, T. Peterle, C. Cioffi, P. Ringler, T. Pfohl, M. Mayor, *Small* **2011**, *7*, 920–929.
- [41] J. P. Hermes, F. Sander, T. Peterle, M. Mayor, *Chin. Int. J. Chem.* **2011**, *65*, 219–222.
- [42] M. Lehmann, E. H. Peters, M. Mayor, *Chem. Eur. J.* **2016**, *22*, 2261–2265.
- [43] M. Lehmann, E. H. Peters, M. Mayor, *Helv. Chim. Acta* **2017**, *100*, e1600395.
- [44] W. M. Pankau, K. Verbist, G. von Kiedrowski, *Chem. Commun.* **2001**, 519–520.
- [45] Y. Hosokawa, S. Maki, T. Nagata, *Bull. Chem. Soc. Jpn.* **2005**, *78*, 1773–1782.
- [46] W. M. Pankau, S. Mönninghoff, G. von Kiedrowski, *Angew. Chem. Int. Ed.* **2006**, *45*, 1889–1891; *Angew. Chem.* **2006**, *118*, 1923.
- [47] J. P. Hermes, F. Sander, T. Peterle, R. Urbani, T. Pfohl, D. Thompson, M. Mayor, *Chem. Eur. J.* **2011**, *17*, 13473–13481.
- [48] J. P. Hermes, F. Sander, U. Fluch, T. Peterle, D. Thompson, R. Urbani, T. Pfohl, M. Mayor, *J. Am. Chem. Soc.* **2012**, *134*, 14674–14677.
- [49] F. Sander, U. Fluch, J. P. Hermes, M. Mayor, *Small* **2014**, *10*, 349–359.
- [50] A. D'Aléo, R. M. Williams, F. Osswald, P. Edamana, U. Hahn, J. van Heyst, F. D. Tichelaar, F. Vögtle, L. De Cola, *Adv. Funct. Mater.* **2004**, *14*, 1167–1177.
- [51] R. McCaffrey, H. Long, Y. Jin, A. Sanders, W. Park, W. Zhang, *J. Am. Chem. Soc.* **2014**, *136*, 1782–1785.
- [52] E. H. Peters, M. Lehmann, M. Mayor, *Part. Part. Syst. Charact.* **2018**, *35*, 1800015.
- [53] T. Sakata, S. Maruyama, A. Ueda, H. Otsuka, Y. Miyahara, *Langmuir* **2007**, *23*, 2269–2272.
- [54] L. Wei, K. Padmaja, W. J. Youngblood, A. B. Lysenko, J. S. Lindsey, D. F. Bocian, *J. Org. Chem.* **2004**, *69*, 1461–1469.
- [55] L. Wei, H. Tiznado, G. Liu, K. Padmaja, J. S. Lindsey, F. Zaera, D. F. Bocian, *J. Phys. Chem. B* **2005**, *109*, 23963–23971.
- [56] H. C. Kolb, M. G. Finn, K. B. Sharpless, *Angew. Chem. Int. Ed.* **2001**, *40*, 2004–2021; *Angew. Chem.* **2001**, *113*, 2056.
- [57] H. C. Kolb, K. B. Sharpless, *Drug Discovery Today* **2003**, *8*, 1128–1137.
- [58] A. de Meijere, F. Diederich, *Metal-Catalyzed Cross-Coupling Reactions Second, Completely Revised and Enlarged Edition*, WILEY-VCH Verlag GmbH & Co. KGaA, Weinheim, **2004**.
- [59] M. M. Alvarez, J. T. Khoury, T. G. Schaaff, M. N. Shafiqullin, I. Vezmar, R. L. Whetten, *J. Phys. Chem. B* **1997**, *101*, 3706–3712.
- [60] "ImageJ," can be found as free download under <https://imagej.net/Welcome> (accessed Jun 17, **2016**).
- [61] P. Siemsen, R. C. Livingston, F. Diederich, *Angew. Chem. Int. Ed.* **2000**, *39*, 2632–2657; *Angew. Chem.* **2000**, *112*, 2740.
- [62] A. S. Hay, *J. Org. Chem.* **1962**, *27*, 3320–3321.
- [63] T. Zaba, A. Noworolska, C. M. Bowers, B. Breiten, G. M. Whitesides, P. Cyganik, *J. Am. Chem. Soc.* **2014**, *136*, 11918–11921.
- [64] R. K. R. Jetti, F. Xue, T. C. W. Mak, A. Nangia, *J. Chem. Soc., Perkin Trans. 2* **2000**, 1223–1232.
- [65] Y. KUBO, K. Nakamura, K. Watanabe, United States Patent Application: 0090227812 - TETRAPHENYLMETHANE SKELETON-CONTAINING COMPOUND, **A1**, 20090227812.

Received: March 18, 2020



Cite this: DOI: 10.1039/d3cc00277b

Received 18th January 2023.
Accepted 24th March 2023

DOI: 10.1039/d3cc00277b

rsc.li/chemcomm

An organic cage controlling the dimension and stability of gold nanoparticles†‡

Erich Henrik Peters^{id}^a and Marcel Mayor^{id}^{*abc}

A molecular cage encapsulating gold nanoparticles is presented. Six benzylic thioethers are pointing into its cavity, stabilizing the particles in a 1:1 ligand-to-particle-ratio in excellent yields. They are bench-stable for several months and can withstand unprecedented thermal stress of up to 130 °C, documenting the advantages of the cage-type stabilization over open-chain analogues.

Owing to their optical,^{1–4} physical^{4,5} and catalytic^{4,6–9} properties, gold nanoparticles (Au NPs) are of major importance in labeling applications^{4,10–16} and as functional building blocks in molecular devices and materials.^{5,17–25} Ever since the pioneering works of Brust *et al.*,^{26,27} great attention has been drawn to thiol-based organic ligands for the stabilization of Au NPs due to the thiolates' affinity for gold.^{28,29}

Based on those seminal works, Pankau *et al.* proposed the use of benzylic thioether-based structures,^{30,31} benefiting from the quasi-reversible character of the dispersion force-type bond between thioether and gold,^{29,32} allowing the ligand to adopt its most favorable conformation upon Au NP formation. This ligand design allowed the synthesis of more complex sulfur-based ligands such as linear,^{33–36} dendritic^{37–39} and branched^{40,41} oligomers that allow the synthesis of Au NPs passivated by a small, discrete number of ligands. While these oligomers were optimized to cover and thereby passivate a well-defined area of the particle surface, the particle itself acted as the template, shaping and arranging the multidentate oligomeric ligand by the attractive

interaction between the ligand's thioether and the particle's gold surface.

As an alternative strategy, the synthesis of a cage-type structure with a well-defined cavity for the nanoparticle is considered in this work. In particular, the impact of a pre-defined organic cage on the particle size and stability is the focus of interest. The difference between both approaches is sketched in Fig. 1. Organic cages to grow metal nanoparticles have been reported for catalytic applications,⁴² and there is also a single example of a rigid cage as the template for Au NP growth.⁴³

The cage design **1** is a variation of our already reported threefold branched ligand structure for Au NPs (**2**)⁴¹ and is displayed in Scheme 1. In analogy to the threefold branched oligomer **2**, the central tetraphenylmethane subunit **7** was

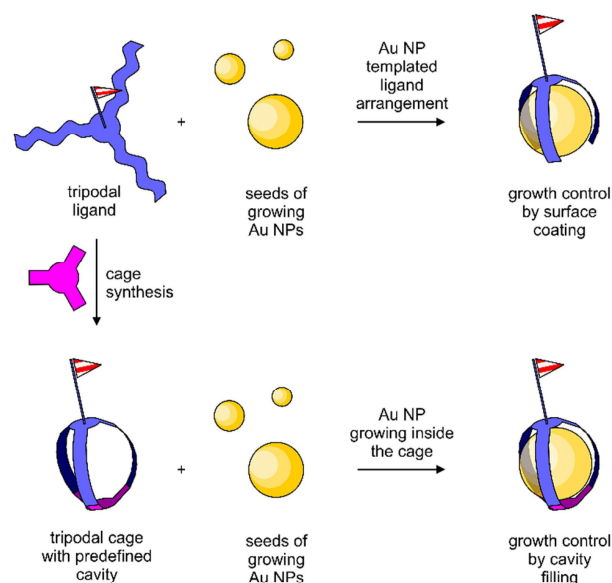


Fig. 1 Conceptual difference between oligomeric ligands passivating the Au NP growth by surface coating (top) and Au NP growth inside an organic cage (bottom).

^a Department of Chemistry, University of Basel, St. Johannis-Ring 19, Basel 4056, Switzerland. E-mail: marcel.mayor@unibas.ch

^b Institute for Nanotechnology (INT), Karlsruhe Institute of Technology (KIT), P. O. Box 3640, Karlsruhe 76021, Germany

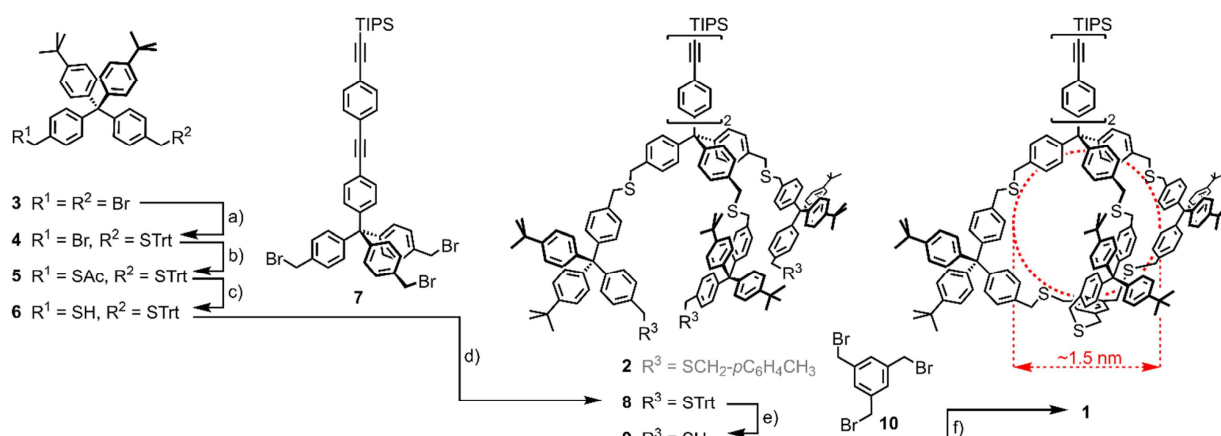
^c Lehn Institute of Functional Materials (LIFM), Sun Yat-Sen University (SYSU), Xingang Xi Rd. 135, Guangzhou 510275, P. R. China

† This work is dedicated to the late Günter Schmid.

‡ Electronic supplementary information (ESI) available: Experimental methods: Synthesis and characterization of compounds **1** and **3–9**, Fig. S1: ¹H NMR of **Au-1**, Fig. S2: TEM image of **Au-1**, Fig. S3: TGA trace of **Au-1**, and Fig. S4: Chem3D MM2 simulation rendering **1**. See DOI: <https://doi.org/10.1039/d3cc00277b>



Communication



Scheme 1 Synthesis of Cage-type ligand **1**. (a) TrtSH, NaH, THF, rt, 2 h, 34%; (b) KSAc, DMF, rt, 30', 93%; (c) (1) K_2CO_3 , MeOH/THF 1:1, rt, 30', (2) HCl (aq.), 96%; (d) THF, NaH, rt, 15 h, 84%; (e) $SiEt_3H$, TFA, CH_2Cl_2 , rt, 5', 93%; (f) **10**, NaH, THF, rt, 72 h, 52%. Trt = trityl, DMF = *N,N*-dimethylformamide, THF = tetrahydrofuran, TFA = trifluoroacetic acid. In red, cage **1**'s cavity's expected dimensions are displayed. Note that the threefold branched oligomer **2** has been previously synthesised⁴¹ and is thus displayed in grey.

decorated with three bifunctional tetraphenylmethane subunits **6** which were subsequently tied together to a cage by reacting with 1,3,5-tris(bromo methyl)benzene (**10**). The central tetraphenylmethane exposes an oligo(phenyleneethynylene) (OPE)-type molecular rod which turned out to be instrumental to define the outer side of the cavity. It is noteworthy that initial attempts without a sterically demanding molecular rod mounted at the central tetraphenylmethane had a pronounced tendency to close the cage with the remaining phenyl subunit of the central building block inside the cage, already occupying the cavity intended for the Au NP growth. Furthermore, the exposed triisopropylsilyl (TIPS)-protected terminal alkyne may act as a functional group, such that monofunctionalized Au NPs are expected.⁴⁴

The synthesis of the cage target structure **1** is displayed in Scheme 1. The assembly of the central benzylic tribromide **7** bearing a lengthy OPE was already reported.⁴¹ The main cage building block **6** was obtained from the benzylic dibromide **3**³³ via the orthogonally protected disulfide **5**. One bromide was substituted by trityl mercaptan (TrtSH) in THF, using sodium hydride (NaH) as a base to give precursor **4** in mediocre yields. The substitution of the second bromide by thioacetate provided the orthogonally protected precursor **5**. Subsequent selective deprotection of the acetate-protected benzylic thiol under basic conditions gave the monoprotected cage building block **6**. Treating the tribromide **7** with 4 equivalents (eq.) of thiol **6** in THF with NaH as the base provided **8** in good 84% isolated yield after gel permeation chromatography (GPC). Acidic deprotection with TFA and triethylsilane ($SiEt_3H$) as a cation scavenger gave trithiol **9** in very good 93% isolated yield.

Threefold nucleophilic substitution of the bromines of **10** with the thiols of **9** resulted in the cage target structure **1**. After a first S_N2 reaction between **9** and **10**, intramolecular ring closure was favored over intermolecular reactions under high-dilution conditions. A 1:1 mixture of **9** and **10** with about 10 eq. of NaH was stirred as 0.4 mM solution in THF for 72 hours at

room temperature, giving cage **1** as a colorless solid after GPC in a very good 52% yield, considering the threefold macrocyclization.

To be able to benchmark the Au NP formation in cage **1** with the one passivated by the coating ligand **2**, a similar Au NP synthesis protocol was used,⁴¹ which is a variation of the one reported by Brust *et al.*²⁶ 1 eq. of tetrachloroauric (III) acid ($HAuCl_4$) for each sulfur atom of the stabilizing structure, *i.e.* 6 eq. with respect to cage **1**, was dissolved in minimum amounts of water (0.3 ml). The transfer of the gold salt from the aqueous to the organic phase was enabled by addition of tetra-*n*-octylammonium bromide (TOAB, 2 eq. with respect to $HAuCl_4$, *i.e.* 12 eq. with respect to **1**) dissolved in minimum amounts of CH_2Cl_2 (0.3 ml). After completion of the phase transfer, indicated by complete decoloration of the aqueous phase, cage **1** as the stabilizing structure (1 eq.) was added as a solid. Nucleation and growth of the Au NPs was triggered by the quick addition of the reducing agent sodium borohydride ($NaBH_4$, 8 eq. with respect to $HAuCl_4$, *i.e.* 48 eq. with respect to **1**) dissolved in minimum amounts of water (0.3 ml). Upon addition of the reducing agent, an immediate color change of the organic phase from bright orange to auburn was observed. After rigorous stirring for 15 min, the organic phase was separated, dried *in vacuo* and the particles were suspended in ethanol. Separation of the Au NPs from excess TOAB, $NaBH_4$ and cage molecules was achieved by three subsequent centrifugations in ethanol, followed by size-exclusion chromatography (SEC) to provide cage **1**-stabilized Au NPs (referred to as **Au-1**) as black powder. The colloidal gold particles grown inside the cage were the only detectable form of gold and were collected in yields exceeding 90% with respect to the gold source. It is noteworthy that Au NPs lacking surface-passivating agents were inherently unstable in our hands and aggregated immediately, *e.g.* on the SEC column. Note that the determined masses were assuming a 1:1 ratio between cage **1** and Au NP, and this hypothesis that the cage structure is controlling the particle's growth by



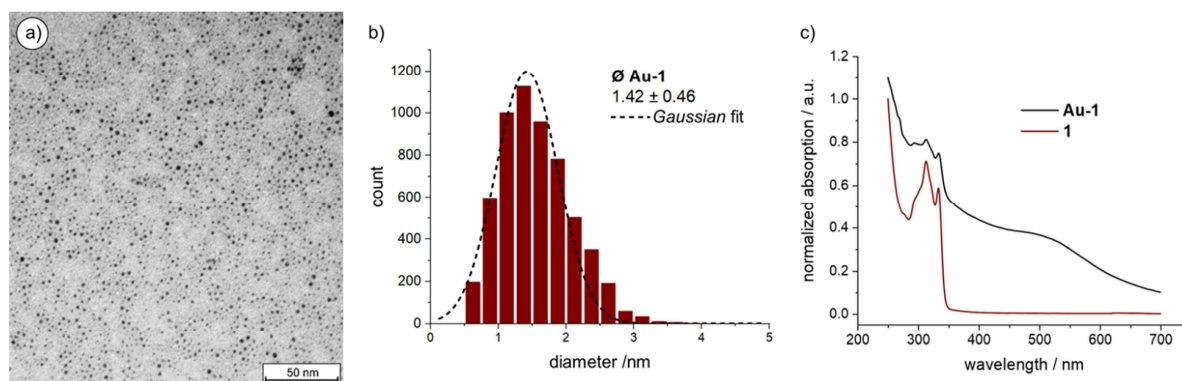


Fig. 2 (a) TEM image of **Au-1**; (b) size-distribution of **Au-1**; (c) Normalized UV-vis absorption spectra of **1** and **Au-1**. Offset for clarity.

encapsulation was corroborated by the analyses discussed in the following. The observed small mass loss most likely occurs during the separation and purification steps.

The Au NPs of **Au-1** were characterized by transmission electron microscopy (TEM, Fig. 2(a) and Fig. S2 in the ESI† displaying a larger area) from which the particle dimensions and their size distribution (Fig. 2(b)) was determined. The mass ratio between organic cage **1** and Au NP was determined by thermogravimetric analysis (TGA). UV-vis absorption spectroscopy (Fig. 2(c)) not only complemented the characterization of **Au-1**, but also allowed the investigation of the thermal stability of the hybrid architecture consisting of the particle inside the organic cage to be carried out.

Over 5000 Au NPs on the TEM micrograph gave an average NP diameter of 1.42 ± 0.46 nm, which is in good agreement with the estimated cavity size of cage **1** of about 1.5 nm obtained by simple MM2 simulation of the structure in Chem3D version 19 (sketched in red in Scheme 1; Fig. S4 in the ESI†). The Au NP size distribution was analyzed using the threshold and particle analysis tools from ImageJ.⁴⁵ The NPs of **Au-1** are enlarged compared with the ones coated and stabilized by the threefold symmetric ligand **2** (1.21 ± 0.36 nm).⁴¹ This suggests a more compact arrangement of the three branches of **2** on the Au NP surface and that the closing of the cage with a mesitylene subunit widens their spatial arrangement in **1**.

Thermogravimetric behavior of **Au-1** was analyzed up to 900 °C with a temperature gradient of 10 °C min^{-1} (Table S1 and Fig. S3 in the ESI†). The sample (2.053 mg) lost 18.1% (0.371 mg) which was attributed to the organic ligand **1**. Thus, 0.16 μmol of **1** were burned from the **Au-1** sample, while 1.682 mg of gold remained, corresponding to 8.54 μmol Au. Thus, on average 53.4 gold atoms are forming the Au NP in the cavity of **1** in the hybrid architecture **Au-1**. The analysis is in excellent agreement with the TEM-based particle size analysis, as the extensively investigated Au₅₅ clusters are reported with diameters of 1.44 ± 0.40 nm.^{46–48} Combined TEM and TGA analyses not only corroborate the 1:1 ratio between organic cage **1** and Au NP in **Au-1**, but also support the hypothesis of Au NP growth inside the cage's cavity.

The comparison between the UV-vis absorption spectra of **Au-1** and **1** (Fig. 2(c)) shows a broad and shallow bump between 450 and 600 nm, characteristic for the Au NPs' plasmon band absorption. The broadness of the absorption points at particle diameters below 2 nm since this is the limit below which the rate of surface scattering exceeds bulk scattering, resulting in a drastic surface plasmon band broadening. The electron-donating nature of the sulfur–gold bond increases the surface electron density below this size, contributing in addition to the surface scattering.⁴⁹ Interestingly, the absorption bands of the OPE subunit between 300 and 350 nm are well-defined for both, **1** and **Au-1**, documenting a well-dissolved OPE subunit in both cases and suggesting that the OPE rod of **Au-1** is exposed to the solvent. At this stage, the accessibility of the OPE is less important but becomes instrumental in the currently ongoing studies, profiting from the exposed alkyne as a reactive handle allowing these monofunctionalized particles to be considered as “massive molecules”.

The remarkable stability of the caged Au NPs in **Au-1** already became apparent in their separation by SEC. To evaluate their thermal stability, a sample was dispersed in *o*-xylene and gradually heated while investigated by UV-vis spectroscopy (Fig. 3). Of particular interest was the plasmon band bump

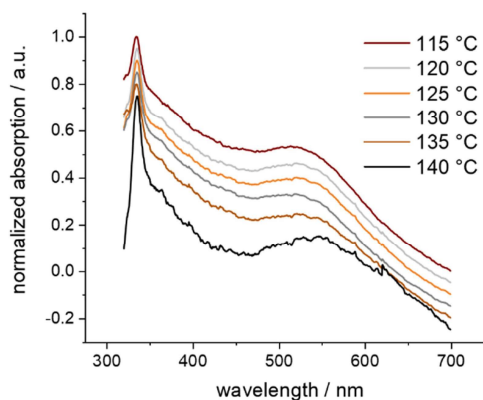
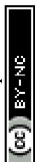


Fig. 3 Normalized UV-vis absorption spectra of **Au-1** in *o*-xylene at selected temperatures, showing thermal aggregation. Offset for clarity.



Communication

between 450 and 600 nm. Starting at 60 °C, the temperature increment was 5 °C per 30 minutes. The series of recorded UV-vis absorption traces displays the first slight redshift of the bump at 135 °C. Exceeding this temperature threshold, the particles aggregated, resulting in a considerable redshift visible to the naked eye. Exposure of samples to temperatures above 135 °C for longer periods resulted in the precipitation of agglomerated Au NPs as a purple solid. Interestingly, the caged Au NPs in **Au-1** have an increased decomposition temperature compared with the ones coated with **2**, which are reported to decompose above 105 °C.⁴¹ We hypothesize that, in **Au-1**, the NP coating sulfides cannot easily detach from the particle surface due to their spatial pre-organization and fixation in the polycyclic cage structure, being reflected in the observed improved resistance against thermal stress. Furthermore, the superior thermal stability features also support the claim of the Au NP grown and caged inside the cavity in the **Au-1** hybrid architecture.

In summary, the cage-type polycyclic ligand **1** is reported which acts as a growth and stabilization cavity for originating Au NPs. Cage **1** not only controls the dimension of the trapped Au NP in **Au-1**, but also protects it better against decomposition and aggregation than uncaged analogues. We are currently exploring the size limitation of the concept as well as the potential of these monofunctionalized Au NPs as labels and building blocks of devices. Furthermore, we intend to explore the catalytic activities of these structures and to investigate the entrapment of other metal clusters in the cage.

The authors thank the Swiss National Science Foundation (Grant no. 200020_207744) for financial support, Patrick Eckert from FHNW Muttensz for providing the TGA measurements, and Dr Michael Pfeffer and Dr Heinz Nadig for measuring ESI-HRMS. M. M. acknowledges support from the 111 project (90002-18011002).

Conflicts of interest

There are no conflicts to declare.

Notes and references

- M. Faraday, *Philos. Trans. R. Soc. London*, 1857, **147**, 145–181.
- G. Mie, *Ann. Phys.*, 1908, **330**, 377–445.
- P. Mulvaney, *MRS Bull.*, 2001, **26**, 1009–1014.
- M.-C. Daniel and D. Astruc, *Chem. Rev.*, 2003, **104**, 293–346.
- G. Schmid, M. Bäuml, M. Geerkens, I. Heim, C. Osemann and T. Sawitowski, *Chem. Soc. Rev.*, 1999, **28**, 179–185.
- C. Wang and D. Astruc, *Chem. Soc. Rev.*, 2014, **43**, 7188–7216.
- L. Pasquato, P. Pengo and P. Scrimin, *Supramol. Chem.*, 2005, **17**, 163–171.
- A. K. Ilunga and R. Meijboom, *Catal. Lett.*, 2019, **149**, 84–99.
- B. I. Kharisov, H. V. R. Dias, O. V. Kharissova and A. Vázquez, *J. Nanopart. Res.*, 2014, **16**, 2665.
- D. Safer, *J. Struct. Biol.*, 1999, **127**, 101–105.
- J. F. Hainfeld, *Science*, 1987, **236**, 450–453.
- J. F. Hainfeld and F. R. Furuya, *J. Histochem. Cytochem.*, 1992, **40**, 177–184.
- D. Safer, L. Bolinger and J. S. Leigh, *J. Inorg. Biochem.*, 1986, **26**, 77–91.
- R. Wilson, *Chem. Soc. Rev.*, 2008, **37**, 2028–2045.
- J. E. Reardon and P. A. Frey, *Biochemistry*, 1984, **23**, 3849–3856.
- H. Yang, J. E. Reardon and P. A. Frey, *Biochemistry*, 1984, **23**, 3857–3862.
- M. A. Mangold, M. Calame, M. Mayor and A. W. Holleitner, *ACS Nano*, 2012, **6**, 4181–4189.
- T. Dadosh, Y. Gordin, R. Krahne, I. Khivrich, D. Mahalu, V. Frydman, J. Sperling, A. Yacoby and I. Bar-Joseph, *Nature*, 2005, **436**, 677–680.
- J. Liao, S. Blok, S. J. van der Molen, S. Diefenbach, A. W. Holleitner, C. Schönenberger, A. Vladyka and M. Calame, *Chem. Soc. Rev.*, 2015, **44**, 999–1014.
- T. A. Gschneidner, Y. A. D. Fernandez and K. Moth-Poulsen, *J. Mater. Chem. C*, 2013, **1**, 7127–7133.
- Y.-S. Chen, M.-Y. Hong and G. S. Huang, *Nat. Nanotechnol.*, 2012, **7**, 197–203.
- H. Gu, J. Chao, S.-J. Xiao and N. C. Seeman, *Nature*, 2010, **465**, 202–205.
- Md. A. Rahman, H.-B. Noh and Yoon-Bo Shim, *Anal. Chem.*, 2008, **80**, 8020–8027.
- G. Schmid, *Adv. Eng. Mater.*, 2001, **3**, 737–743.
- L. Ma, F. Li, T. Fang, J. Zhang and Q. Wang, *ACS Appl. Mater. Interfaces*, 2015, **7**, 11024–11031.
- M. Brust, M. Walker, D. Bethell, D. J. Schiffrin and R. Whyman, *J. Chem. Soc., Chem. Commun.*, 1994, 801–802.
- M. Brust, J. Fink, D. Bethell, D. J. Schiffrin and C. Kiely, *J. Chem. Soc., Chem. Commun.*, 1995, 1655–1656.
- H. Häkkinen, *Nat. Chem.*, 2012, **4**, 443–455.
- J. R. Reimers, M. J. Ford, S. M. Marcuccio, J. Ulstrup and N. S. Hush, *Nat. Rev. Chem.*, 2017, **1**, 0017.
- W. M. Pankau, K. Verbist and G. von Kiedrowski, *Chem. Commun.*, 2001, 519–520.
- W. M. Pankau, S. Mönninghoff and G. von Kiedrowski, *Angew. Chem., Int. Ed.*, 2006, **45**, 1889–1891.
- M. S. Inkpen, Z.-F. Liu, H. Li, L. M. Campos, J. B. Neaton and L. Venkataraman, *Nat. Chem.*, 2019, **11**, 351.
- M. Lehmann, E. H. Peters and M. Mayor, *Chem. – Eur. J.*, 2016, **22**, 2261–2265.
- M. Lehmann, E. H. Peters and M. Mayor, *Helv. Chim. Acta*, 2017, **100**, e1600395.
- T. Peterle, A. Leifert, J. Timper, A. Sologubenko, U. Simon and M. Mayor, *Chem. Commun.*, 2008, 3438–3440.
- T. Peterle, P. Ringler and M. Mayor, *Adv. Funct. Mater.*, 2009, **19**, 3497–3506.
- J. P. Hermes, F. Sander, T. Peterle, R. Urbani, T. Pfohl, D. Thompson and M. Mayor, *Chem. – Eur. J.*, 2011, **17**, 13473–13481.
- F. Sander, U. Fluch, J. P. Hermes and M. Mayor, *Small*, 2014, **10**, 349–359.
- J. P. Hermes, F. Sander, U. Fluch, T. Peterle, D. Thompson, R. Urbani, T. Pfohl and M. Mayor, *J. Am. Chem. Soc.*, 2012, **134**, 14674–14677.
- E. H. Peters, M. Lehmann and M. Mayor, *Part. Part. Syst. Charact.*, 2018, **35**, 1800015.
- E. H. Peters and M. Mayor, *Eur. J. Inorg. Chem.*, 2020, 2325–2334.
- R. Saha, B. Mondal and P. S. Mukherjee, *Chem. Rev.*, 2022, **122**, 12244–12307.
- R. McCaffrey, H. Long, Y. Jin, A. Sanders, W. Park and W. Zhang, *J. Am. Chem. Soc.*, 2014, **136**, 1782–1785.
- E. H. Peters and M. Mayor, *Chimia*, 2021, **75**, 414–426.
- ImageJ, <https://imagej.nih.gov/ij/download.html>, (accessed December 27, 2019).
- G. Schmid, R. Pfeil, R. Boese, F. Bandermann, S. Meyer, G. H. M. Calis and J. W. A. van der Velden, *Chem. Ber.*, 1981, **114**, 3634–3642.
- T. Mori and T. Hegmann, *J. Nanopart. Res.*, 2016, **18**, 295.
- D. H. Rapoport, W. Vogel, H. Cölfen and R. Schlögl, *J. Phys. Chem. B*, 1997, **101**, 4175–4183.
- M. M. Alvarez, J. T. Khoury, T. G. Schaaff, M. N. Shafiqullin, I. Vezmar and R. L. Whetten, *J. Phys. Chem. B*, 1997, **101**, 3706–3712.



Conclusion and Outlook

In this thesis, a series of branched, benzylic thioether-based ligands for the monofunctionalization of gold nanoparticles was presented. We have shown that breaking the linearity of oligomeric ligands by introducing a central linking unit gives a better surficial covering of gold nanoparticles and results in an enhanced stability in comparison with parent linear ligands. This was demonstrated by attaching previously reported benzylic thioether ligands three times to a tripodal central tetraphenylmethane moiety. It was observed that ligands with bulkier thioether side-chains were more stable than their less bulky parent structures and were more effective in giving gold nanoparticles stabilized by a single ligand.

In a next step, we showed that this approach reliably gives monofunctionalized gold nanoparticles by introducing a protected acetylene-terminated OPE moiety to the free phenyl of the central linking tripod. Deprotection of the acetylene and subsequent homocoupling or CuAAC “click” reaction to 1,3,5-tris(4-(azidomethyl)phenyl)benzene gave gold nanoparticles dimers and trimers, respectively, with no notable observation of higher-order structures. The near-to-complete lack thereof points at the favorable surface passivation of the ligand. It was, nonetheless, found that a fraction of the gold nanoparticle dimers had a very short interparticle distance. Statistical analysis of the latter showed two distinct peaks which speaks against dimers that may not lie flat on the sample surface but rather for dimers where the acetylene is directly coupled to an exposed part of the neighboring gold nanoparticle surface.

Finally, the monofunctionalized ligand’s side-chains were tied together, closing a cage with a cavity diameter of approximately 1.5 nm. The particles synthesized in presence of this cage had a diameter in close agreement with the expected cavity size and were measured to contain 53.5 gold atoms in average, which compares well with reported Au₅₅ clusters. A most striking feature of these gold nanoparticles is the spontaneous di- and polymerization which was observed without subjecting the compound to deprotecting or acetylene-homocoupling conditions. While a direct attachment of a naked acetylene to an exposed gold atom of a neighboring particle seems an obvious structural explanation and is also supported by the very narrow interparticle distance, the mechanism polymerization has not been elucidated and is, as of this moment, still subject of further research.

This point of the work gives several opportunities for pushing our research further. The monofunctionalized tripodal ligand can be decorated with larger side-chains in order to investigate how far such systems can be enlarged to give bigger gold nanoparticles that still bear a single functionality. Owing to its favorable stabilization conditions, the closing benzene of the cage can be swapped for alternate, bulkier moieties, giving the cage a larger cavity and thus the prospect of optically more interesting gold nanoparticles. Since the present systems have proven to be suitable for further wet chemical processing, screening their suitability as labels for biomolecules or as catalysts should be envisaged. Finally, the ligands can be decorated with water-solubilizing groups, e.g cyclodextrin introduced by “click” chemistry with suitably modified ligands, in order to obtain the first ever reported water-soluble monofunctionalized gold nanoparticles stabilized by a single benzylic thioether-based ligand.

Copyright WILEY-VCH Verlag GmbH & Co. KGaA, 69469 Weinheim, Germany, 2018.

Particle

& Particle Systems Characterization

Supporting Information

for *Part. Part. Syst. Charact.*, DOI: 10.1002/ppsc.201800015

Gold Nanoparticles Stabilized by Single Tripodal Ligands

*Erich Henrik Peters, Mario Lehmann, and Marcel Mayor**

WILEY-VCH

Copyright WILEY-VCH Verlag GmbH & Co. KGaA, 69469 Weinheim, Germany, 2013.

Supporting Information

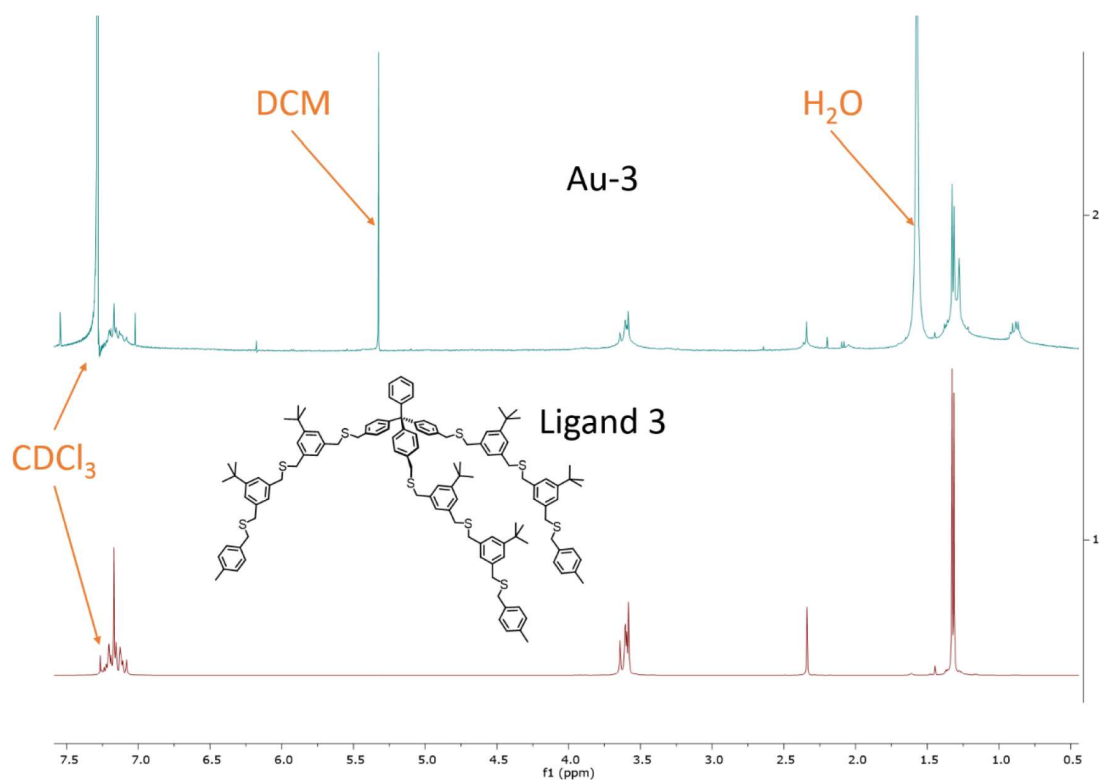
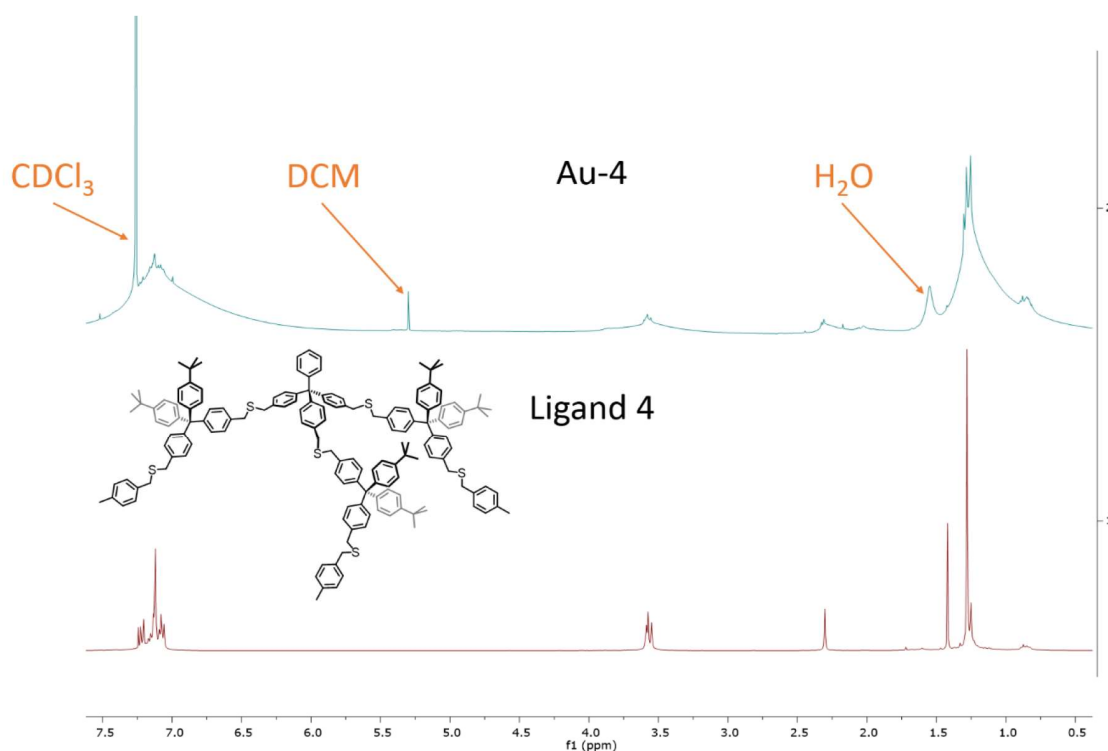
Gold Nanoparticles Stabilized by Single Tripodal Ligands*Erich Henrik Peters, Mario Lehmann, and Marcel Mayor**

Table of Contents

Analysis of AuNPs	S2-S6
¹ H-NMR of AuNPs	S2-S3
TGA Traces of Au-3, Au-4, and Au-5	S3
TGA Data of Au-4 ₁₂ eq, Au-5 ₁₈ eq, Au-5 ₃₆ eq, and Au-5 ₇₂ eq	S4
Monitoring of Heated AuNPs by UV-vis Absorption Spectroscopy	S4
TEM Micrographs and Size Analysis of Bigger NPs	S5-S6
Syntheses	S7-S13
Central Tripodal Linking Unit	S7-S9
<i>m</i> -Xylene-Based Oligomeric Side-Chains	S9-S10
Tetraphenylmethane-Based Oligomeric Side-Chains	S10-S13
NMR-Spectra of compounds 1 - 5	S14-S18
¹ H- and ¹³ C-NMR of Ligand 1	S14
¹ H- and ¹³ C-NMR of Ligand 2	S15
¹ H- and ¹³ C-NMR of Ligand 3	S16
¹ H- and ¹³ C-NMR of Ligand 4	S17
¹ H- and ¹³ C-NMR of Ligand 5	S18
References	S19

WILEY-VCH

Analysis of AuNPs

 $^1\text{H-NMR}$ of AuNPs**Figure S1.** $^1\text{H-NMR}$ spectrum of Au-3 (above) and of the pure ligand 3 (below).**Figure S2.** $^1\text{H-NMR}$ spectrum of Au-4 (above) and of the pure ligand 4 (below).

WILEY-VCH

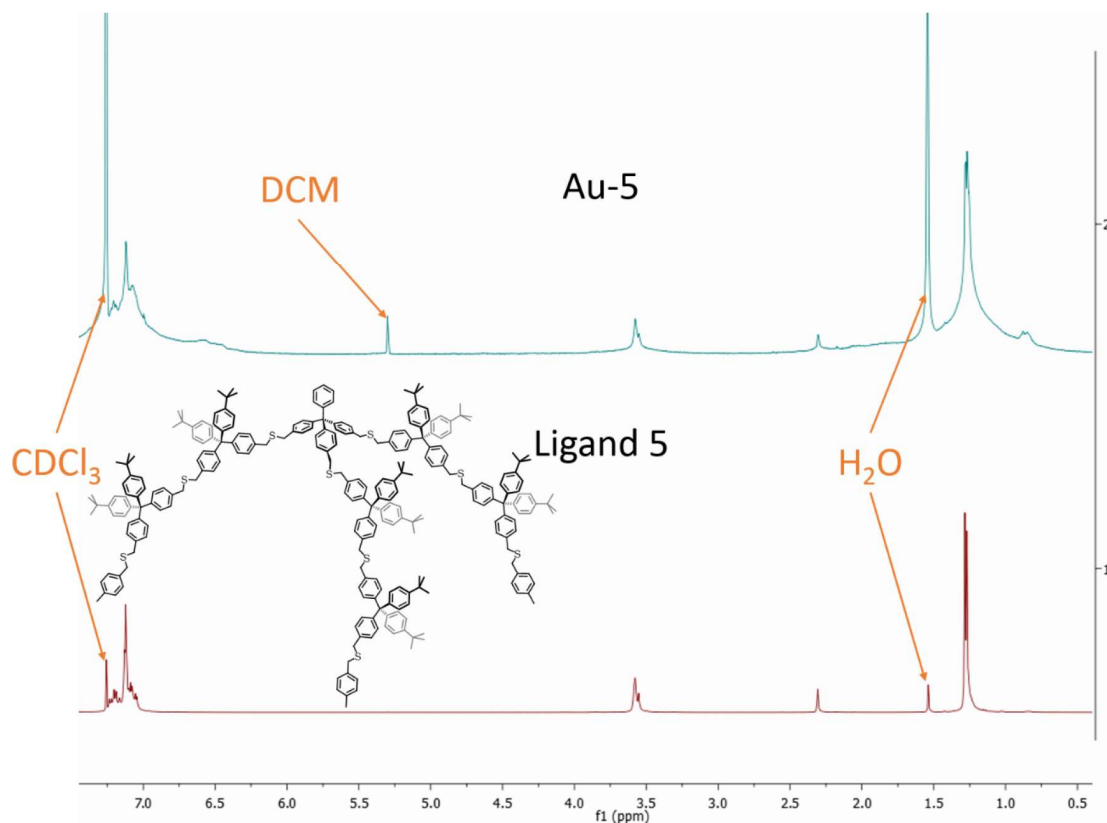


Figure S3. $^1\text{H-NMR}$ spectrum of **Au-5** (above) and of the pure **ligand 5** (below).

TGA Traces of Au-3, Au-4, and Au-5

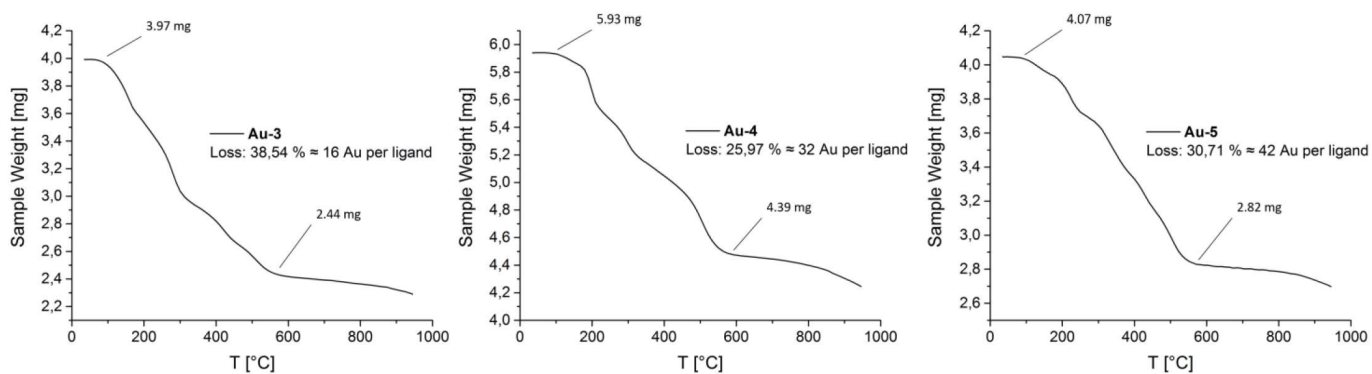


Figure S4. TGA traces of **Au-3**, **Au-4** and **Au-5**.

WILEY-VCH

TGA Data of Au-4_{12eq}, Au-5_{18eq}, Au-5_{36eq}, and Au-5_{72eq}

Table S1. Ligand-to-gold ratio based on TGA analysis data (*m*Lig: mass of disappearing ligand; *M*Lig: ligand molar mass; *n*Lig: number of moles of ligand; *m*Au: mass of remaining gold; *n*Au: number of moles of gold; Au/Lig: average number of gold atoms per ligand; NP Ø: NP diameter; Au/NP: average number of gold atoms per NP; Lig/NP: average number of ligand per NP; Molar mass of gold: MAu: 196.97 g mol⁻¹).

Entry	<i>m</i> Lig [mg]	<i>M</i> Lig [g mol ⁻¹]	<i>n</i> Lig [mol]	<i>m</i> Au [mg]	<i>n</i> Au [mol]	<i>n</i> Au [mol]	NP Ø [nm]	Au/NP	Lig/NP
Au-4 _{12eq}	1.45	2243	6.46 × 10 ⁻⁷	1.00	5.09 · 10 ⁻⁵	7.87	N/A	N/A	N/A
Au-5 _{18eq}	0.79	3716	2.13 × 10 ⁻⁷	1.65	8.38 · 10 ⁻⁶	39.29	1.18 ± 0.37	47.04	1.29
Au-5 _{36eq}	0.97	3716	2.61 × 10 ⁻⁷	1.59	8.07 · 10 ⁻⁶	30.92	1.30 ± 0.41	50.82	2.20
Au-5 _{72eq}	0.96	3716	2.58 × 10 ⁻⁷	0.70	3.56 · 10 ⁻⁶	13.78	1.62 ± 0.55	131.49	N/A

Monitoring of Heated AuNPs by UV-vis Absorption Spectroscopy

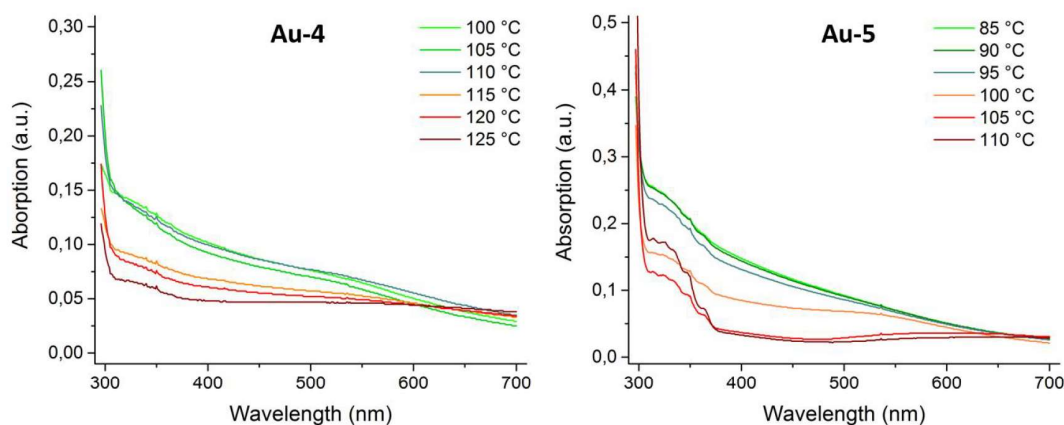


Figure S5. UV-vis absorption spectra of heated AuNPs at selected temperatures showing the thermal agglomeration of the particles due to ligand detaching visible by significant loss of absorption. Left: **Au-4**; right: **Au-5**. Offset for clarity.

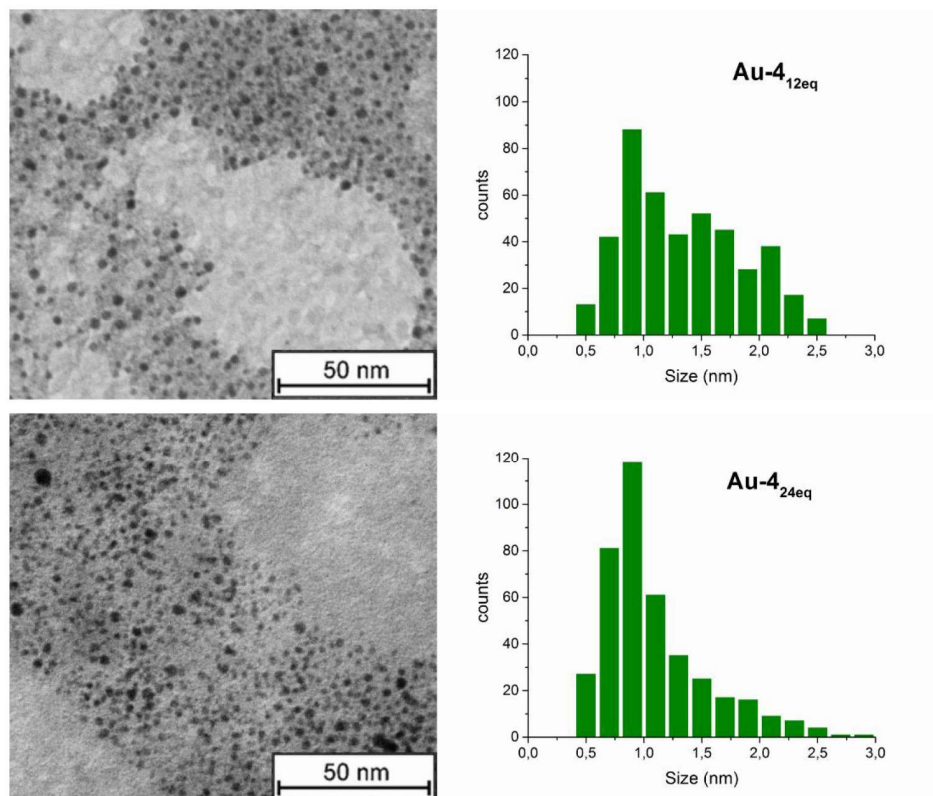
TEM Micrographs and Size Analysis of Bigger NPs

Figure S6. Representative TEM micrograph extracts and size distributions of the respective AuNPs. AuNPs synthesized using 12 (above) and 24 (below) equivalents of HAuCl₄ stabilized by ligand **4**. No statistics were made on these distributions for the lack of meaningfulness.

WILEY-VCH

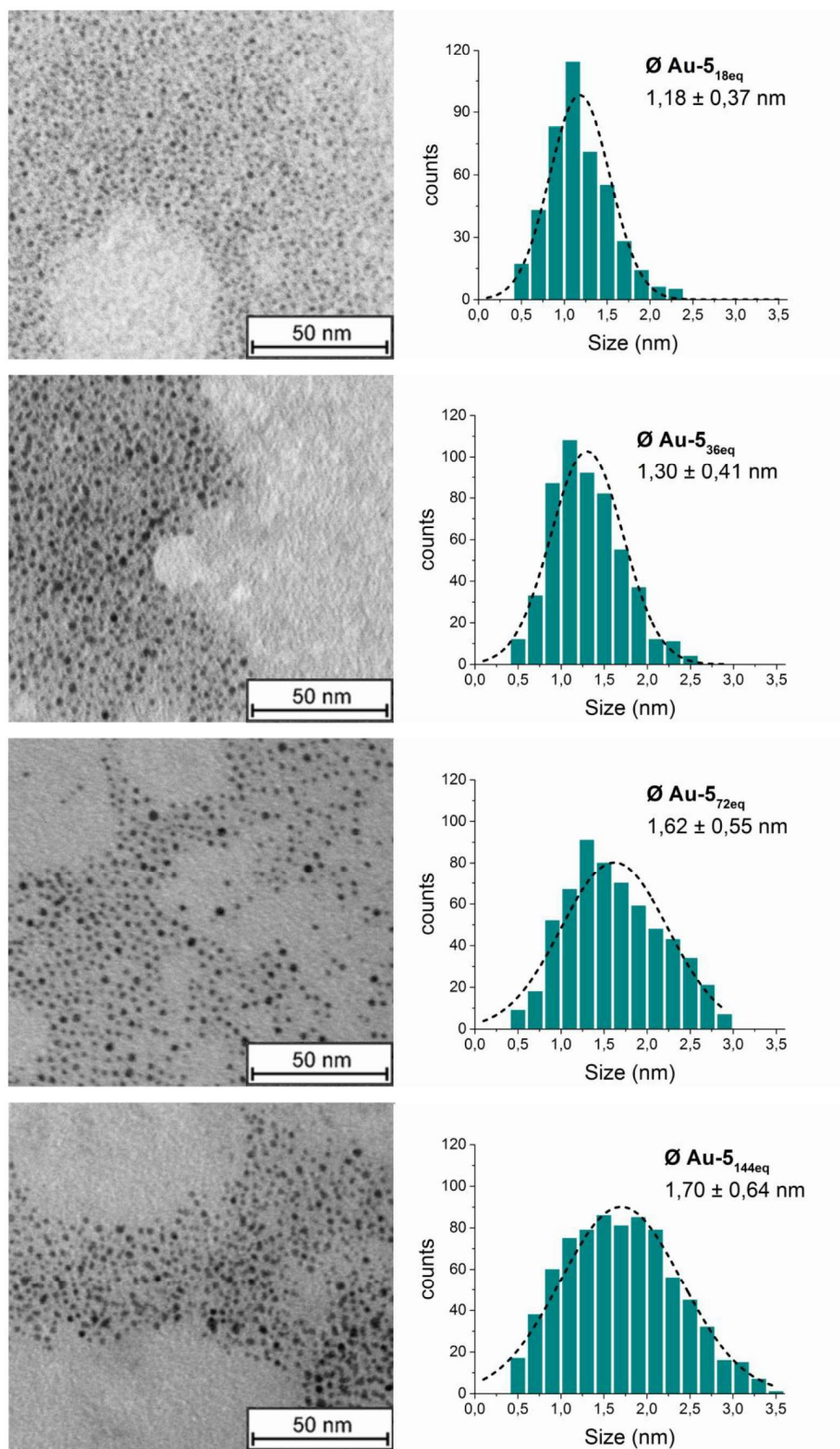


Figure S7. Representative TEM micrograph extracts and size distributions of the respective AuNPs. AuNPs synthesized using 18 (top), 36 (second), 72 (third) and 144 (bottom) equivalents of HAuCl₄ stabilized by ligand **5**. Note that the bottom micrograph was obtained from a crude, unpurified sample. *Gaussian* fits: dashed curves.

Syntheses

Central Tripodal Linking Unit

tri-p-tolylmethanol (11)^[1]

In a dry degassed 500 ml three-neck flask equipped with rubber septum, reflux condenser and addition funnel, Mg turnings (2.02 g, 83.2 mmol, 2.5 eq) were suspended in dry, degassed THF (100 ml) under argon atmosphere. 4-bromotoluene (14.2 g, 83.2 mmol, 2.5 eq) dissolved in dry, degassed THF (50 ml) were added drop-wise. In order to activate the *Grignard* reagent, the mixture was heated with a heat gun until a reaction was observed, and subsequently stirred for three hours. Methyl *p*-toluate (5 g, 33.3 mmol, 1 eq) was dissolved in dry, degassed THF (50 ml) and added to the mixture, which was then allowed to stir at 75 °C for 24 hours. After cooling to room temperature, the reaction was worked up with a saturated aqueous solution of NH₄Cl. The aqueous phase was washed twice with TBME. The combined organic phases were washed twice with water, dried over MgSO₄ and the solvent was evaporated. The crude product was subjected to CC (n-hexane 5:1 DCM) to obtain **11** as a white solid (9.87 g, 32.7 mmol, 98 %). ¹H-NMR (400 MHz, Chloroform-d δ): 7.17-7.12 (m, 6H), 7.09 (m, 6H), 2.70 (s, 1H), 2.32 (s, 9H).

4-(tri-p-tolylmethyl)aniline (12)^[2]

To a 250 ml two-neck flask, freshly distilled aniline (11.1 ml, 121 mmol, 4 eq) was added and dissolved in concentrated HCl (7.7 ml, cat.) and acetic acid (AcOH, 30 ml). Compound **11** (9.17 g, 30.4 mmol, 1 eq) was dissolved in AcOH (15 ml) and added portion-wise. The mixture was heated to 140 °C and refluxed during three hours, then allowed to cool to room temperature. The volatile was evaporated by rotavapor, the remaining solid was dissolved in DCM and neutralized with 1 M NaOH. The organic phase was washed three times with water, dried over Na₂SO₄ and concentrated. The product was allowed to precipitate by addition of

WILEY-VCH

cold MeOH to afford **12** as a white solid (7.6 g, 66 %). ¹H-NMR (400 MHz, Chloroform-d δ): 7.08 (m, 6H), 7.02 (m, 6H), 6.98-6.93 (m, 2H), 6.57 – 6.52 (m, 2H), 3.55 (s, 2H), 2.30 (s, 9H).

Tris(p-tolyl)methylbenzene (13)^[3]

To a dry, degassed 500 ml two-neck flask, BF₃OEt₂ (1.7 ml, 13.2 mmol, 2 eq) was added and cooled to -10 °C. Compound **12** (2.50 g, 6.62 mmol, 1 eq) was dissolved in dry, degassed THF (35 ml) in a separate dry and degassed flask, and was added drop-wise. The mixture was stirred at -10 °C for 2 hours after which time ^tBuNO₂ (1.4 ml, 11.6 mmol, 1.75 eq) dissolved in ml THF (35 ml) was added drop-wise. A 500 ml flask was prepared with FeSO₄ (1.11 mg, 7.32 mmol, 1.1 eq) dissolved in DMF (200 ml). The crude reaction mixture was slowly poured into the FeSO₄ solution, leading to evolution of N₂. The mixture was stirred at room temperature for 2.5 hours, then poured into ice water. The mixture was extracted twice with DCM, washed twice with 1 M aqueous HCl, twice with water and dried over MgSO₄. After evaporation of the volatile in vacuo, **13** was purified by CC (c-hexane 20:1 EtOAc) as a pale solid (1.92g, 80 %). ¹H-NMR (400 MHz, Chloroform-d δ): 7.24-7.19 (m, 4H), 7.18-7.13 (m, 1H), 7.12-7.00 (m, 12H), 2.30 (s, 9H).

Tris((p-bromomethyl)phenyl)methylbenzene (6)^[3]

A dry, degassed 500 ml two-neck flask was equipped with a reflux condenser and a glass stopper. Compound **13** (1.87 g, 5.16 mmol, 1 eq), NBS (5.51 g, 31 mmol, 6 eq) and AIBN (169 mg, 1.03 mmol, 0.2 eq) were suspended in methyl formate (200 ml) under argon atmosphere. The suspension was bubbled with argon for 30 minutes, then illuminated with a 500 W halogen lamp. The mixture was refluxed for 15 hours and then allowed to cool to room temperature. The crude precipitate was concentrated, and redissolved in DCM. The solution was washed four times with water, dried over MgSO₄, and the solvent was evaporated in

WILEY-VCH

vacuo. The crude product was subjected to automated CC (c-hexane 20:1 DCM, c-hexane 10:1 DCM after 4 column volumina) to give **6** as a white solid (1.56 g, 50 %). ¹H-NMR (400 MHz, Chloroform-d δ): 7.30-7.27 (m, 6H), 7.26-7.20 (m, 3H), 7.20-7.16 (m, 8H), 4.47 (s, 6H).

*m-Xylene-Based Oligomeric Side-Chains**1,3-bis(bromomethyl)-5-(tert-butyl)benzene (20)^[4]*

In a 500 ml two-neck flask 1-(tert-butyl)-3,5-dimethylbenzene (5 g, 30.8 mmol, 1 eq) was suspended in methyl formate (300 ml). NBS (21.9 g, 123 mmol, 4 eq) and AIBN (1.01 g, 6.16 mmol, 0.2 eq) were added to the suspension which was then bubbled with argon for 30 minutes. The mixture was illuminated by a 500 W halogen lamp and refluxed for 15 hours. The solvent was evaporated in vacuo, and the crude mixture redissolved in DCM. The mixture was washed once with a saturated aqueous solution of Na₂S₂O₃ and four times with water. The organic phase was dried over Na₂SO₄, and the solvent evaporated. The purification was afforded by automated CC (c-hexane 20:1 DCM and c-hexane 10:1 DCM after 4 column volumes) to yield **20** as a white solid (6.36 g, 65 %). ¹H-NMR (400 MHz, Chloroform-d δ): 7.33 (d, J = 1.6 Hz, 2H), 7.26–7.25 (m, 1H), 4.48 (s, 4H), 1.32 (s, 9H).

(3-(bromomethyl)-5-(tert-butyl)benzyl)(trityl)sulfane (14)^[5]

In a dry, degassed 100 ml 3-neck flask, compound **20** (871 mg, 2.72 mmol, 1 eq) and tritylthiol (465 g, 1.63 mmol, 0.6 eq) were dissolved in dry, degassed THF (25 ml). NaH (60% dispersed in mineral oil, 326 mg, 8.16 mmol, 3 eq) was added to the solution which was then allowed to stir at room temperature for 2 hours. The reaction mixture was quenched with water, then extracted three times with TBME, dried over Na₂SO₄ and the solvent removed in vacuo. The crude product was subjected to CC (c-hexane 10:1 DCM), yielding **14** as a white

WILEY-VCH

solid (528 mg, 38 %). ¹H-NMR (400 MHz, Chloroform-d δ): 7.50-7.42 (m, 6H), 7.35-7.20 (m, 10H), 7.02 (s, 1H), 6.95 (s, 1H), 4.43 (s, 2H), 3.32 (s, 2H), 1.27 (s, 9H).

*Tetraphenylmethane-Based Oligomeric Side-Chains**bis(4-(tert-butyl)phenyl)(p-tolyl)methanol (21)*^[6]

In a dry degassed 500 ml two-neck flask equipped with rubber septum, reflux condenser and addition funnel, magnesium turnings (4.0 g, 166.7 mmol, 2.5 eq) were suspended in dry, degassed THF (100 ml) under argon atmosphere. 1-Bromo-4-*tert*-butylbenzene (29.1 ml, 166.7 mmol, 2.5 eq) dissolved in dry degassed THF (100 ml) was added drop-wise. In order to activate the *Grignard* reagent, one pellet of iodine was added to the mixture, which was subsequently stirred for 3 hours. Methyl *p*-toluate (10 g, 66.7 mmol, 1 eq) was dissolved in 100 ml dry degassed THF and was added to the mixture, which was then allowed to stir at 75 °C for 22 hours. After cooling to room temperature, saturated aqueous ammonium chloride and water were added. The aqueous phase was extracted three times with TBME. The combined organic phases were washed twice with water, dried over MgSO₄, filtrated and the solvent was evaporated. The crude product was subjected to CC (c-hexane 1:1 DCM) to obtain compound **21** as a white solid (22.5 g, 87 %). ¹H-NMR (400 MHz, Chloroform-d): δ 7.33-7.28 (m, 4H), 7.20-7.16 (m, 6H), 7.13-7.09 (m, 2H), 2.70 (s, 1H), 2.34 (s, 3H), 1.30 (s, 18H).

4-(bis(4-(tert-butyl)phenyl)(p-tolyl)methyl)aniline (22)^[7]

To a solution of freshly distilled aniline (22.7 ml, 248.6 mmol, 4.75 eq) and conc. HCl (21 ml) in AcOH (150 ml) in a 500 ml two-neck flask, compound **21** (20.1 g, 52.3 mmol, 1 eq) was added portionwise. The reaction mixture was refluxed and stirred at 140 °C for 15 hours. After cooling to room temperature, the acetic acid was evaporated. The solid was dissolved in

WILEY-VCH

DCM, washed four times with water, dried over magnesium sulfate, filtrated and the solvent evaporated. The crude product was subjected to CC (c-hexane 5:1 EtOAc and 1 % Et₃N) to give **22** as a white solid (17.0 g, 71 %). ¹H-NMR (400 MHz, Chloroform-d δ): 7.21 (d, J = 8.6 Hz, 4H), 7.11-7.06 (m, 6H), 7.05-7.01 (m, 2H), 6.96 (d, J = 8.6 Hz, 2H), 6.56 (d, J = 8.6 Hz, 2H), 2.31 (s, 3H), 2.34 (s, 3H), 1.29 (s, 18H)

4,4'-((4-iodophenyl)(p-tolyl)methylene)bis(tert-butylbenzene) (23)^[7]

To a dry, degassed 1000 ml three-neck flask equipped with thermometer and rubber septa, boron trifluoride diethyl etherate (8.23 ml, 65 mmol, 2 eq) was added and the flask was cooled to -10 °C. Compound **22** (15 g, 32.5 mmol, 1 eq) dissolved in dry, degassed DCM (200 ml) was added drop-wise. *tert*-butyl nitrite (7.58 ml, 56.9 mmol, 1.75 eq) was dissolved in dry, degassed THF (200 ml) and added drop-wise. The mixture was allowed to stir for 3 hours. Potassium iodide (8 g, 48.7 mmol, 1.5 eq) and iodine (10.9 g, 42.2 mmol, 1.3 eq) were added to the mixture. The reaction mixture was allowed to gradually warm up to room temperature, stirred for 15 hours and then quenched with saturated aqueous sodium thiosulfate. A pale solid precipitated which was filtrated through hyflo, and redissolved in DCM. The organic phase was washed three times with water, dried over MgSO₄ and the solvent was removed in vacuo. The crude product was subjected to CC (c-hexane) to afford **23** as a colorless solid (15.7 g, 84 %). ¹H-NMR (400 MHz, Chloroform-d δ): 7.23-7.21 (m, 4H), 7.11-7.06 (m, 8H), 7.03 (d, J = 8.3 Hz, 4H), 2.31 (s, 6H), 1.29 (d, J = 1.1 Hz, 18H).

bis(4-(tert-butyl)phenyl)di-p-tolylmethane (24)^[7]

Under inert atmosphere, compound **23** (16 g, 27.9 mmol, 1 eq) was dissolved in dry, degassed THF (250 ml) in a dry, degassed 500 ml two-neck flask. The solution was cooled to -60 °C and methyl lithium (1.6 M solution in hexane, 52.3 ml, 83.8 mmol, 3 eq) was added drop-wise. The mixture was allowed to slowly warm up to room temperature and was stirred for 2

WILEY-VCH

hours. The reaction mixture was quenched upon addition of water, extracted three times with DCM and dried over MgSO₄. After filtration, the volatile was evaporated by rotavapor to afford **24** as a white solid (12.6 g, quant.). ¹H-NMR (400 MHz, Chloroform-d δ): 7.56-7.52 (m, 1H), 7.25-7.21 (m, 2H), 7.09-7.03 (m, 4H), 6.98-6.94 (m, 1H), 2.31 (s, 1H), 1.29 (s, 9H).

bis(4-(bromomethyl)phenyl)bis(4-(tert-butyl)phenyl)methane (25)^[7]

In a dry, degassed 500 ml two-neck flask equipped with a reflux condenser and a glass stopper, compound **24** (5 g, 10.9 mmol, 1 eq), NBS (7.8 g, 43.4 mmol, 4 eq) and catalytic amounts of AIBN (180 mg) were suspended in methyl formate (150 ml) under inert atmosphere and bubbled with argon for 30 minutes. The reaction was activated by illumination with a 500 W halogen lamp and refluxed for 15 hours, then cooled to room temperature. The solvent was evaporated, and the residue dissolved in DCM. The mixture was washed four times with water and dried over MgSO₄. After filtration, the volatile was evaporated and the crude product subjected to automated CC (*c*-hexane 20:1 DCM and *c*-hexane 10:1 DCM after 4 column volumes) to afford **25** as a white solid (4.0 g, 60 %). ¹H-NMR (400 MHz, Chloroform-d δ): 7.28-7.27 (m, 2H), 7.25 (s, 6H), 7.23 (d, *J* = 2.0 Hz, 2H), 7.20-7.16 (m, 2H), 7.10-7.05 (m, 4H), 4.48 (s, 4H), 1.30 (s, 18H).

(4-((4-(bromomethyl)phenyl)bis(4-(tert-butyl)phenyl)methyl)benzyl)(trityl)sulfane (15)^[7]

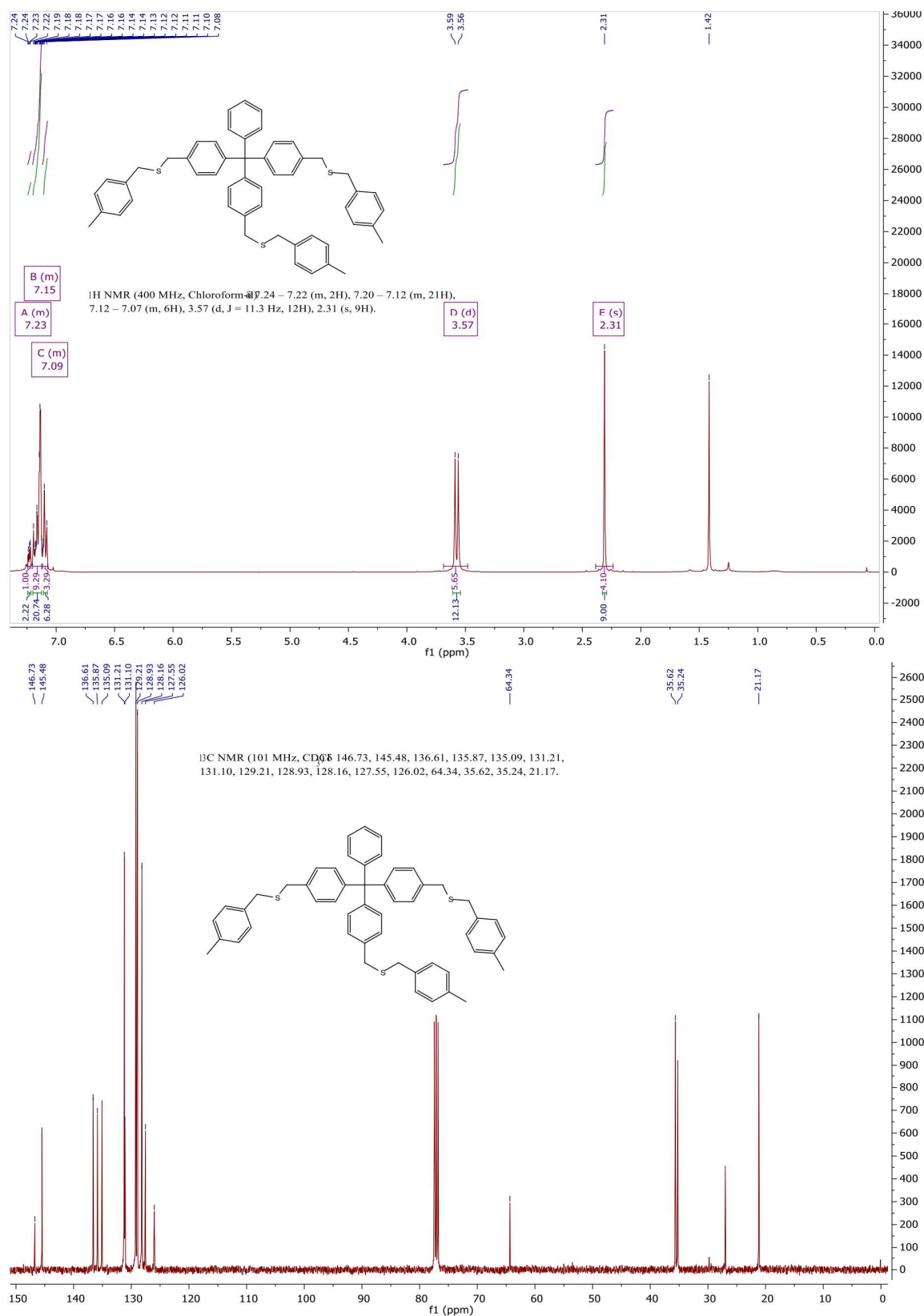
Compound **25** (100 mg, 0.162 mmol, 1 eq) was dissolved in dry THF (5 ml) in a 10 ml Schlenk tube. Trithylthiol (27.6 mg, 0.097 mmol, 0.6 eq) was added to the solution, which was then degassed for 30 minutes with argon. Sodium hydride (60 % dispersion in mineral oil, 2 eq) was added to the flask. The mixture was stirred at room temperature for 15 hours, and then quenched by addition of water, extracted two times with TBME, washed twice with water, dried over MgSO₄, filtrated and the solvent was removed in vacuo. The crude product was subjected to CC (*c*-hexane 2:1 DCM) to afford compound **15** as white foam (37.9 mg,

WILEY-VCH

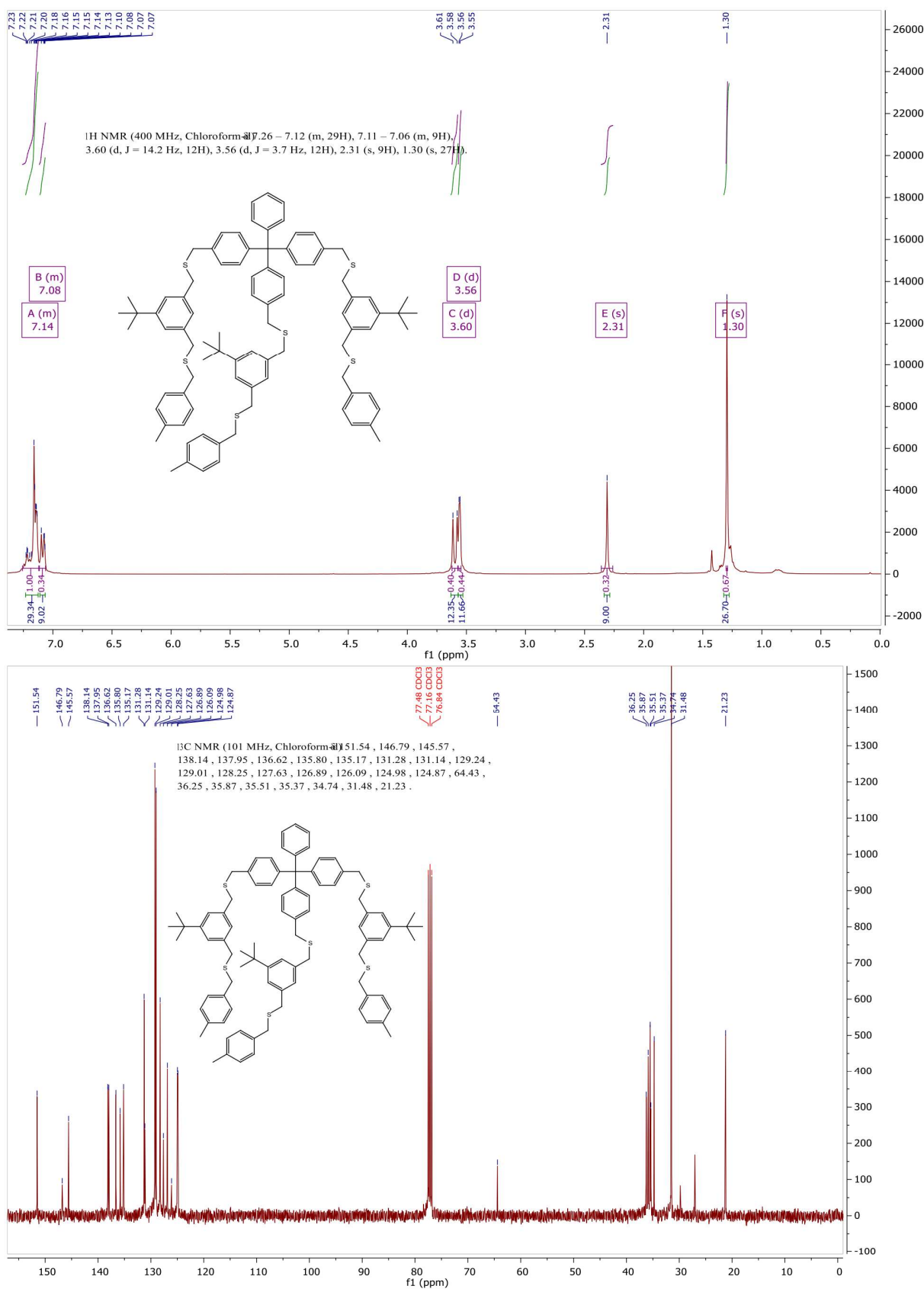
48%). ¹H-NMR (400 MHz, Chloroform-d δ): 7.48-7.43 (m, 5H), 7.30 (s, 4H), 7.26 (d, J = 1.7 Hz, 6H), 7.24-7.18 (m, 7H), 7.15 (d, J = 8.4 Hz, 2H), 7.08-7.04 (m, 5H), 7.00 (d, J = 8.3 Hz, 2H), 4.47 (s, 2H), 3.28 (s, 2H), 1.29 (s, 18H).

WILEY-VCH

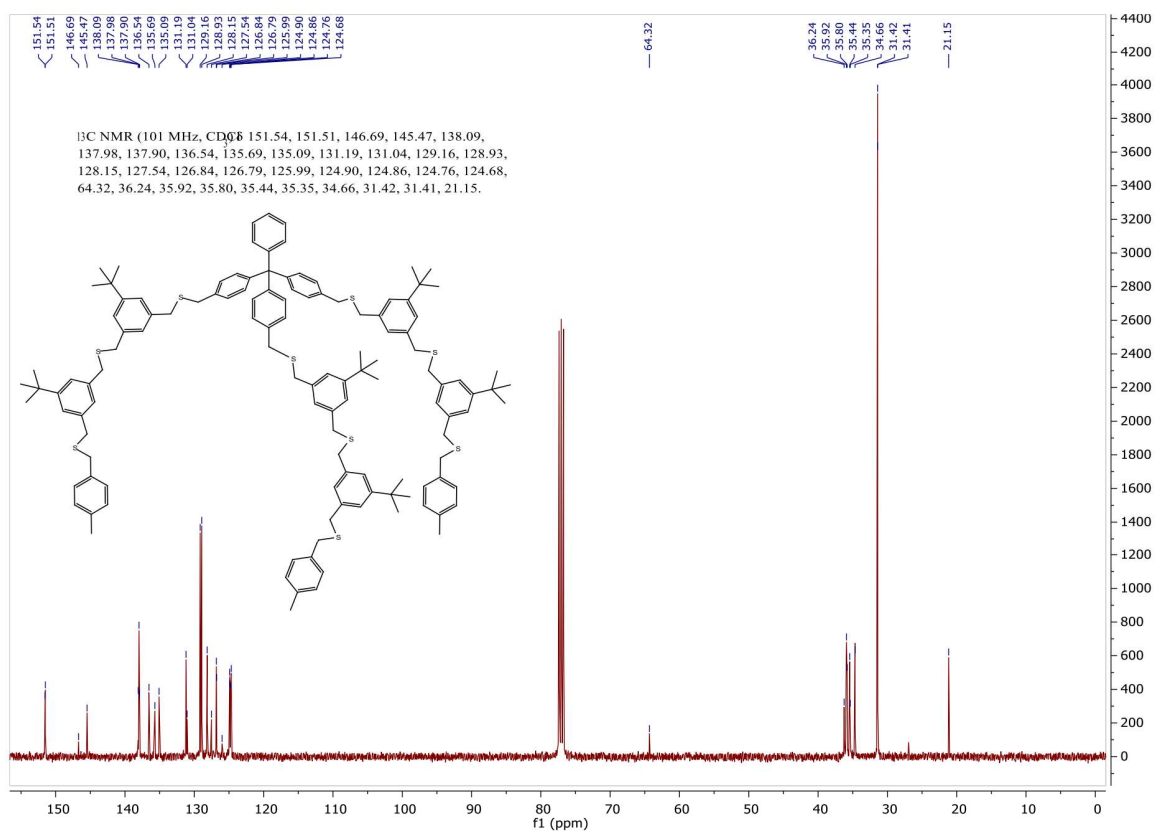
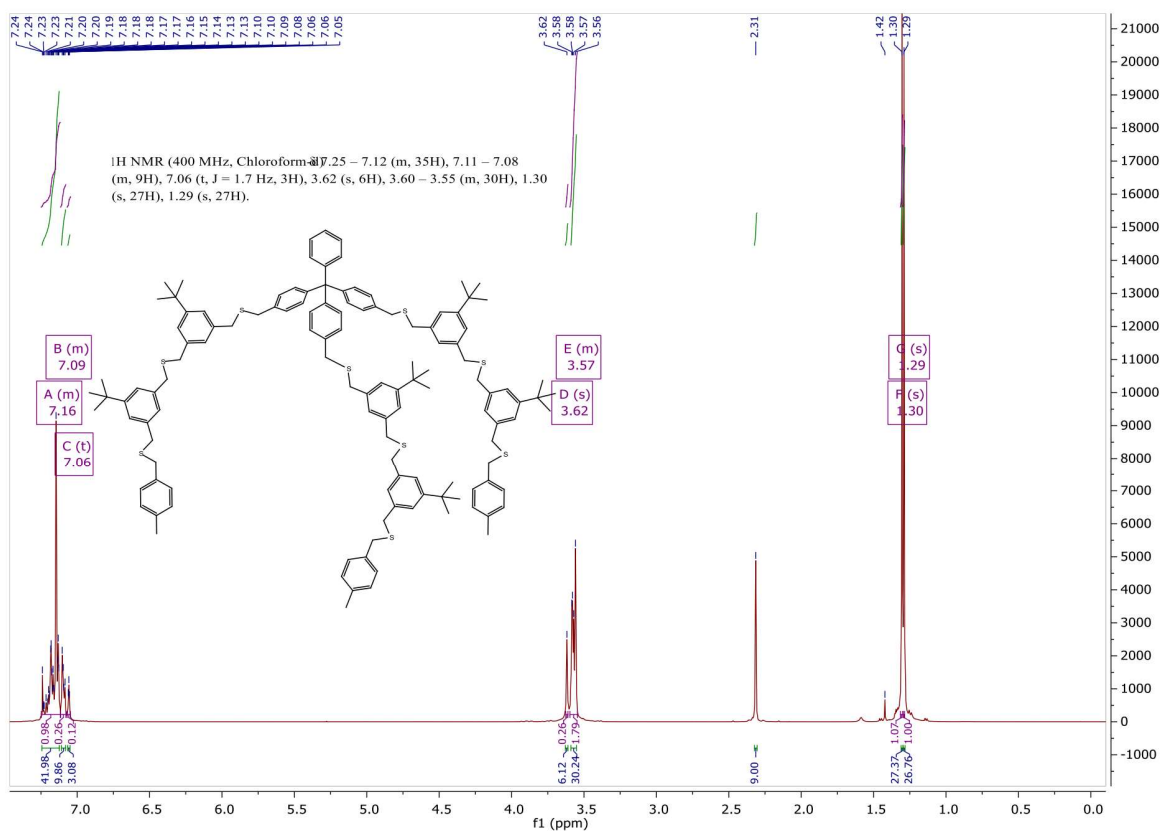
NMR-Spectra of compounds 1 - 5

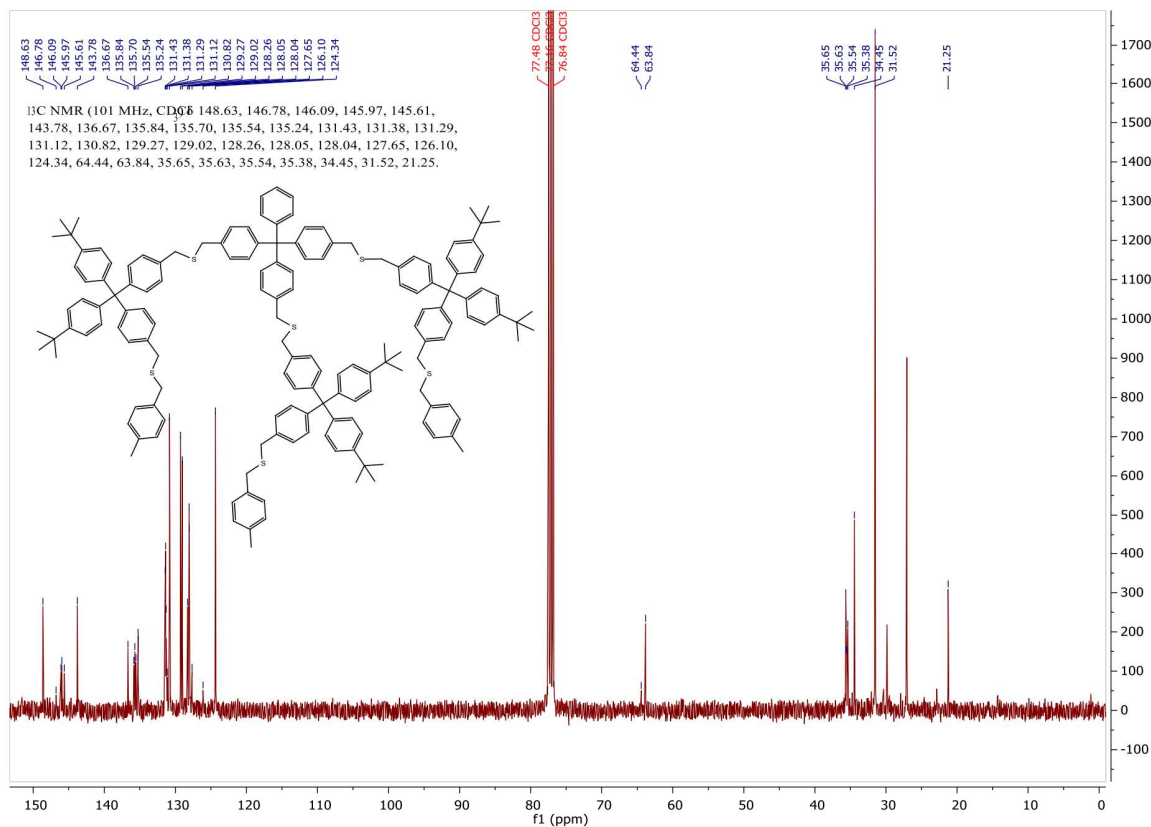
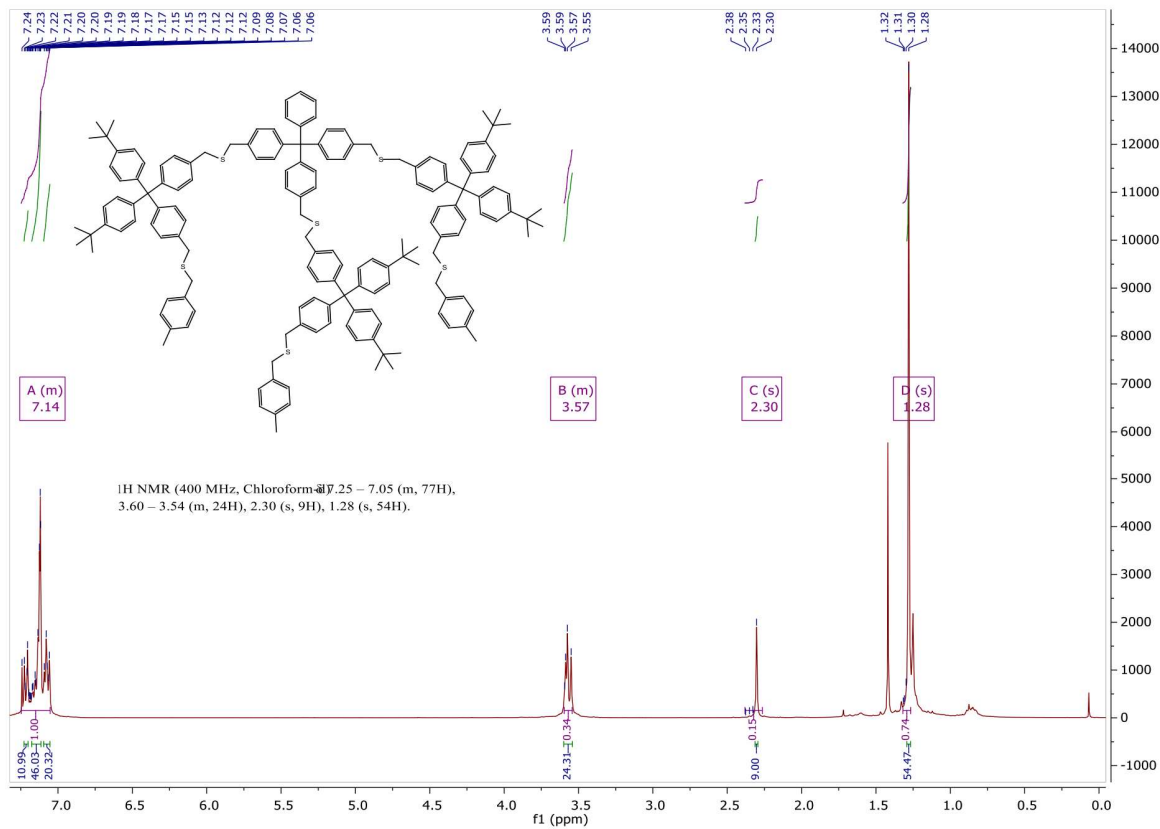
¹H- and ¹³C-NMR of Ligand 1

WILEY-VCH

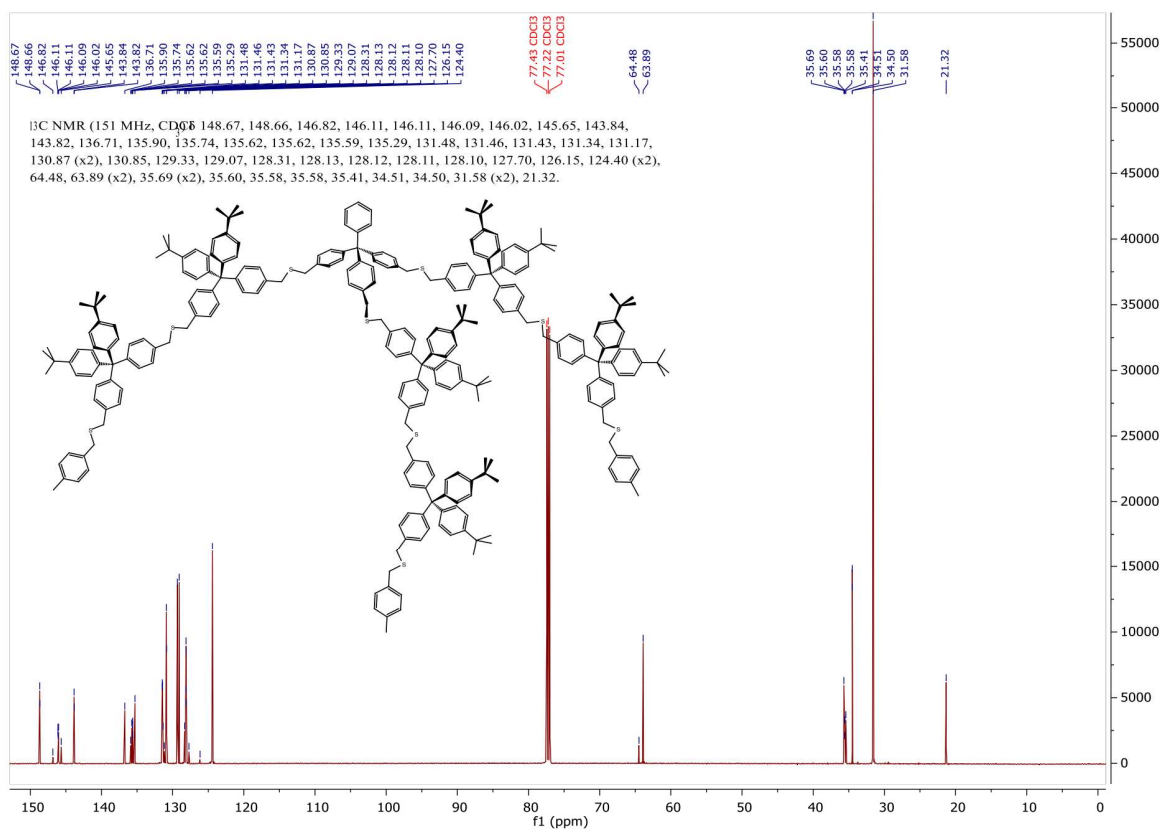
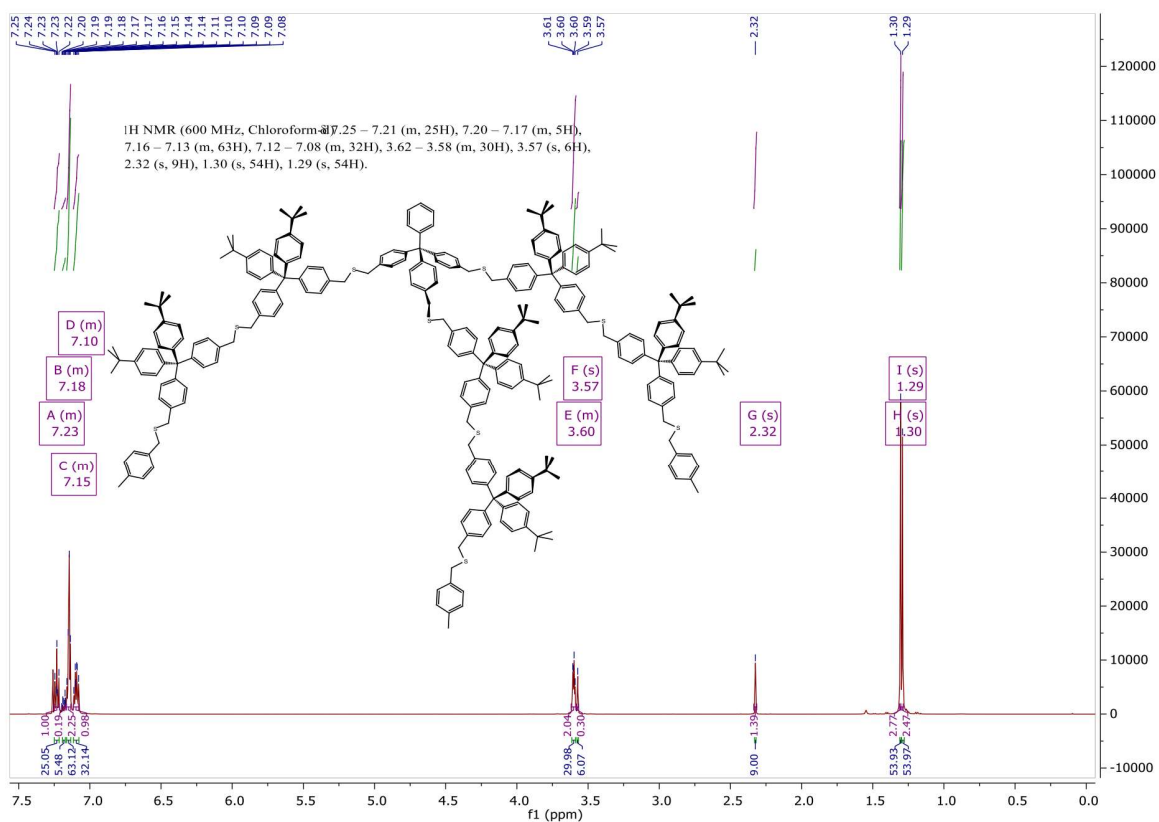
¹H- and ¹³C-NMR of Ligand 2

WILEY-VCH

 ^1H - and ^{13}C -NMR of Ligand 3

¹H- and ¹³C-NMR of Ligand 4

WILEY-VCH

 ^1H - and ^{13}C -NMR of Ligand 5

WILEY-VCH

References

- [1] R. B. Moodie, T. M. Connor, R. Stewart, *Can. J. Chem.* **1959**, *37*, 1402.
- [2] C. Heim, A. Affeld, M. Nieger, F. Vögtle, *Helv. Chim. Acta* **1999**, *82*, 746.
- [3] J. Tian, Y.-D. Ding, T.-Y. Zhou, K.-D. Zhang, X. Zhao, H. Wang, D.-W. Zhang, Y. Liu, Z.-T. Li, *Chem Eur J* **2014**, *20*, 575.
- [4] S. S. Moore, T. L. Tarnowski, M. Newcomb, D. J. Cram, *J. Am. Chem. Soc.* **1977**, *99*, 6398.
- [5] T. Peterle, A. Leifert, J. Timper, A. Sologubenko, U. Simon, M. Mayor, *Chem. Commun.* **2008**, 3438.
- [6] C. S. Marvel, J. F. Kaplan, C. M. Himel, *J. Am. Chem. Soc.* **1941**, *63*, 1892.
- [7] M. Lehmann, E. H. Peters, M. Mayor, *Chem. Eur. J.* **2016**, *22*, 2261.



Supporting Information

Alkyne-Monofunctionalized Gold Nanoparticles as Massive Molecular Building Blocks

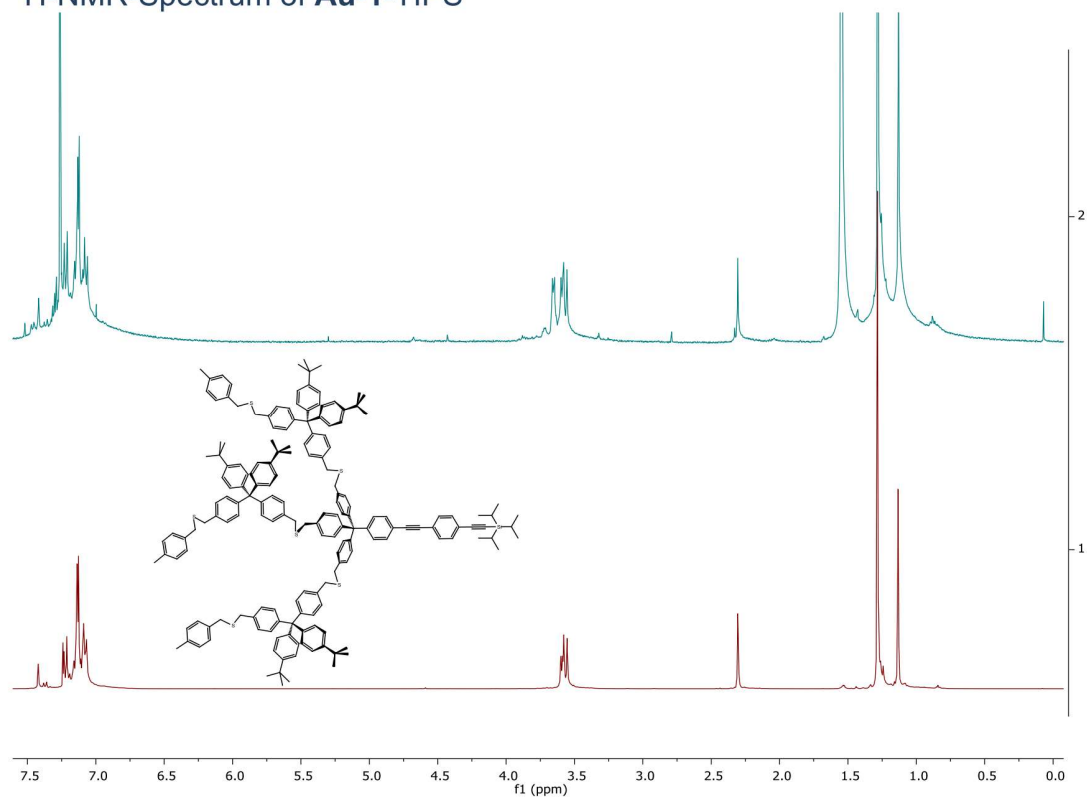
Erich Henrik Peters and Marcel Mayor*

Contents

Analysis of AuNPs	2
¹ H-NMR-Spectrum of Au-1-TIPS	2
TEM micrographs	3
Thermogravimetric Analysis of Au-1-TIPS	5
Analytical Data of Compounds 6–8, 2 and 1	6
¹ H- and ¹³ C-NMR-Spectra of compound 6	6
Mass Spectrum of Compound 6	7
¹ H- and ¹³ C-NMR-Spectra of compound 7	7
Mass Spectrum of Compound 7	8
¹ H- and ¹³ C-NMR-Spectra of Compound 8	9
Mass Spectrum of Compound 8	10
¹ H- and ¹³ C-NMR-Spectra of Compound 2	10
Mass Spectrum of Compound 2	11
¹ H- and ¹³ C-NMR-Spectra of Compound 1	12
Mass Spectrum of Compound 1	13

Analysis of AuNPs

$^1\text{H-NMR}$ -Spectrum of **Au-1-TIPS**



Blue: $^1\text{H-NMR}$ -Spectrum of **Au-1-TIPS**, **red:** $^1\text{H-NMR}$ -spectrum of ligand **1**. The close similarity corroborates the coating of the Au NP by the ligand. Furthermore, the line-broadening caused by the restricted tumbling motion documents the immobilization of the ligand on the NP surface.

TEM micrographs

Au-1-TIPS

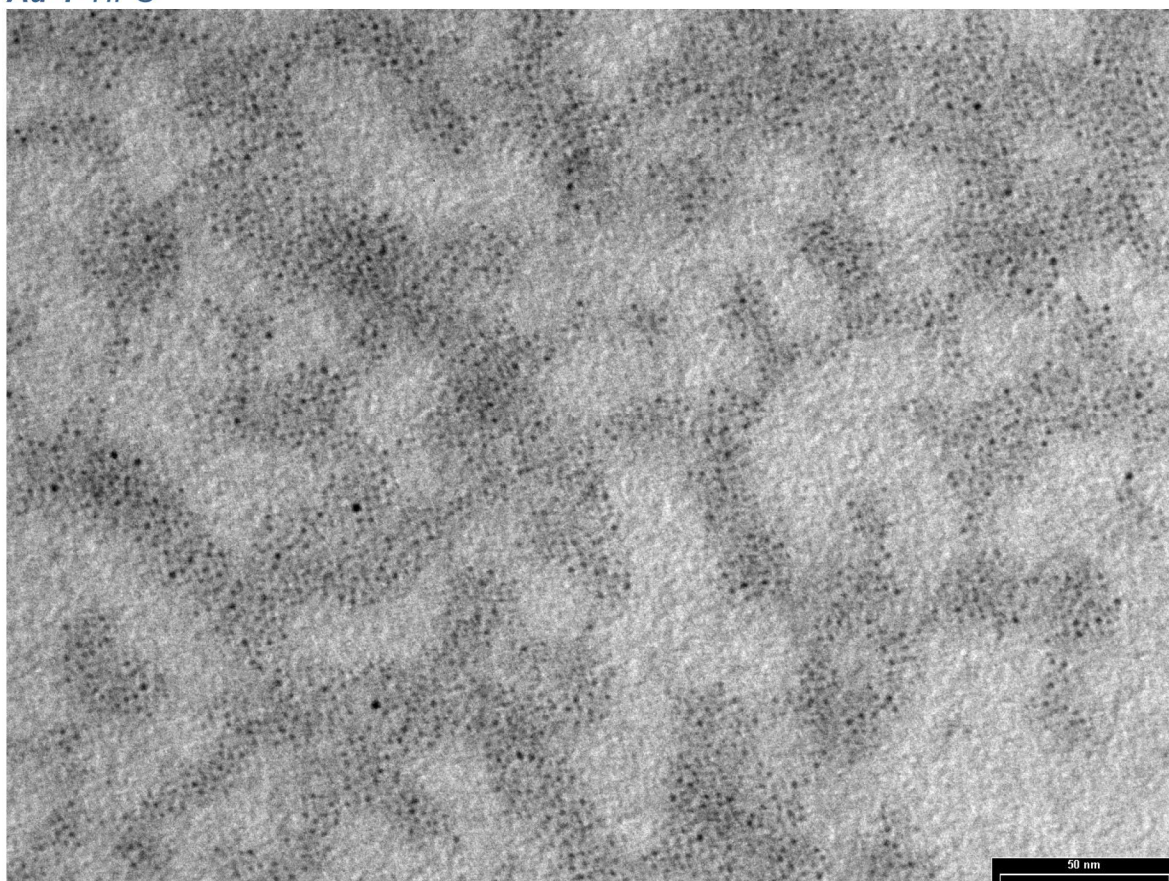


Figure S1. Representative TEM micrograph of **Au-1-TIPS**

(Au-1)₂

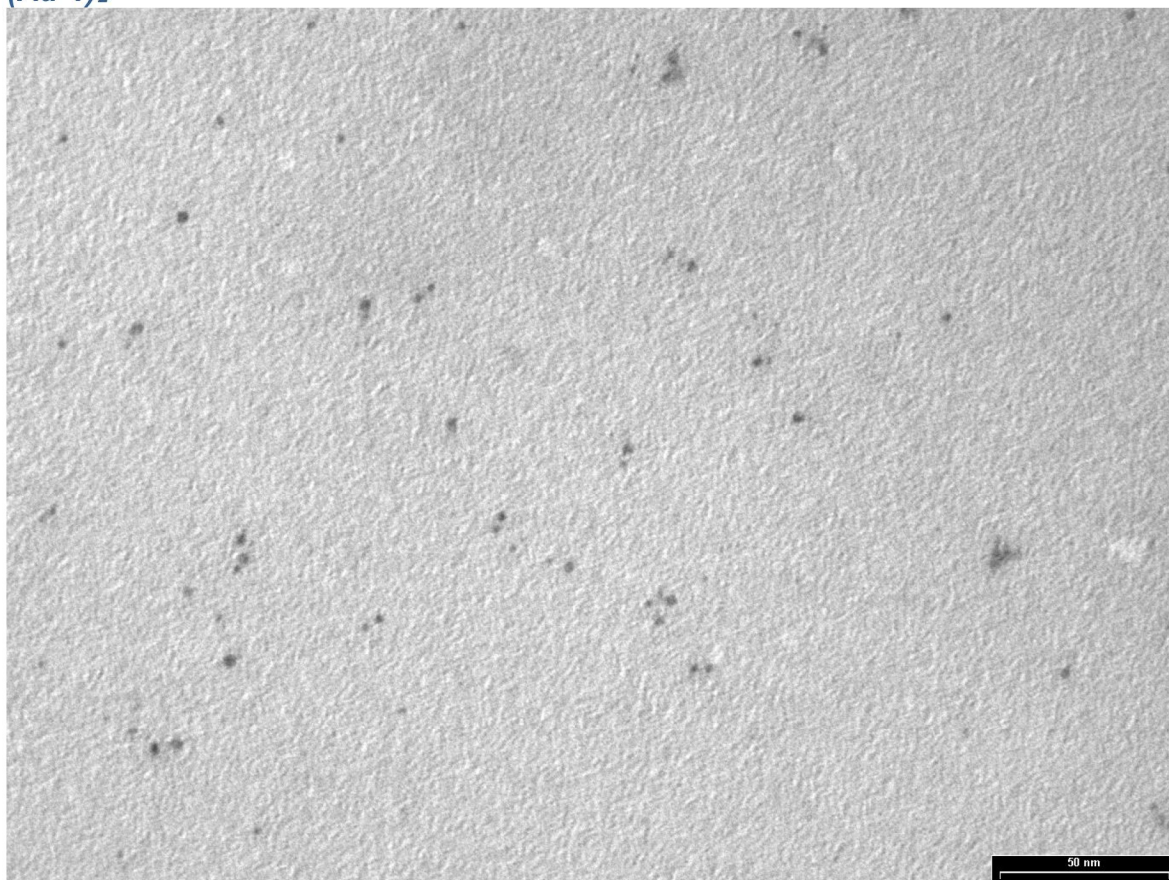


Figure S2. Representative TEM micrograph of dimers **(Au-1)₂** from the homocoupling reaction.

(Au-1)₃9

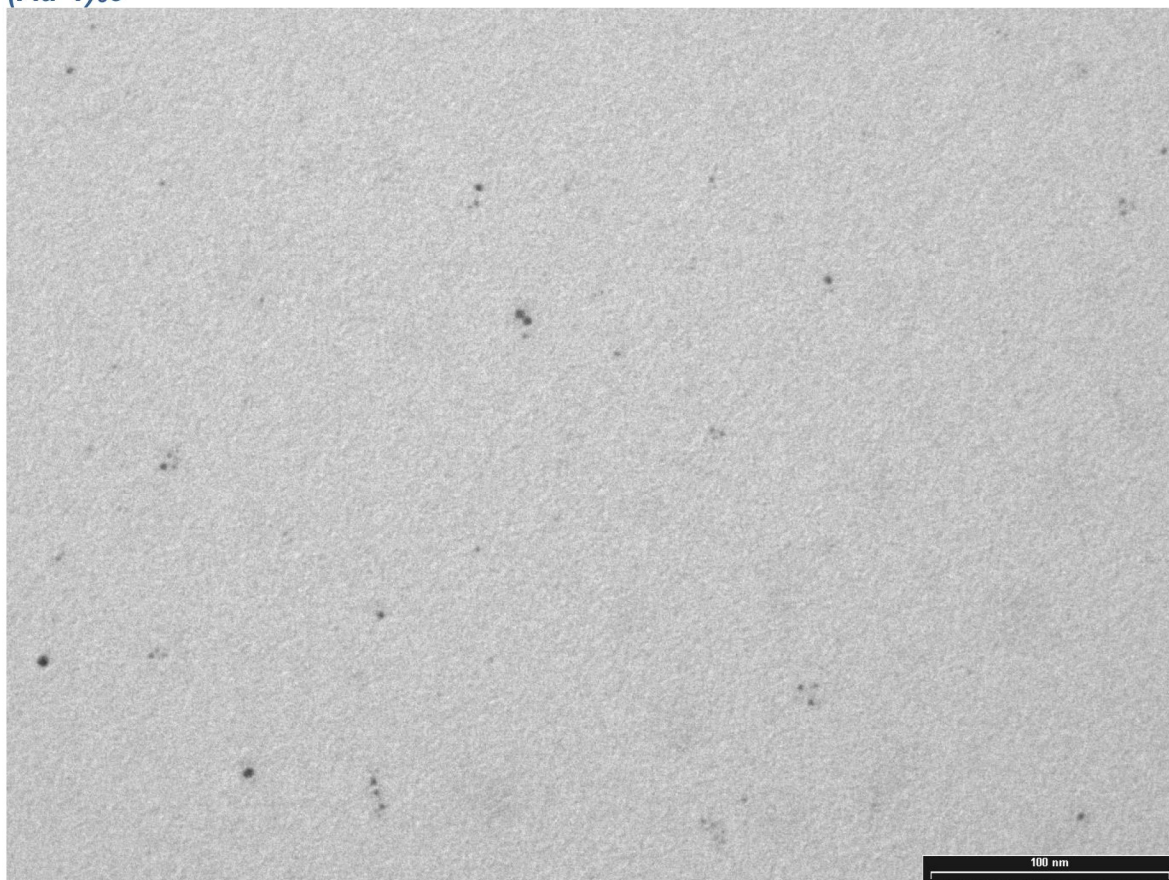


Figure S3. Representative TEM micrograph of the “click” reaction comprising dimers and **(Au)₃9** trimers.

Thermogravimetric Analysis of **Au-1-TIPS**

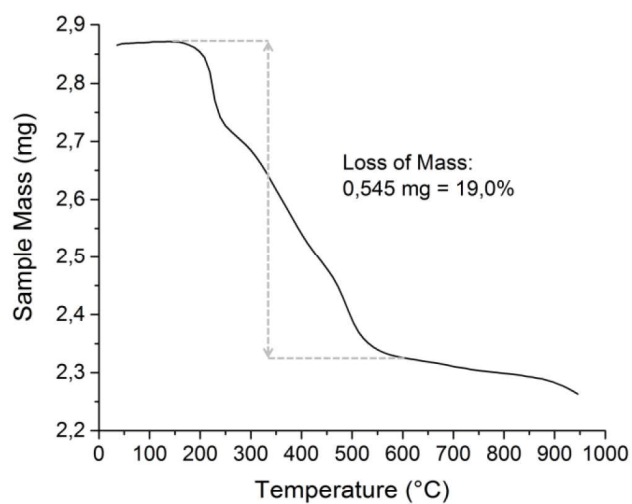
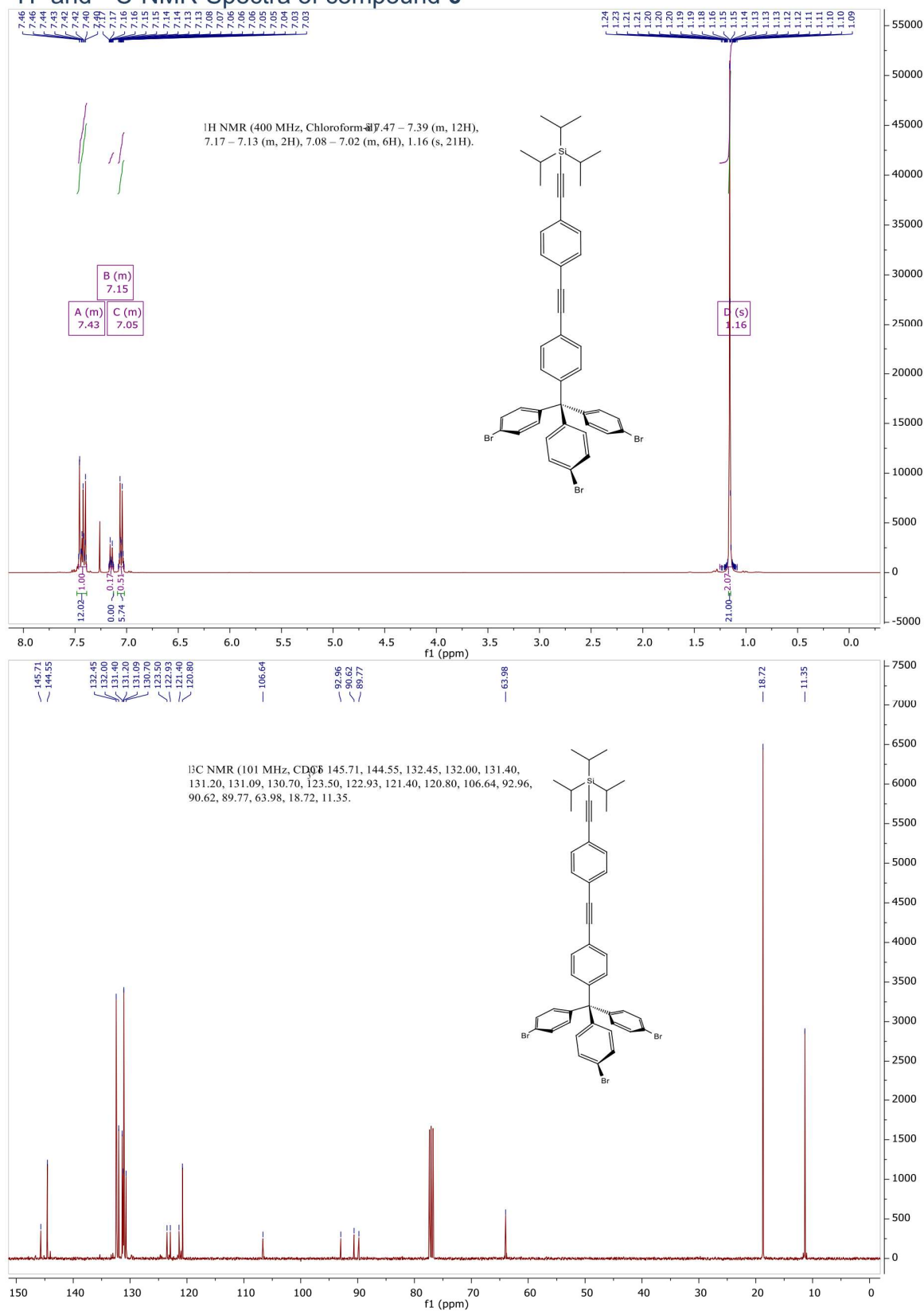
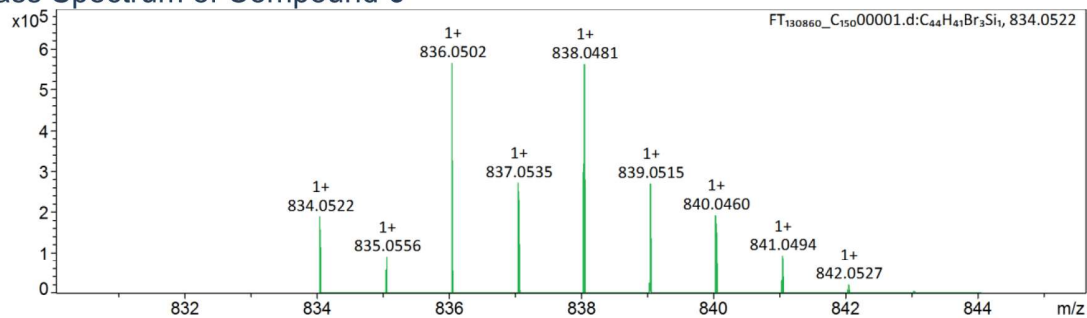


Figure S4. TGA mass loss trace for **Au-1-TIPS**.

Analytical Data of Compounds 6–8, 2 and 1

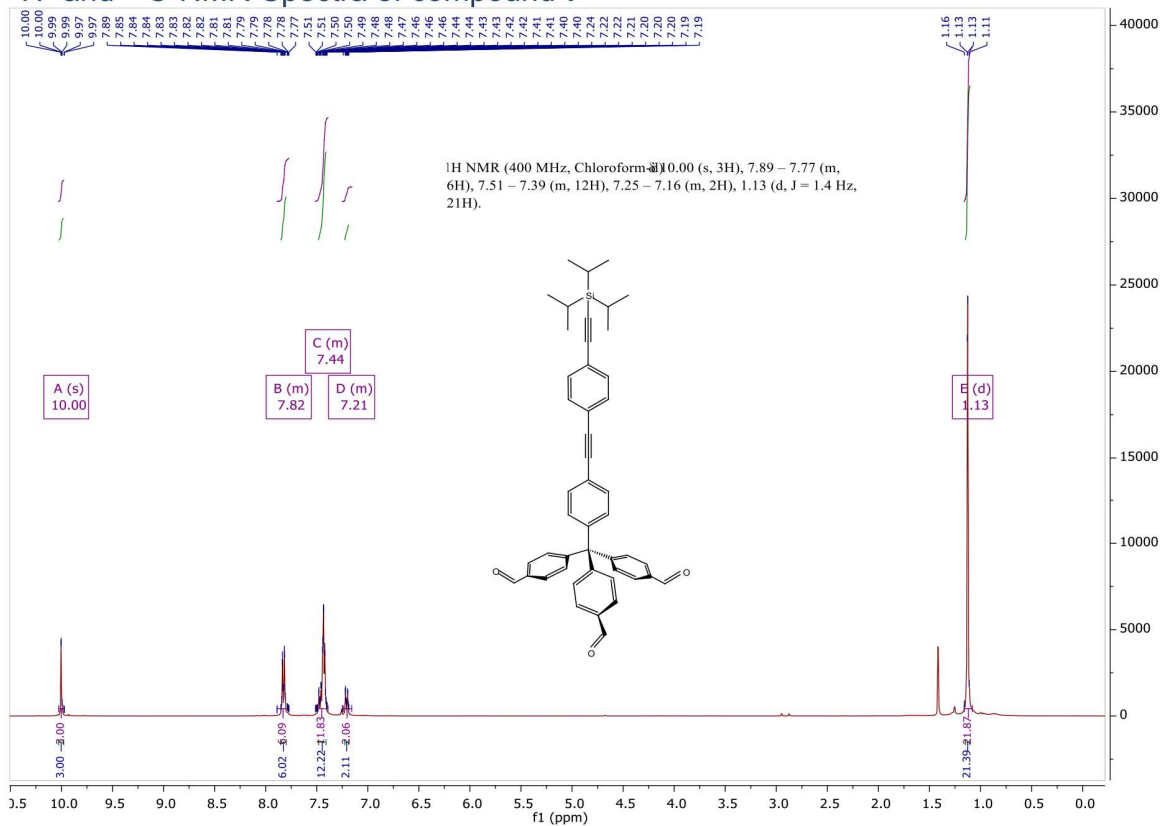
 ^1H - and ^{13}C -NMR-Spectra of compound 6

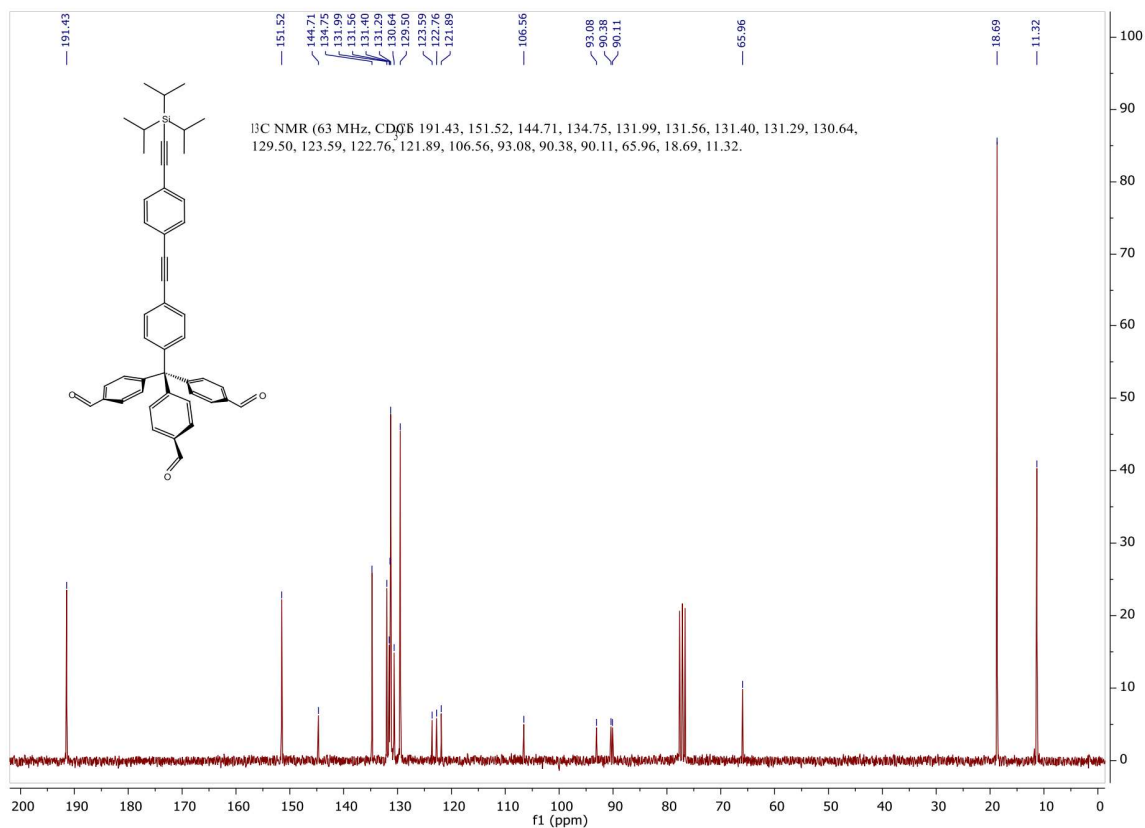
Mass Spectrum of Compound 6



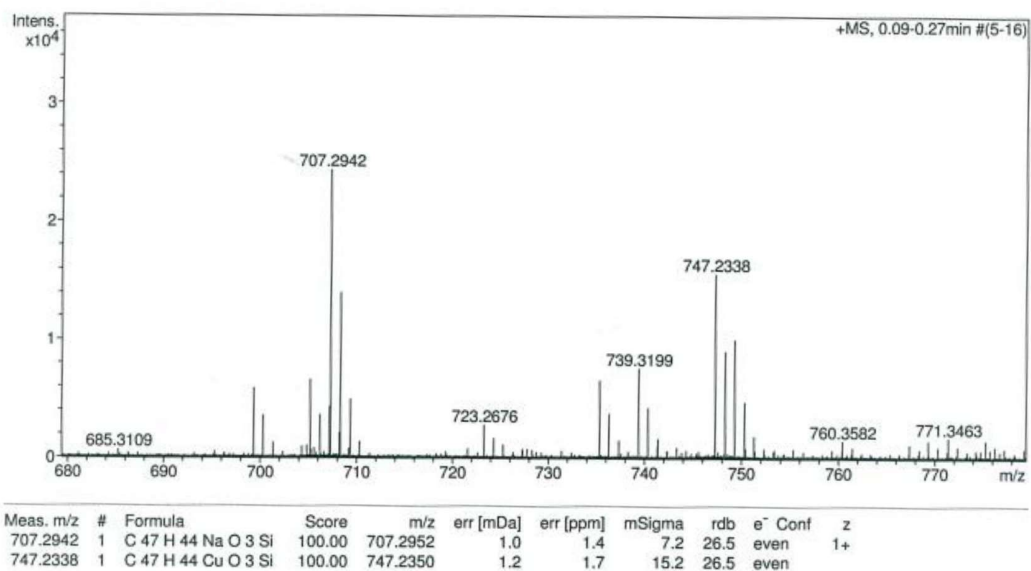
Evaluation Spectra / Validation Formula:

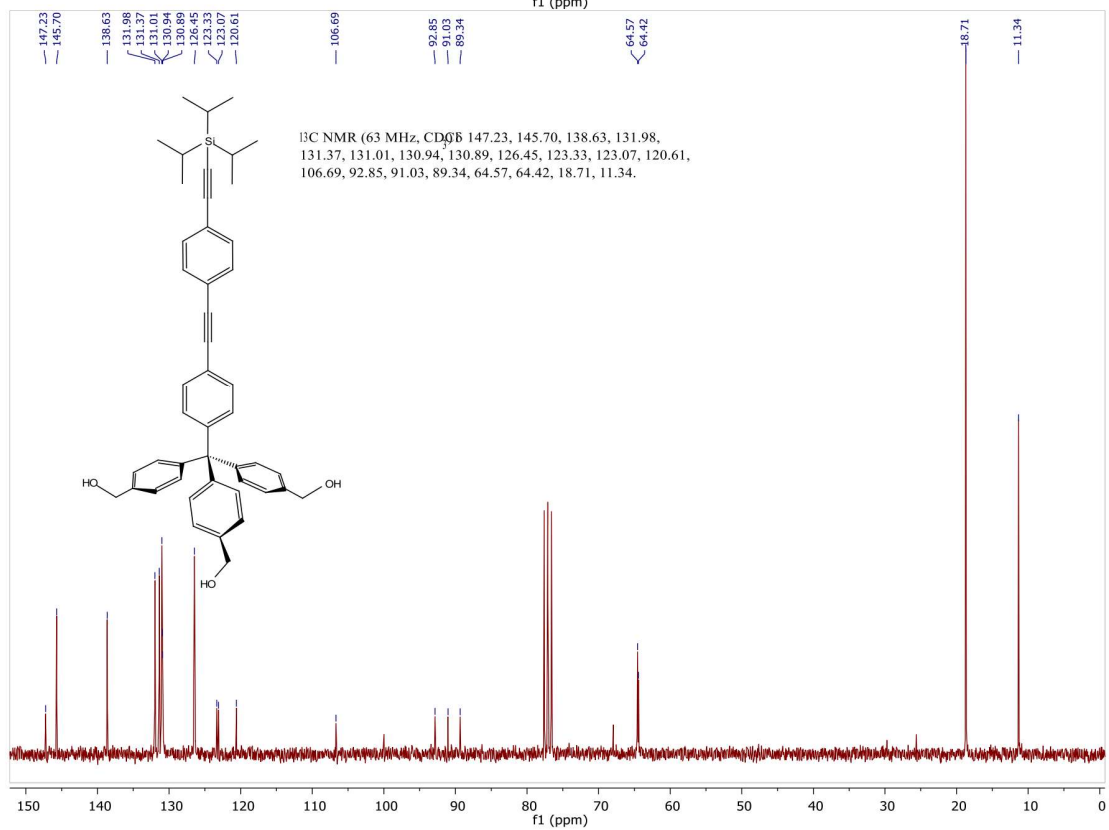
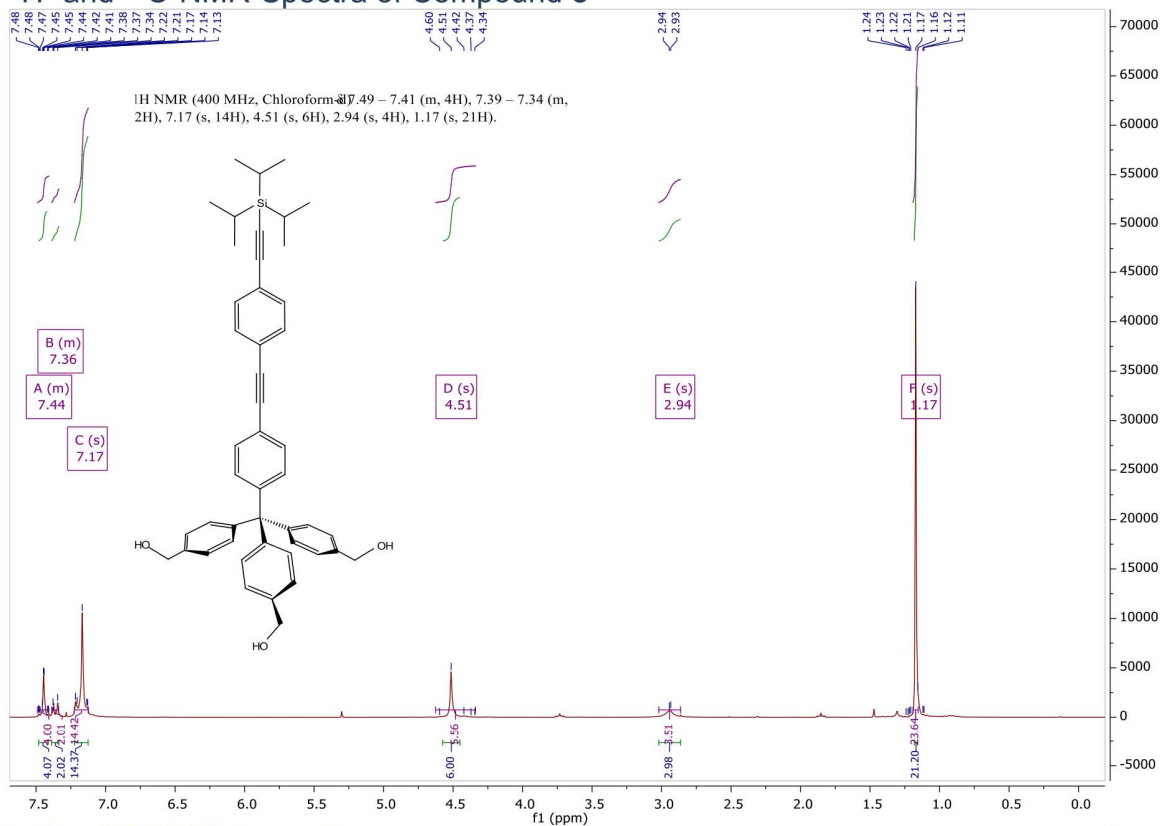
#	Ion Formula	Adduct	m/z	z	Meas. m/z	mSigma	N-Rule	err [mDa]	err [ppm]
1	C ₄₄ H ₄₁ Br ₃ Si	M	834.0522	1+	834.0531	325.1	ok	-0.9	-1.1

¹H- and ¹³C-NMR-Spectra of compound 7

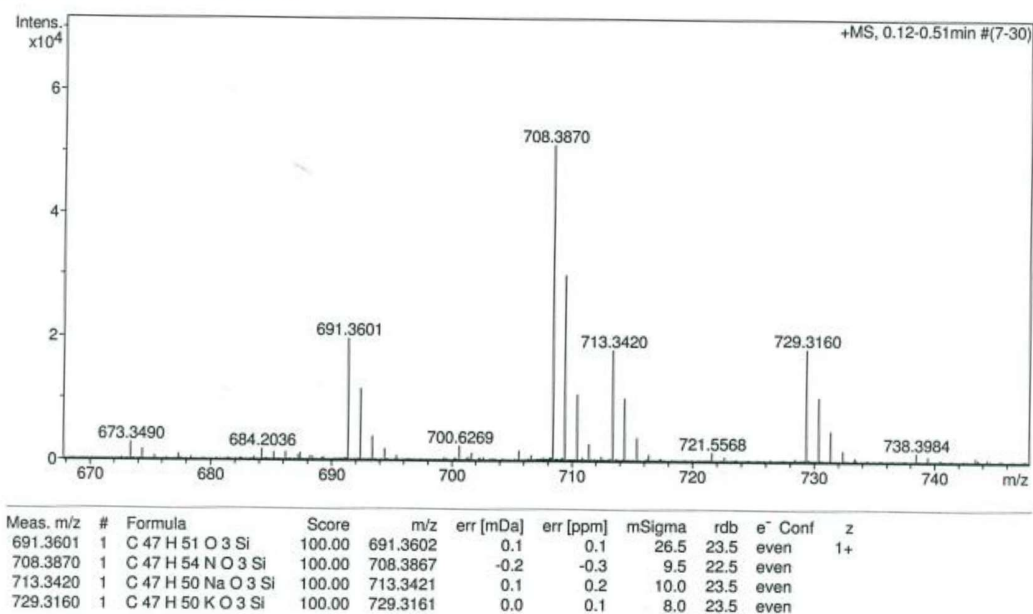
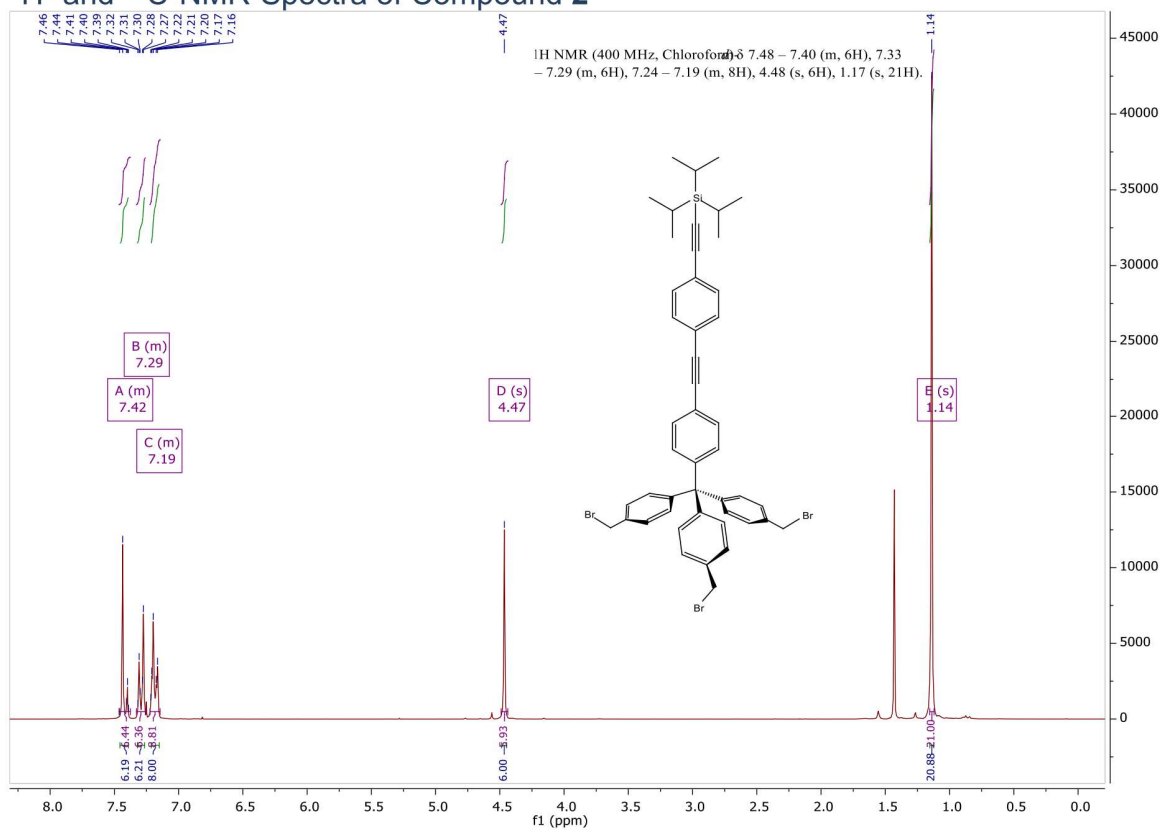


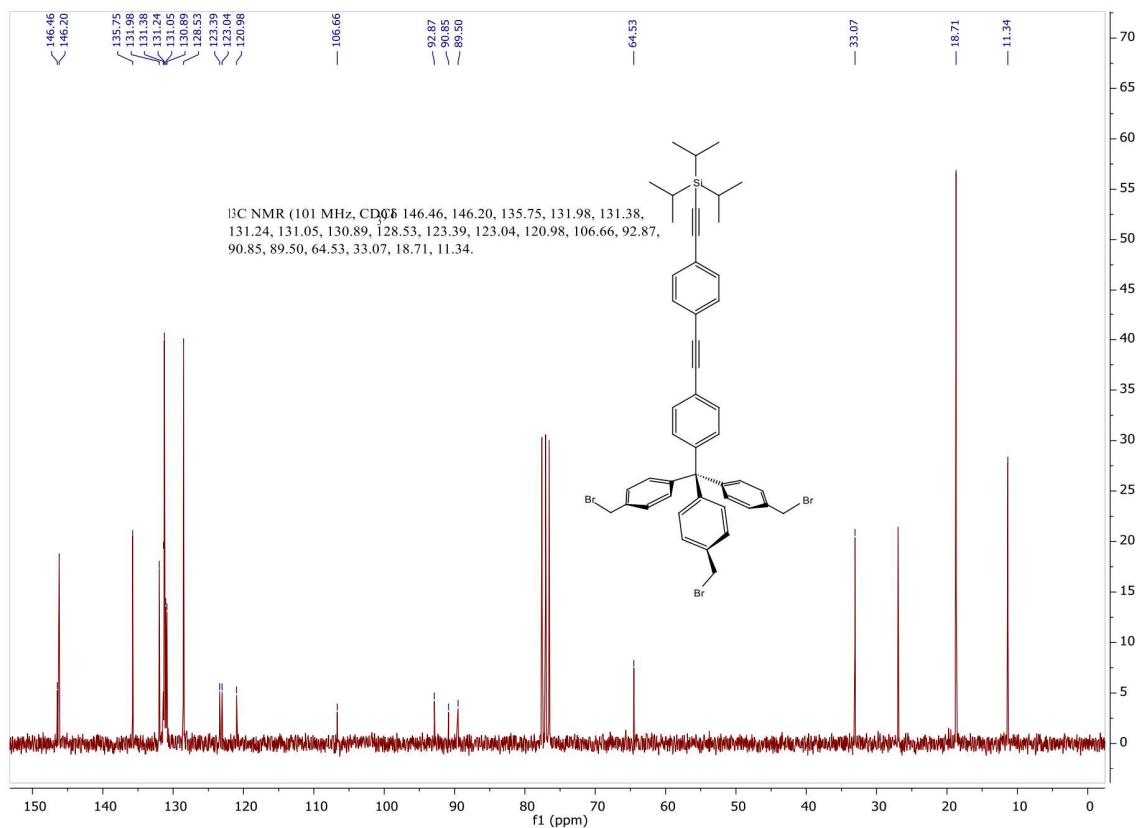
Mass Spectrum of Compound 7



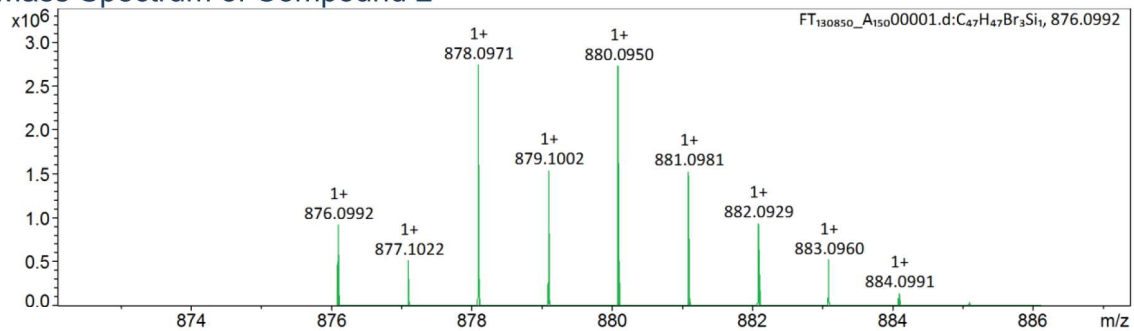
¹H- and ¹³C-NMR-Spectra of Compound 8

Mass Spectrum of Compound 8

¹H- and ¹³C-NMR-Spectra of Compound 2

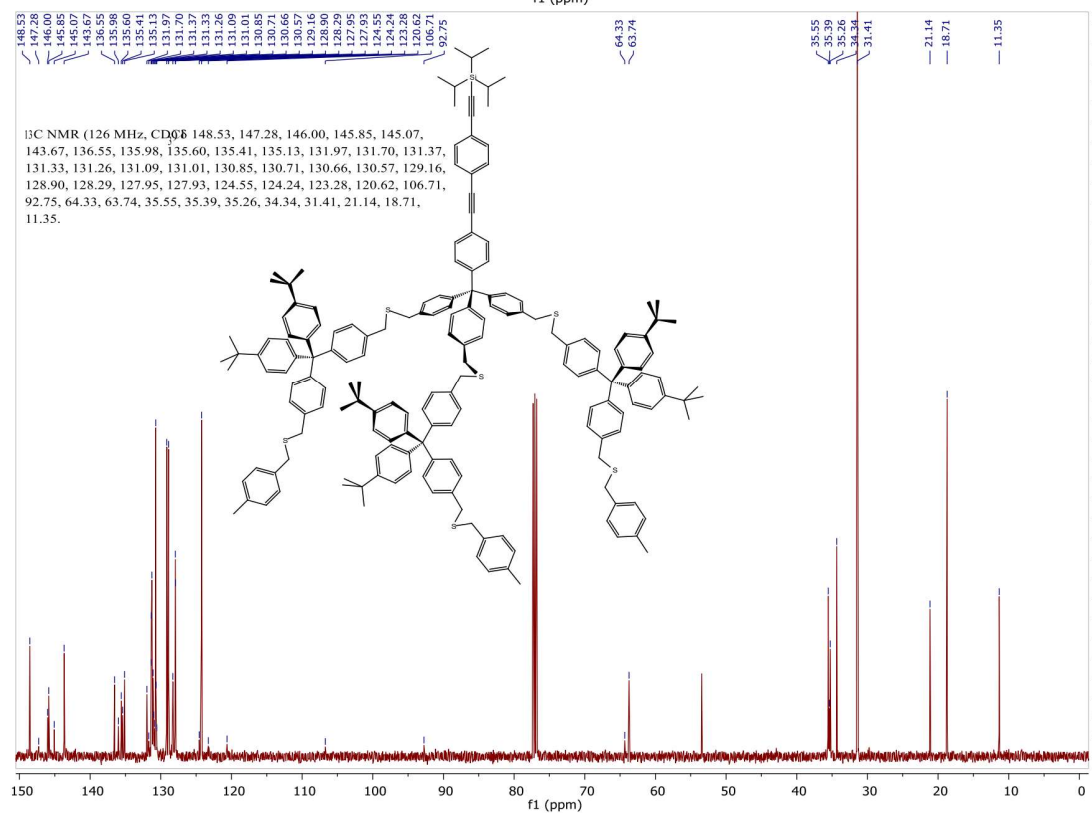
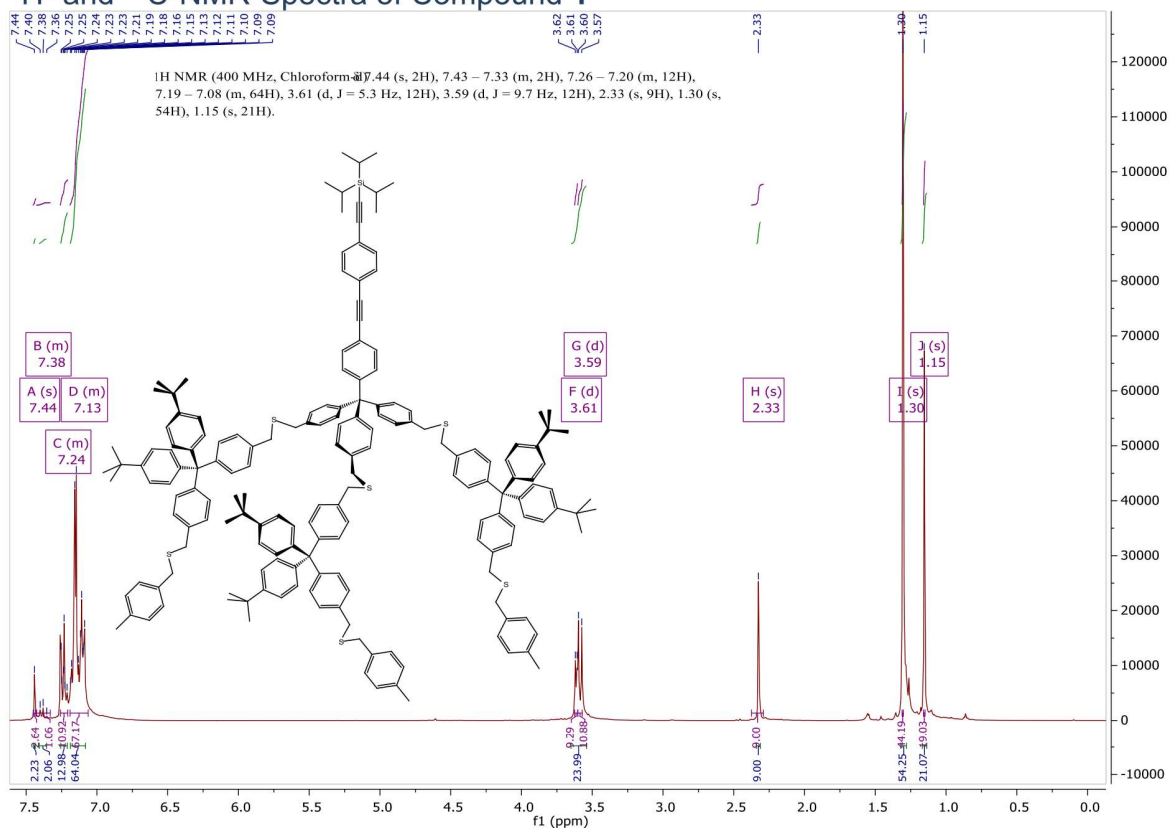


Mass Spectrum of Compound 2

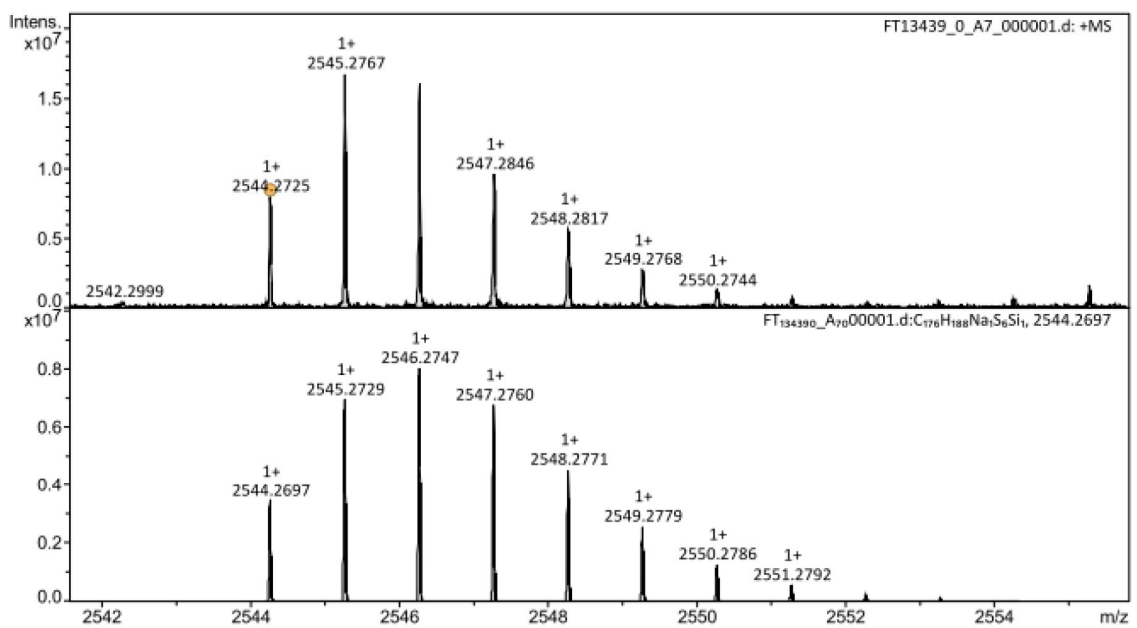


Evaluation Spectra / Validation Formula:

#	Ion Formula	Adduct	m/z	z	Meas. m/z	mSigma	N-Rule	err [mDa]	err [ppm]
1	C ₄₇ H ₄₇ Br ₃ Si	M	876.0992	1+	876.1003	96.8	ok	-1.1	-1.3

¹H- and ¹³C-NMR-Spectra of Compound 1

Mass Spectrum of Compound 1



Evaluation Spectra / Validation Formula:

#	Ion Formula	Adduct	m/z	z	Meas. m/z	mSigma	N-Rule	err [mDa]	err [ppm]
1	C ₁₇₆ H ₁₈₈ Na ₆ Si	M+Na	2544.2697	1+	2544.2725	139.2	ok	-2.8	-1.1

Supporting Information

for the manuscript:

Organic Cage Controlling Dimension and Stability of Gold Nanoparticles

*Erich Henrik Peters and Marcel Mayor**

Contents

Analysis of Au-1	2
¹ H-NMR Spectra of 1	2
TEM micrograph of Au-1	3
Thermogravimetric Analysis of Au-1	4
Materials	6
Equipment and Measurements	6
Synthesis and Analytical Data of Cage 1 and Compounds 3–9	7
tris(p-(bromomethyl)phenyl)-p-(p-(triisopropylsilylethynyl)phenylethynyl)phenylmethane (7) ¹	7
bis(p-(bromomethyl)phenyl)-bis(p-tert-butylphenyl)methane (3) ²	7
p-(tritylthiomethyl)phenyl-p-(bromomethyl)phenyl-bis(p-tert-butylphenyl)methane (4) ²	7
p-(tritylthiomethyl)phenyl-p-(acetylthiomethyl)phenyl-bis(p-tert-butylphenyl)-methane (5)	8
p-(mercaptomethyl)phenyl-p(tritylthiomethyl)phenyl-bis(p-tert-butylphenyl)-methane (6)	10
Tris(p-(p-(p-(tritylthiomethyl)phenyl-bis(p-tert-butylphenyl)methyl)phenylmethylthiomethyl)phenyl)-p-(p-(triisopropylsilylethynyl)phenylethynyl)phenylmethane (8).....	12
Tris(p-(p-(p-(mercaptomethyl)phenyl-bis(p-tert-butylphenyl)methyl)phenylmethylthiomethyl)phenyl)-p-(p-(triisopropylsilylethynyl)phenylethynyl)phenylmethane (9).....	14
Cage-Type Ligand 1	17
References	19

Analysis of Au-1

^1H -NMR Spectra of **1**

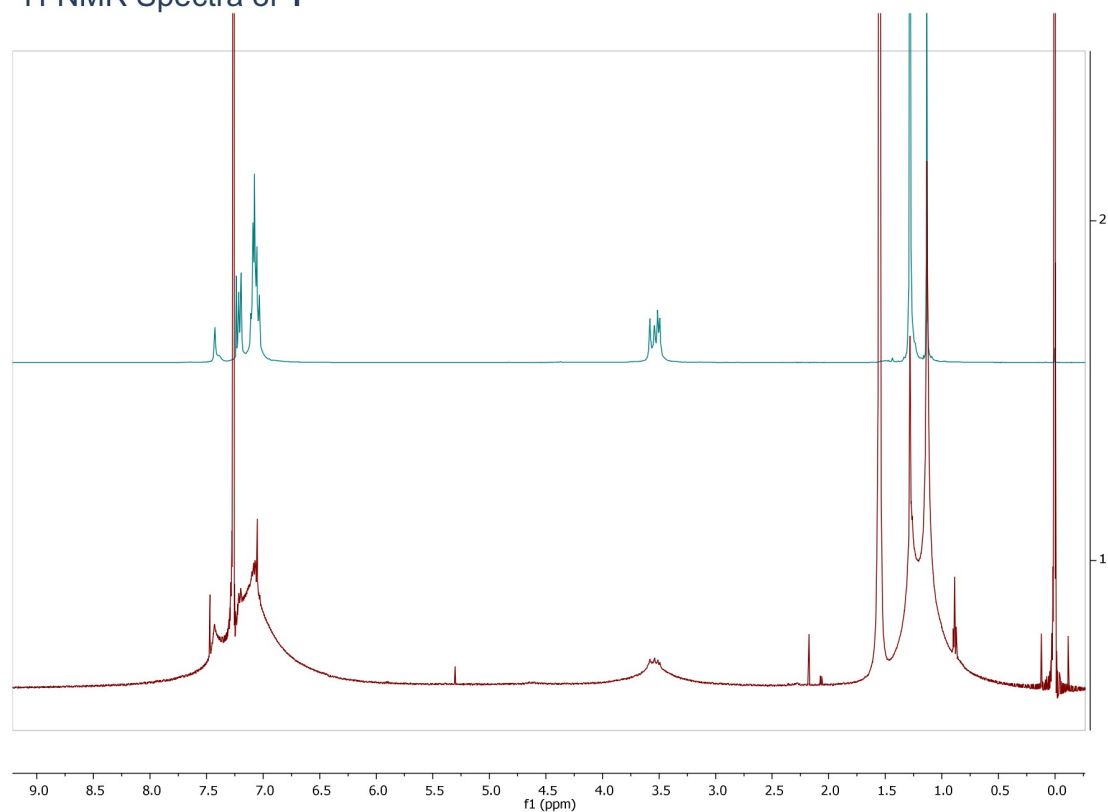


Fig. S1 ^1H NMR spectrum of cage **1** (blue) and **Au-1** (red). The close similarity corroborates the coating of the Au NP by the ligand. The characteristic line-broadening caused by the restricted tumbling motion documents the immobilization of the ligand on the NP surface.

TEM micrograph of **Au-1**

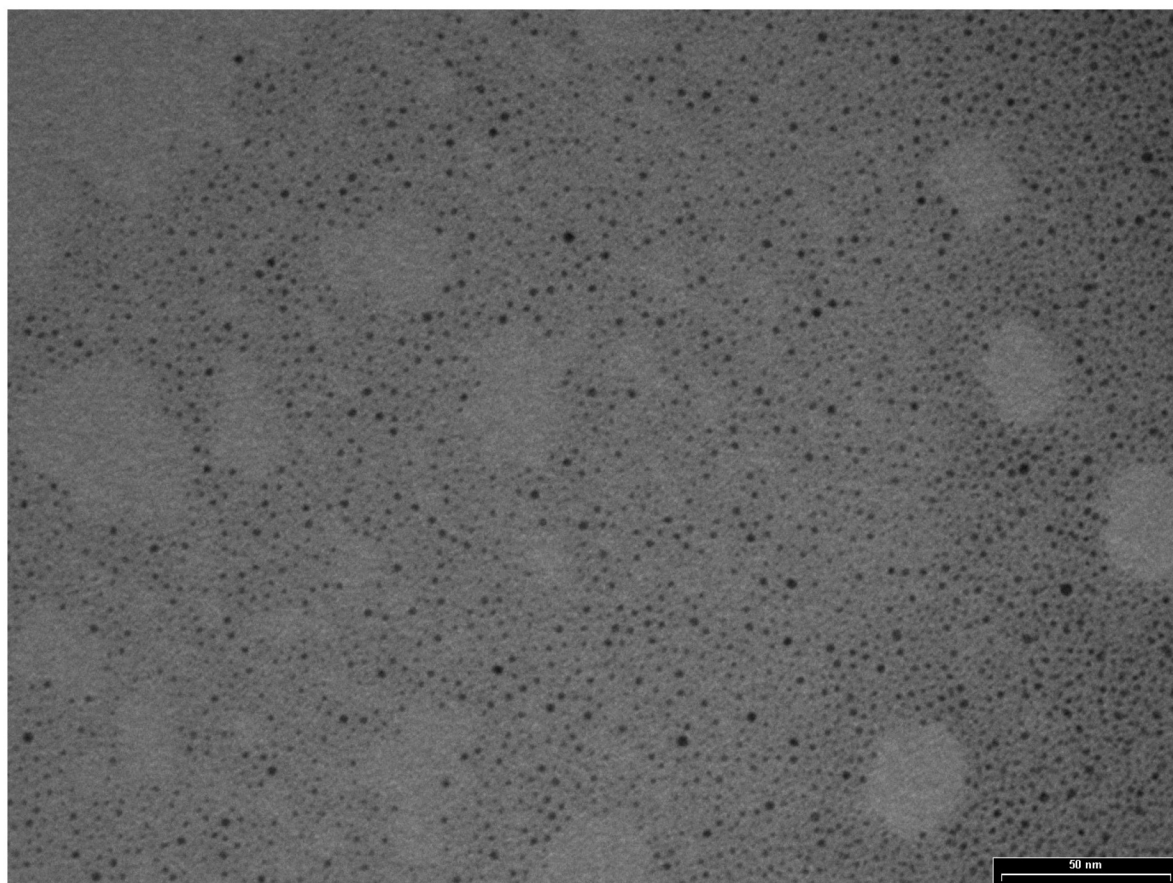
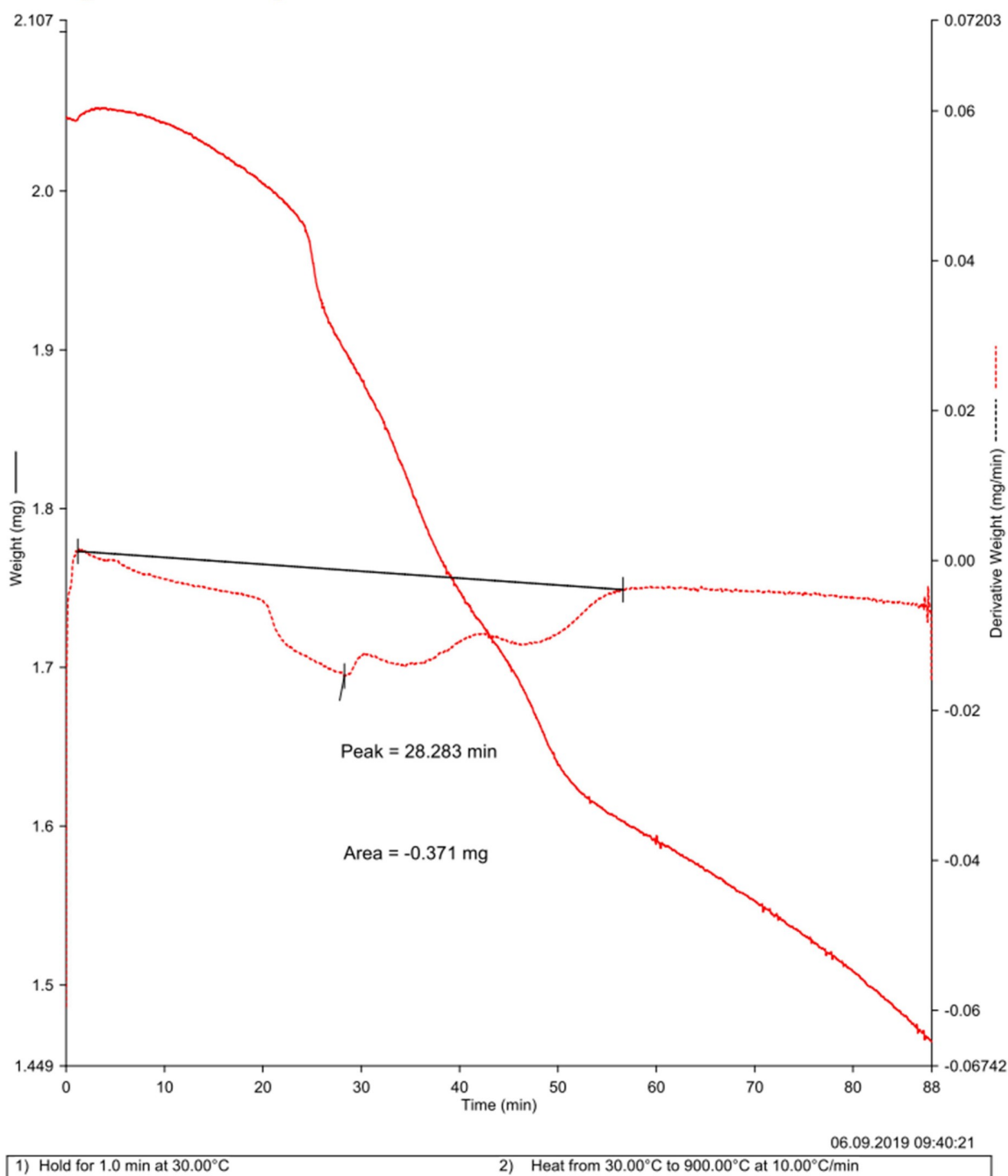


Fig. S2. Representative TEM micrograph of **Au-1**

Thermogravimetric Analysis of **Au-1****Fig. S3.** TGA mass loss trace for **Au-1**.**Table S1.** Ligand-to-gold ratio as taken from TGA and TEM images.

Au-1	$m(1)$ [mg]	$M(1)$ [g/mol]	$n(1)$ [mol]	m_{Au} [mg]	n_{Au} [mol]	M_{Au} [g mol ⁻¹]	$n_{Au}/n(1)$
TGA	2.053	2325.58	$1.60 \cdot 10^{-7}$	1.682	$8.54 \cdot 10^{-6}$	196.97	53.5

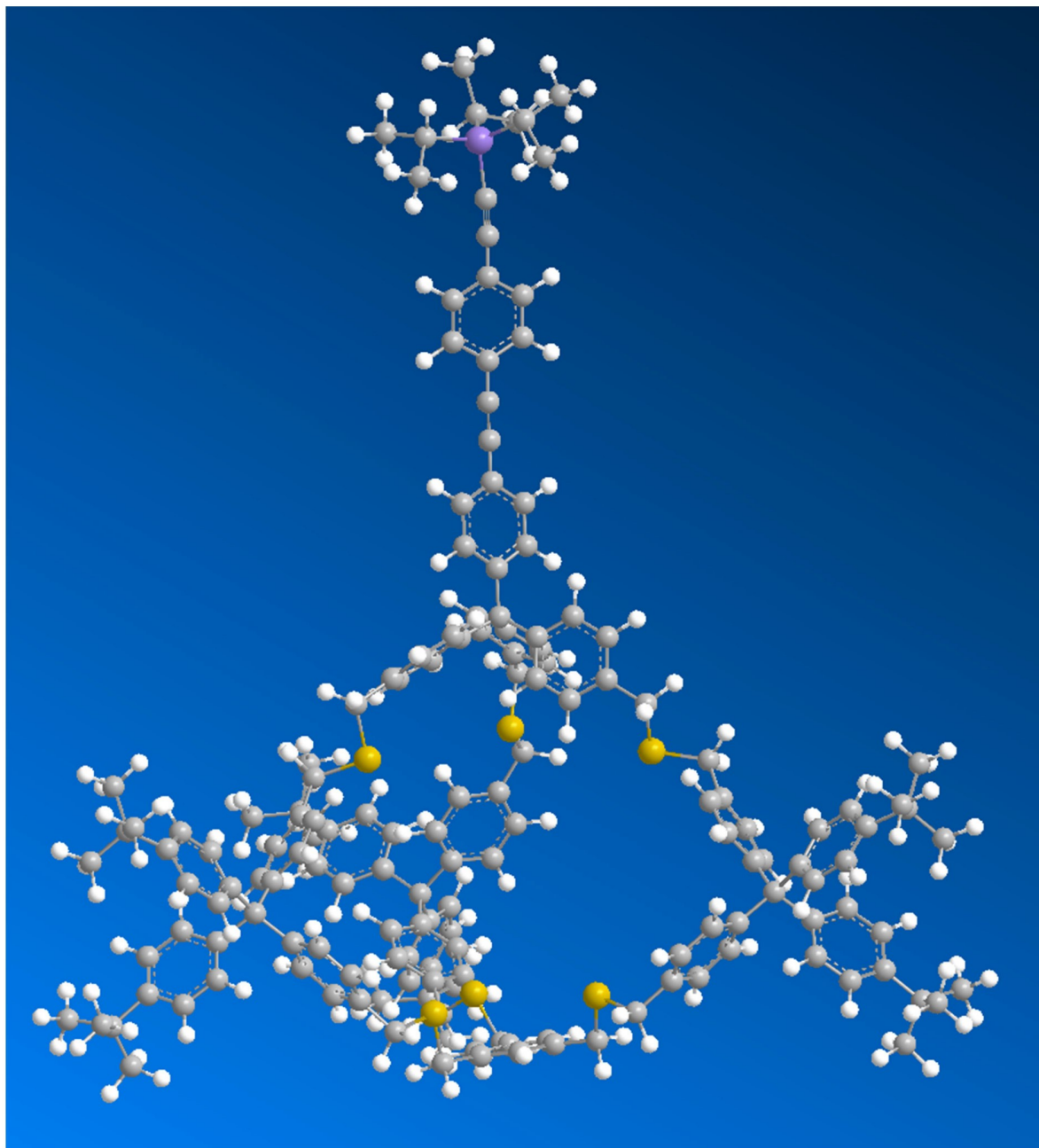


Fig. S4. Chem3D MM2 simulation render of **1**.

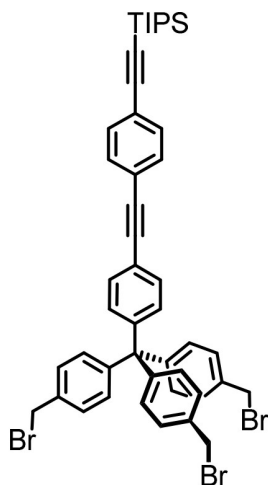
Materials

All commercially available starting materials were of reagent grade and used as received, unless stated differently. Absolute THF was purchased from Acros, stored over 4 Å molecular sieves, pre-dried with CaH, handled under argon and freshly distilled over sodium before each use. Pure CH₂Cl₂ was purchased from J. T. Baker. Pure toluene was purchased from Acros. Pure DMF was purchased from Acros Organics. *tert*-butylmethylether (TBME), *n*-hexane, ethyl acetate (EtOAc), and CH₂Cl₂ from Biosolve were used for purification and were of technical grade. Column chromatography was carried out on SiliaFlash P60 (particle size 40–63 μm) from SiliCycle. SEC for the purification of AuNPs mono-, di- and trimers was performed manually using Bio-Rad Bio-Beads S-X1 (operating range 600–14 000 g mol⁻¹) with CH₂Cl₂ or toluene as eluent. Deuterated solvents were purchased from Cambridge Isotope Laboratories.

Equipment and Measurements

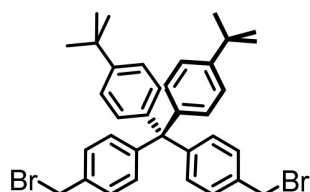
¹H and ¹³C NMR spectra were recorded with a Bruker DPX 400 instrument (¹H resonance 400 MHz, ¹³C resonance 101 MHz) or a Bruker DRX 500 instrument (¹H resonance 500 MHz, ¹³C resonance 126 MHz) at 298 K. The chemical shifts (δ) are reported in ppm and are referenced to the residual proton signal of the deuterated solvent (Chloroform-d: 7.26 ppm) for ¹H spectra or the carbon of the solvent (Chloroform-d: 77.1 ppm) for ¹³C spectra. The coupling constants (*J*) are given in Hertz (Hz), the multiplicities are denoted as: s (singlet), d (duplet), t (triplet), m (multiplet), and br (broad). High-resolution mass spectra (HRMS) were measured as HR-ESI-ToF-MS with a Maxis 4G instrument from Bruker or a Bruker UltraFlex II – MALDI-ToF-MS. For purification of the ligands, a (automated) Shimadzu Prominence System was used with SDV preparative columns from Polymer Standards Service (two Showdex columns in series, 20 mm × 600 mm each, exclusion limit: 30 000 g mol⁻¹) with chloroform as eluent. UV–vis measurements were recorded on a Jasco V-770 spectrophotometer using 117.100F-QS cuvettes from Hellma Analytics (10 mm light path). TEM was performed on a Philips CM100 TEM at 80 kV using copper grids (Cu-400HD) from Pacific Grid Tech. TGA was measured on a Mettler Toledo TGA/SDTA851^e with a heating rate of 10 °C min⁻¹.

Synthesis and Analytical Data of Cage **1** and Compounds **3–9**



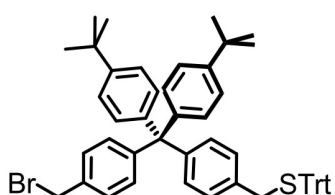
tris(p-(bromomethyl)phenyl)-p-(p-(triisopropylsilylethynyl)phenylethynyl)phenylmethane (**7**)¹

Compound **7** was synthesized as described in Ref. 1.



bis(p-(bromomethyl)phenyl)-bis(p-tert-butylphenyl)methane (**3**)²

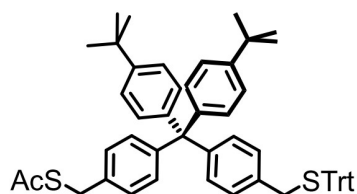
Compound **3** was synthesized as described in Ref. 2.



p-(tritylthiomethyl)phenyl-p-(bromomethyl)phenyl-bis(p-tert-butylphenyl)methane (**4**)²

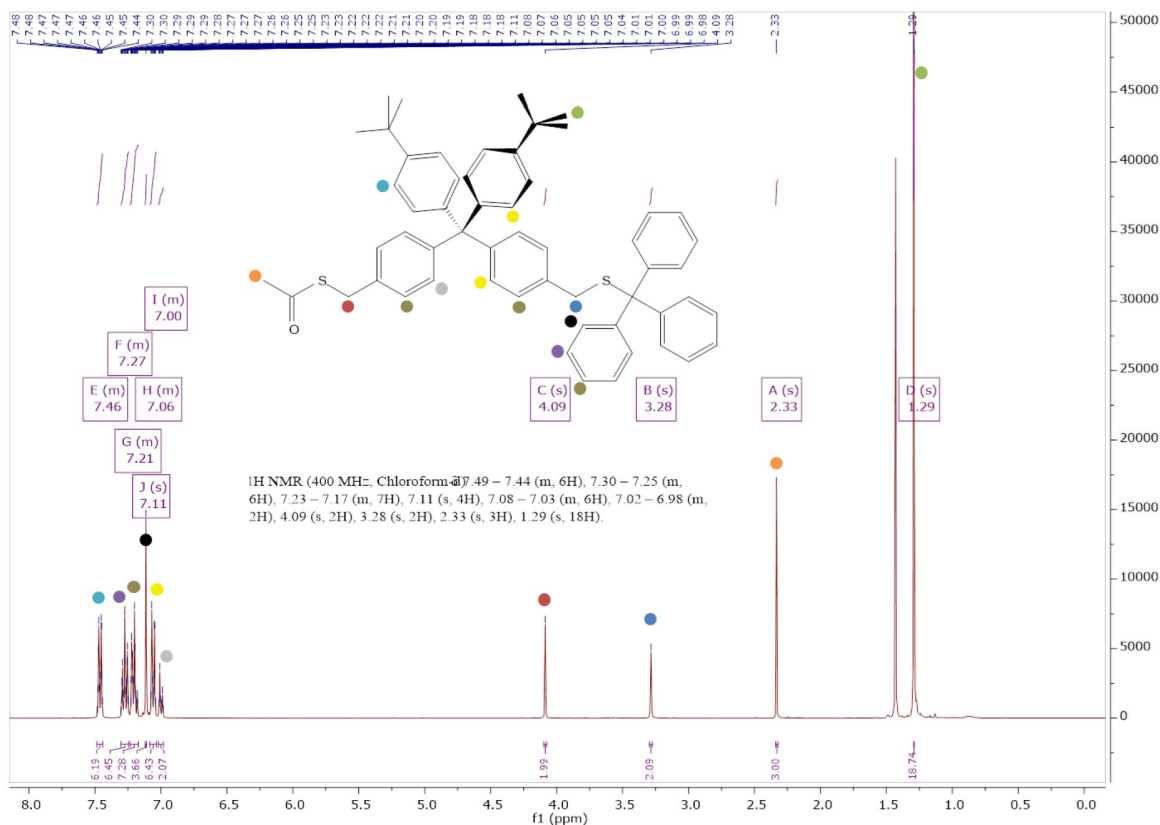
In a 250 ml flask, compound **3** (2.75 g, 4.45 mmol, 1 eq.) was dissolved in 100 ml freshly distilled THF in. Tritylthiol (1.27 g, 4.45 mmol, 1 eq.) was added to the solution which was then bubbled with argon for 15 minutes. NaH (60% dispersion in mineral oil, 200 mg, 5.03 mmol, 1.1 eq.) was added to the flask. The mixture was stirred at rt for 2 hours, quenched by careful addition of minimum amounts of water, dried over Na₂SO₄ and evaporated to dryness. The crude product was subjected to automated column chromatography (c-hexane: CH₂Cl₂ 10:1 and 2:1) to afford compound **4** (1.22 g, 1.50 mmol, 34%) as a white foam. ¹H NMR (400 MHz, Chloroform-d) δ 7.48 - 7.43 (m, 5H), 7.30 (s, 4H), 7.26 (d, J = 1.7 Hz, 6H), 7.24 - 7.18 (m, 7H), 7.15 (d, J =

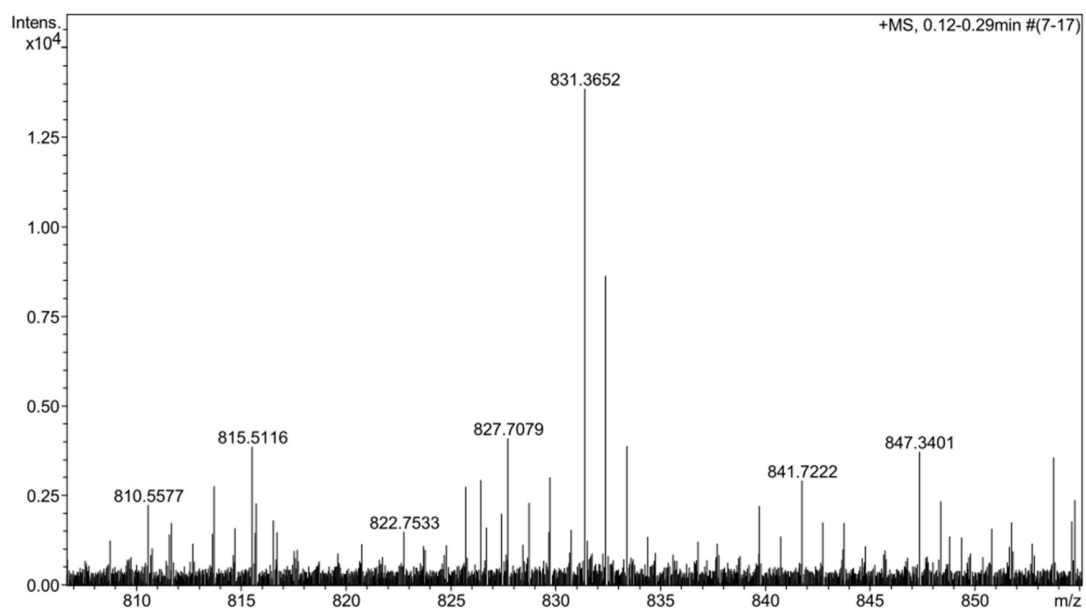
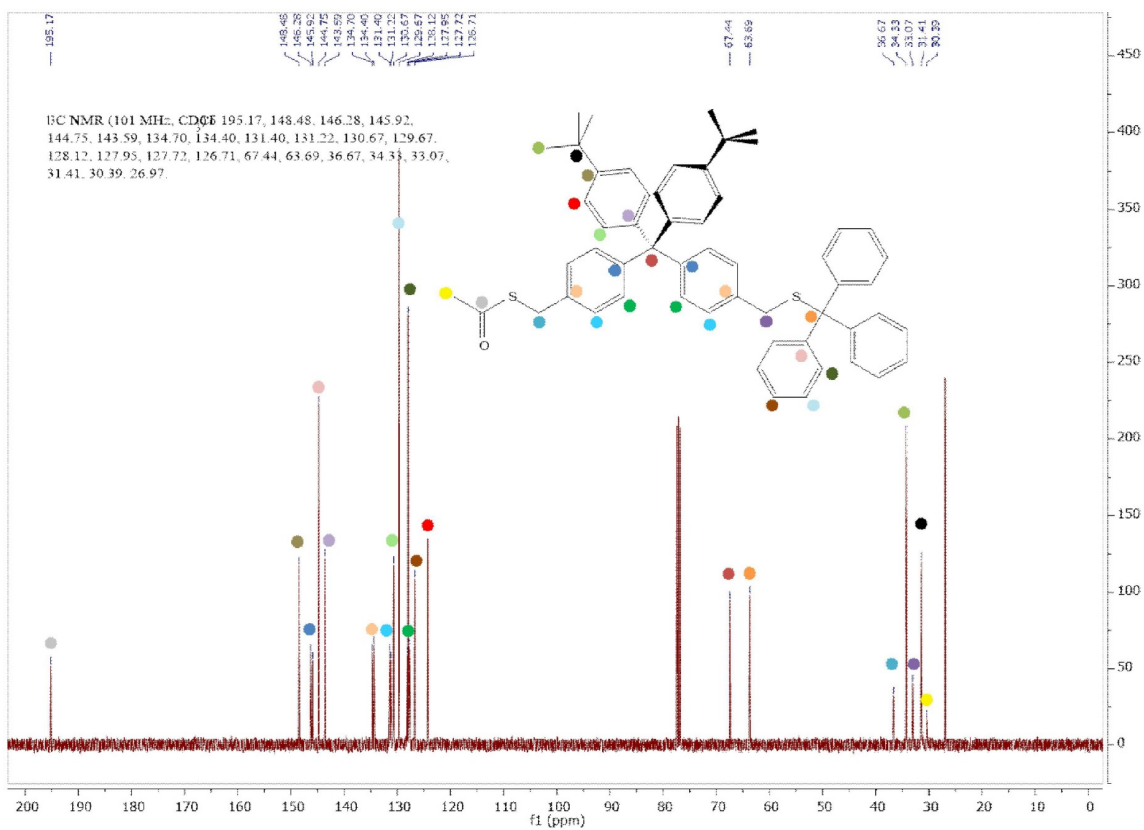
8.4 Hz, 2H), 7.08 -7.04 (m, 5H), 7.00 (d, J = 8.3 Hz, 2H), 4.47 (s, 2H), 3.28 (s, 2H), 1.29 (s, 18H).



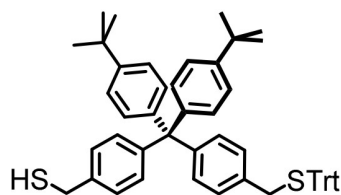
p-(tritylthiomethyl)phenyl-p-(acetylthiomethyl)phenyl-bis(p-tert-butylphenyl)-methane (**5**)

In a 100 ml flask, **4** (1.22 g, 1.50 mmol, 1 eq.) was dissolved in 50 ml dry DMF. Potassium thioacetate (0.343 g, 3.00 mmol, 2 eq.) was added and the mixture was stirred for 30 minutes after which time the mixture was diluted in excess TBME and washed five times with water to remove the DMF. The mixture was dried over Na₂SO₄, evaporated to dryness and subjected to column chromatography (c-hexane: CH₂Cl₂ 1:1) to give asymmetrically protected side-chain **5** as a green foam (1.13 g, 1.40 mmol, 93%). ¹H-NMR (400 MHz, Chloroform-d) δ 7.49 – 7.44 (m, 6H), 7.30 – 7.25 (m, 6H), 7.23 – 7.17 (m, 7H), 7.11 (s, 4H), 7.08 – 7.03 (m, 6H), 7.02 – 6.98 (m, 2H), 4.09 (s, 2H), 3.28 (s, 2H), 2.33 (s, 3H), 1.29 (s, 18H). ¹³C-NMR (101 MHz, CDCl₃) δ 195.17, 148.48, 146.28, 145.92, 144.75, 143.59, 134.70, 134.40, 131.40, 131.22, 130.67, 129.67, 128.12, 127.95, 127.72, 126.71, 67.44, 63.69, 36.67, 34.33, 33.07, 31.41, 30.39. HRMS (ESI-ToF): m/z = [M+Na]⁺ calcd. for C₅₆H₅₆OS₂Na⁺: 831.3665, found: 831.3652.



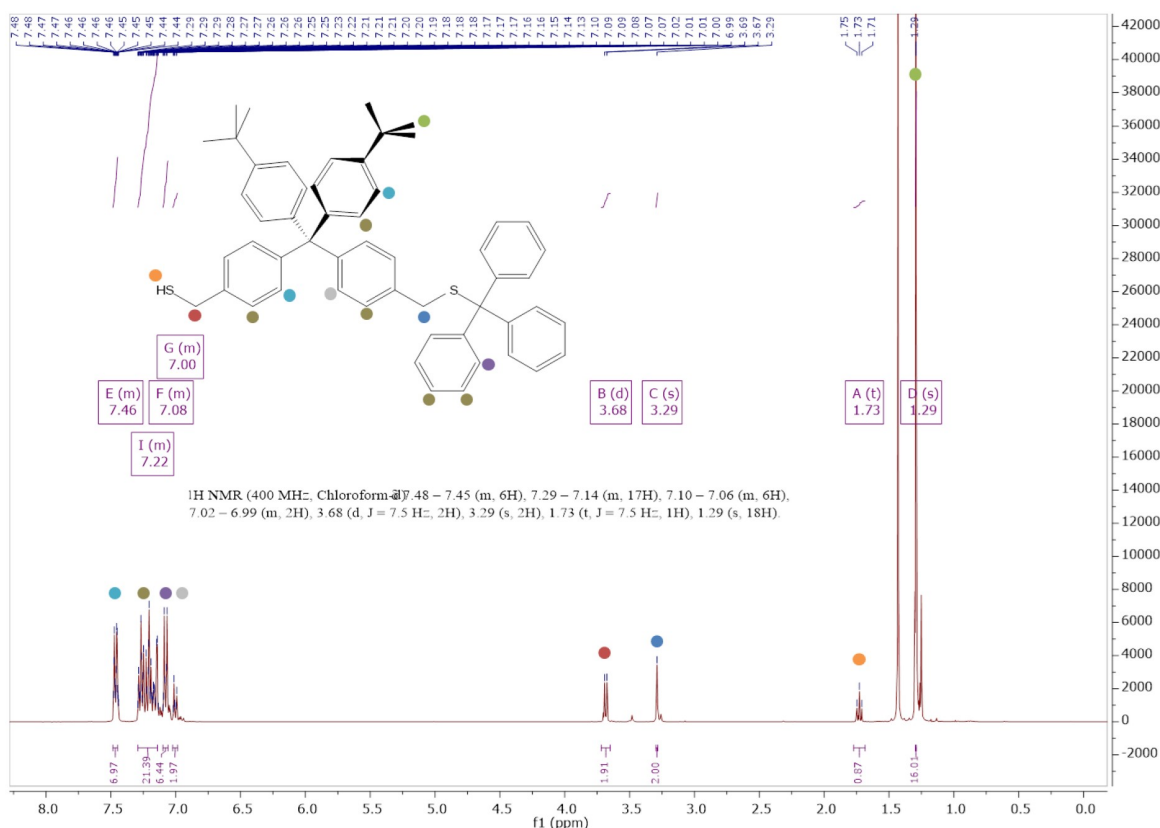


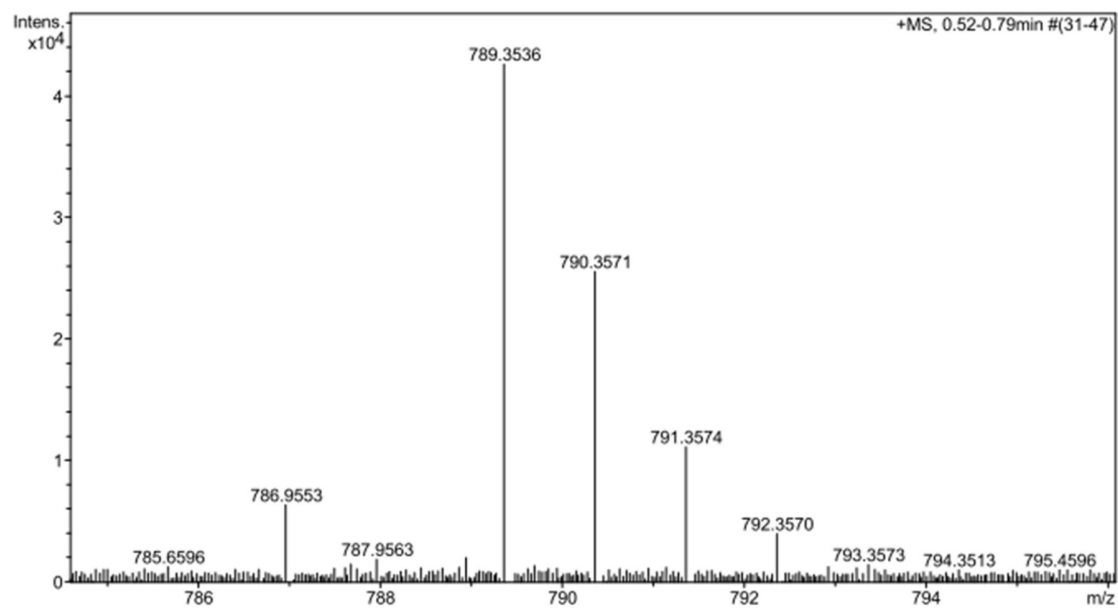
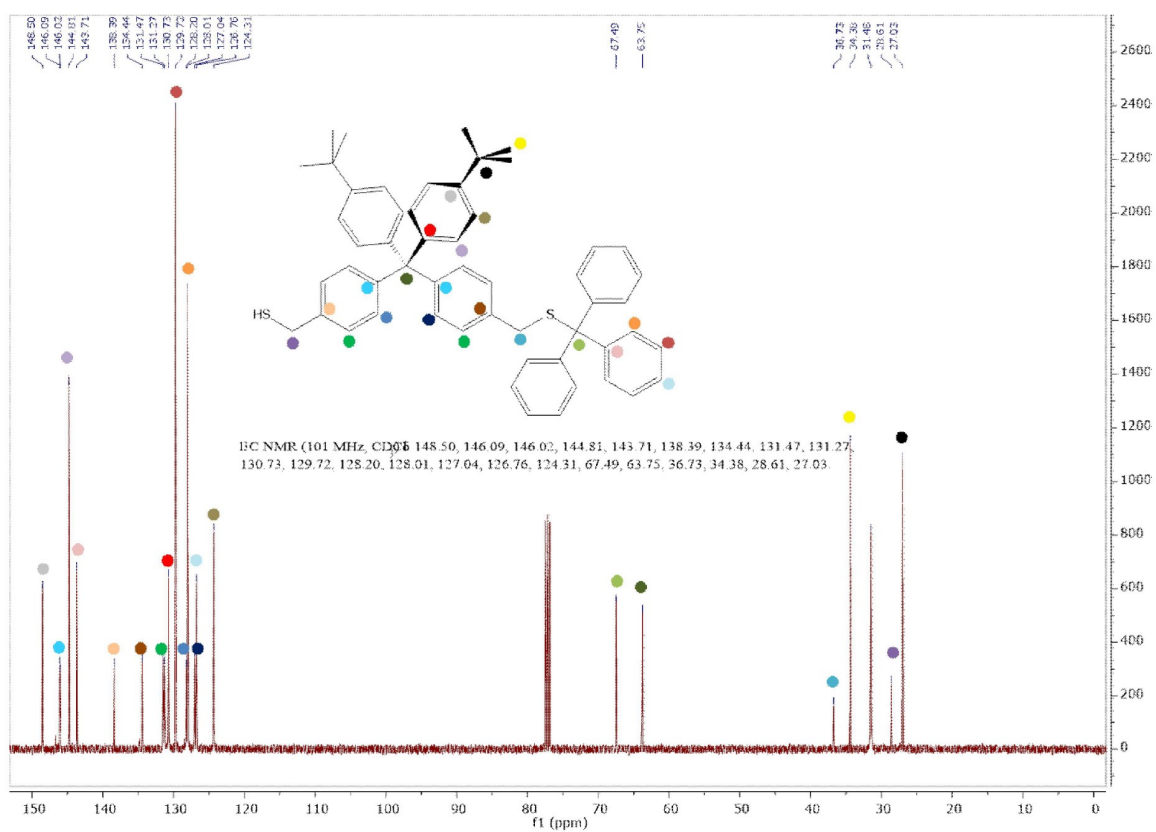
Meas. m/z	#	Formula	Score	m/z	err [mDa]	err [ppm]	mSigma	rdb	e ⁻ Conf	z
831.3652	1	C ₅₆ H ₅₆ NaO ₂ S	100.00	831.3665	1.2	1.5	10.1	28.5	even	1+



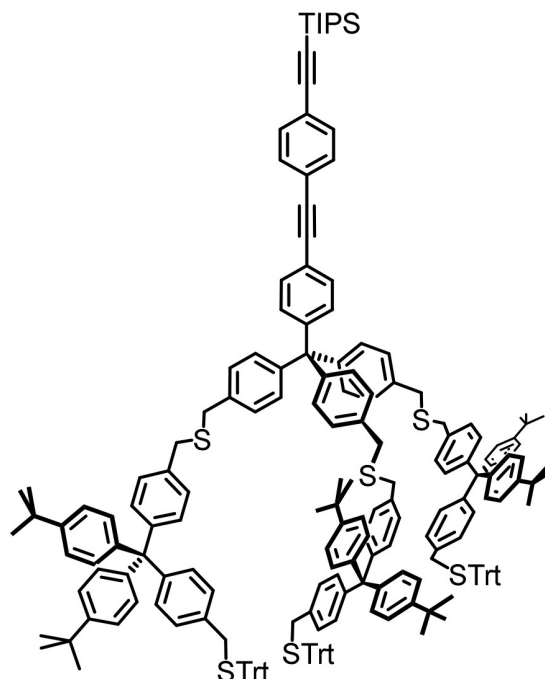
p-(mercaptomethyl)phenyl-p(tritylthiomethyl)phenyl-bis(p-tert-butylphenyl)-methane (**6**)

In a 100 ml flask, **5** (939 mg, 1.16 mmol, 1 eq.) was dissolved in 30 ml MeOH:THF 1:1 and degassed with argon for 20 minutes after which time K_2CO_3 (321 mg, 2.32 mmol 2 eq.) was added. The mixture was stirred for 4 hours and thereafter acidified by addition of 10% aqueous HCl (50 ml). The mixture was extracted three times with CH_2Cl_2 , dried over Na_2SO_4 and subjected to automated column chromatography (c-hexane: CH_2Cl_2 gradient 4:1 to 1:1) to afford thiol **6** as a white foam (854 mg, 1.11 mmol, 96%). 1H NMR (400 MHz, Chloroform- d) δ 7.48 – 7.45 (m, 6H), 7.29 – 7.14 (m, 17H), 7.10 – 7.06 (m, 6H), 7.02 – 6.99 (m, 2H), 3.68 (d, $J = 7.5$ Hz, 2H), 3.29 (s, 2H), 1.73 (t, $J = 7.5$ Hz, 1H), 1.29 (s, 18H). ^{13}C NMR (101 MHz, $CDCl_3$) δ 148.50, 146.09, 146.02, 144.81, 143.71, 138.39, 134.44, 131.47, 131.27, 130.73, 129.72, 128.20, 128.01, 127.04, 126.76, 124.31, 67.49, 63.75, 36.73, 34.38, 28.61, 27.03. HRMS (ESI-ToF): $m/z = [M+Na]^+$ calcd. for $C_{54}H_{54}S_2Na^+$: 789.3559, found: 789.3536.



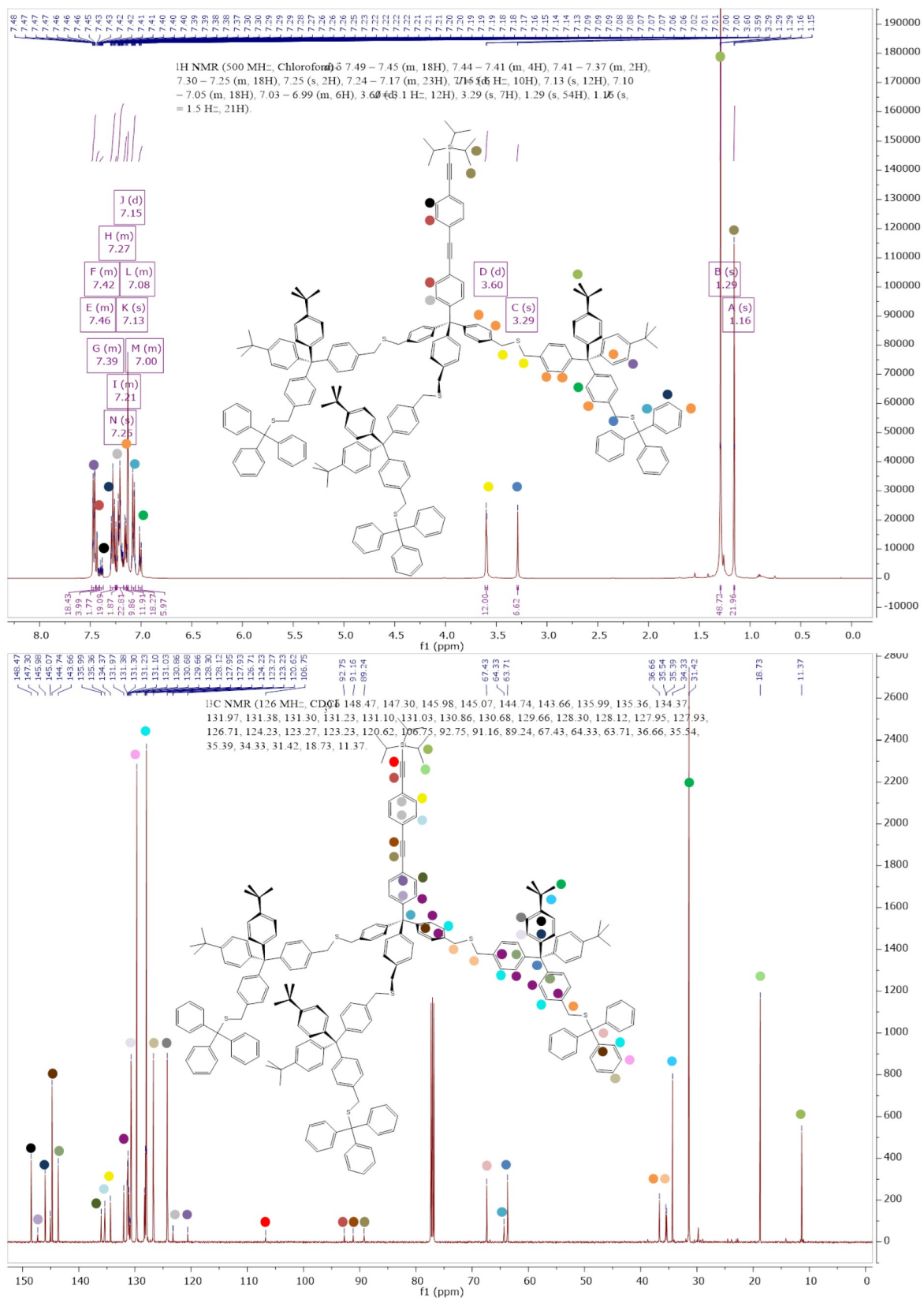


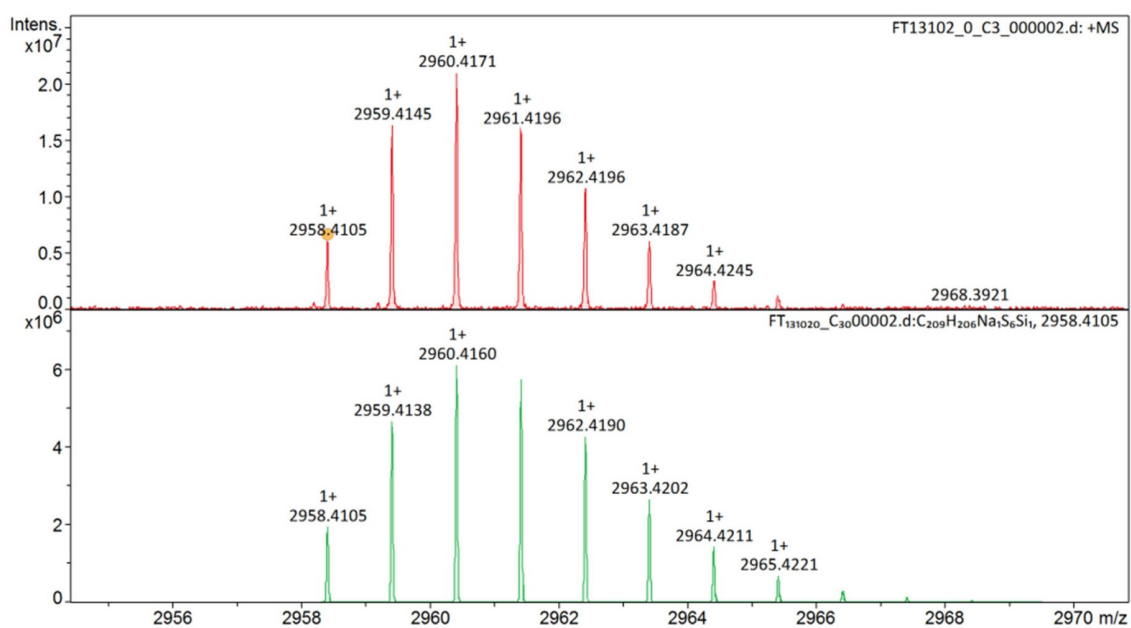
Meas. m/z	#	Formula	Score	m/z	err [mDa]	err [ppm]	mSigma	rdb	e ⁻ Conf	z
789.3536	1	C ₅₄ H ₅₄ NaS ₂	100.00	789.3559	2.4	3.0	8.1	27.5	even	1+



Tris(p-(p-(p-(tritylthiomethyl)phenyl-bis(p-tert-butylphenyl)methyl)phenylmethylthio-methyl)phenyl)-p-(p-(triisopropylsilylethynyl)phenylethynyl)phenylmethane (**8**)

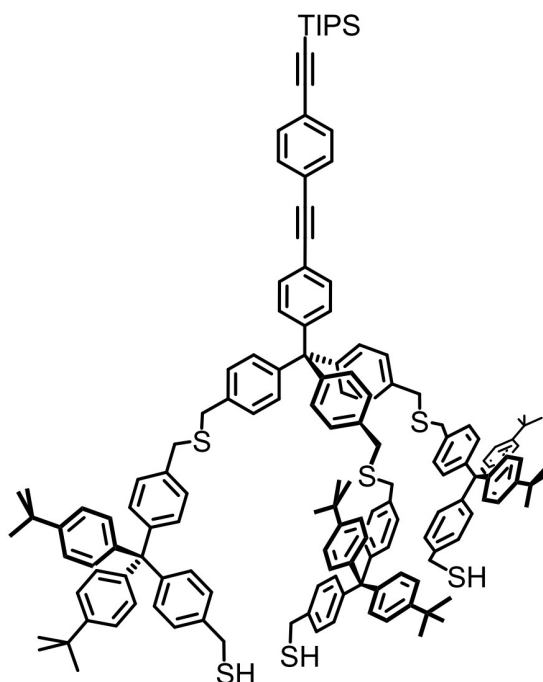
In a 25 ml flask, tribromide **7** (100 mg, 0.114 mmol, 1 eq.) and thiol **6** (350 mg, 0.456 mmol, 4 eq.) were dissolved in 10 ml dry THF and bubbled with argon for 30 minutes. NaH (60% dispersion in mineral oil, 50 mg, 1.25 mmol, 11 eq.) was added and the mixture was stirred at rt for 15 hours after which the reaction was quenched by careful addition of minimum amounts of water. The mixture was dried over Na₂SO₄, filtrated over a silica plug (CH₂Cl₂) and evaporated to dryness. Isolation by automated GPC (chloroform) gave S-protected cage precursor **8** as a yellow solid (279 mg, 0.096 mmol, 84%). ¹H NMR (500 MHz, Chloroform-*d*) δ 7.49 – 7.45 (m, 18H), 7.44 – 7.41 (m, 4H), 7.41 – 7.37 (m, 2H), 7.30 – 7.25 (m, 18H), 7.25 (s, 2H), 7.24 – 7.17 (m, 23H), 7.15 (d, *J* = 5.6 Hz, 10H), 7.13 (s, 12H), 7.10 – 7.05 (m, 18H), 7.03 – 6.99 (m, 6H), 3.60 (d, *J* = 3.1 Hz, 12H), 3.29 (s, 6H), 1.29 (s, 54H), 1.16 (s, 21H). ¹³C NMR (126 MHz, CDCl₃) δ 148.47, 147.30, 145.98, 145.07, 144.74, 143.66, 135.99, 135.36, 134.37, 131.97, 131.38, 131.30, 131.23, 131.10, 131.03, 130.86, 130.68, 129.66, 128.30, 128.12, 127.95, 127.93, 126.71, 124.23, 123.27, 123.23, 120.62, 106.75, 92.75, 91.16, 89.24, 67.43, 64.33, 63.71, 36.66, 35.54, 35.39, 34.33, 31.42, 18.73, 11.37. HRMS (MALDI-ToF): *m/z* = [M+Na]⁺ calcd. for C₂₀₉H₂₀₆S₆SiNa⁺: 2958.4105, found: 2958.4105.





Evaluation Spectra / Validation Formula:

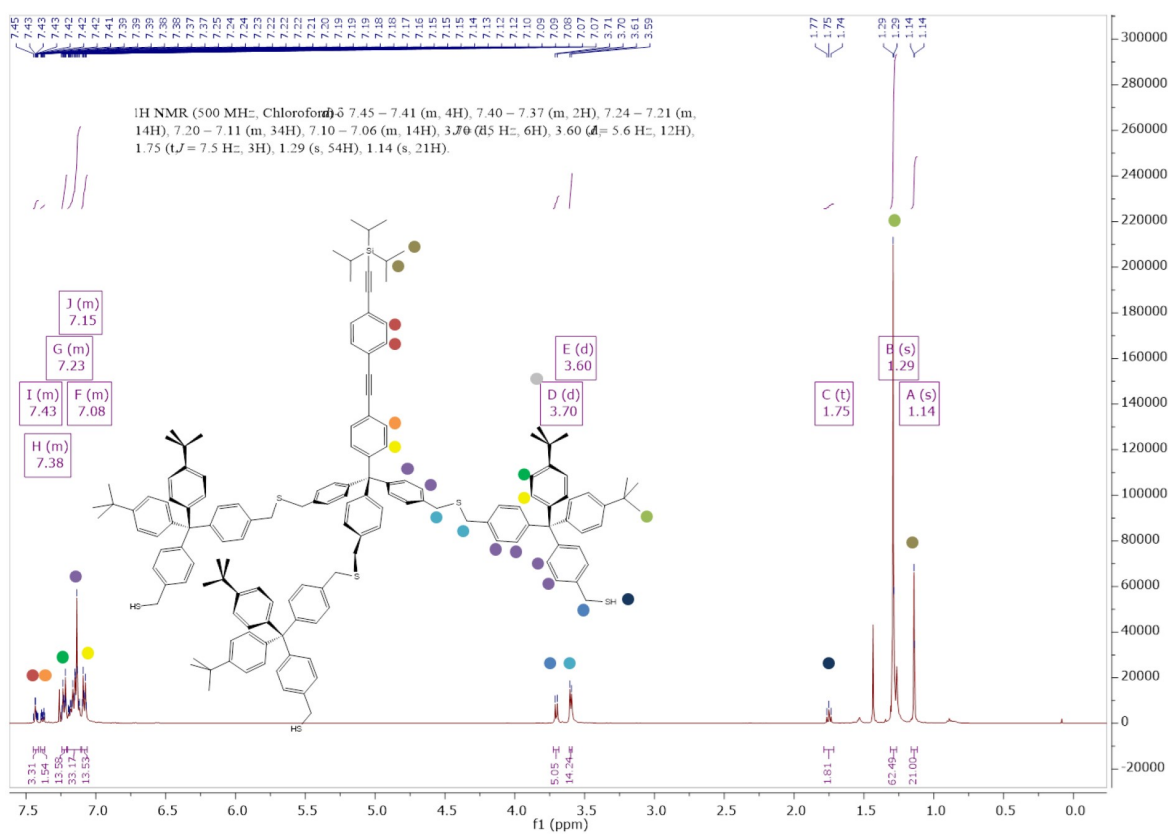
#	Ion Formula	Adduct	m/z	z	Meas. m/z	mSigma	N-Rule	err [mDa]	err [ppm]
1	C ₂₀₉ H ₂₀₆ NaS ₆ Si	M+Na	2958.4105	1+	2958.4105	102.4	ok	-0.0	-0.0

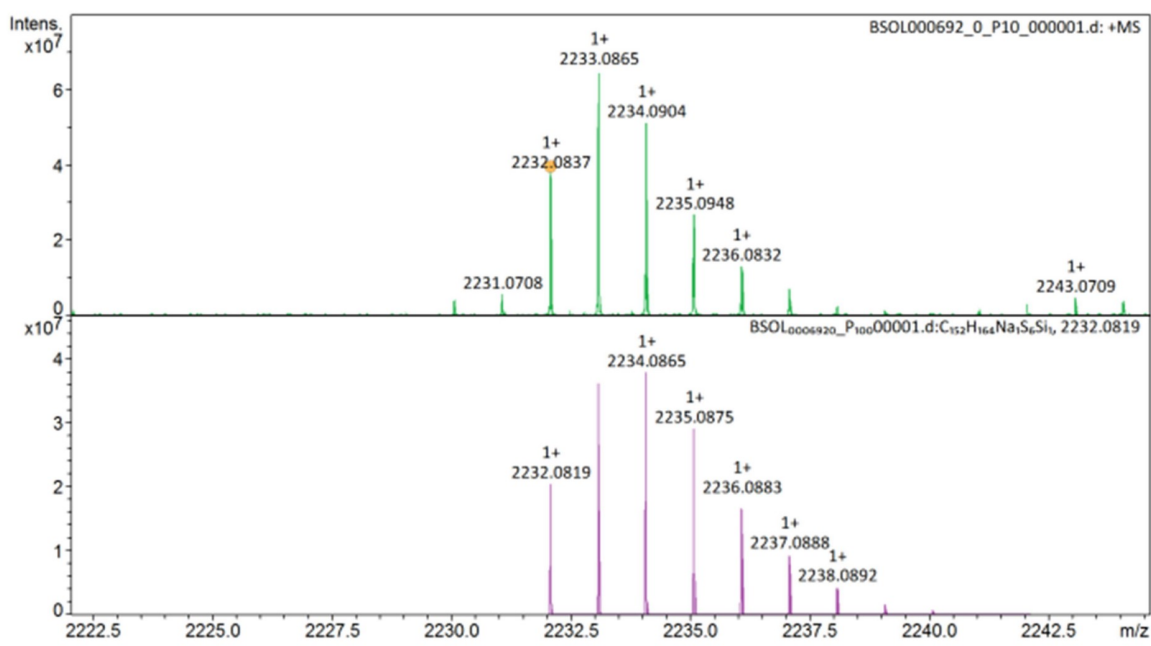
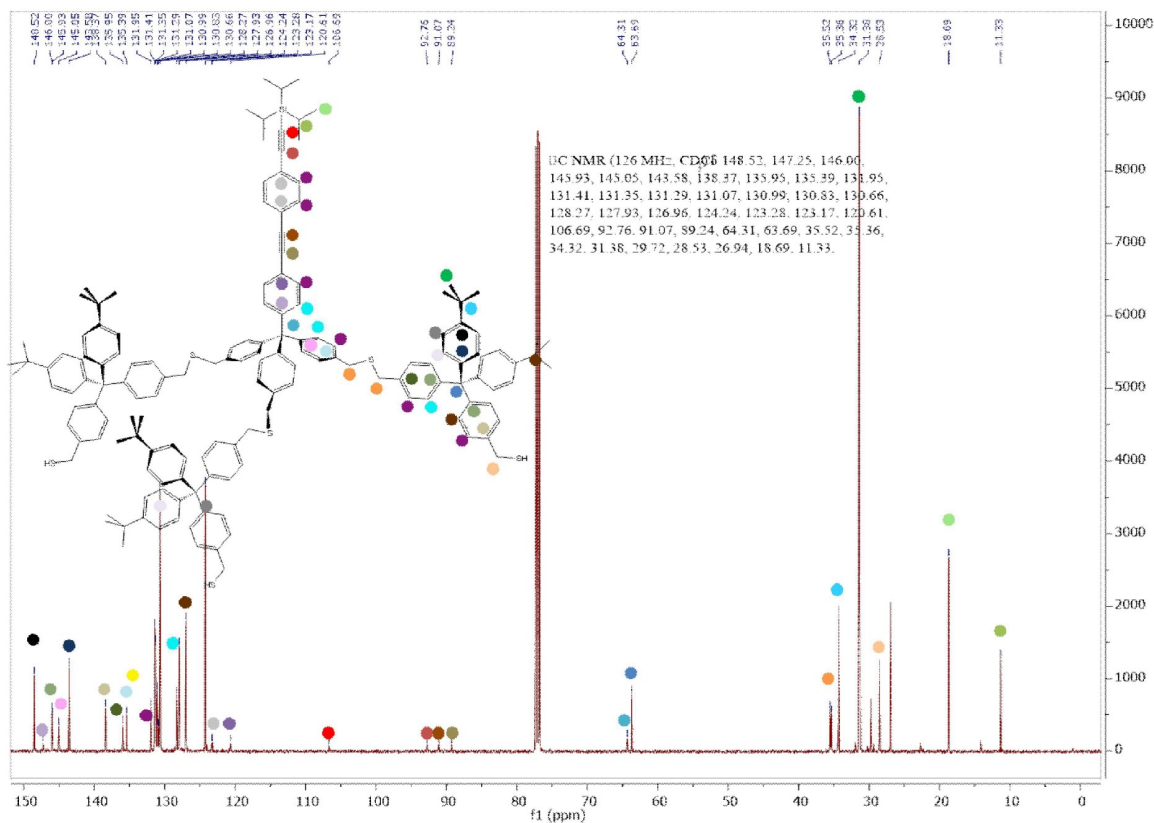


Tris(p-(p-(p-(mercaptomethyl)phenyl-bis(p-*tert*-butylphenyl)methyl)phenylmethylthio-methyl)phenyl)-p-(p-(triisopropylsilylethynyl)phenylethynyl)phenylmethane (**9**)

In a dry, degassed 25 ml flask, cage precursor **8** (576 mg, 0.196 mmol, 1 eq.) and SiEt₃H (0.20 ml, 0.745 mmol, 3.8 eq.) were dissolved in 20 ml CH₂Cl₂ and degassed for 30 minutes. The deprotection was started upon addition of 0.8 ml TFA (4 vol-%) which was visible from the color change to bright orange. The mixture was stirred

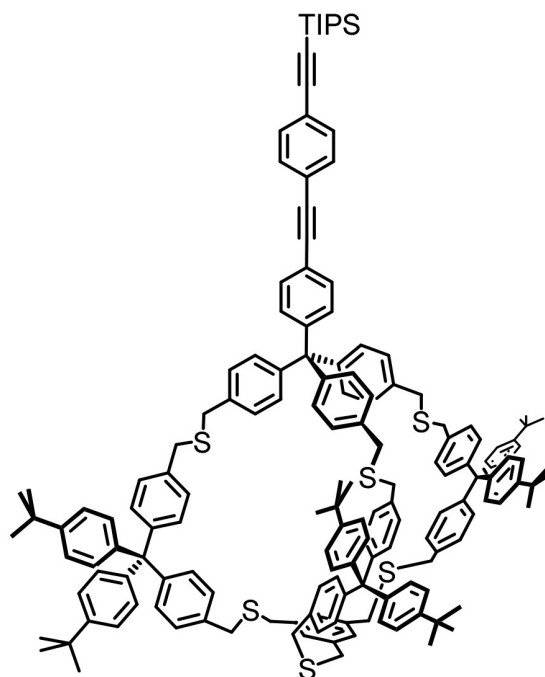
until the color had faded, indicating completion of the reaction (5 minutes) and quenched by addition of saturated aqueous NaHCO_3 . The phases were separated and the aqueous phase extracted twice with CH_2Cl_2 . The organic phase was dried over Na_2SO_4 and evaporated in vacuo. Purification was performed by column chromatography (c-hexane: CH_2Cl_2 gradient 4:1 to 1:1) to yield cage precursor trithiol **9** (404 mg, 0.183 mmol, 93%) as a white solid. ^1H NMR (500 MHz, Chloroform- d) δ 7.45 – 7.41 (m, 4H), 7.40 – 7.37 (m, 2H), 7.24 – 7.21 (m, 14H), 7.20 – 7.11 (m, 34H), 7.10 – 7.06 (m, 14H), 3.70 (d, $J = 7.5$ Hz, 6H), 3.60 (d, $J = 5.6$ Hz, 12H), 1.75 (t, $J = 7.5$ Hz, 3H), 1.29 (s, 54H), 1.14 (s, 21H). ^{13}C NMR (126 MHz, CDCl_3) δ 148.52, 147.25, 146.00, 145.93, 145.05, 143.58, 138.37, 135.95, 135.39, 131.95, 131.41, 131.35, 131.29, 131.07, 130.99, 130.83, 130.66, 128.27, 127.93, 126.96, 124.24, 123.28, 123.17, 120.61, 106.69, 92.76, 91.07, 89.24, 64.31, 63.69, 35.52, 35.36, 34.32, 31.38, 28.53, 18.69, 11.33. HRMD (MALDI-ToF): $m/z = [\text{M}+\text{Na}]^+$ calcd. for $\text{C}_{152}\text{H}_{164}\text{S}_6\text{SiNa}^+$: 2232.0819, found: 2232.0837.





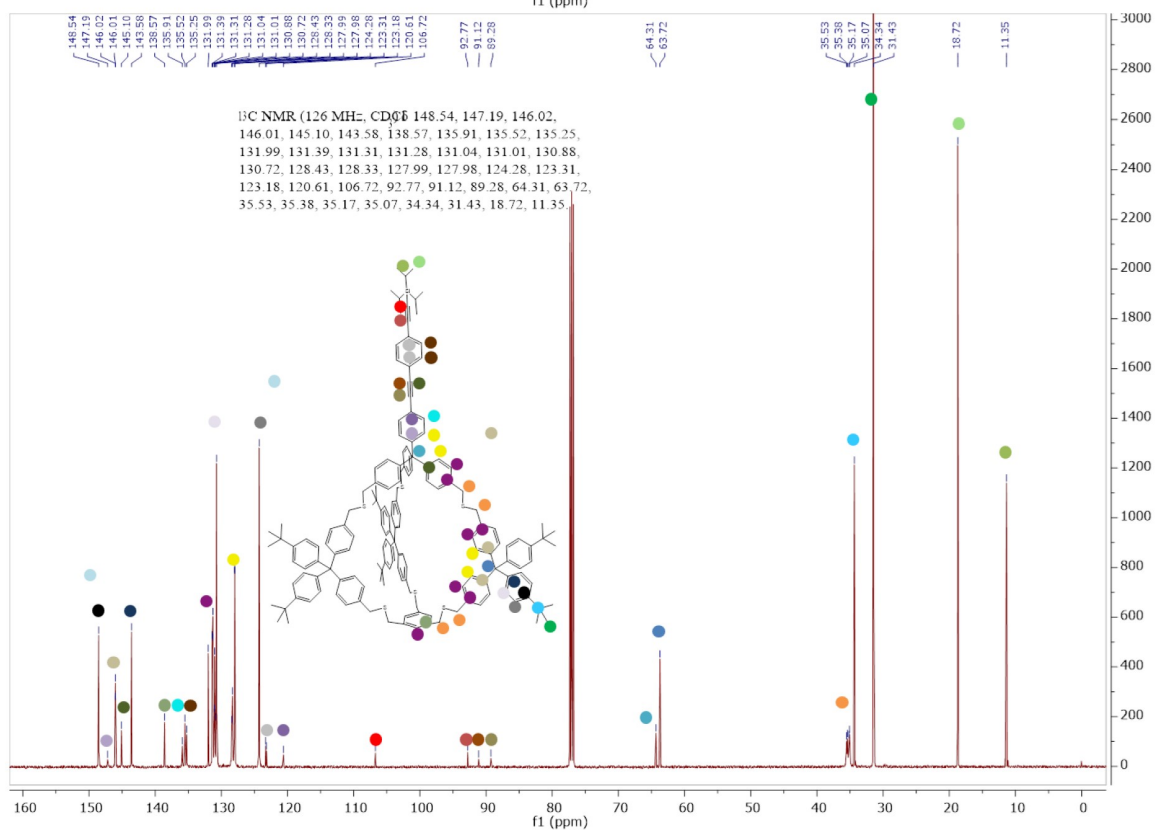
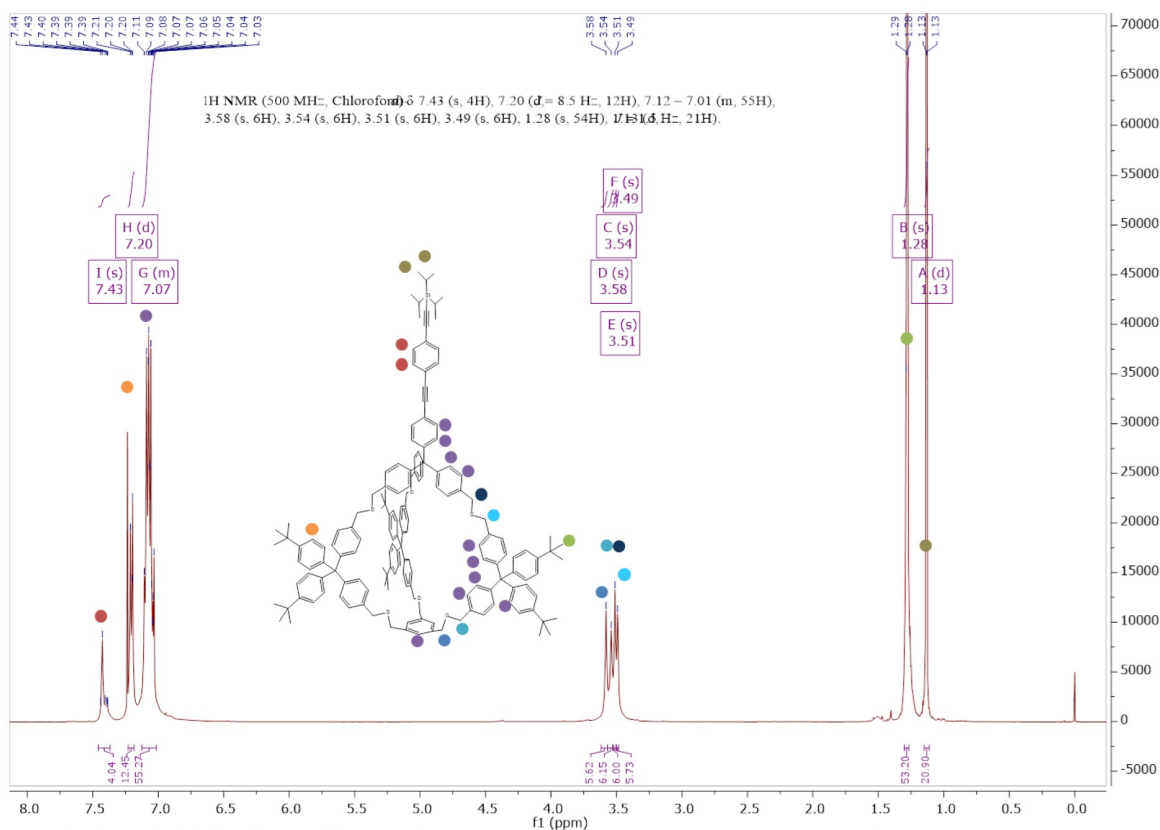
Evaluation Spectra / Validation Formula:

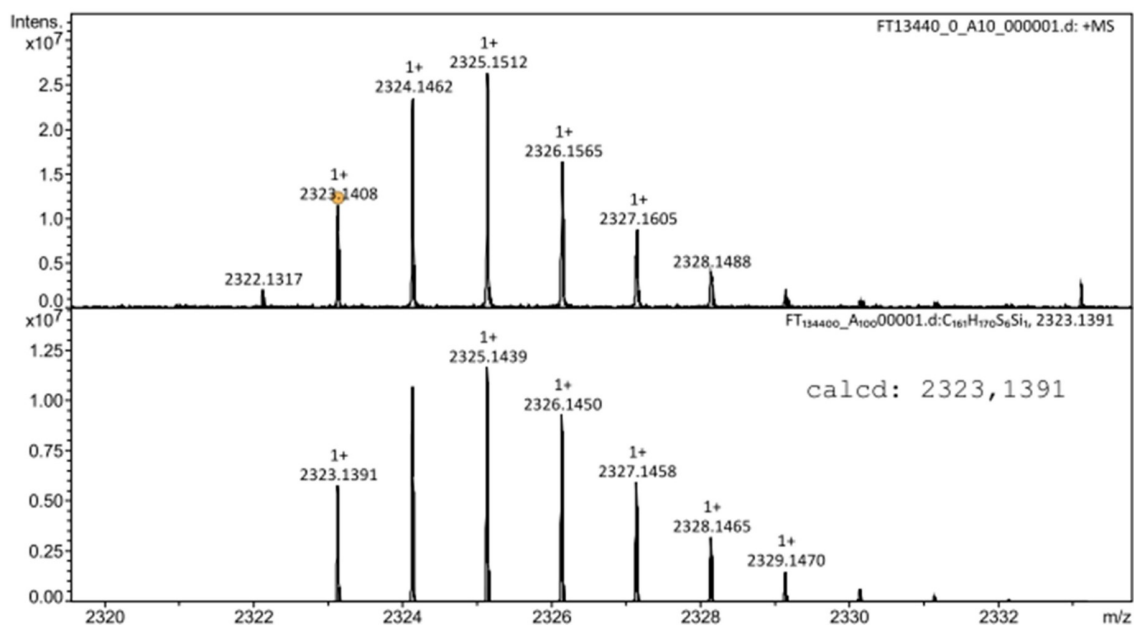
#	Ion Formula	Adduct	m/z	z	Meas. m/z	mSigma	N-Rule	err [mDa]	err [ppm]
1	C ₁₅₂ H ₁₆₄ Na ₆ Si ₆	M+Na	2232.0819	1+	2232.0837	177.6	ok	-1.8	-0.8



Cage-Type Ligand 1

In a 250 ml flask, trithiol **9** (175 mg, 0.079 mmol, 1 eq.) and 1,3,5-tris(bromomethyl)benzene (28 mg, 0.079 mmol, 1 eq.) were dissolved in 200 ml dry THF and degassed with an argon stream for 30 minutes. NaH (60% dispersion in mineral oil, 30 mg, 0.751 mmol, 9.5 eq.) was added and the reaction mixture was allowed to stir at rt for 3 days. The reaction was quenched upon careful addition of minimum amounts of water, dried over Na₂SO₄ and the solvent removed in vacuo. The crude was filtrated over a silica plug (CH₂Cl₂) and cage **1** was isolated by automated GPC (chloroform) to give a colorless solid (95 mg, 0.041 mmol, 52%). ¹H NMR (500 MHz, Chloroform-*d*) δ 7.45 – 7.38 (m, 4H), 7.20 (d, *J* = 8.5 Hz, 12H), 7.12 – 7.01 (m, 55H), 3.58 (s, 6H), 3.54 (s, 6H), 3.51 (s, 6H), 3.49 (s, 6H), 1.28 (s, 54H), 1.14 – 1.12 (m, 21H). ¹³C NMR (126 MHz, CDCl₃) δ 148.54, 147.19, 146.02, 146.01, 145.10, 143.58, 138.57, 135.91, 135.52, 135.25, 131.99, 131.39, 131.31, 131.28, 131.04, 131.01, 130.88, 130.72, 128.43, 128.33, 127.99, 127.98, 124.28, 123.31, 123.18, 120.61, 106.72, 92.77, 91.12, 89.28, 64.31, 63.72, 35.53, 35.38, 35.17, 35.07, 34.34, 31.43, 18.72, 11.35. HRMS (MALDI-ToF): *m/z* = [M]⁺ calcd. for C₁₆₁H₁₇₀S₆Si⁺: 2323.1391, found: 2323.1408.





Evaluation Spectra / Validation Formula:

#	Ion Formula	Adduct	m/z	z	Meas. m/z	mSigma	N-Rule	err [mDa]	err [ppm]
1	C16H17O5Si	M	2323.1391	1+	2323.1408	213.8	ok	-1.7	-0.7

References

- 1 E. H. Peters and M. Mayor, *Eur. J. Inorg. Chem.*, 2020, **2020**, 2325–2334.
- 2 M. Lehmann, E. H. Peters and M. Mayor, *Chem. – Eur. J.*, 2016, **22**, 2261–2265.

Erich Henrik PETERS

PERSONAL DATA

PLACE AND DATE OF BIRTH: Welwyn Garden City, UK; June 28, 1990
 ADDRESS: Güterstrasse 229, 4053 Basel, Switzerland
 NATIONALITY: Swiss and French
 PHONE: +41 76 308 59 52
 EMAIL: e.henrik.peters@gmail.com



WORK EXPERIENCE

SINCE | **SCIENTIST R&D, InnoMedica Schweiz AG, Marly**
SEP 2021 | Scale-up project lead | research and development of active pharmaceutical compounds encapsulated in liposomes to improve drug targeting | analytical development | planning, execution and knowledge transfer of production scale-up in cGMP environment (clean room) | literature research | IT power user | collaboration and negotiations with external partners.

AUG 2020 | **POST-DOCTORAL FELLOW, Universität Bern, Group of Prof. Dr. Robert Häner**
THROUGH | Synthesis and functionalization of self-assembling supramolecular polymers | analysis of intermediates and target structures
AUG 2021 | by MS, NMR, chromatography, UV-vis and fluorescence | literature research | project management | advisor for junior staff.

AUG 2015 | **INTERNSHIP, University of Applied Sciences and Arts Northwestern Switzerland (FHNW), Muttenz,**
THROUGH | **Group of Prof. Dr. Patrick Shahgaldian**
JAN 2016 | Co-immobilization and shielding of multiple enzymes on silica nanoparticles to create a non-diffusion-limited enzymatic cascade reaction in order to facilitate the removal of sulfonamide antibiotics residues from wastewater.

JAN 2013 | **MARTIAL ARTS COACH, Kampfsportcenter Kun-Tai-Ko, Füllinsdorf**
THROUGH | Teaching karate and kickboxing lessons to children and adults.
AUG 2021

EDUCATION

APR 2020 | **Ph.D. in CHEMISTRY, Universität Basel, Switzerland, Group of Prof. Dr. Marcel Mayor**
 Thesis: "Monofunctionalized Gold Nanoparticles via Branched Thioether-Based Ligands" | Final grade: 5.5/6.0 (*magna cum laude*)
 Synthesis of dendron- and cage-type organic ligands for the stabilization of monofunctionalized gold nanoparticles | analysis of intermediates and target structures by MS, NMR, chromatography and UV-vis | literature research | teaching undergraduates.

AUG 2015 | **M.Sc. in NANOSCIENCE, Universität Basel, Switzerland, Group of Prof. Dr. Marcel Mayor**
 Thesis: "Synthesis and Characterization of a Central Tripodal Subunit Enabling Dendritic Coverage of Gold Nanoparticles"
 Final Grade: 5.8/6.0 (*summa cum laude*) | Major: Organic Chemistry

SEP 2013 | **B.Sc. in NANOSCIENCE, Universität Basel, Switzerland**
 Final Grade: 5.0/6.0 (*cum laude*)

FEB 2010 | **Basic Military Education and Service, Rettungsunteroffiziers- und Rekrutenschule 75,**
THROUGH | **Wangen a/A, Switzerland**
AUG 2010 | Corps: Rettungskompanie 75-1 (rescue troops and emergency aid in case of natural disasters) | Rank: Soldier

LABORATORY SKILLS

PREPARATIVE SKILLS

Organic synthesis (milligram to multi-gram scale)
 cGMP manufacturing of drug products
 Work in cleanroom environment
 Automated solid-phase oligonucleotide synthesis
 Magnetron sputtering

ANALYTICAL SKILLS

Chromatography | TLC, HPLC, GPC, SEC, flash chromatography
 Mass spectrometry | GC-EI, GC-FID, LC-ESI, MALDI-ToF, DART
 Spectroscopy | ¹H-NMR, ¹³C-NMR, UV-Vis, IR, XPS, fluorescence
 Particle analysis | TEM, AFM, DLS, TFF
 Biological assays | Bradford, Lowry

COMPUTER SKILLS

Documenting	Word, Writer, LaTeX 2 _ε
Presentations	Powerpoint, Impress
Data Analysis	Excel, Calc, Origin, MestreNova, Chromeleon
Graphics	ChemDraw, Gimp, Gwyddion, ImageJ

SOFT SKILLS

Project management and careful documentation of experiments
Organization of studies and negotiations with external partners
Report writing and knowledge transfer
Oral presentations at international conferences

LANGUAGE SKILLS

MOTHER TONGUES

German
French

FOREIGN LANGUAGES

English	Fluent in speaking, reading, and writing
Spanish	Advanced level in speaking, reading, and writing
Swedish	Advanced level in reading, beginner level in speaking and writing

PUBLICATIONS

FIRST AUTHOR	<p>“An organic cage controlling the dimension and stability of gold nanoparticles” <i>Chem. Commun.</i>, 2023, 59, doi: 10.1039/D3CC00277B.</p> <p>“Monofunctionalized Gold Nanoparticles: Fabrication and Applications” <i>Chimia</i>, 2021, 75,5, 414–426, doi: 10.2533/chimia.2021.414.</p> <p>“Alkyne-Monofunctionalized Gold Nanoparticles as Massive Molecular Building Blocks” <i>Eur. J. Inorg. Chem.</i>, 2020, 24, 2325–2334, doi: 10.1002/ejic.202000273.</p> <p>“Gold Nanoparticles Stabilized by Single Tripodal Ligands” <i>Part. Part. Syst. Char.</i>, 2018, 35, 1800015, doi: 10.1002/ppsc.201800015.</p>
CO-AUTHOR	<p>“Size Matters: Influence of Gold-to-Ligand Ratio and Sulfur-Sulfur Distance of Linear Thioether Heptamers on the Size of Gold Nanoparticles” <i>Helv. Chim. Acta.</i> 2017, 100, e1600395, doi: 10.1002/hlca.201600395.</p> <p>“Linear Tetraphenylmethane-Based Thioether Oligomers Stabilising an Entire Gold Nanoparticle by Enwrapping” <i>Chem. Eur. J.</i> 2016, 22, 2261–2265, doi: 10.1002/chem.201504575.</p> <p>“Enzyme Shielding in an Enzyme-thin and Soft Organosilica Layer” <i>Angew. Chem. Int. Ed.</i> 2016, 55, 6285–6289, doi: 10.1002/anie.201600590.</p>

POSTERS AND TALKS

JAN 2020	<p>“Monofunctional Organic Cage for Gold Nanoparticles” (talk) Swiss Snow Symposium, Saas-Fee (CH)</p>
DEC 2019	<p>“Monofunctional Organic Cage for Gold Nanoparticles” (poster and elevator pitch) PCC Christmas Symposium, Basel (CH)</p>
SEP 2019	<p>“Chemistry with Monofunctionalized Gold Nanoparticles” (talk) 39th Regio Symposium, Mittelwihr (F)</p>
JUN 2018	<p>“Gold Nanoparticle Dimers via Acetylene Homocoupling” (poster) Swiss Nanoscience Convention 2018, Zürich (CH)</p>
AUG 2015	<p>“Gold Nanoparticles for Molecular Electronics via Tailor-Made Ligands” (poster) 9th International Nanoscience Students Conference, Basel (CH)</p>

INTERESTS AND ACTIVITIES

SPORTS

Karate (black belt, II. dan)
Kickboxing (black belt, II. dan)
Aikido (white belt, V. kyū)
Iaido (beginner)

HOBBIES

Cooking and eating out with friends
Rock, rap and jazz music and concerts of which
Makeshift repairs on everyday devices and practical solutions for small problems
Reading comic books
Growing tomatoes, chilies and spices